Refinery Integration of By-Products from Coal-Derived Jet Fuels

SEMI-ANNUAL PROGRESS REPORT

March 18, 2006 – September 30, 2006

Caroline E. Burgess Clifford, André Boehman, Chunshan Song,
Bruce Miller, Gareth Mitchell

Date Issued: November 30, 2006

Grant DE-FC26-03NT41828

The Pennsylvania State University
The Energy Institute
C205 Coal Utilization Laboratory
University Park, PA 16802

Disclaimer

Abstract

This report summarizes the accomplishments toward project goals during the second six months of the third year of the project to assess the properties and performance of coal based products. These products are in the gasoline, diesel and fuel oil range and result from coal based jet fuel production from an Air Force funded program. Specific areas of progress include generation of coal based material that has been fractionated into the desired refinery cuts and examination of carbon material, the use of a research gasoline engine to test coal-based gasoline, and modification of diesel engines for use in evaluating diesel produced in the project. At the pilot scale, the hydrotreating process was modified to separate the heavy components from the LCO and RCO fractions before hydrotreating in order to improve the performance of the catalysts in further processing. Characterization of the gasoline fuel indicates a dominance of single ring alkylcycloalkanes that have a low octane rating; however, blends containing these compounds do not have a negative effect upon gasoline when blended in refinery gasoline streams. Characterization of the diesel fuel indicates a dominance of 3-ring aromatics that have a low cetane value; however, these compounds do not have a negative effect upon diesel when blended in refinery diesel streams. Both gasoline and diesel continue to be tested for combustion performance. The desulfurization of sulfur containing components of coal and petroleum is being studied so that effective conversion of blended coal and petroleum streams can be efficiently converted to useful refinery products. Activated carbons have proven useful to remove the heavy sulfur components, and unsupported Ni/Mo and Ni/Co catalysts have been very effective for hydrodesulfurization. Equipment is now in place to begin fuel oil evaluations to assess the quality of coal based fuel oil. Combustion and characterization of the latest fuel oil (the high temperature fraction of RCO from the latest modification) indicates that the fraction is

heavier than a No. 6 fuel oil. Combustion efficiency on our research boiler is ~63% for the heavy RCO fraction, lower than the combustion performance for previous co-coking fuel oils and No. 6 fuel oil. An additional coal has been procured and is being processed for the next series of delayed co-coking runs. Work continues on characterization of liquids and solids from co-coking of hydrotreated decant oils; liquid yields include more saturated and hydro- aromatics, while the coke quality varies depending on the conditions used. Pitch material is being generated from the heavy fraction of co-coking. Investigation of coal extraction as a method to produce RCO continues; the reactor modifications to filter the products hot and to do multi-stage extraction improve extraction yields from ~50 % to ~70%. Carbon characterization of co-cokes for use as various carbon artifacts continues.

TABLE OF CONTENTS

List of Tables

List of Figures

Refinery Integration of By-Products from Coal-Derived Jet Fuels

Introduction

This program is investigating the fate of each major product from a refinery complex, except jet fuel, resulting from the refinery integration of coal-derived jet fuel production via a combined RCO/LCO strategy by studying the physical and chemical nature of all products that are perturbed by introduction of coal components into the refinery.

The impact of the proposed research is to provide the scientific and fundamental engineering basis to integrate the production of coal-based jet fuel into existing refinery operations in a time frame consistent with availability and economic forecasts related to petroleum-derived as opposed to coal-based feedstocks. The results of these studies lead to the integration of all non-jet-fuel streams into current refinery operations in concert with desired production of coal-based jet fuel engine testing toward the end of the first decade of the new century. For successful utilization of coal-based jet fuels all non-jet-fuel components must fit existing and future product stream specifications.

Executive Summary

Penn State has been working for more than a decade on the development of an advanced, thermally stable, coal-based jet fuel, JP-900. Two process routes to JP-900 have been identified, one involving the hydrotreating of blends of refined chemical oil (RCO, a by-product of the coal tar industry) with light cycle oil (LCO), and the other involving the addition of coal to delayed cokers. However, no refinery is operated for the primary purpose of making jet fuel. The conversion of the jet fuel section of a refinery to production of coal-based JP-900 would necessarily impact the quantity and quality of the other refinery products, such as gasoline, diesel fuel, fuel oil, and coke. The overall objective of this project is to examine the characteristics and quality of the streams *other than the jet fuel*, and to determine the effect those materials would have on other unit operations in the refinery.

The present report documents the activities of the second six months of year three of what is envisioned to be a four-year program. Our collateral work on jet fuel, funded by the Air Force Office of Scientific Research, is focused exclusively on that product. Thus as we branch out into the study of the other refinery streams, under this present contract, much of the effort in the last year has been devoted to the evaluation of product streams to streamline operations.

The overall project involves pilot-scale production of materials at Intertek PARC Technical Services (Harmarville, PA). The coal-based gasoline and diesel fuel is being evaluated in appropriate internal combustion engines. Desulfurization, denitrogenation, and saturation of aromatics are being tested. There is also a component to examine the production of high-value aromatic compounds. The initial products of coal-based fuel oil were tested in a research boiler, although not enough fuel was available to do complete characterization. The pitch and coke co-coking from initial runs has been characterized. These interrelated activities are designed to evaluate the full range of products from coal-based thermally stable jet fuel production and to lead toward process integration in existing refineries.

The first run for hydrotreatment of blends of refined chemical oil and light cycle oil, followed by fractionation of the total product, was performed at Intertek PARC. The various distillation cuts have been provided to the researchers at Penn State for analytical characterization and for use in the appropriate evaluation tests. In addition, decant oil was hydrotreated at several levels of severity for use in the co-coking work. In this report period, Intertek PARC has distilled samples of RCO (75% yield) and LCO (63% yield) separately before hydrotreatment, and is in the process of finishing hydrotreatment to provide new fuels for Year 4 evaluation. The fuel oil fraction has been separated and provided to those in Task 4 for evaluation.

Characterization of the gasoline fuel indicates a dominance of single ring alkylcycloalkanes that have a low octane rating (Research Octane Number is 61.0 for EI-174); however, blends containing these compounds do not have a negative effect upon gasoline when blended in refinery gasoline streams.

Characterization of the diesel fuel indicates a dominance of 3-ring aromatics that have a low cetane value; however, these compounds do not have a negative effect upon diesel when blended in refinery diesel streams. The two compounds that have been chosen to represent the coal-based diesel are fluorene and phenanthrene. These compounds were blended with a low sulfur diesel fuel from BP (BP-15). This reporting period, ethylhexyl nitrate (EHN) slightly improved the combustion performance of the blend of BP-15 and 5% phenanthrene, but did not appear quite as effective with fluorene.

The desulfurization of sulfur containing components of coal and petroleum is being studied so that effective conversion of blended coal and petroleum streams can be efficiently converted to useful refinery products. The development of unsupported finely dispersed Ni/Mo and Co/Mo catalyst prepared in house shows increased sulfur removal compared to commercial Ni/Mo catalyst. Adsorptive desulfurization of LCO using activated carbon worked well, by removing the heavy sulfur and nitrogen compounds before hydrogenation. For the saturation of two-ring aromatics component of Task 3, zeolite catalyst supports exhibit higher sulfur tolerance.

Equipment is now in place to begin fuel oil evaluations to assess the quality of coal based fuel oil. It was reported in the last report that combustion and characterization of a the initial co-processed fuel oils indicates that the fuel oil is somewhere in between a No. 4 and a No. 6 fuel oil. Emission testing indicates the fuel burns similarly to these two fuels, but trace metals for the coal-based material are different than petroleum-based fuel oils. The boiler efficiency of the most recent fuel oil, the bottom fraction of RCO (62.3%), is lower than the efficiency than No. 6 fuel oil (70%). Trace metal evalution of this fuel oil will be included in the next semi-annual report.

A significant amount of work has progressed on Task 5, which is the evaluation of co-coking using coal and refinery solvents. Previously, we showed that co-coking studies using the

first cleaned coal are highly reproducible in the pilot-scale delayed coker. Evaluation of the coke indicated that while the coke produced is of very good quality, the metals content of the carbon is still high in iron and silica. The most recent work has focused on obtaining a coal with a lower mineral matter content, from the Marfolk mine in West Virginia. Preparation of the coal is in progress. The best conditions for co-coking of hydrotreated decant oil with coal in tubing reactors are under atmospheric conditions at 18 h. Hydrotreatment reduced levels of heteroatoms and increased coke quality under atmospheric conditions; however, when using autogeneous conditions, the original decant oil produced the best quality products. When co-coking with hydrotreated decant oil in the lab scale coker, increased hydrotreatment improved the quality of the liquids produced. Introduction of coal into the co-coking process increased the aromatic content of the liquids. Coal extraction using refinery solvents is being evaluated as a method to produce a material similar to the blend of RCO and LCO. The most recent research indicates that filtering the product hot and engineering a multi-stage unit will increase the extraction yield to ~70% and reduce the LCO/RCO ratio. Methods to improve the quality of pitch produced from the liquids from co-coking have been helpful (soaking and oxidation); the methods of distillation and extraction will also be evaluated. Coke is being evaluated for other possible uses. The effect of coal on calcination of cokes from co-coking was an increase in weight loss and an increase in Lc (determined from XRD). Increasing the amount of coal above 20% caused processing problems and decreased the quality of the carbon product.

Experimental

The respective experimental details for each of the tasks of this project are described within the individual Tasks I – V detailed later in this report.

Results and Discussion

The results of each task of this project are documented and discussed within the appropriate Task I – V detailed later in this report.

Conclusions

Each of the individual tasks of this project has progressed as proposed or to a greater extent than originally proposed. Each task individually contributes to the ultimate goal of refinery integration. This report describes the procurement of equipment into the appropriate

laboratories, the establishment of experimental procedures and the generation of results that indicate the relevance and feasibility of the proposed work.

Progress has been made to produce hydrotreated products, differing from conventional refinery products but also compatible with conventional materials. Specific areas of progress include generation of coal based material that has been fractionated into the desired refinery cuts, acquisition and installation of a research gasoline engine, and modification of diesel engines for use in evaluating diesel produced in the project. In this year's work, distillation was done at the beginning of the process to remove components potentially detrimental to hydrotreatment catalysts. When fractionating, ~63% of LCO and ~75% of RCO was distilled for further hydrotreatment; hydrotreatment is in progress, in which gasoline, jet fuel, and diesel will be produced. Currently, the only fuel tested from the process change is fuel oil, as hydrotreatment continues on the light fractions.

Characterization of the gasoline fuel indicates a dominance of single ring alkylcycloalkanes that have a low octane rating (Research Octane Number is 61.0 for EI-174); however, blends containing these compounds do not have a negative effect upon gasoline when blended in refinery gasoline streams. The method for condensing products from low temperature oxidation has been upgraded using a dry ice/acetone bath. Characterization of the diesel fuel indicates a dominance of 3-ring aromatics that have a low cetane value; however, these compounds do not have a negative effect upon diesel when blended in refinery diesel streams. The two compounds that have been chosen to represent the coal-based diesel are fluorene and phenanthrene. These compounds were blended with a low sulfur diesel fuel from BP (BP-15). This reporting period, ethylhexyl nitrate (EHN) slightly improved the combustion performance

of the blend of BP-15 and 5% phenanthrene, but did not appear quite as effective with fluorene. For both the gasoline and diesel fuels, the performance of engines will continue to be evaluated.

The desulfurization of sulfur containing components of coal and petroleum is being studied so that effective conversion of blended coal and petroleum streams can be efficiently converted to useful refinery products. The development of a finely unsupported dispersed Ni/Mo and Co/Mo catalyst prepared in house shows increased sulfur removal compared to commercial Ni/Mo catalyst. Adsorptive desulfurization of LCO using activated carbon worked well, by removing the heavy sulfur and nitrogen compounds before hydrogenation. For the saturation of two-ring aromatics component of Task 3, zeolite catalyst supports exhibit higher sulfur tolerance. Metal aluminophosphate catalysts have been synthesized for use in making value-added chemicals from two-ring aromatics. Currently, ZSM 5 2 shows the best catalytic activity.

Equipment is now in place to begin fuel oil evaluations to assess the quality of coal based fuel oil. It was reported in the last report that combustion and characterization of the first co-processed fuel oil indicates that the fuel is somewhere in between a No. 4 and a No. 6 fuel oil. Emission testing indicates the fuel burns similarly to these two fuels, but trace metals for the coal-based material are different than petroleum-based fuel oils. The boiler efficiency of the most recent fuel oil, the bottom fraction of RCO (62.3%), is lower than the efficiency than No. 6 fuel oil (70%). Trace metal evalution will be included in the next semi-annual report.

Previous co-coking studies using cleaned coal are highly reproducible in the pilot-scale delayed coker. Evaluation of the coke indicated that while the coke produced is of very good quality, the metals content of the carbon is still high in iron and silica. The most recent work has focused on obtaining a coal with a lower mineral matter content, from the Marfolk mine in West Virginia. Preparation of the coal is in progress.

The best conditions for co-coking of hydrotreated decant oil with coal in tubing reactors are under atmospheric conditions at 18 h. Hydrotreatment reduced levels of heteroatoms and increased coke quality under atmospheric conditions; however, using autogeneous conditions, the original decant oil produced the best quality products. When co-coking with hydrotreated decant oil in the lab scale coker, increased hydrotreatment improved the quality of the liquids produced, by increasing the saturated cyclic compounds. Introduction of coal into the co-coking process increased the aromatic content of the liquids.

Coal extraction using refinery solvents is being evaluated as a method to produce a material similar to the blend of RCO and LCO. Early work indicated that a 10/1 ratio of LCO to coal can extract ~50% of coal, but the final ratio of LCO to RCO is only 9/1. The most recent research indicates that filtering the product hot and engineering a multi-stage unit will increase the extraction yield to ~70% and reduce the LCO/RCO ratio.

Methods to improve the quality of pitch produced from the liquids from co-coking have been helpful (soaking and oxidation); the methods of distillation and extraction will also be evaluated.

Coke is being evaluated for other possible uses. Bireflectance measurement for relative anisotropy of green and calcined cokes could have limited application, but is not as conclusive a measurement as XRD, density, or CTE. The effect of coal on calcination of cokes from co-coking was an increase in weight loss and an increase in Lc (determined from XRD). Increasing the amount of coal above 20% caused processing problems and decreased the quality of the carbon product.

Technical Discussion

Background

Penn State has been involved in a multi-phase fifteen-year program to develop an advanced thermally stable jet fuel for the Air Force **[1-1 -1-4]**. This fuel would resist breaking down at high temperatures (900°F), so it could be used for cooling sensitive parts on high-performance aircraft, as well as providing the propulsion. It is provisionally called JP-900.

At its inception, the JP-900 program presumed that this new fuel would be made entirely or substantially from coal. There are three reasons for this.

Scientific validity. Penn State's researchers have shown clearly that the kinds of chemicals in the fuel that make it stable at 900°F (hydroaromatics and naphthenes) can be derived in abundant amounts from coal. This has been demonstrated in numerous peer-reviewed publications **[1-5 – 1-10].**

Long-term security. Unlike petroleum, coal is a secure, domestic energy resource, for which centuries' worth of reserves remain in the U.S.

Stable procurement. Both petroleum and natural gas are vulnerable to significant price spikes. In contrast, coal companies are willing to write twenty-year delivery contracts at a guaranteed stable price. In turn, this would help stabilize the price of military fuel for decades to come.

To ultimately produce an advanced thermally stable coal-based jet fuel a practical and economically viable process, compatible with current refinery practice, is necessary. The evaluation of this scenario is the subject of this proposal. No refinery is operated for the specific purpose of making jet fuel. Furthermore, refineries are highly integrated, in that many of the individual operations are dependent on, or use streams from, other operations. Therefore, in order to insure that the production of coal-based JP-900 in the jet fuel section of a refinery is acceptable to refinery operators, it is crucial to have data showing the effect of the by-products from coal-based JP-900 production (i.e., the $<180^{o}C$ and the $>270^{o}C$ fractions) on the quantity and quality of the other refinery products: gasoline, diesel, fuel oil, pitch, and coke.

Options for integrating coal, or a coal liquid product that is currently available commercially (a by-product coal tar distillate from the metallurgical coke industry) into existing refineries are illustrated in **Figure 1-1**. With respect to the first two options, coal can either be added to the coker directly or be co-processed with the resid. Of these, addition of the coal to coker has been selected – in consultation with our refinery partner – as the better option to produce sufficient quantities of coal-based fuel for thermal stability and combustion testing. Each of these approaches has a unique set of technical challenges in terms of specifying the proper feedstocks (for both petroleum- and coal-based components), process conditions (temperature and pressure) and processing approaches.

Previous work at Penn State has resulted in significant progress in identifying the remaining critical barriers to realization of coal-based fuels **[1-11 – 1-20].**

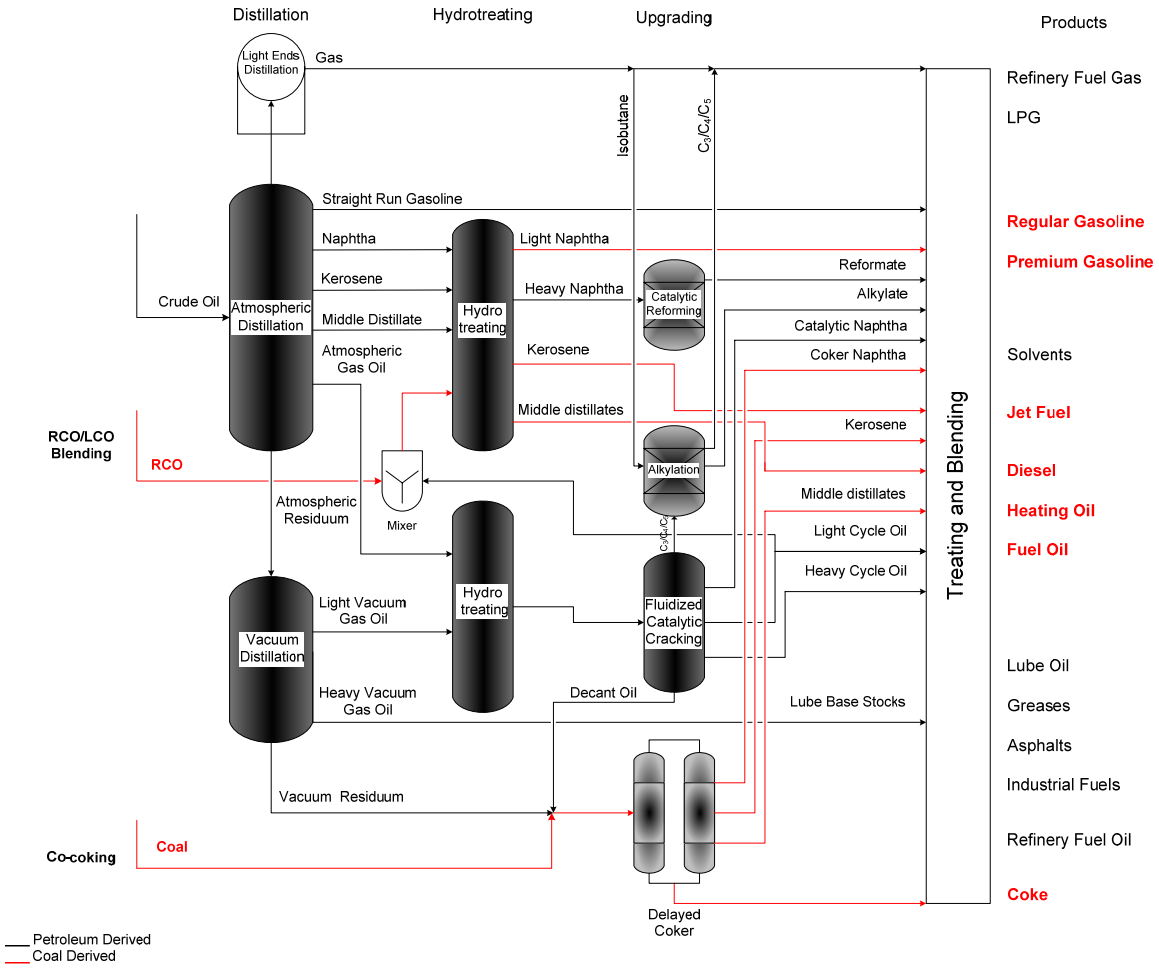

Figure 1-1. Possible Integration of Coal into Existing Refineries.

Objectives

A number of potential JP-900-type jet fuels have been produced by Pennsylvania Applied Research Corporation (PARC) from the hydrotreatment of a coal-derived refined chemical oil (RCO) and its mixture with a petroleum-derived light cycle oil (LCO).

The overall objective of this project is to examine the characteristics and quality of the streams other than the jet fuel, and what effect those materials would have on the other unit operations in the refinery, the quality and value of the other products. Broadly,

these additional by-products are the liquids lighter and heavier than jet fuel itself, i.e., the <180^{o}C and the >270^{o}C fractions produced after hydrotreating the RCO/LCO blend and fractionating to recover the jet fuel and other refinery streams.

Prior to the beginning of this project, virtually all work was focused on the jet fuel. However, as we have noted above, no refinery is run for the specific purpose of making jet fuel. Therefore, to make these processes acceptable for adoption in refineries, it is vital to assess their impact on the other major operations and products in a refinery. The acquisition of that knowledge is the basis of this project.

These studies will impact all of the major product streams in a conventional petroleum-based refinery. Therefore, replacing petroleum feedstock with domestic coal, gasoline, diesel, fuel oil and pitch components will favorably impact reducing dependence on, and security of supply of, foreign petroleum resources.

The objectives of the project are to:

- Investigate and develop an understanding of the most promising refinery integration of all process streams resulting from the production of coal-based jet fuel.
- Demonstrate the quality of each of the process streams in terms of refinery requirements to maintain a stable, profitable refinery operation.
- Demonstrate the performance of key process streams in practical testing used for application of these streams.

This fundamental research was proposed as a four-year program. In this document we report activities and accomplishments for the first half of the second contract year. The approach chosen draws on previous work that has now successfully

produced a coal-based JP-900 fuel at pilot-plant scale for initial investigations in the fuel stabilization and combustion studies **[1-21 – 1-23]**. In that work, it has been shown that hydrotreated blends of light cycle oil and refined chemical oil (a coal-derived liquid) resulted in the most thermally stable product to date.

This program is investigating the fate of each major product from a refinery complex, except jet fuel, resulting from the refinery integration of coal-derived jet fuel production via a combined RCO/LCO strategy by studying the physical and chemical nature of all products that are perturbed by introduction of coal components into the refinery.

The impact of the proposed research is to provide the scientific and fundamental engineering basis to integrate the production of coal-based jet fuel into existing refinery operations in a time frame consistent with availability and economic forecasts related to petroleum-derived as opposed to coal-based feedstocks. The results of these studies lead to the integration of all non-jet-fuel streams into current refinery operations in concert with desired production of coal-based jet fuel engine testing toward the end of the first decade of the new century. For successful utilization of coal-based jet fuels all non-jet-fuel components must fit existing and future product stream specifications.

Coal tar fractions have been successfully demonstrated to be suitable feedstocks for the production of jet fuels for high-speed aircraft **[1-22, 1-23]**. The jet fuel, as prepared and evaluated in our Air Force project, is a 180-270^{o}C product, cut from a mixture of RCO/LCO total liquid product. Of this product the <180^{o}C cut represents ~4% of the total product and the >270^{o}C fraction represents just over 40% of the total

liquid product **[1-24]**. These streams must either be blended as is, chemically converted and then blended, converted to chemicals, or used as feed to the coker.

Scope of Work for Year 3

The technical approach consists of five carefully planned goals whose successful completion will lead to the achievement of the project objectives. These goals include:

- pilot-scale fuel production at PARC,
- evaluation of coal-based gasoline and diesel products in internal combustion engines,
- desulfurization and denitrogenation of coal-based fuels, the saturation of aromatics to improve stability, and the development of chemicals from coal,
- evaluation of coal-based fuel oil, and
- evaluation of pitch and coke materials from coal-based fuel production.

These interrelated goals are designed to evaluate the full utilization of products from coal-based thermally stable jet fuel production and lead toward process integration into existing refineries.

Tasks to be Performed

We are critically analyzing the performance and value of the streams produced from combination of coal-derived components and normal refinery process streams.

The critical analyses include:

- evaluation of gasoline range material in spark-ignited gasoline engines
- evaluation of diesel-range product for use in compression-ignited diesel engines
- evaluation of heavier range materials as heating oils and boiler fuels
- evaluation of products from co-coking strategies as precursors to higher value cokes and carbons.

The following summarizes the technical achievements for the first six months of the third project year.

Task 1. Pilot-Scale Fuel Production at PARC

C. Burgess Clifford (PSU), J. Banes (PARC)

Subtask 1.1 LCO and RCO Procurement

Intertek PARC prepared to do a new run of blended light cycle oil (LCO) and refined chemical oil (RCO); the LCO was procured from United Refining Company in Warren, PA. The RCO was procured from Koppers, Inc., Harmarville, PA. The process was modified at this point in the program to reduce the impact of the coal-derived material on typical refinery catalysts. It was discovered in the previous runs that the 570˚F+ material in the 1:1 LCO/RCO feed was reducing the efficiency of the catalyst. The feed was distilled in order to remove the 570˚F+ fraction. Each of the feed components were distilled separately and then blended together to obtain the final feed for processing. A schematic of the previous runs and the current modifications is shown in **Figure 1-2 (a)-(c).**

The RCO (PR-1660) was distilled in the 150-gallon batch still to remove the 570°F+ material. Three distillations were needed to distill the nine drums of RCO. The first two distillations were done by taking an atmospheric cut at 435°F to take out the light ends and the naphthalene. Once that cut was completed the still was then cooled and vacuum was added to make three additional cuts at 560, 570 and 580°F. The 10°F cuts were taken to best match the desired cut point. The third distillation was done atmospherically.

The first distillation (X-1318) went smoothly during the atmospheric cut to 445°F. Then the still was cooled and 120 mm Hg of vacuum was pulled down. The

vacuum lines to the pump plugged with naphthalene crystals and the still was shut down to clean the system. The still was restarted with a vacuum of 150 mm Hg. It ran and finished the three cuts with no further interruptions.

The second distillation (X-1332) ran very similarly to the first distillation. The atmospheric cut came off at 437°F. Again the still was cooled and the vacuum was pulled down to 150 mm Hg. The vacuum came down to 115 mm Hg before the unit had to be shut down to clean out the vacuum system and change the vacuum oil. Once cleaned, the still was restarted with 100 mm Hg of vacuum and ran at this condition throughout the three cuts with no other problems.

The third and final distillation (X-1333) did not run as the other two had. It started the same with an atmospheric cut first, however it was only taken to 426°F. The still was then shutdown during the weekend and started back up with 150 mm Hg of vacuum. This caused a considerable amount of naphthalene to plug the vacuum system. Due to time constraints the distillation was finished at atmospheric conditions to make a final cut of 560°F. The vacuum lines were later cleaned out and the naphthalene added back into the first cut. This distillation yielded a total loss of only 2.2 wt%. The still data sheets and the simulated distillations, ASTM method D-2887, are in Appendix A. The yield of RCO that will be used for further processing was ~75%.

After the distillations were finished a simulated distillation (SIMDIS GC) was taken on each cut from each distillation. With this information and the yield data, a calculated SIMDIS GC was done to determine the amount of each cut to blend to achieve the proper end point. The calculation as well as the still data sheets and the SIMDIS GC, ASTM method D-2887, are in Appendix A.

The LCO distillation was done at the United Refining Plant in Warren, PA. They cut nine drums of LCO which had a 95 wt% point of 684°F to 594°F. Both the full range and the distilled LCO simulated distillations, ASTM method D-2887, are in Appendix B. The yield of LCO that will be used for further processing is ~63%.

The final blend of RCO and LCO was done at a 1:1 ratio by weight. The LCO was added to the blend tank first at a weight of 2,676 lbs. This was done to keep the 570°F- RCO liquid in the blend to ensure the complete mixture of the two components. If the components were not blended in this way, the naphthalene in the RCO may have set up on the walls of the tank and would not mix completely. The RCO was added next to the blend tank at a weight of 2,676 lbs also. The blend was mixed in the tank for three hours and then drummed off into 55-gallon drums for processing in P67.

In previous work, a simulated distillation (D2887) of LCO and RCO samples was done, and is shown in **Table 1-1**. **[1-25]** Intertek PARC sent LCO and RCO samples of the current run for analysis, and will be compared to the previous analyses. The RCO bottoms was also collected in 55-gal drums (2 drums) and sent to Penn State for testing as a fuel oil for combustion. Discussion on this aspect will be included in Task 4.

(a)

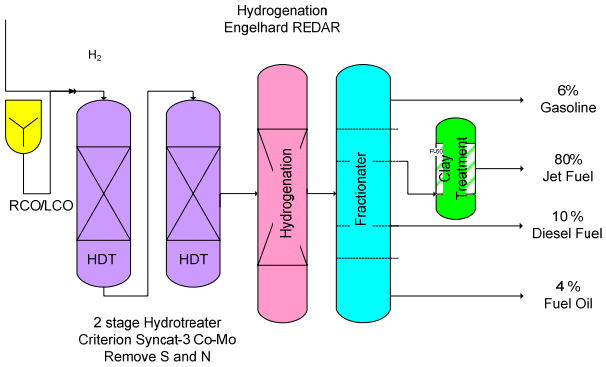

(b)

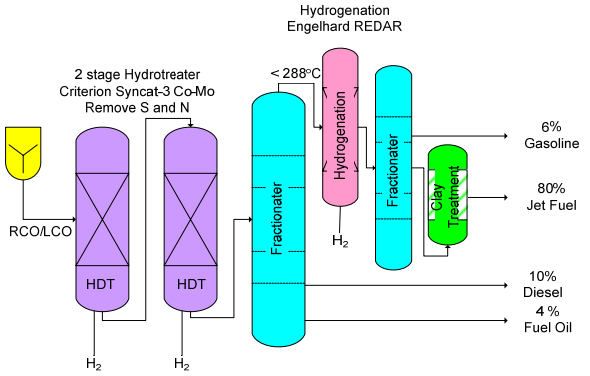

(c)

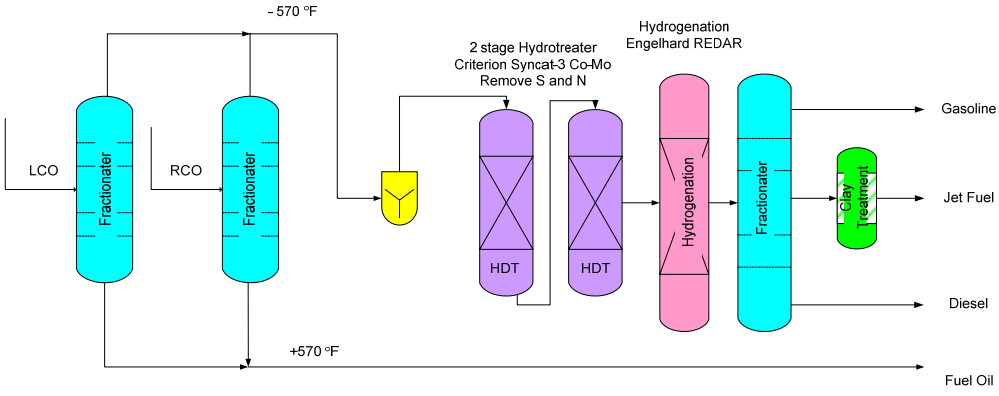

Figure 1-2: (a) Schematic of Fuel Hydrotreating and Hydrogenation, first runs, **(b)** Schematic of Fuel Hydrotreating and Hydrogenation, second runs, **(c)** Modification of Schematic of Fuel Hydrotreating and Hydrogenation currently being run at Intertek PARC, Harmaville, PA.

Subtask 1.2 Catalyst Preparation

Catalyst, necessary for the deep hydrotreating of total liquid product (TLP), was obtained in this task. In previous work **[1-1, 1-24]**, PARC has identified a Criterion Syncat-3 cobalt-molybdenum or Syncat 37, nickel-molybdenum catalysts as effective in converting the coal-based blend to a deeply hydrotreated total liquid product. This product has been found to be rich in hydroaromatic components and as a result the jet fuel is thermally very stable. These catalysts must be activated by presulfiding after drying in a flow of hydrogen. The SYNCAT catalyst is received by PARC pre-impregnated with a sulfur compound, however, PARC employs a treatment with kerosene containing 0.25 wt% dimethyldisulfide to ensure proper sulfiding prior to use.

Subtask 1.3 Hydrotreatment of Blended Product

Production of deeply hydrotreated total liquid product (TLP) to provide material for other tasks in this project by large-scale production of TLP is necessary. The full description of the previous runs is provided in previous semi-annual reports. **[1-25]** The production of drum quantities of liquid products is being done currently, with the expectation to have jet fuel, diesel, and gasoline by mid-January. The hydrotreatment will be done similarly to previous runs.

Subtask 1.4: Fractionation into Refinery Product Slate

Additional work has been done on this part of the project with regards to the solids production. Analysis of the cokes generated from co-coking of hydrotreated decant oils with coal is described in Task 5 of the report.

Table 1-1 United LCO and Koppers RCO
Simulated Distilllations – Previous Run

SAMPLE	LCO PR 1244	RCO PR 1238	1:1 RCO:LCO PR 1251
Instrument	5880	5880	5880
IBP	350	335	341
5%	451	390	396
10%	485	429	431
20%	516	433	436
30%	533	435	440
40%	553	437	486
50%	570	438	534
60%	593	451	551
70%	618	500	577
80%	651	545	625
90%	684	598	667
95%	705	650	704
FBP	771	894	813
% at 356ºF (180ºC)	0.15	1.91	1.36
% at 518ºF (270ºC)	31.2	74.0	45.5
% at 572ºF (300ºC)	50.9	85.1	68.1

Task 2. Evaluation of Coal-based Gasoline and Diesel Products in IC Engines and Related Studies (A. Boehman, Y. Yang, S. Kirby, Y. Zhang)

By introducing coal-derived streams into the refinery, several perturbations to the quality and quantity of refinery streams may result and directly impact vehicular fuels production. The coal contribution to the refinery streams will affect the quality, composition and performance of the resulting vehicular fuels. The fraction of the hydrotreated streams that boils below 180°C will be directed to the gasoline pool. Having components from coal is expected to boost octane number and aromatic content, and therefore, boost value. The >270°C cut of the hydrotreated stream would be low in sulfur due to the severe hydrotreatment. The effect on flash point will need to be determined if this stream is sent to the fuel oil pool and/or diesel pool. If this stream is combined with diesel fuel, it will add cycloparaffins, which will increase energy density and boost value. However, the impact on cetane number and sooting tendency is unclear. The following task structure permits assessment of the impact of refinery integration of JP-900 production on gasoline and diesel fuel.

Subtask 2.1. Impact on Gasoline Quality and Performance

Under this subtask, our efforts have consisted of continuing preparation and refinement of facilities for the SI engine testing activity and ignition studies of relevant compounds to understand the impact of the coal-derived compounds on knocking and flame propagation.

Subtask 2.1.1 Preparation of Laboratory and Instrumentation

Combustion and emission properties of the coal-based gasoline in SI engine applications has been studied in a single-cylinder Waukesha CFR octane rating engine and will be studied in the single-cylinder Ricardo Hydra research engine. Under this subtask, we acquired and installed the Ricardo Hydra single-cylinder research engine for use under Task 2.1.2 and developed instrumentation for combustion analysis. And we modified the fuel delivery system on a CFR Octane Rating engine for ignition quality and reaction pathway tests.

GC-MS results have shown that the major components in the coal-based gasoline samples are cycloalkanes, whose octane ratings are lower than that of the commercial-grade gasoline and therefore may cause knocking in SI engine combustion. Flame propagation across the combustion chamber and the auto-oxidation chemistry of the unburned mixture (end gas) have been identified as the two determining factors in engine knock **[2-1]**. The auto-oxidation chemistry of the end gas is being performed at a Waukesha CFR octane rating with modified intake system and running at the motoring mode. To date, our examination of the decomposition chemistry of methyl cyclohexane (a model for coal-derived gasoline) has resulted in an ACS preprint **[2-2]**.

The two devices designed for studying the flame propagation in SI engine have been obtained. The signal conditioning and data acquisition system for these probes has been built and is ready for testing.

A head gasket equipped with 6 ion probes (**Figure 2-1**) has been designed and fabricated for the Hydra engine which enables detecting the flame arrival along the plane of head gasket. The related signal conditioning board has been build and data acquisition

boards have been purchased. Another in-cylinder flame detector, optical sensor equipped spark plug, has also been obtained (**Figures 2-2 and 2-3)** which allows the flame detection on the top of the combustion chamber.

The two devices designed for studying the flame propagation in SI engine have been obtained. Description for the ion-probe head gasket was included in the previous annual report. The recently received fiber-optic spark plugs (**Figures 2-2 and 2-3**) utilize eight optical probes installed on the plug rim (**Figures 2-2**) to "see" the flame propagation during engine combustion. Two such spark plugs were obtained and will be installed in the Ricardo Hydra engine and CFR octane rating engine. The signal conditioning and data acquisition system are being built.

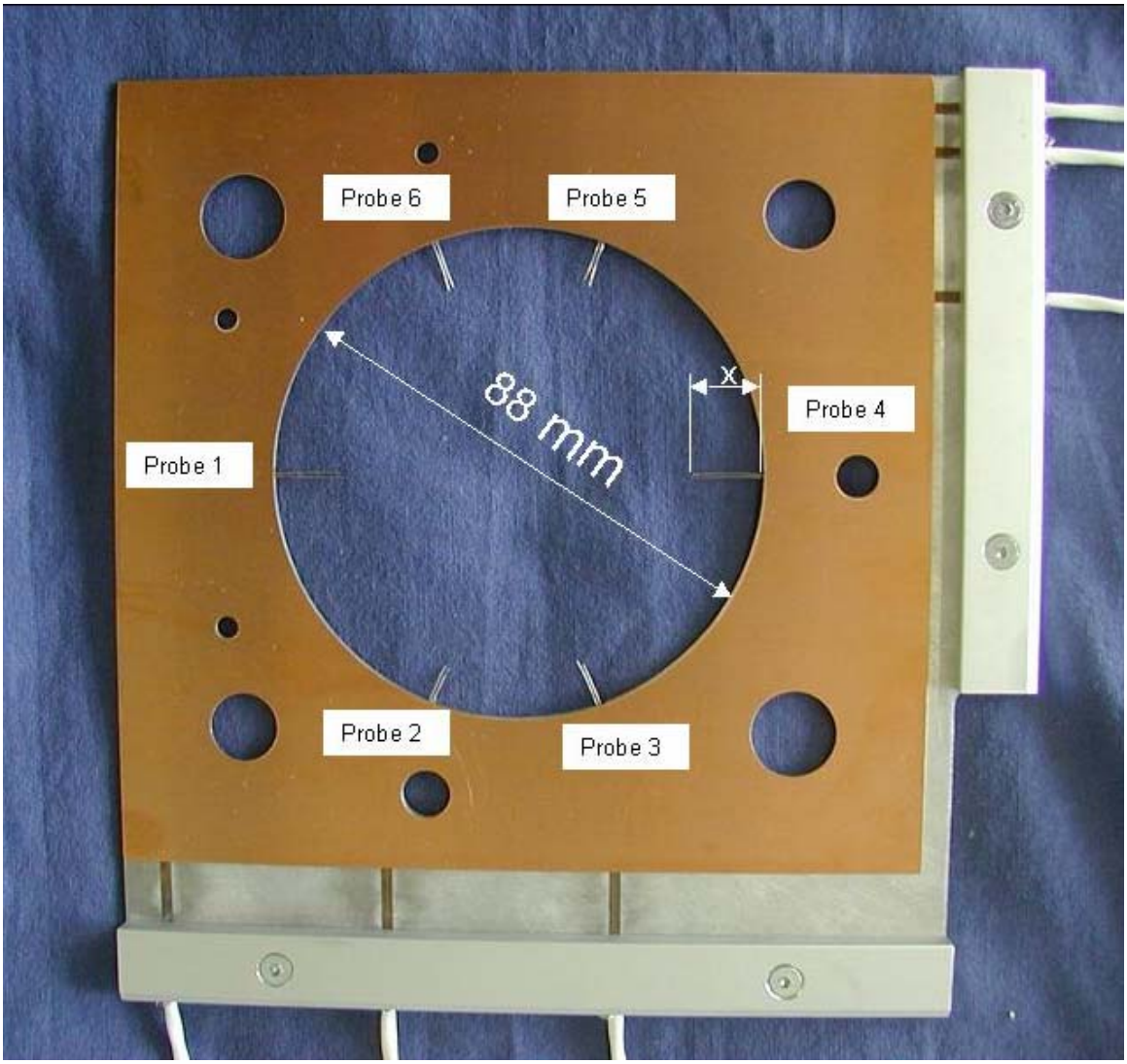

Figure 2-1 Ion probe equipped head gasket for the Hydra engine

Figure 2-2 Optic-fiber Spark Plug for the CFR Octane Rating Engine

Figure 2-3 Close-up of the Electrodes and Eight Optical Openings

Low temperature heat release during the oxidation of model compound methylcyclohexane was observed with modified operation conditions. Two-stage ignition of methylcyclohexane was also detected. This is in contrast to previous tests where no heat release was detected prior to the sudden autoignition (knocking). Comparison of the operation condition is listed in **Table 2-1**. The decreased engine speed gives more time for the low temperature oxidation to occur. Lowered intake temperature shifts the reaction from the intermediate region that has the negative temperature dependence (heat release is inhibited) to the low temperature region where heat release can be easily detected.

Table 2-1 CFR Engine Operation Conditions for Previous and Current Autoignition Study

	Previous	Current
Engine speed (RPM)	900	600
Intake Temperature (K)	533	393

Finally, the method has been upgraded for condensing products from the low temperature oxidation. A dry-ice/acetone bath replaced the previous ice/water bath. A gas bubbler containing a known volume of dichloromethane is immersed in the bath. Gas flow rate into the bubbler is regulated and measured, which enables the quantification of the condensed species. The obtained dichloromethane solution is then directly analyzed by GC-MS without water extraction. Non-condensed gases after the cold trap are collected in Tedlar bags and analyzed by GC-FID/TCD. With these improvements, a much more complete picture of methylcyclohexane low temperature oxidation was obtained.

Subtask 2.1.2 Impact on Chemical and Physical Properties

Under this subtask, we have performed detailed chemical analyses and physical analyses of fuel samples. From several runs at PARC, fuel fractions were provided representing the gasoline and diesel fuel cuts. To date the primary fuel characterization for the gasoline cut has been through ignition studies which are presented under Subtask 2.1.3 below. Octane rating measurements of the coal-derived gasoline, blends of the coal-derived gasoline in a reference gasoline ("UTG 96," 96 RON fuel provided by ConocoPhillips in support of this project) and blends of model compounds in the reference gasoline have been completed. The research octane number was measured on the CFR octane rating engine according to the ASTM D2699 standard.

Octane number measurements of coal-based gasoline (CBG) and its blends with other components are measured on the Waukesha CFR octane rating engine. The engine was calibrated according to the ASTM D2699 standard, as shown in **Table 2-2**. In most cases calibration is within the rating tolerance, and the largest deviation (RON=85 vs. 84.1) is less than 1 RON unit, showing the engine is in good shape.

Table 2-2 Calibration results of CFR octane rating engine by using toluene standardization fuels

Octane No.	Measurement	Rating tolerance
65.2	65.4	±0.4
85.0	84.1	±0.3
89.3	89.3	±0.3
93.4	93.0	±0.3
96.9	96.8	±0.2
99.6	99.3	±0.3

Research octane number (RON) of the coal-based gasoline, EI-174, the latest from JP-900 production, was measured as 61.0. EI-174 was blended with a commercial gasoline provided by Conoco-Phillips which has the RON of 96. Research octane number at various blending levels were tested and plotted in **Figure 2-4**. The measured RON is seen very close to that is predicted by the linear relationship based on volumetric percentage v_i, $RON_{mix} = \sum RON_i \times v_i$.

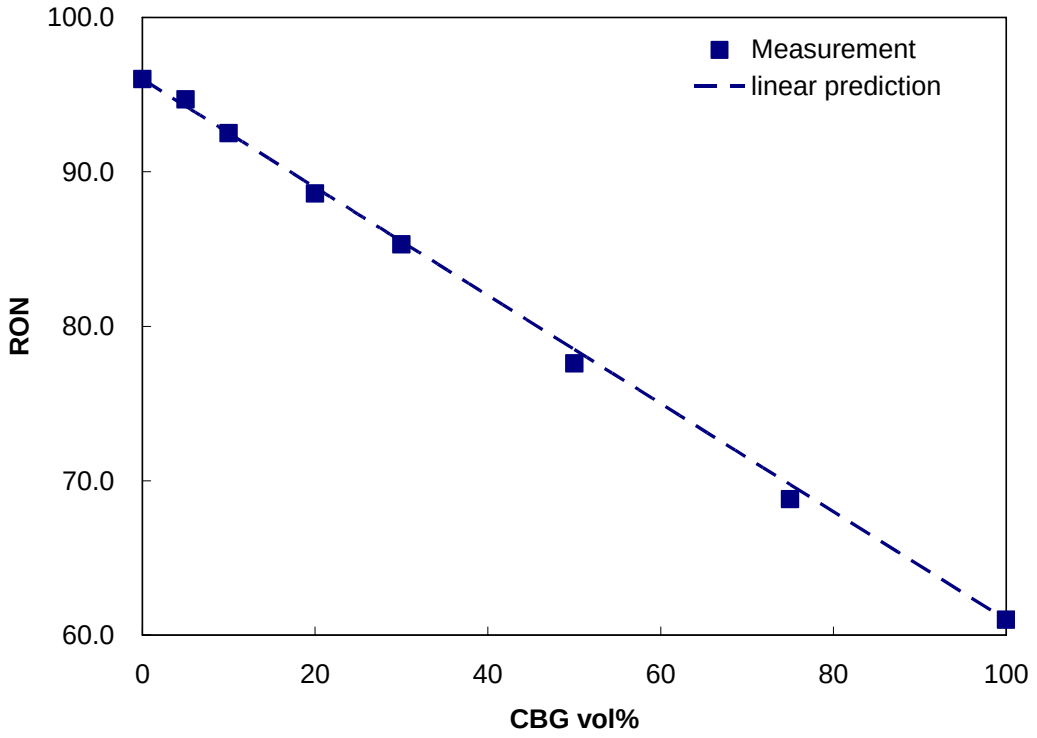

Figure 2-4. RON vs. CBG blending level in RON 96 gasoline. Dots: experiment measurements. Line: $RON_{mix} = \sum RON_i \times v_i$.

Subtask 2.1.3 Impact on SI Engine Emissions and Performance

The low temperature oxidation of methylcyclohexane has been successfully achieved in the CFR engine with the recent modifications on engine operation conditions.

Heat release from the low temperature oxidation is shown in **Figure 2-4**. This low temperature heat release does not lead to main combustion because reaction is quenched during the expansion stroke. Note the maximum temperature during this cycle is only 886 K, well below the normal combustion temperature (>1800K). The start of cool flame ignition, which is defined as the point where heat release rate turns from negative to positive, occurs at 1.8 crank angles after TDC with the temperature of 831 K and pressure of 1314 kPa. The ignition temperature of methylcyclohexane is comparable with the 1^{st}-stage ignition of n-heptane (~780 K, in the last report) under similar conditions. However, the cool flame combustion of methylcyclohexane occurs at a much later timing than that of n-heptane which is well before TDC. This is consistent with the longer ignition delay of methylcyclohexane observed in rapid compression machine studies **[2-3]**. The later-than-TDC ignition timing also implies that two-stage ignition, which is commonly observed for n-heptane and other straight-chain alkanes, occurs only under a narrow range of conditions for methylcyclohexane. Later tests at high compression ratios confirmed this speculation.

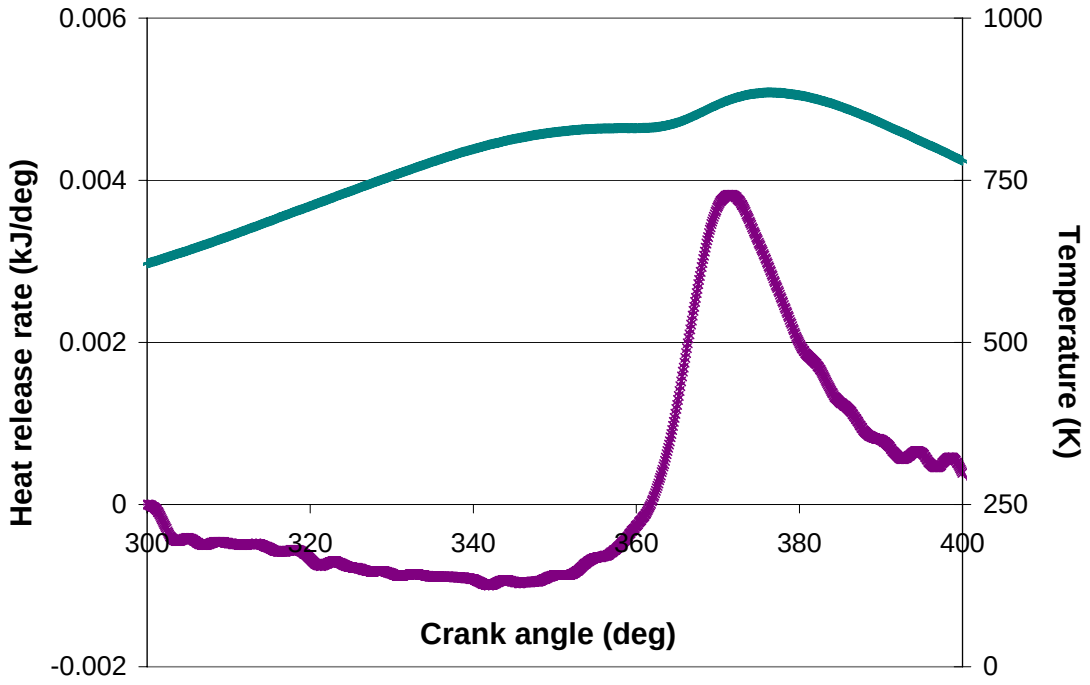

Figure 2-5 **Heat release and cylinder temperature of methylcyclohexane during cool flame combustion. Condition: intake 120°C, 600 rpm, compression ratio 7.47, equivalence ratio 0.13 (nitrogen 50 SCFH).**

To further investigate methylcyclohexane oxidation in an SI engine, especially the formation of aromatic compounds, a series of tests were conducted. While the other conditions are kept constant, the engine compression ratio was increased so that the transition from low temperature heat release to the major combustion can be studied.

The oxidation products were collected and analyzed by the methods described above. GC results of non-condensable species after the cold trap have been studied. **Figure 2-6** shows the concentration variation of O_2, CO, and CO_2 with compression ratio detected by TCD. **Figure 2-7** shows the concentration variations of methane, ethane & ethylene, propylene, and unreacted methylcyclohexane with compression ratio by FID.

Note that except methylcyclohexane, all species in **Figures 2-6 and 2-7** are only present in the gas phase. Most methylcyclohexane is absorbed by the cold dichloromethane liquid and appears on GC-MS spectra. It is seen that as compression ratio increases, fuel consumption increases as indicated by the steady decrease of O_2 and fuel concentrations. Significant amount of CO, methane, ethane and ethylene are formed as compression ratio increases. They are relatively stable comparing to other intermediates and can be consumed if the combustion is complete. The build-up of CO concentration retards CO_2 formation, therefore the CO_2 concentration stays at low concentration (<0.5%) during the course of the test. A considerable amount of propylene is also formed whose concentration increases at early stage (lower compression ratio) and decreases at late stage. This means that propylene is a relatively reactive intermediate and is converted to other species at higher temperature.

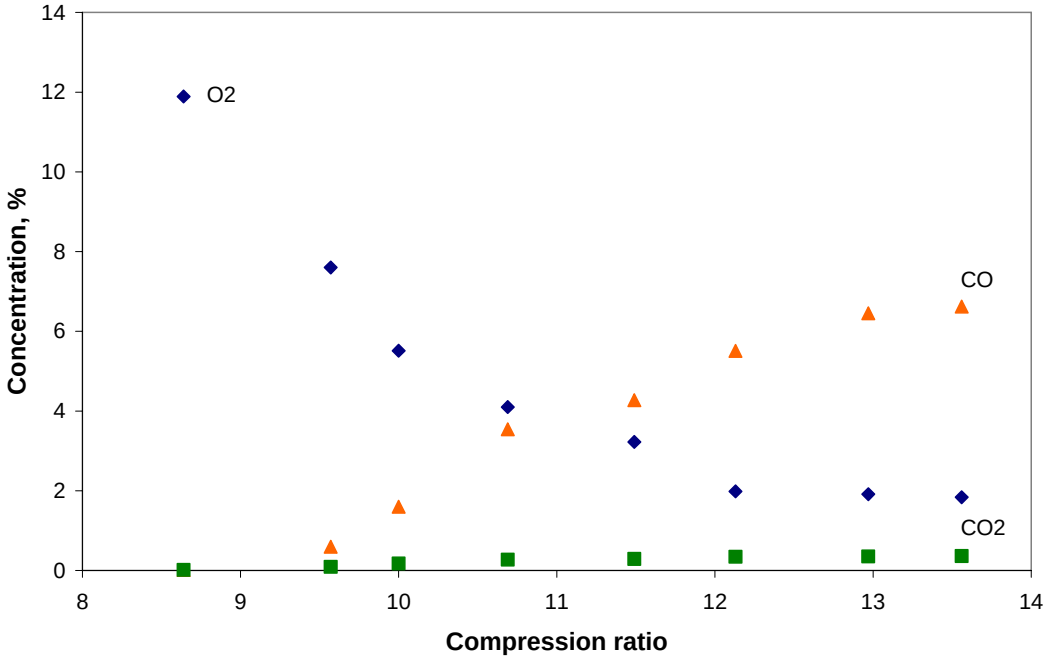

Figure 2-6 Concentrations of O_2, CO, and CO_2 vs. compression ratio by TCD. Condition: intake 120°C, 600 rpm, equivalence ratio 1.2 (nitrogen 125 SCFH).

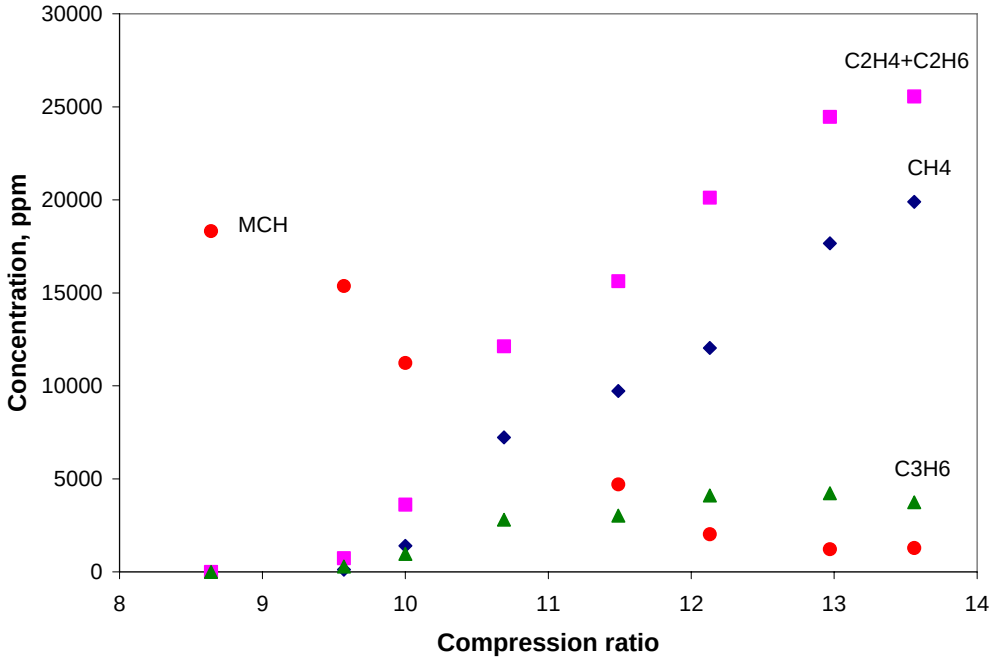

Figure 2-7 Concentration of CH_4, C_2H_4+C_2H_6, C_3H_6, and methylcyclohexane vs. compression ratio by FID. Conditions are same as in Figure 2-6.

GC-MS results of the condensable species are still being analyzed. A preliminary result suggests that the intermediate species are formed via two pathways: dehydrogenation and partial oxidation. Methylcyclohexenes are the major products at low compression ratio while benzene and toluene are the major products at high compression ratio, indicating that the dehydrogenation is the dominant reaction path. Benzene formation is directly from such dehydrogenation reactions. On the other hand, partial oxidation products, such as cycloketones and cycloepoxides, are observed at low compression ratio but disappeared at high compression ratio, which suggests these early formed intermediates are consumed at high temperature.

Note that the previous results only reported the oxygen-containing species in the condensed phase because the gas-collecting method was not able to effectively condense the unreacted fuel and related dehydrogenation products. The new method will enable us to study the complete product compositions (in both liquid and gas) of many hydrocarbons from the current system.

Subtask 2.2 Impact on Diesel Fuel Quality and Performance

Under this subtask, our focus shifted from facility development activities to fuel and combustion characterization. The facilities work has been refinement and enhancement of two existing engine test stands, one housing a Navistar V-8 7.3L turbodiesel engine and the other housing a DDC 4-cylinder 2.5L turbodiesel engine.

2.2.1 Acquisition, Installation and Instrumentation of Ignition Test Equipment

This work has been completed, with some updated information on configuration and procedures given in Section 2.1.1. The equipment was applied to ignition studies of diesel and other fuels and has resulted in the submission of a manuscript to *Combustion & Flame* **[2-4]**.

2.2.2. Development of Analytical Methods and Test Procedures

The modification of the CFR Octane Rating engine to serve as a rapid compression machine for ignition studies represents a unique adaptation of a standard instrument and will provide a means of comparing experimental data with kinetic models of the ignition process.

In addition, through other DOE and industrial sponsored research, we have developed extensive capabilities and methodologies for characterization of diesel soot, with the intention of determining how fuel and how combustion conditions can alter the morphology of soot aggregates, primary particle nanostructure and the surface chemistry of diesel soot. Some of these observations have been reported in journals and conferences recently **[2-5 – 2-7]**.

2.2.3. Evaluation of Capabilities and Needs for Supplemental Measurements and Analyses

The analytical methods developed for the characterization of the fuel cuts from the PARC runs can now serve as the basis for subsequent fuel and SOF chemical analyses. We have developed procedures for use of an existing FTIR spectrometer to speciate the products of our ignition tests, which has already highlighted significant differences in the intermediate species present as we pass through first and second stage ignition for different fuels. We have also developed a plan for upgrading an existing gas chromatograph for hydrocarbon speciation from engine exhausts. We intend to perform the upgrade of the GC (from packed to capillary columns) and use a method that is the same as in the Shimadzu GC-MS. This will allow the GC results to be interpreted through the species identification capabilities of the GC-MS.

Given the impact observed in Year 2 of the coal derived diesel fuel (CDD) on particulate emissions, in Year 3 we acquired a scanning mobility particle sizer (SMPS) to enable observation of the impact of fuel composition on the particle size distribution of

diesel soot and particulates. The instrument became operational near the end of Year 3 and the first data from this instrument will be reported in the Year 4 semi-annual report.

2.2.4. Impact on Chemical and Physical Properties

We have completed tests on the impact of coal-derived compounds on the DCN of base diesel fuels. This work resulted in the preparation of an ACS preprint **[2-8]**.

Two major components of coal-derived diesel fuel (cut #3) were identified by GC-MS. Fluorene and phenanthrene were found to be present in sample # EI 175 in concentrations of 3 wt% and 1.5 wt%, respectively. These compounds were used as representatives for similar compounds, such as hydrophenanthrenes, that form a large portion of the coal-derived diesel.

Physical property analyses were performed on solutions of various concentrations of fluorene, or phenanthrene, in an ultra low-sulphur diesel fuel (BP15). BP15 is petroleum-derived and primarily comprises of long chain aliphatic compounds (C8 to C13). Both fluorene and phenanthrene are already present in BP15 at concentrations of <1 wt%. Solubility issues arose at concentrations greater than 5 wt% for fluorene, in all likelihood due to the aliphatic nature of BP15.

Evaluation of combustion characteristics of doped BP15 will be performed. To remove the influence of ignition delay ethyl hexyl nitrate (EHN) was added to 5% phenanthrene doped BP15 at 250, 500, and 750 ppm. The ignition delay of these mixtures was determined using the IQT and results are presented in **Table 2-3**.

Table 2-3 Fuel Properties of Ultra Low Sulfur Diesel Fuel Doped with Three-Ringed Aromatics

Fuel	**BP15**	**BP15/5%Phenathrene/EHN**			
Additive (ppm)	-	0	250	500	750
DCN	47.2	46.7	50.8	50.2	49.9

The derived cetane number (DCN) for each of the fuel blends was measured in accordance with ASTM D6890-03a. A correlation has been developed to convert the measured ignition delay into a DCN, which is correlated with the CN measured by ASTM D613 (CFR Cetane Rating engine). The ignition delay (defined as the elapsed time from injection to where the chamber pressure reaches $P_{initial}$ + 50 psi) under specified conditions is measured using the Ignition Quality Tester (IQT) (**Figure 2-8**). The system is fully automated and an experiment consists of 15 pre-injections (to equilibrate system temperatures) followed by 32 injections. The reported DCNs are the averages of these 32 injections of pre-filtered fuels. A sample of data from a single injection is presented as a screen shot in **Figure 2-9**.

Very little affect on DCN was observed with the addition of varying concentrations of EHN. This result is confusing and work is continuing to determine what might be neutralizing the affect of the EHN. Similar trends, or lack thereof, in fuel properties related to phenanthrene-doped BP15 have been presented in previous reports. Methods used in sample preparation are being examined.

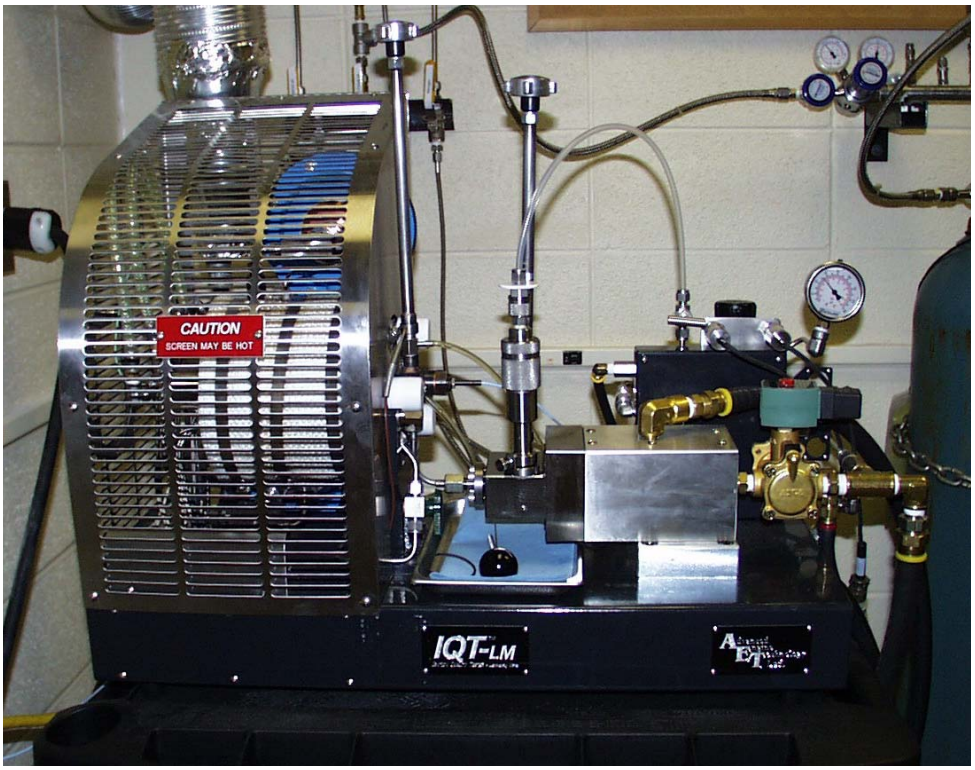

Figure 2-8 Photograph of the Ingnition Quality Tester (IQT) at the Penn State Energy Institute

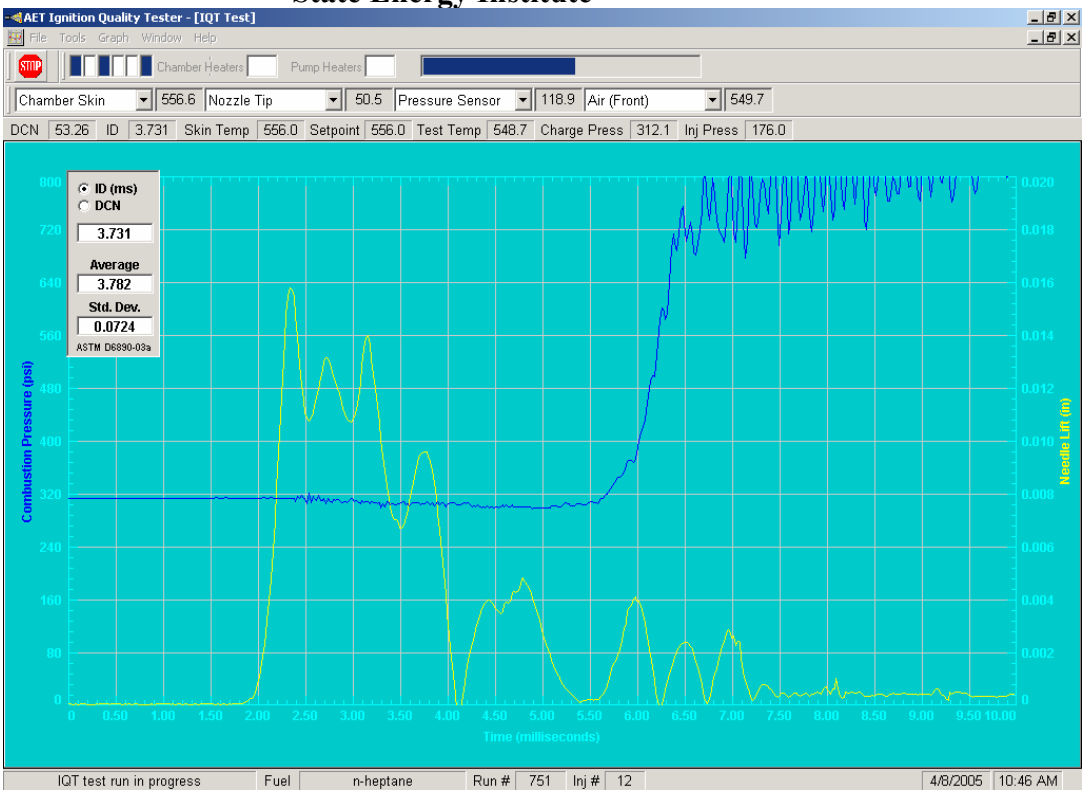

Figure 2-9 Sample data readout from the IQT. Needle lift is displayed in yellow and combustion pressure in blue.

A recent effort has focused on the impact of coal-derived compounds on the smoke point (and thereby the sooting tendency) of diesel fuel. To that end, tests were performed using Ultra Low Sulfur Diesel (BP15) and a mixture of 20 vol% biodiesel in BP15 (B20) as basestocks into which fluorene was added. The biodiesel used was SoyGold.

Smoke Point (SP) - Smoke Point data were recorded using a Smoke Point Lamp. Each sample preparation and measurement followed the ASTM D-1322 Standard Test Method for Smoke Point of Kerosene and Aviation Turbine fuel. A fuel sample was burned in the smoke point lamp, and the maximum flame height (millimeters) obtainable without smoking was measured.

Ramsbottom Carbon Residues (RCR %) - Each sample preparation and measurement followed the ASTM D-524, Standard Test Method for Ramsbottom Carbon Residue of Petroleum Products. The carbon residue of a fuel is the tendency to form carbon deposits under high temperature conditions. A 4 g sample of a filtered bulk was placed in a tared glass-coking bulb and heated at 550°C for 20 minutes. The heating expels all volatile material, leaving only the carbon residue. After cooling, the bulb was re-weighed to determine the amount of residue, which is reported as a percent RCR. The carbon residue is a measurement of the tendency of a hydrocarbon to form coke, expressed in weight percent. Equation (1) was used to obtain the weight percent carbon residues (RCR %).

$$RCR\% \approx \frac{(residuebulb - emptybulb)}{(samplebulb - emptybulb)} * 100 \qquad (1)$$

In the smoke point analysis the effects of adding Fluorene to BP15 and B20 were observed, **Figure 2-10**. Generally flame height decreased with the addition of Fluorene, therefore sooting tendency increased **[2-9]**. An unexpected result was recorded for the affect of 1 wt % Fluorene addition to BP15. Previous work has established that increasing aromatic composition in the fuel will produce a key shift to soot precursors **[2-10]**. However, a slight suppression of sooting tendency is suggested by the small increase in the SP.

SP of B20 samples were higher than their respective BP15 counterparts. This result may be due to the presence of oxygen in the fuel molecule, or simple dilution of the affect from aromatics already present in BP15 (6.9 wt% PAH).

RCR % reached a minimum at 1 wt % Fluorene in both BP15 and B20. This decrease in the coke formation may be due to Hydrogen Abstraction. Hydrogen Abstraction occurs when the concentration of radicals is below critical limits i.e. low enough to increase the frequency for the radicals to react with other non-radical molecules instead of recombination (condensation) reactions with itself. **Figure 2-11**, shows how Fluorene may perform this function.

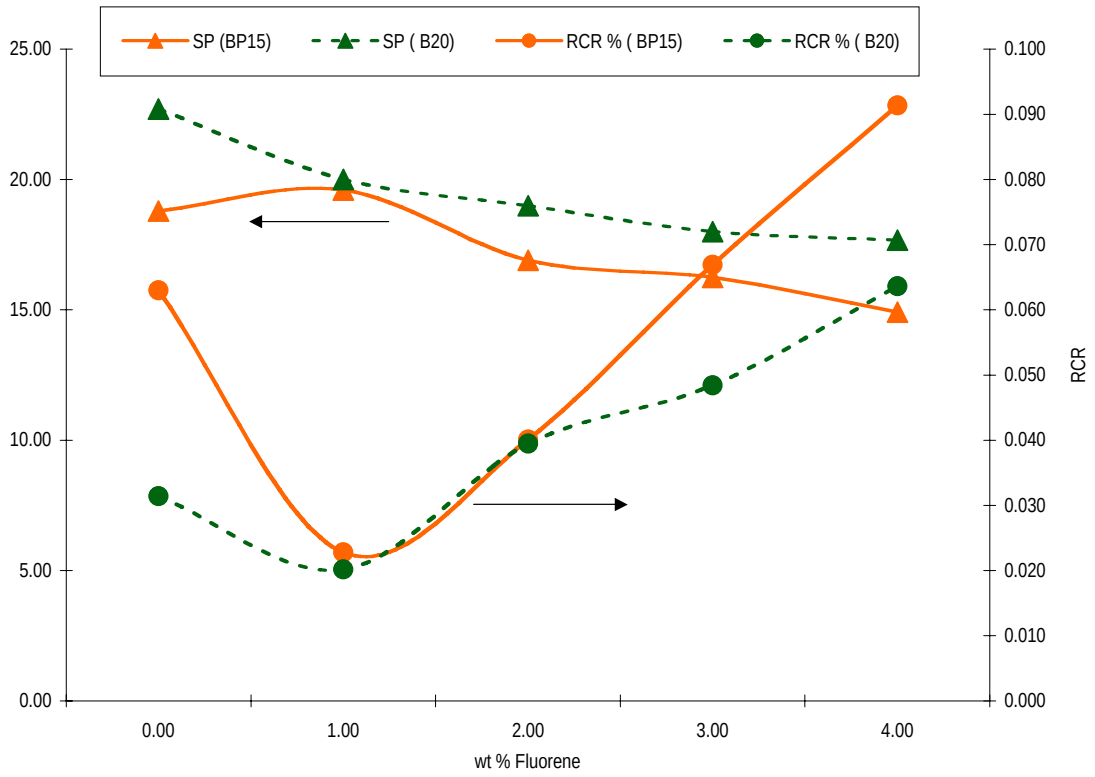

Figure 2-10 Affect of Fluorene addition on the Smoke Point (SP) and Ramsbottom Carbon Residue (RCR) of both Ultra Low Sulfur Diesel (BP15) and a biodiesel blend (B20)

Previous research revealed that Fluorene provides five hydrogens, the first to be released being those in sp^3 configurations (Carbon-9) **[2-11]**. sp^3 Carbons require lower amounts of energy to transform a chemical bond to radicals, whilst the associated aromatic rings can delocalize, and thus stabilize, the radical. Once Fluorene concentrations increase, so does the concentration of Fluorene radicals and the benefits of hydrogen radical production are lost due to Fluorene radical recombination.

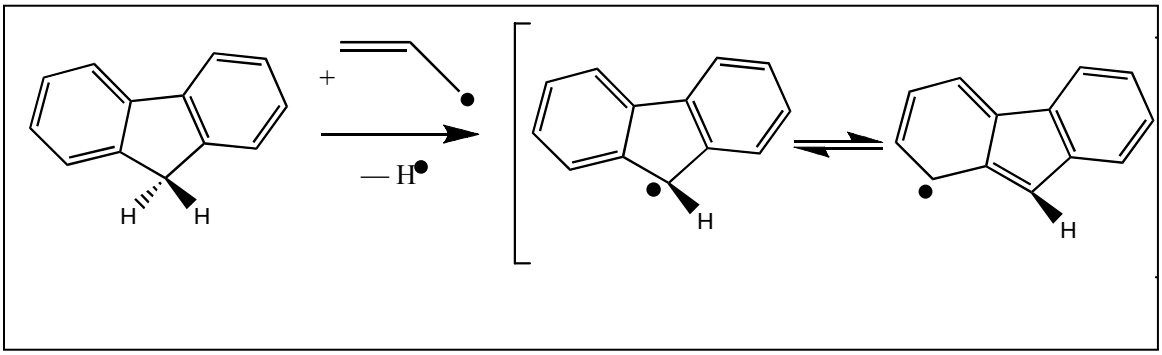

Figure 2-11 Hydrogen abstraction mechanism for Fluorene

Similar RCR%s were recorded for 1 and 2 wt% Fluorene with BP15 and B20, respectively. Initially, the addition of 20 vol% biodiesel to BP15 (B20) improved the RCR% (0.063 to 0.031). Once Fluorene was added this degree of improvement was not attained again. Improvement in coking tendency due to Fluorene addition was not as pronounced for B20 as for BP15, hinting at the presence of two competing processes.

In summary, Fluorene addition to diesel and B20 fuels increases sooting tendency. Some suppression of sooting tendency was apparent when 1 wt% Fluorene was added to diesel fuel. Coking tendency of both diesel and B20 was suppressed by the addition of low concentrations of Fluorene. At higher concentrations Fluorene increased the coking tendency of both diesel and B20 (>2.9 and >1.6 wt% Fluorene, respectively). A larger affect on the coking tendency of diesel, compared to B20, suggests competing mechanisms for coking suppression between biodiesel and Fluorene.

2.2.5 Impact on CI Engine Emissions and Performance

The engine testing was performed on a DDC/VM 2.5L common-rail diesel engine. Engine specifications are listed in **Table 2-4**. Coal derived diesel fuel (5% volume) blended with BP15 (CDD5) was selected for the engine testing with BP15 performed as the baseline fuel. AVL mode 2 and mode 3 represent the low load and

medium load conditions with low engine speeds. Theses two modes were chosen as the engine testing conditions at this stage. Detailed engine testing conditions can be seen in **Table 2-5**.

Table 2-4 Engine specification

Engine	DDC 2.5L TD DI-4V automotive diesel engine
Displacement	2.5L
Bore	92mm
Stroke	94mm
Compression Ratio	17.5
Connecting rod length	159mm
Rated Power	103KW@4000 RPM
Peak Torque	340Nm@1800 RPM
Injection system	Electronically controlled common-rail(Bosch)
Valve train	4 valves/cylinder

Table 2-5 Engine testing conditions

Mode	Speed (rpm)	Load (ft.lb)	BMEP (MPa)	Pilot SOI (Deg BTDC)	Main SOI (Deg BTDC)
AVL2	1330	46.5	0.32	22	-4
AVL3	1630	153.8	1.05	34	3

As shown in **Figure 2-12** and **Figure 2-13**, there were no observably significant differences found in the bulk overall combustion characteristics between coal derived diesel blend and BP15 under both AVL mode2 and mode 4 conditions. As the engine condition was changed from AVL mode2 to mode 3, both pilot injection and main injection were advanced. As a result, reduction of premixed heat release due to main injection was observed. As to the heat release due to pilot injection, when the pilot injection timing was advanced from AVL mode 2 to mode 3, a small amount of low temperature heat release prior to the main premixed heat release was found. Also, there was a significantly increase in the diffusion combustion fraction as the engine load was increased with the change of injection timings.

From the needle lift characteristics shown in **Figures 2-14** and **2-15**, there was no injection timing difference observed between coal derived diesel blend and BP15 under both of the engine conditions despite that there was a bulk modulus difference between these two fuels. In conventional pump-line-nozzle diesel engines, there was a fuel pressure propagation speed difference due to the different fuel bulk modulus. However, in the common-rail diesel engines, bulk modulus effect can be eliminated due to different fuel injection system features.

Also, as shown from **Figures 2-16** to **2-19**, almost the same pressure traces and bulk cylinder temperature profiles were observed between coal derived diesel blend and baseline BP15. Although, 5% coal derived diesel fuel blend and baseline BP15 shared almost same injection and overall combustion characteristics, there were emissions results differences found between these two fuels. Error bars in the testing results represent the 95% confidence interval for random error and 1% full-scale system calibration error.

NO_x emissions were found higher for the coal derived diesel blend consistently through the increased engine load conditions (**Figures 2-20**). A 0.9% NO_x increase at mode 2 conditions and 3.8% NO_x increase at mode 3 for 5% coal derived diesel blend were observed. Since there was no injection timing and overall combustion characteristics difference, adiabatic flame temperature difference between these two fuels were expected to be the reason causing the increased NO_x emissions for coal derived diesel blend. It is known that the addition of aromatic content will increase the adiabatic flame temperature and NO_x emission is very sensitive to the flame temperature and produced in the local high flame temperature regions. Coal derived diesel fuel has a

significantly higher aromatic content than normal diesel fuel, therefore the addition of coal derived diesel fuel in the baseline fuel will increase the adiabatic flame temperature and NO_x emissions. Under this condition, although there was no difference in the bulk cylinder gas temperature profile, there were locally higher flame temperature regions formed for the coal derived diesel fuel blend.

As engine load was increased, significant decrease in the total unburned hydrocarbon and carbon monoxide emissions were observed (**Figures 2-21** and **2-22**). This decrease is mainly due to the significant increase in the combustion temperature when the engine load was increased. This increase facilitates more complete oxidation for hydrocarbon and carbon monoxide. Also, under low load condition, coal derived diesel fuel was observed to produce more carbon monoxide emissions. This can be explained by the lower air-fuel ratio for the coal derived diesel fuel blend as shown in **Figures 2-24**. Also, the addition of coal derived diesel fuel increases the quantity of ring structures in the fuel, which will tend to increase the unburned hydrocarbon emissions.

Finally, a slightly higher brake specific fuel consumption for coal derived diesel blend was observed throughout the engine testing conditions as shown in **Figures 2-23**.

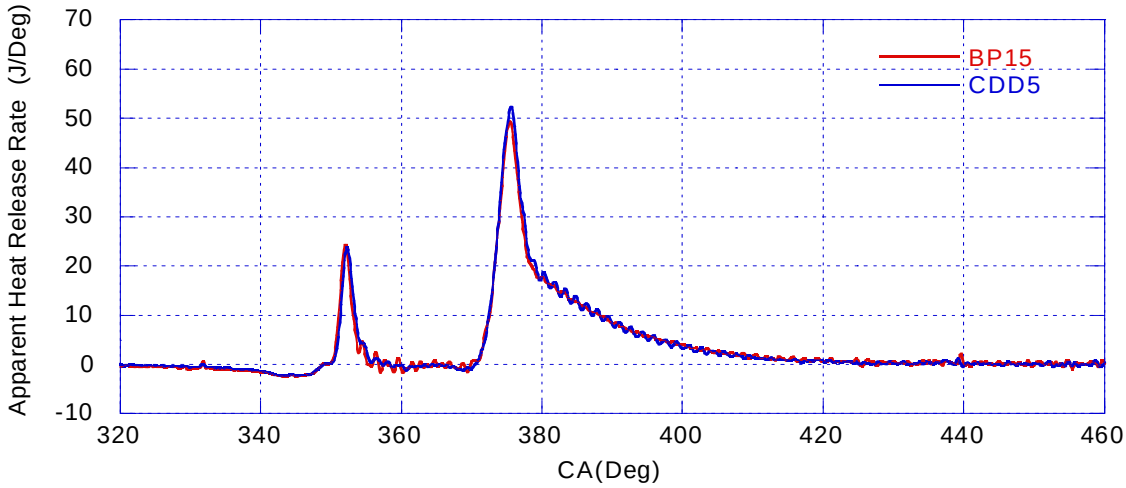

Figure 2-12 Apparent heat release rate at AVL mode 2

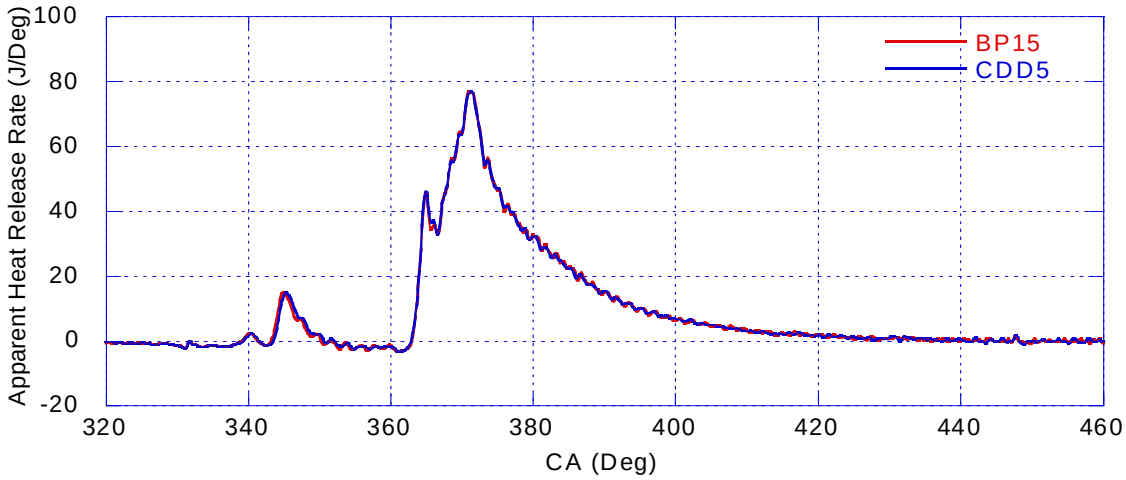

Figure 2-13 Apparent heat release rate at AVL mode 3

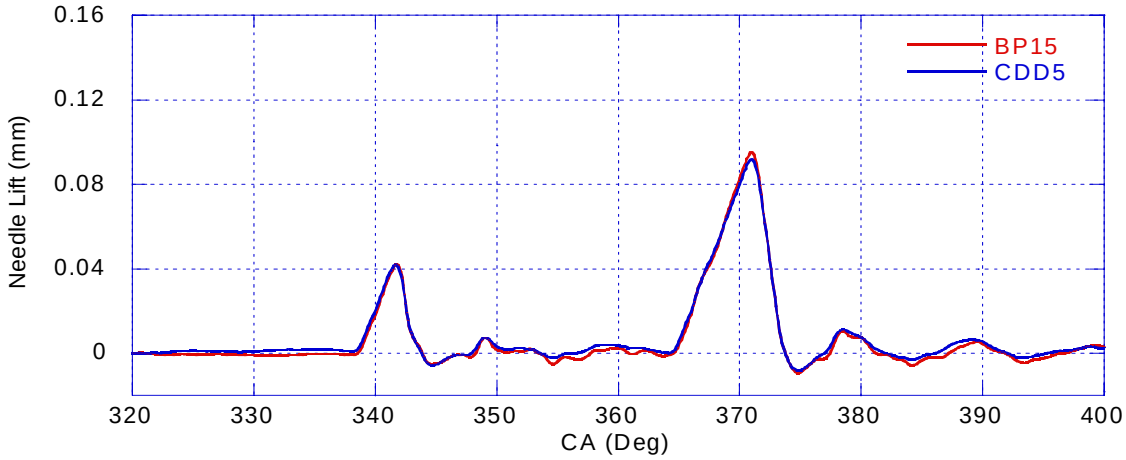

Figure 2-14 Needle lift signal at AVL mode 2

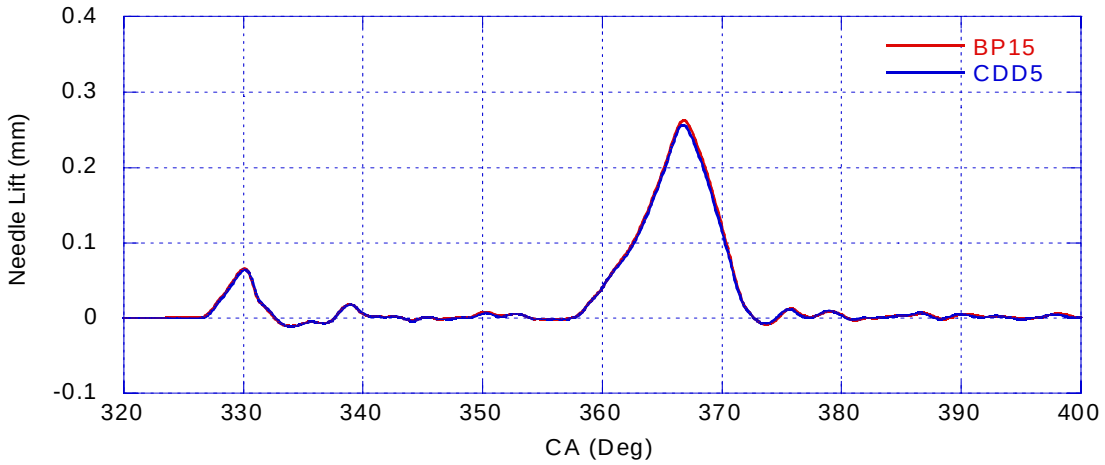

Figure 2-15 Needle lift signal at AVL mode 3

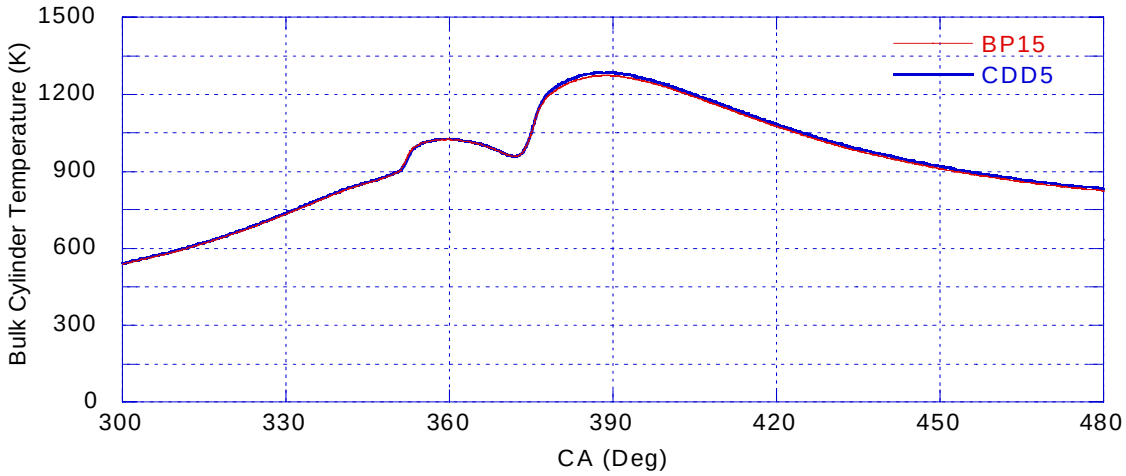

Figure 2-16 Bulk cylinder gas temperature at AVL mode 2

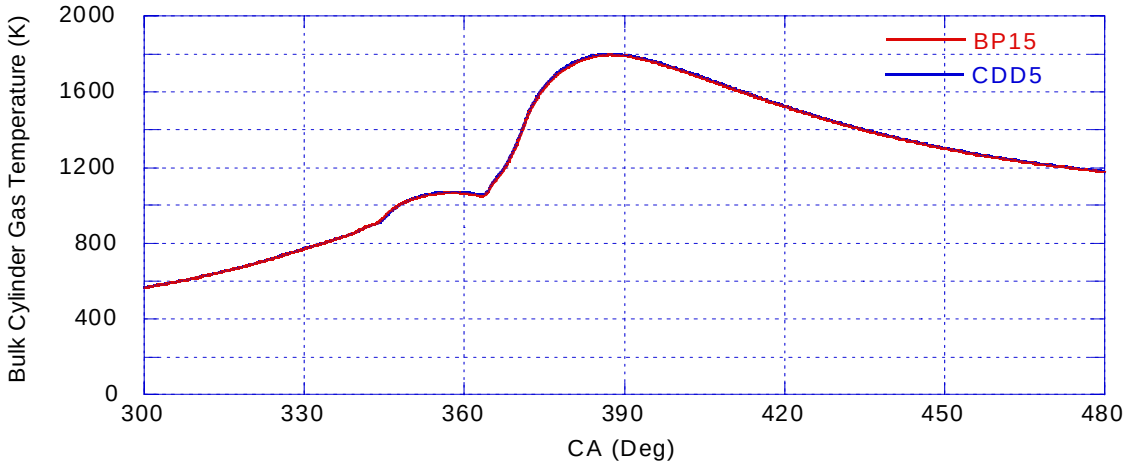

Figure 2-17 Bulk cylinder gas temperature at AVL mode 3

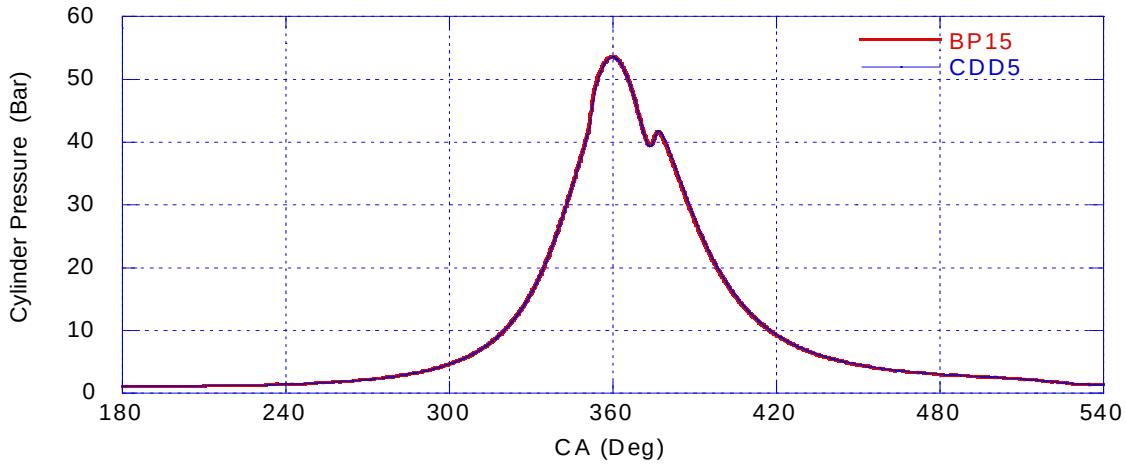

Figure 2-18 Cylinder pressure trace at AVL mode 2

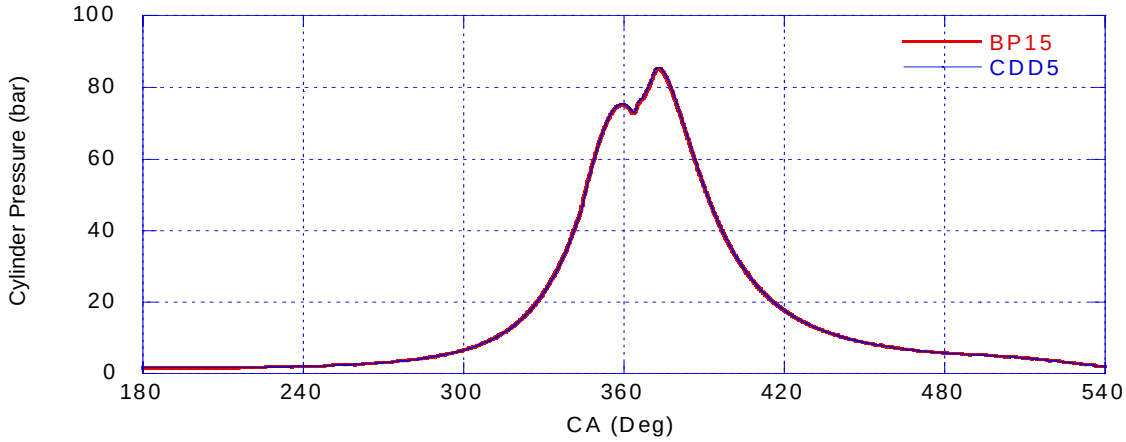

Figure 2-19 Cylinder pressure trace at AVL mode 3

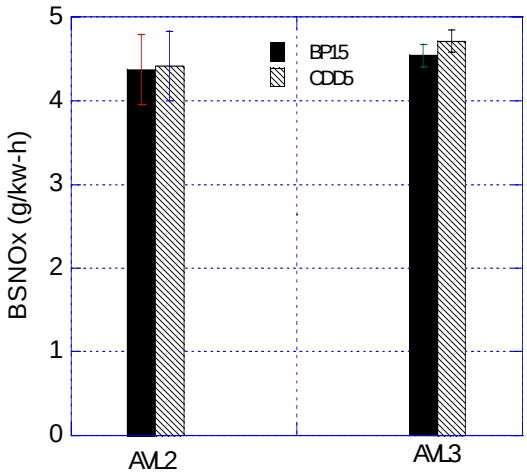

Figure 2-20 Brake specific NOx emissions

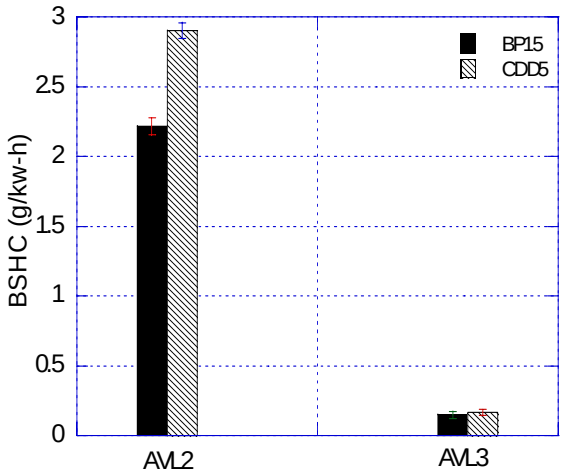

Fig. 2-21 Brake specific unburned hydrocarbon emissions

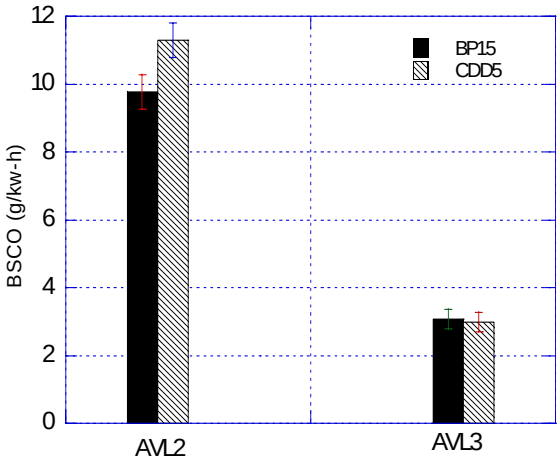

Figure 2-22 Brake specific CO emissions

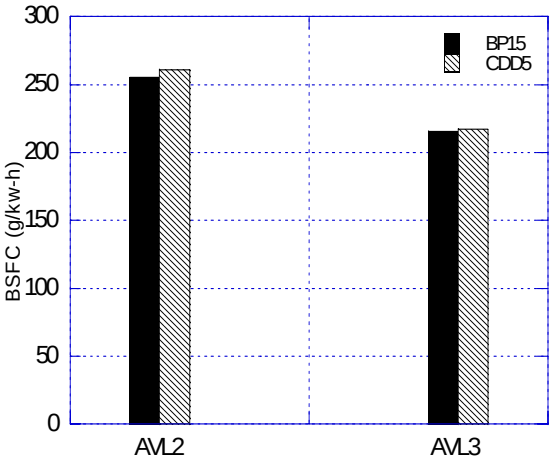

Figure 2-23 Brake specific fuel consumption

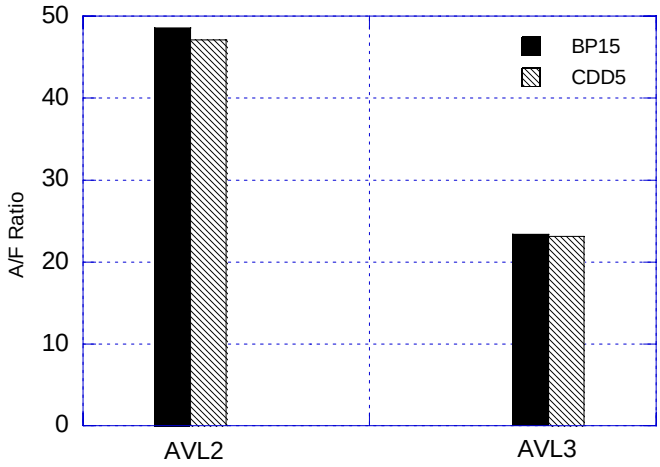

Figure 2-24 Air to fuel ratio

Impacts of Addition of Phenanthrene on Engine Performance and NOx Emissions

Since phenanthrene has been identified in the coal-based diesel fuel and similar compounds form a large portion of the coal based diesel fuel, it is of interest to investigate the impacts of addition of phenanthrene on engine performance and emissions. To that end, 1 wt.% and 5 wt.% phenanthrene were doped into neat biodiesel fuel for engine tests. The engine was operated at 1350 rpm, high load conditions.

All of the three test fuels had very similar needle lift and heat release rate profiles, as shown in Figure **2-25** and Figure **2-26**. Figure **2-27** shows that the brake

specific fuel consumption decreased as more phenanthrene was added into the baseline biodiesel fuel. Since phenanthrene has significantly higher sooting tendency than biodiesel, more soot will be expected to form in the diffusion flame region when phenanthrene is added. Higher soot formation in the flame zone can cause increases in soot radiative heat transfer from the diffusion flame, which can lead to decreases of actual flame temperatures. Due to the high sensitivity of thermal NO formation on flame temperature, NO_x emissions were anticipated to decrease as the actual flame temperature decreases. Therefore, the addition of phenanthrene is expected to result in the decrease of NO_x emissions. However, on the other hand, the addition of phenanthrene into biodiesel will also increase the adiabatic flame temperature of the blend. Hence, two competing effects co-exist in the NO formation when phenanthrene is added. Figure **2-28** shows the NO_x emissions for the three test fuels under different load conditions. As can be seen, 1% addition of phenanthrene causes an increase in NO_x emissions at 13.2 bar gIMEP condition. But, at lower load conditions, it generally showed no obvious effect on NO_x emissions. When 5% pheneathrene is added, an evident decrease in NO_x emissions throughout the load conditions was observed, which indicated the soot radiation effects had become more dominant at this concentration of phenanthrene. Exhaust temperatures shown in Figure **2-29** were also found decreased for 5% phenanthrene blend, which was also an indication of lower combustion temperatures for the biodiesel containing 5% phenenthrene. Further investigation will be performed to confirm the results from this study.

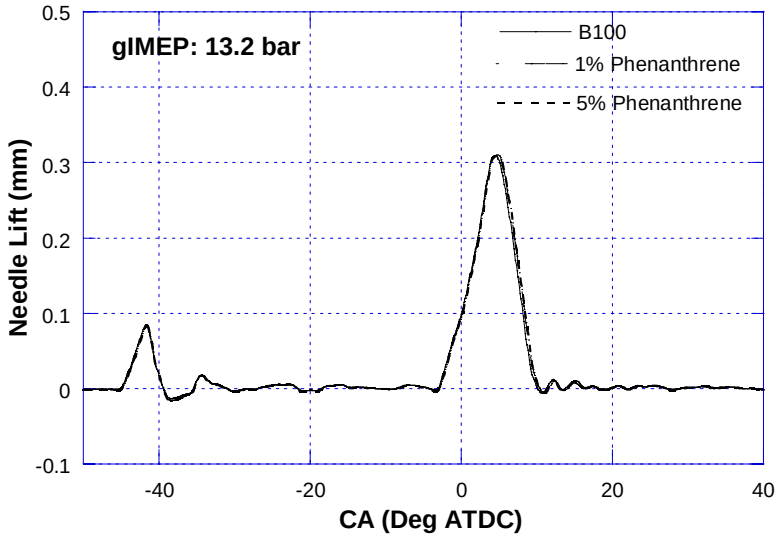

Figure 2-25: Needle Lift Profile at 13.2 bar gIMEP Condition

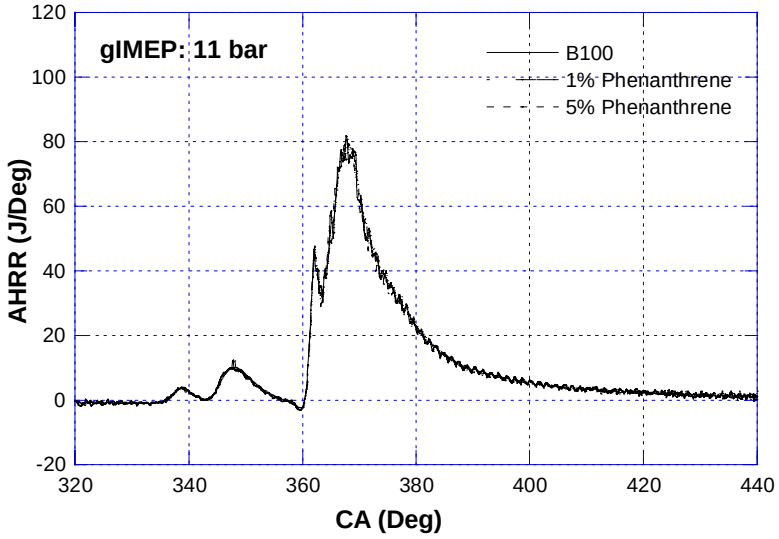

Figure 2-26: Apparent Heat Release Rate at 11 bar gIMEP Condition

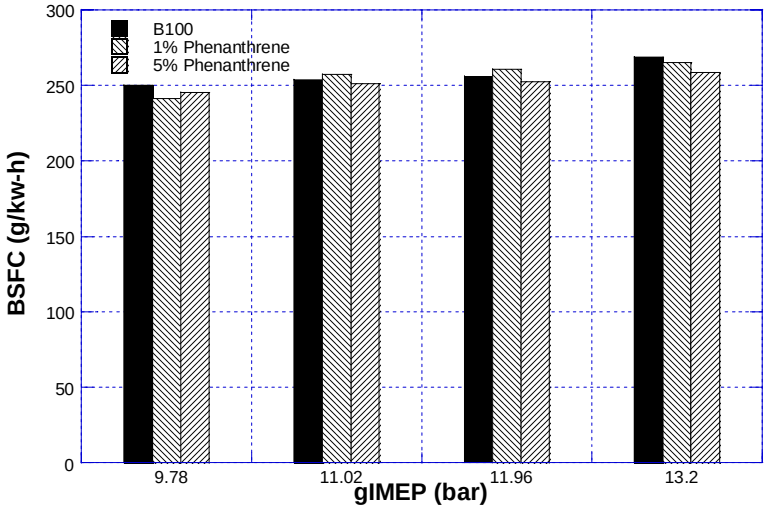

Figure 2-27: Brake Specific Fuel Consumption

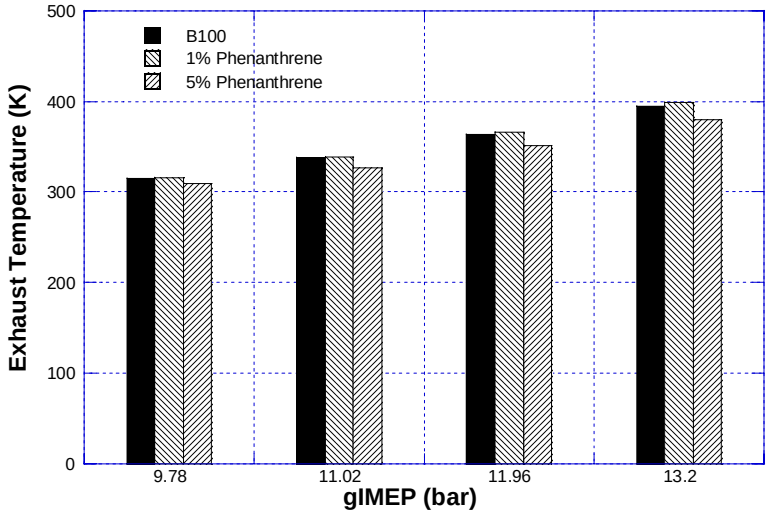

Figure 2-28: Brake Specific NO_x Emissions

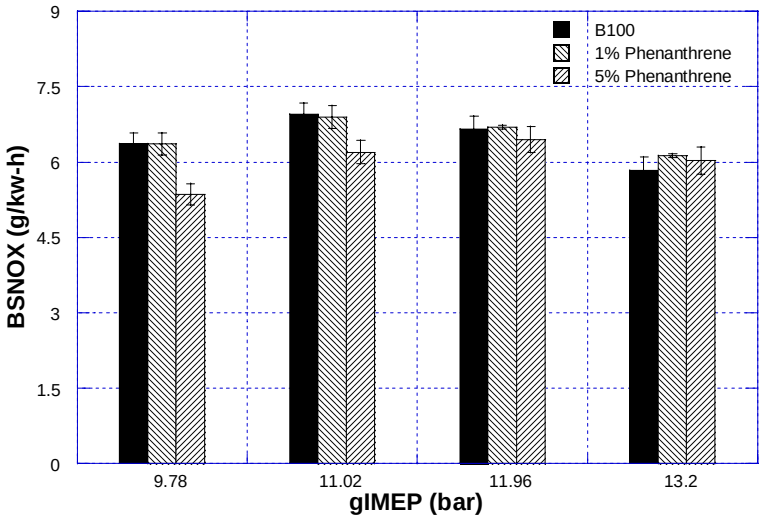

Figure 2-29: Exhaust Temperature

In-Cylinder Imaging of Coal-Derived Diesel Combustion

For the purpose of better understanding the impact of the coal-derived compounds on the injection, ignition and combustion of diesel fuels in a practical engine, we have developed an installation of an existing AVL 513D Engine Videoscope (purchased under an NSF Research Equipment Grant, # CTS-0079073) in our Navistar V-8 7.3L turbodiesel engine. This required design and machining access for an endoscope probe and a light guide to visualize the fuel spray and the spray flame. The modified cylinder head is ready for use and will be implemented after some other preliminary emissions studies are completed.

(a)

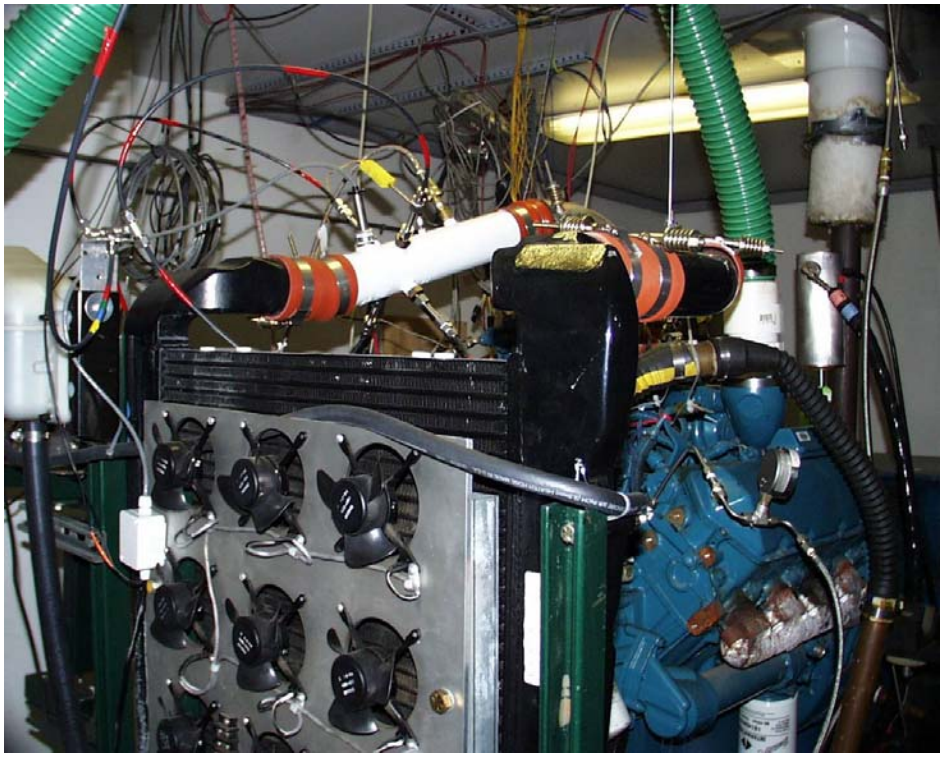

(b)

Figure 2-30 Digital Photograph of (a) Optically Accessible Cylinder Head and (b) Navistar 7.3L Turbodiesel Engine

Impact of Fuel Composition on Combustion and the Properties of Diesel Soot

Previously in the Year 2 Annual Report we presented a comparison between BP15, 10%CDD, and 20%CDD. Emission data was obtained for BP15 and 20%CDD fuels. The oxidation behavior of the soot from engine combustion of BP15 and 10%CDD was determined by using the thermogravimetric and Differential Scanning Calorimetry (TGA-DSC). The engine used in this experiment is a single cylinder DI diesel engine operated at 75% load and 3600 rpm. This section of the report provides a comparison between BP15, 10%CDD, and 20%CDD.

Emission data was obtained for BP15 and 20%CDD fuels. The oxidation behavior of the soot from engine combustion of BP15 and 10%CDD was determined by using the thermogravimetric and Differential Scanning Calorimetry (TGA-DSC). The engine used in this experiment is a single cylinder DI diesel engine operated at 75% load and 3600 rpm.

Single-Cylinder DI diesel Engine - A highly instrumented, single-cylinder direct injection (DI) diesel engine with a maximum power output of 7 hp. Cylinder pressure and fuel-line pressures will be measured using Kistler piezoelectric pressure transducer models 6052B1 and 601B1, respectively. A Hall-effect proximity sensor will be used to measure needle-lift in the injector. An AVL 364 shaft encoder installed on the engine crankshaft, along with a Keithley DAS 1800 data acquisition board enabled 0.1 CA degree resolutions of these signals. NOx emissions will be measured using an Eco-Physics NOx analyzer integral in an AVL GEM 110 emissions bench.

Fuels - The test fuels considered in this work are: an ultra low sulfur diesel with 15ppm sulfur content (BP15) and BP15 blended with 10% and 20% CDD.

Soot Oxidation Reactivity - In this study, The BP15 and 10% CDD soots were collected from the raw exhaust of a single-cylinder DI diesel engine. The soot oxidation

behavior was conducted on the Thermogravimetric Analysis (TGA) and Differential Scanning Calorimetry (DSC). TGA-DSC provides data on soot mass reduction as a function of temperature and the oxidation temperature and time.

Emissions - The preliminary investigations on the effects of the coal-derived diesel on engine emissions were conducted on the single-cylinder DI engine. The engine was operated at 75% load and 3600rpm.

Table 2-6 shows emission data for BP15 and 20%CDD. The injection of 20%CDD (-7.6 CA BTDC) is advanced relative to the BP15 fuel (-6.98 CA BTDC). As a result, the 20%CDD produces higher NOx than the BP15 fuel.

Figure 2-31 shows pressure data for BP15 and 20%CDD. BP15 has a relatively higher peak temperature. As seen in the heat release profile in **Figure 2-32**, the start of combustion is retarded for the 20%CDD relative to the BP15 fuel, due to the low cetane number of the 20%CDD fuel.

Table 2-6. Emission data for BP15 and 20%CDD

	BP15	20%CDD
NOx (ppm)	569	616
CO2 (%)	7.9	8.3
CO (ppm)	831	1060
UHC (ppm)	286	404

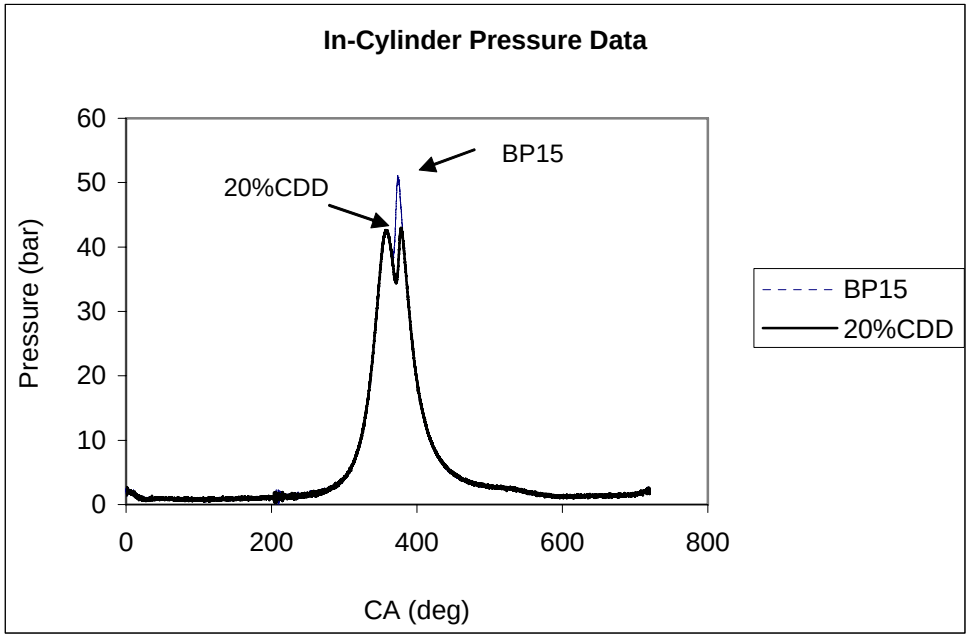

Figure 2-31 In-cylinder pressure data for BP15 and 20%CDD fuels.

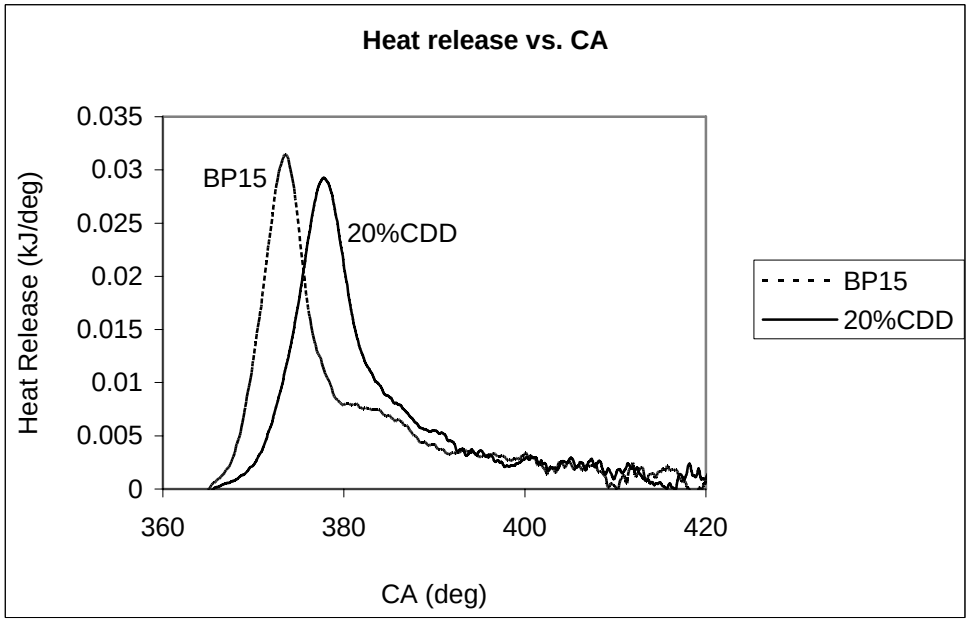

Figure 2-32 Heat release profile for BP15 and 20%CDD fuels.

Soot Characterization - For temperature programmed oxidation (TPO) experiments, TGA-DSC tests were performed on a Q-600 thermogravimetric analyzer.

Soot particles were collected from the raw exhaust of the single-cylinder DI diesel engine. The soot was collected on Teflo filters and then removed and heated at 500°C for 1 hour under nitrogen gas to remove the soluble organic fraction. Soot samples were then placed in TGA-DSC furnace and heated in air in the temperature range 20-700 °C using heating rate of 10 °C/min. **Figure 2-33** shows the mass reduction and heat release profiles as a function of temperature for BP15 and 10%CDD. It is obvious that the oxidation characteristics of the soot from both fuels are identical. This would indicate that the soot formation mechanisms and the physical/chemical properties of both soots are similar. **Table 2-7** shows some important thermal parameters of both soots.

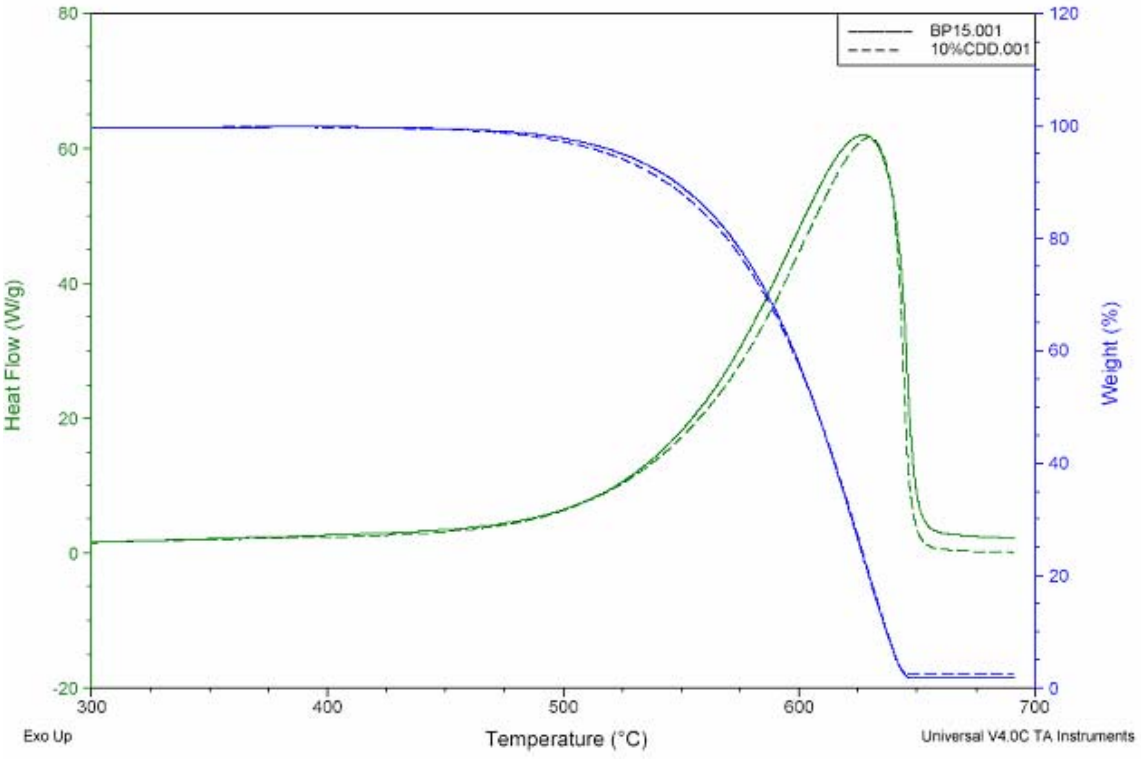

Figure 2-33 TGA-DSC profiles for different soot samples.

Table 2-7. Thermal properties of diesel soot.

	BP15	10%CDD
*Onset temp. (°C)	525	519
Maximum peak temp. (°C)	627.65	630.43
Heat of reaction (kJ/g)	24.4	23.5

*T_{onset}: temperature at 5 wt.% weight loss

Soot Structure - To gain better understanding about structural properties of diesel soot, the HRTEM imaging was obtained. The experiment was conducted on a field emission JEOL 2010F instruments located in the Materials Research Institute (MRI) of Penn State. For the HRTEM imaging, thermophoretic sampling unit was used to capture soot particles from the raw exhaust. Soot particles were captured on a 3 mm diameter cupper grid coated with a lacey carbon film. **Figure 2-34** shows the nanostructure of the 20% CDD soot. It exhibits the classical soot nanostructure: long fringes arranged concentrically at the edges and randomly oriented fringes in the center.

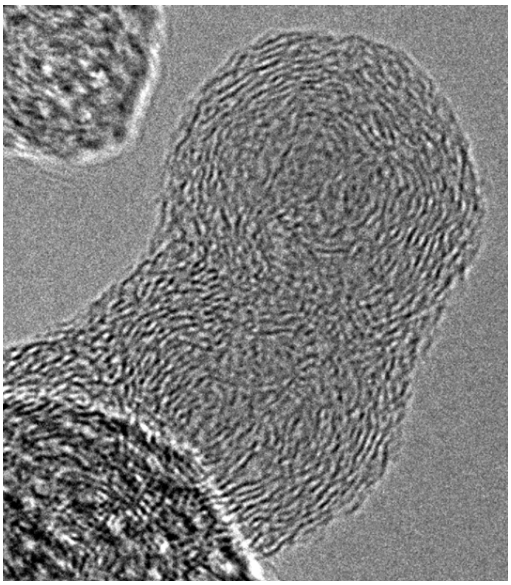

Figure 2-34 Soot Nanostructure of 20% CDD soot.

Future Work - The impacts of engine operating conditions such as EGR, injection timing and injection strategies on soot oxidative reactivities will be evaluated. Bulk soot samples will be collected from the raw exhaust of the DDC engine. Further experiments will be conducted on the TGA-DSC to obtain the oxidation kinetics of diesel soot.

X-Ray Diffraction (XRD) will be used to obtain the interlayer spacing (d002) and the layer dimension (La). Raman Spectroscopy (RS) will be used to obtain the intensities of the amorphous and graphitic peaks and the intensity ratio will be interpreted as a measure of the in-plane crystallite dimensions. The density, pore size distribution, and active surface areas of different soots will also be determined. The CHN analyzer will be used to obtain information about the elemental composition of the soot. FTIR will provide data about the functional groups.

Impact of EGR on Combustion and the Properties of Diesel Soot

In the Year 2 Annual Report for future work, we proposed to examine the impacts of engine operating conditions such as EGR, injection timing and injection strategies on soot oxidative reactivity. Bulk soot samples were to be collected from the raw exhaust of the DDC engine. Experiments were to be conducted on the TGA-DSC to obtain the oxidation kinetics of diesel soot and various characterization techniques were to be applied to these soot samples, for comparison with the fuel effects.

Recent findings in our laboratory have shown that fuel formulation can affect the oxidative reactivity of the soot (see for instance the Year 2 Annual Report **[1-**). The inclusion of biodiesel in the fuel lowers the ignition temperature of soot and consequently lowers the temperature required for regeneration of the diesel particulate filter (DPF) and

this was attributed to the high surface oxygen content of biodiesel soot. In addition, the oxidation rate of biodiesel was found to be two times faster than that of diesel soot **[2-5]**.

Here, we present a potential method to improve the regenerability of the DPF by enhancing the oxidative reactivity of diesel soot. We show that EGR can be utilized to generate more reactive soot. Carbon dioxide CO_2 was used to simulate particle free and cold EGR, which is proposed as a possible pathway to generate soot that is more prone to oxidize in DPF.

Soot Origin and Sampling. A highly instrumented single cylinder direct injection diesel engine was used to produce the soot samples. The engine was running under fixed load (75%) and speed (3600 rpm). Diesel particulate matter samples were collected from the raw exhaust of the engine on teflo filters. The diesel particulate matter was subsequently removed from the filters and thermally treated under UHP nitrogen at 500°C to remove volatile compounds. Thus, the soot considered in this work is the volatile-free fraction of the diesel particulate. Simulated EGR (SEGR) was introduced to the engine intake system from high pressure cylinders of CO2 at different concentrations: 0, 3, 6, and 9 vol.%. The fuel considered was an ultra low sulfur diesel with 15 ppm sulfur content (BP15).

Soot Oxidative Reactivity. A Thermogravimetric Analyzer (TGA) was used to investigate the difference in reactivity between the soot samples. Two experiments were considered to elucidate the soot reactivity: (1) the isothermal in which the soot was heated in air (100cc/min) at 475°C and, (2) the nonisothermal in which the soot was heated in air (100cc/min) from 30°C to 600°C at a heating rate of 2.5°C/min. The kinetic parameters of soot oxidation were derived from the nonisothermal profiles **[2-14]**.

Raman Spectroscopy. A visible Renishaw spectroscopy was used to determine the degree of graphitization of the soot samples. The excitation laser was an Ar ion laser (λ_0 =514 nm, source power 10mW). The laser was focused on the sample through a microscope with 100X objective lens. Two soot samples, designated as S0 and S9 were considered, where 0 and 9 correspond to the CO_2 concentrations under which the soot was formed. The integrated intensity ratio IG/ID was used to investigate the degree of graphitization of the soot samples and Tuinstra and Koenig (TK) expression was used to determine the crystallite width (La) **[2-14]**.

X-Ray Diffraction (XRD). The XRD investigation was done using a Philips MPD instrument. The XRD spectra of S0 and S9 were recorded and the interlayer spacing (d002) was calculated according to Bragg's equation **[2-12]**, the stacking height (Lc) and the crystallite width (La) were calculated according Scherrer's equation **[2-12]**.

Soot Nanostructure Imaging. To investigate the nanostructure of the diesel soot, the high resolution transmission electron microscopy (HRTEM) images were recorded using a Joel 2010F instrument operated at 200kV and equipped with a field emission gun. A small amount of the sample was suspended and sonicated in ethanol. A drop of the solution was then transferred to a copper grid coated with a lacy carbon film for analysis.

Soot Reactivity. **Figure 2-35a** shows the isothermal TGA profiles for S0 and S9. The impact of CO2 is obvious. Increasing the CO_2 enhances the oxidation behavior of the soot. **Figure 2-35a** also shows that by increasing the CO_2 concentration in the engine intake, further increase in the reactivity is observed. The oxidation rate of

S9 was found to be two times faster than that of S0. The results here suggest that low temperature combustion via high EGR level is advantageous.

Figure 2-35b shows the nonisothermal and differential TGA (DTG) profiles of S0 and S9. Compared to S0, S9 exhibits a lower ignition temperature by about 50°C. The oxidation time was cut nearly by 50%. The activation energies were estimated to be 145 kJ/mol and 105 kJ/mol for S0 and S9, respectively. The reported activation energies were independent of gas flow rate and sample mass and therefore free from heat and mass transfer limitations. From the DTG, it can be seen that the reaction rate of S0 increases with temperature as expected, is higher than the reaction rate of S0 and reaches a maximum at lower temperature than S0.

XRD. From the XRD patterns (not shown), the key structural parameters can be determined. The d002 results obtained from Bragg's equation **[2-12]** were calculated as 0.345 nm and 0.354 for S0 and S9, respectively. Using Scherrer's equation **[2-12]**, Lc values were found to be 1.19 nm and 1.15 nm for S0 and S9, respectively. The crystallite width (La) was determined as 2.24 nm and 1.65 nm for S0 and S9, respectively. From these data it can be seen that the difference in reactivities between S0 and S9 is not explained by the d002 or Lc. The crystallite width, on the other hand, is shorter for S9. It is well-known that soot with short fringes is more prone to oxidation because of the increase in the ratio between edge carbon and basal plane carbon **[2-13]**. Accordingly, it is expected that the number of active sites in S9 is higher than those in S0. This speculation can be proved by performing oxygen chemisorption analysis on both samples.

Raman Spectroscopy. **Figure 2-26** shows the Raman spectra obtained for S0 and S9. Two distinct peaks are shown: the G peak (1580 cm-1), which is referred to the graphitic band, and the D peak (1350 cm-1), which can be assigned to the disordered band. The integrated intensity ratio IG/ID can be used as a reactivity index. The IG/ID for S0 and S9 was found to be 0.443 and 0.375, respectively. These values indicate that S0 has more graphitic structure than S9 in agreement with the TGA data. According to the Tuinstra and Koenig (TK) expression **[2-14]**, the crystallite width (La) is found to be 1.95 nm and 1.65 for S0 and S9, respectively. Despite the fact that the TK expression holds well only for La between 2.5 and 250 nm **[2-15]**, the values of La from the Raman spectra agrees with those from XRD.

Soot Nanostructure. The HRTEM investigations were conducted in order to obtain information about soot structure at the atomic level. The HRTEM images of S0 and S9 are shown in **Figure 2-37**. Both soots have a classic core/shell structure. S0 soot is characterized by a small disordered core which was estimated to be about 2-3 nm. The outermost part is built of straight fringes arranged concentrically and parallel to the particle perimeter. On the other hand, S9 soot has a larger disordered core of about 9-10 nm. The core is characterized by randomly oriented short fringes. The outermost regions of the primary particles are characterized by wavy-long graphene layers. The coexistence of the wavy layers and short fringes in S9 are partly responsible for the observed higher reactivity.

The results presented here show that changing the combustion conditions via CO2 alters the soot properties. EGR can be utilized to enhance the oxidative reactivity of diesel soot. We employed CO_2 to simulate cold and particle free EGR; a condition that

can be achieved in real world engines by recirculation of the EGR from downstream of the DPF (particle free EGR) and to increase the cooling of the EGR (cold EGR).

It is well-known that CO_2 suppresses the soot formation through its dilution, thermal, and chemical effects [**2-16 – 2-17**]. It can be speculated that adding CO_2 results in different pyrolysis chemistry. The nature of the pyrolysis species and the way they contribute to soot formation and growth are altered. Due to its higher heat capacity (the thermal effect of CO_2), incorporating CO_2 into the combustion process results in lowering the flame temperature. Therefore, one can expect that the degree of carbonization/graphitization of the soot is lowered and less mature soot is produced. The chemical effect of CO_2, on the other hand, is believed to also influence the soot reactivity. The dissociation of CO_2 leads to an increase in O atoms and the reaction of CO_2 with H atoms results in increasing the OH and decreasing the H concentration **[2-16]**. Hence, the oxidation rates increase as a result of high O and OH concentrations and the formation of large PAH is suppressed due to the lack of H atoms, the key component for soot formation via the HACA mechanism **[2-18]**. Accordingly, small particle size, and hence higher surface area, and short fringe length are formed; the characteristics of more oxidatively reactive soot. However, further work is necessary to determine the mechanism by which CO_2 influences the soot reactivity.

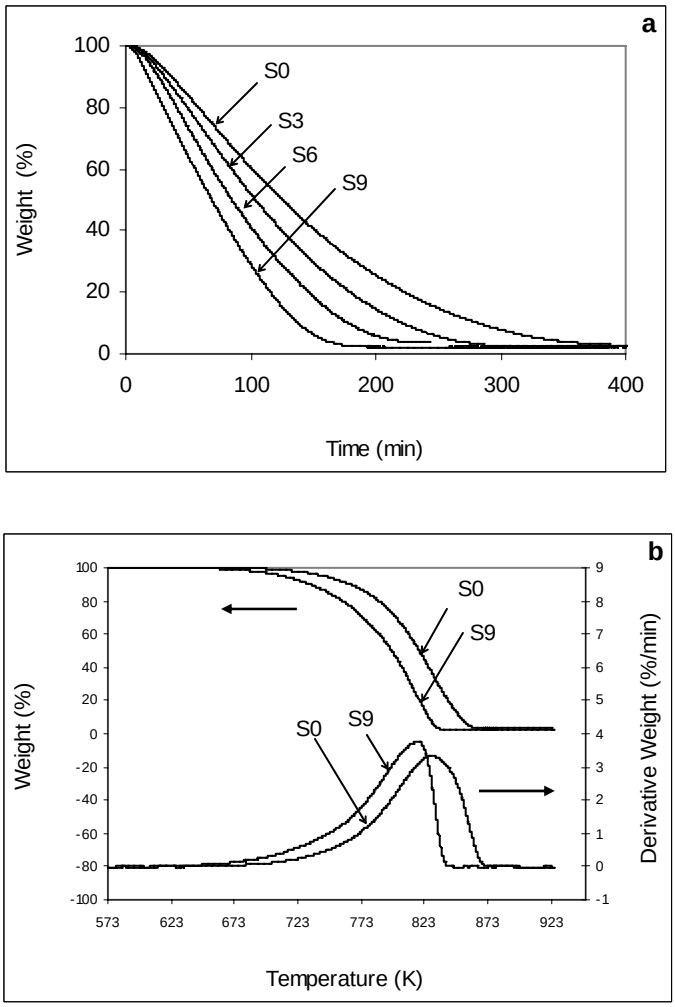

Figure 2-35(a) Isothermal profiles at 475°C under air ; 0, 3, 6, and 9 correspond to the concentrations of CO2 injected to engine intake (b) Weight loss profiles of S0 and S9.

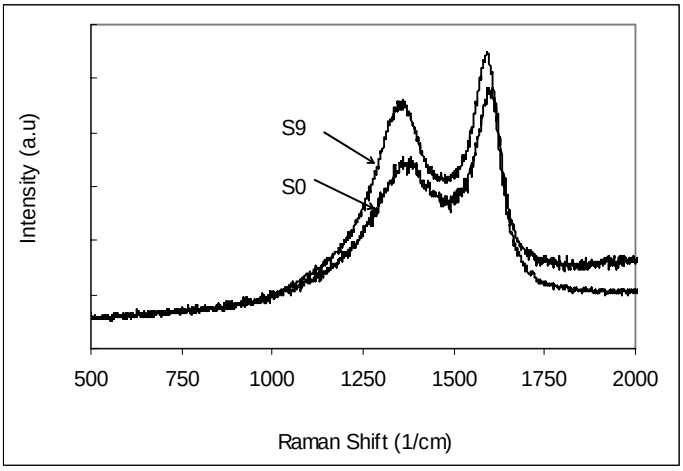

Figure 2-36. Raman spectra of S0 and S9 (λ_0 = 514 nm)

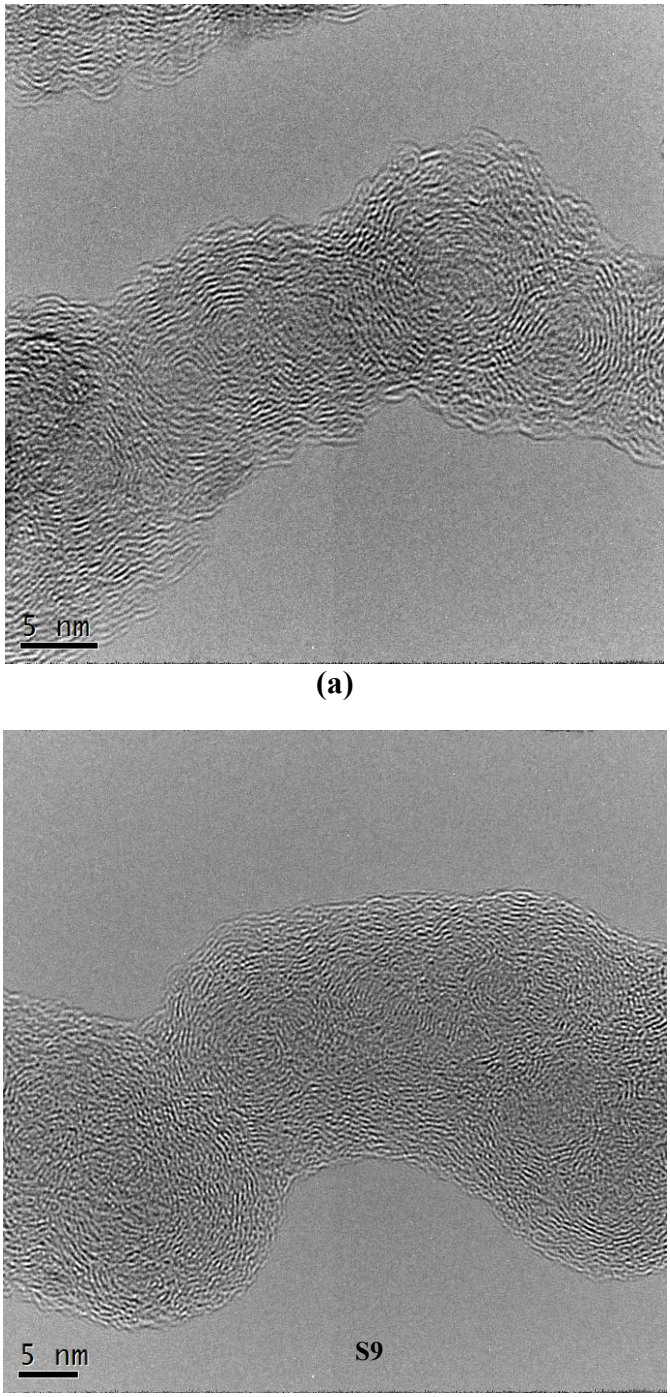

Figure 2-37. HRTEM images of (a) S0 and (b) S9.

Future Work - A Santoro-type diffusion flame will be used to assess the impacts of aromatics on soot reactivity by examining the role that the polyaromatic hydrocarbon (PAH) compounds play during the inception and growth stages of soot formation. Two

aromatic compounds are of particular interest: Phenanthrene ($C_{14}H_{10}$) and fullerene ($C_{13}H_{10}$). These compounds will be heated in a vaporizer to temperatures above the respective melting points, and their vapors will be entrained into the flowing burner fuel (ethylene). Soot will then be collected from the resulting sooting flame.

Task 3. Desulfurization, Denitrogenation, Saturation of Aromatics, Chemicals from Coal

Jae Hyung Kim, Shamal Kumar Saha, Hyun Jae Kim, Vasudha Dhar, Boonyawan Yoosuk and Xiaoliang Ma, Chunshan Song

Subtask 3.1: Desulfurization and Denitrogenation

Ultra-deep hydrodesulfurization (HDS) of diesel fuel has become an important research area because of increasingly stringent environmental regulations on sulfur content in fuel **[3-1]**. On June, 2006, it has been effective that the sulfur level must be lower than 15 ppm S in diesel fuels by US EPA. In order to improve efficiency of HDS, therefore, many studies on deep hydrodesulfurization of model and real diesel fuels are being conducted with various methods and different catalysts by many research groups **[3-1 – 3-7]**. Hydrodesulfurization is currently a major process in petroleum refineries to reduce the sulfur in the liquid hydrocarbon fuels. However, it was found by many researchers that the nitrogen compounds coexisting in middle–distillate oil inhibit the deep hydrodesulfurization and the removal of such nitrogen compounds from the middle–distillate oil can improve significantly the deep hydrodesulfurization performance **[3-2, 3-3, 3-8]**. Recently, a new concept called selective adsorption for removing sulfur has been explored at Penn State (PSU-SARS), which aims at removing sulfur in the fuels by selective adsorption on adsorbents at ambient temperature. The major advantages of this process are that the process can run at ambient temperature and pressure without using hydrogen gas and the spent adsorbents can be regenerated either by solvent washing or by

oxidation using air. The idea in PSU-SARS process can be also applied to pre-denitrogenation of the middle–distillate oil to improve the deep hydrodesulfurization performance.

In the adsorption part of this study, we are focusing on the adsorptive denitrogenation of basic or very reactive nitrogen compounds such as quinoline or indole, which influences very much hydrodesulfurization. It is expected that these nitrogen compounds may be removed easily by adsorption as compared with sulfur compounds because they are much more reactive than sulfur compounds in hydrotreating process. Therefore, the performance of HDS may be improved, even though basic or reactive nitrogen compounds are removed from middle-distillate oil.

3.1.1. Experimental

3.1.1.1. Adsorptive desulfurization and denitrogenation of LCO

The adsorptive denitrogenation/desulfurization of light cycle oil (LCO, EI-163 from United Refinery) was performed on the activated carbon which had shown the best adsorption properties on sulfur and nitrogen compounds in a model fuel as reported in the previous report. The activated carbon was provided from MeadWestvaco and has surface area of 1843 m^2/g and pore size of 28.6 Å. It was pretreated in nitrogen flow at 200 °C for 1 h in order to remove water and other contaminants adsorbed in their surface which might significantly influence the adsorption properties. Then the adsorbent was cooled down to room temperature and the adsorption experiment was performed in a flow system with LHSV of 4.8 h^{-1}. Analysis of fuel samples was conducted using Antek 9000 series nitrogen and sulfur analyzer for more accurate quantitative analysis and also HP

GC equipped with a capillary column (XTI-5, Restek) and a pulsed flame photometric detector (PFPD) for identification of sulfur compounds.

3.1.1.2. Unsupported Mo sulfide catalysts with promoters

The unsupported Mo sulfide catalysts with/without Co promoter were synthesized by the hydrothermal method developed in our laboratory. The catalysts were compared with commercial catalysts and unsupported Mo and NiMo sulfides which were reported in the previous report. Aqueous ammonium tetrathiomolybdate (ATTM) and a promoter precursor $Co(NO_3)_2 \cdot 6H_2O$ was mixed with organic solvent (decalin) and decomposed and reacted under 400 psi of hydrogen pressure and 350 $^{\circ}$C in 25 ml of microautoclave. All catalysts were evaluated with simultaneous HDS of DBT and 4,6-DMDBT, which was carried out in a horizontal micro-reactor. The HDS reaction conditions were 400 psi of H_2 pressure and 350ºC of reaction temperature. The liquid products were collected and analyzed by Shimadzu GC/MS (GC12A/QP-500) for identification and HP GC-FID (HP5890) with XTI-5 capillary column (Restek) for quantification. For kinetics study, HDS reaction was conducted under 300 psi of H_2 pressure and 300^{o}C in order to obtain reliable kinetics data. In general, HDS of individual sulfur compound follows the pseudo-first-order kinetics. To calculate individual rate constant for each reaction pathway, the kinetic equation was combined with the ratio of initial selectivity of primary products for each reaction pathway which provides more reliable kinetic data because the initial selectivity is calculated at the initial rate **[3-9]**. The unsupported Mo sulfide catalysts were characterized by XRD (Scintag Powder Diffractometer with Cu K_α emission, 30 mA 35 KV), N_2 adsorption (Micromeritics ASAP 2000) and TEM (JEOL JEM-2010F electron microscope operated at 200 kV).

3.1.2. Results and discussion

3.1.2.1. Adsorption of light cycle oil (LCO) on activated carbon

As reported in previous year, the adsorptive denitrogenation and desulfurization of light cycle oil (LCO) was performed at 25°C and 4.8 h^{-1} LHSV on the activated carbon which showed excellent adsorption properties of the model fuel and very high adsorption capacity of sulfur and nitrogen compounds. LCO used in this study contains 1.5 wt% S and 464 ppmw N. **Figure 3-1** shows the breakthrough of sulfur and nitrogen. The breakthrough amount of the treated fuel for sulfur was less than 1.3 g-F/g-A, and the C/C_o values for sulfur increased sharply to around 1.0 after the breakthrough. Nitrogen concentration broke through with a treated-fuel amount of 4.9 g-F/g-A. Then, the C/C_0 value increased sharply to 0.8 and then slowly to 1.0 until the breakthrough amount up to 45 g-F/g-A.

To investigate fuel compositions, LCO was analyzed by GC-PFPD which detects only sulfur compounds and the results of GC-PFPD are shown in **Figure 3-2**. The LCO contains wide range of sulfur compounds from two-ring sulfur compounds, BT (benzothiophene), to three-ring sulfur compounds, DBT (dibenzothiophene) with alky groups. Major compounds are C_2-BT (specifically 2,3-DMBT) and C_1-DBT (specifically 4-MDBT). As well, 4,6-DMDBT, one of the most refractory sulfur compounds, is contained although its amount is relatively lower than the major compounds. To investigate the adsorption mechanism, the LCO treated by adsorptive desulfurization and denitrogenation was analyzed. **Figure 3-3** shows the GC-PFPD charts of the LCO treated by adsorption. After treated at 1.3 g-F/g-A (grams of treated LCO per grams of

adsorbent), the LCO contains 2878 ppm S (analyzed by Antek S/N analyzer) only and small amount of 2,3-DMBT and C_3-BT were detected on GC-PFPD chart while nitrogen compounds were not detected at this sample on the basis of Antek nitrogen analysis. In the GC-PFPD analysis, the sample fuels were diluted solvent and therefore, the peaks of sulfur compounds might look less. After treated at 3.1 g-F/g-A, sulfur concentration almost reached to the initial concentration of LCO and it was 1.47 wt% S and most of sulfur compounds contained in untreated LCO were detected. Further treated LCO samples contain almost same amount of sulfur and show same GC-PFPD chart as shown in **Figure 3-3** while nitrogen concentration was still lower than 50 ppm N after treated at 6.7 g-F/g-A.

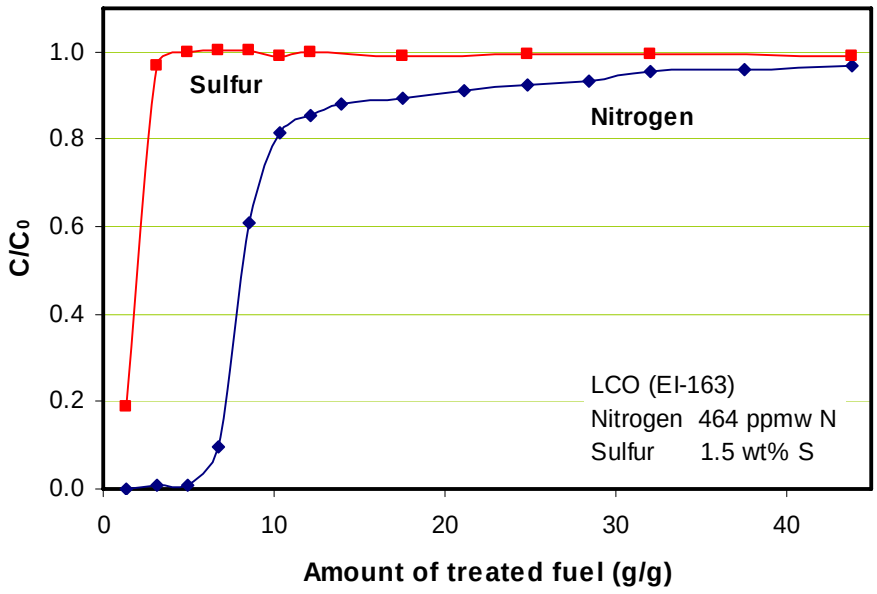

Figure 3-1. The breakthrough of sulfur and nitrogen in LCO over activated carbon.

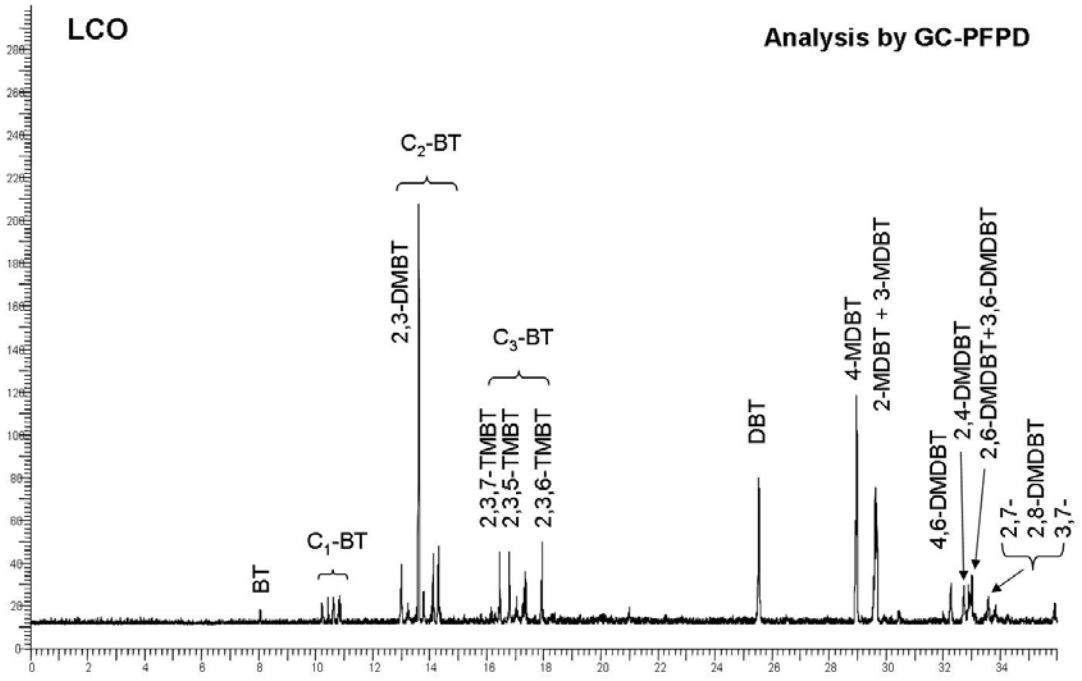

Figure 3-2.GC-PFPD analysis of light cycle oil (LCO).

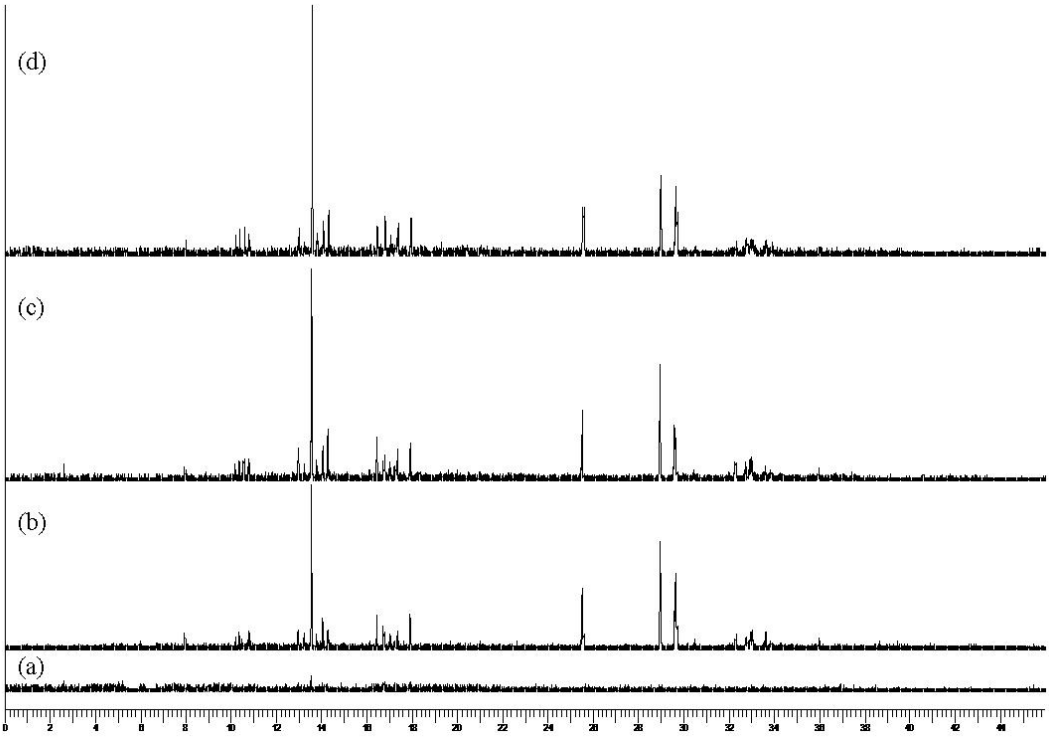

Figure 3-3. GC-PFPD analysis of LCO treated by adsorption on activated carbon after the amount treated of (a) 1.3 g-F/g-A, (b) 3.1 g-F/g-A, (c) 4.9 g-F/g-A and (d) 6.7 g-F/g-A.

3.1.2.2. Hydrotreating of LCO treated by adsorption

For hydrotreating of LCO treated by adsorption, the samples treated by 6.7 g-F/g-A were collected and it contains 1.3 wt% S and 14 ppm N. HDS of LCOs untreated and treated by adsorption was performed at 300°C and 300 psi of H_2 pressure for 30 min. First, the products were analyzed by GC-PFPD as shown in **Figure 3-4**. Based on the GC-PFPD analysis, the hydrotreating removed all range of sulfur compounds and specifically sulfur compounds in BT range was removed more significantly than those in DBT range as compared between (a) and (b) in **Figure 3-4**. On the other hand, adsorption treatment removed more sulfur compounds in DBT range than those in BT range as compared between (a) and (c) in **Figure 3-4**. It is because the activated carbon has excellent adsorption properties of heavy and alkylated DBTs as reported in the previous year. **Figure 3-4** (d) shows sulfur compounds in LCO treated by adsorption followed by hydrotreating. All range of sulfur compounds were removed significantly although C_2-BT and C_2-DBT remain still. Therefore, it is certain that hydrodesulfurization (HDS) of LCO is improved significantly after following adsorption treatment. However, quantitative analysis of LCO treated by hydrotreating and adsorption was not conducted with GC-PFPD due to its poor reliability. Therefore, reliable quantitative analysis is required further in future research.

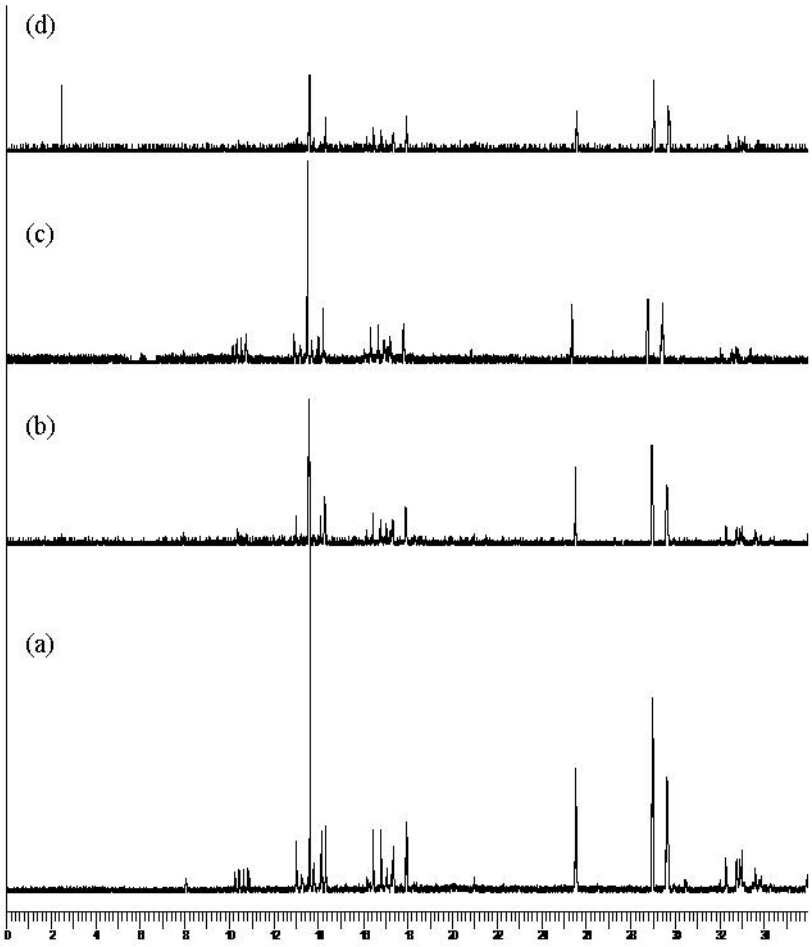

Figure 3-4. The improvement of HDS of LCO after treatment by adsorption. (a) LCO, (b) hydrotreated, (c) treated by adsorption and (d) treated by adsorption followed by hydrotreating.

3.1.2.3. Development of unsupported Mo sulfide catalysts for HDS

3.1.2.3.1. Comparison of unsupported Mo sulfide catalysts with commercial catalysts

The study of the simultaneous DBT and 4,6-DMDBT HDS was performed and the catalytic activity of unsupported Mo sulfide catalysts with Ni and Co were compared with commercial HDS catalysts. **Figure 3-5** shows the comparison of DBT and 4,6-DMDBT conversion on the unsupported NiMo and CoMo sulfide catalysts with sulfided

commercial catalysts. The conversion of DBT and 4,6-DMDBT on the unsupported Mo sulfides are significantly higher than those of the commercial catalysts (Cr424 and Cr344). On the conversion of 4,6-DMDBT, specifically, the unsupported NiMo sulfide showed two times higher than commercial NiMo catalyst (Cr424) while the unsupported CoMo sulfide did three times higher than commercial CoMo catalyst (Cr344). The results indicate that the unsupported NiMo and CoMo sulfide catalysts are certainly superior to the commercial HDS catalysts on the HDS activity of the refractory sulfur compounds because 4,6-DMDBT is one of the most refractory sulfur compound to be desulfurized. This improvement of HDS performance is not only due to the higher surface area and metal loading on the unsupported catalysts, but also their higher HDS activity than commercial catalysts. Based on the kinetic evaluation as shown in **Figure 3-6**, the high HDS activity of unsupported Mo sulfide catalysts came from their high activity for hydrogenation (HYD) pathway. The unsupported NiMo and CoMo sulfides have higher HYD activity than commercial catalysts on HDS of both sulfur compounds. Particularly, the unsupported CoMo sulfide has interestingly high HYD activity on 4,6-DMDBT HDS and even higher than the unsupported NiMo sulfide.

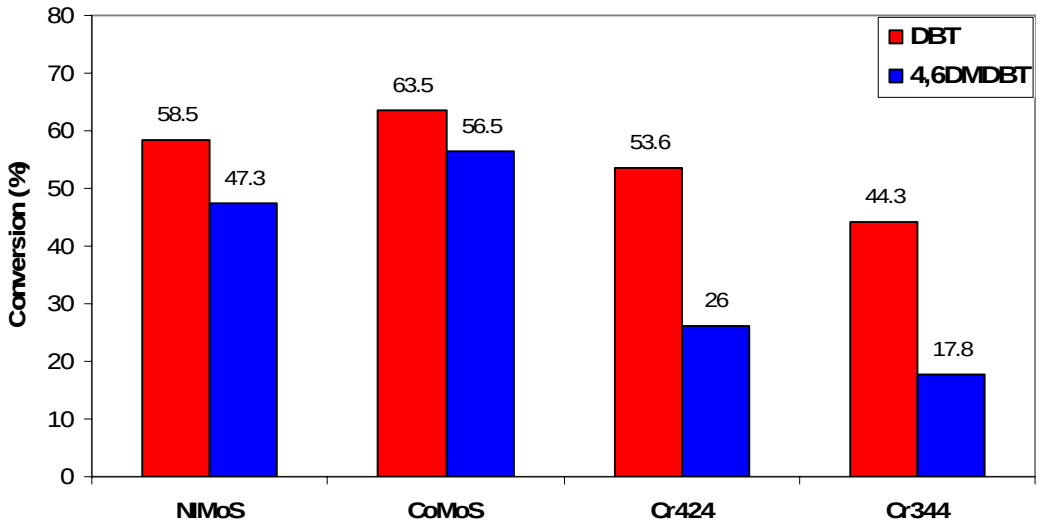

Figure 3-5. The conversion of DBT and 4,6-DMDBT on simultaneous HDS over the unsupported NiMo and CoMo sulfide catalysts and sulfided commercial $NiMo/Al_2O_3$ (Cr424) and $CoMo/Al_2O_3$ (Cr344).

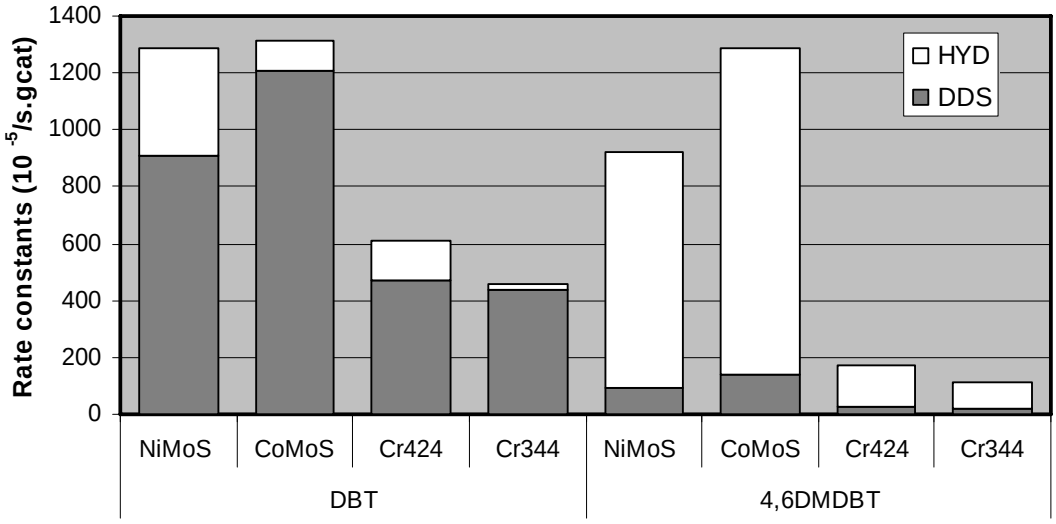

Figure 3-6. The rate constants for simultaneous HDS of DBT and 4,6-DMDBT over the unsupported sulfide catalysts and sulfided commercial catalysts.

3.1.2.3.2. The promoter effects on HDS over unsupported Mo sulfide catalysts

Table 3-1 shows the reactivity and product distribution of DBT and of 4,6-DMDBT on unsupported Mo sulfide catalyst and compared to those obtained with NiMo and CoMo sulfide catalysts. Surprisingly, the conversion of 4,6-DMDBT was higher than that of DBT over the unsupported Mo sulfide. This is mainly due to high activity for HYD pathway, which was the prominent pathway for HDS of both compounds on the sulfide catalyst. However, as far as the HDS activity (desulfurized products) is considered, DBT is about twice as reactive than 4,6-DMDBT. The promoted Mo sulfide catalysts were much more active than the Mo sulfide catalysts for the HDS of both DBT and 4,6-DMDBT. However, the promoting effect was essentially due to the enhancement of the rate of the DDS pathway on both promoted sulfides. The promoters may decrease the strength of the bond between molybdenum and the sulfur atoms resulting from the decomposition of the organic molecules. In the same way it can be supposed that the promoter decreases the metal–sulfur bond in the sulfide itself and increases the electronic density on the sulfur atoms **[3-10]**. Unlike other HDS catalysts, the unsupported Mo sulfides have quite high activity on 4,6-DMDBT HDS as compared with DBT HDS (approximately 0.8 times compare with 2-6 times as reported in the literature).

The effect of the Me/(Me+Mo) atomic ratio (Me=Co or Ni) on the HDS activity of both NiMo and CoMo catalyst is shown in **Figure 3-7**. The effect of Ni promoter was reported in previous year and compared with that of Co promoter in this study. For both series of catalysts, the HDS activity increased with increasing amount of Co or Ni, but it reached a maximum at the 0.5 of Me/(Me+Mo) ratio and then decreased at higher ratio. Higher addition of promoters may help to generate more active phase on the catalysts

because of better incorporation with the crystallites of Mo sulfide in small cluster. In this study, therefore, it is certainly observed the significant synergetic effect of Ni and Co promoters on the unsupported Mo sulfide catalysts for simultaneous HDS of DBT and 4,6-DMDBT as shown in **Figure 3-7**.

Table 3-1. Product distribution for the simultaneous HDS of DBT and 4,6-DMDBT over unsupported Mo, NiMo and CoMo sulfide catalysts

Catalysts	Mo	NiMo[c]	CoMo[c]
DBT Conversion (%)	28.0	58.5	63.5
Selectivity(%)			
THDBT	42.9	6.2	4.0
BP	30.0	41.1	78.1
CHB	20.6	42.6	12.9
BCH	6.5	10.1	5.0
THDBT/CHB	2.1	0.1	0.3
HYD/DDS[a]	2.4	1.4	0.3
4,6-DMDBT Conversion (%)	32.2	47.3	56.5
Selectivity (%)			
THDMDBT	87.0	37.8	33.4
3,3'DMBP	7.7	33.2	43.1
MCHT	4.0	27.0	20.1
DMBCH	1.2	2.0	3.4
THDMDBT/MCHT	21.5	1.4	1.7
HYD/DDS[b]	12.2	2.0	1.3

[a] HYD/DDS = Selectivity (THDBT+CHB+BCH)/Selectivity (BP)
[b] HYD/DDS = Selectivity (THDMDBT+MCHT+DMBCH)/Selectivity (3,3'DMBP)
[c] Me/(Me+Mo) = 0.43

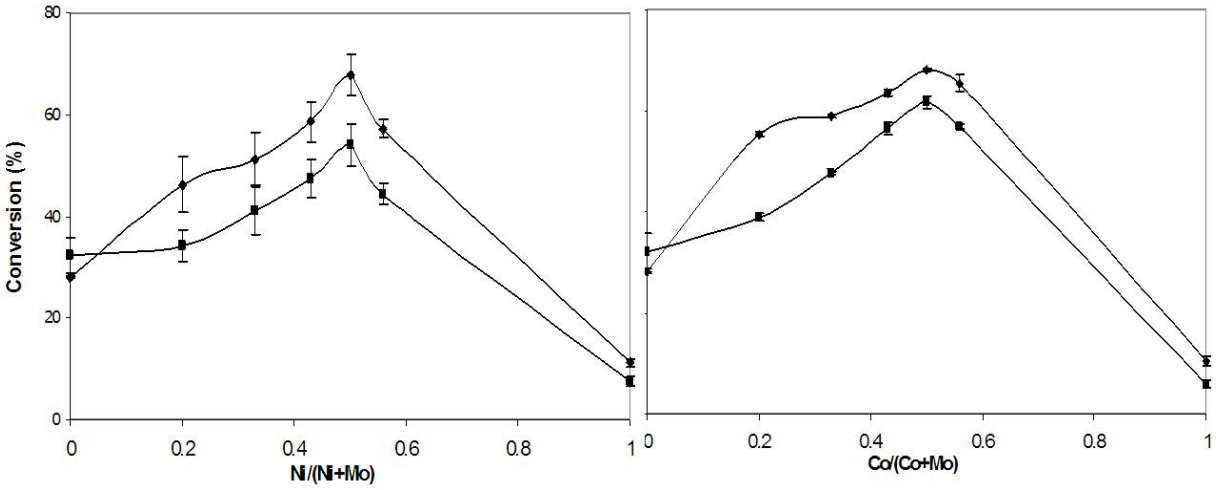

(a) (b)

Figure 3-7. The effect of Me/(Me+Mo) atomic ratio (Me=Ni or Co) on HDS of DBT and 4,6-DMDBT over unsupported (a) NiMo and (b) CoMo sulfide catalysts (◆ DBT conversion ,■ 4,6-DMDBT conversion).

3.1.2.3.3. Comparison between unsupported Mo sulfide catalysts

Table 3-2 shows the physical properties of unsupported Mo sulfides synthesized by the hydrothermal method. The unsupported Mo sulfide has 283 m^2/g of surface area and 0.68 cm^3/g of pore volume. These values are considerably higher than those of other Mo sulfide catalysts in literature where, generally, Mo sulfide has less than 50 m^2/g of surface area. After the addition of promoters, it was observed that the decreases on surface area and pore volume were significant. In the pore size distribution (**Figure 3-8**), the unsupported Mo sulfides show bimodal pore systems and the volume of larger pore size is higher than that of smaller pore size on unsupported Mo sulfide without promoters. However, the volume of larger pore size to smaller pore size was decreased

when the promoters were added. These results indicate that the promoter influences the morphology the unsupported Mo sulfides.

Table 3-2. Surface area, pore volume and average pore size of fresh catalysts prepared from ATTM

Sulfide Catalysts	Surface Area (m^2/g)	Pore volume (cm^3/g)
MoS	283	0.68
NiMoS	199	0.28
CoMoS	168	0.19

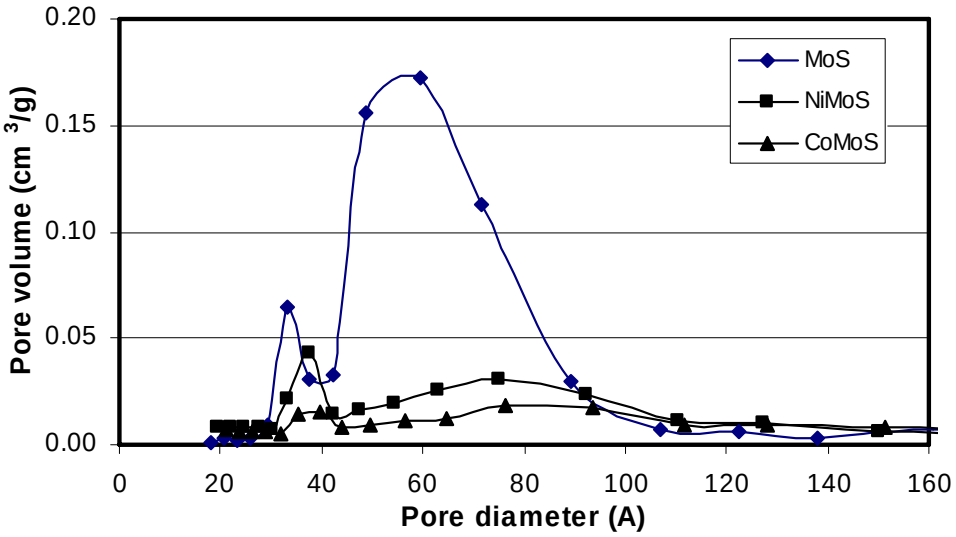

Figure 3-8. Pore distribution of unsupported Mo sulfides with promoters (Ni and Co).

For further characterization of unsupported Mo sulfides, XRD and TEM analysis were conducted. From XRD patterns (**Figure 3-9**) in the comparison to commercial available MoS_2, all unsupported Mo sulfides showed broad X-ray reflections characteristic of a poorly crystallized MoS_2 structures and particularly it become more broad when the promoters were presented. The intensity of most MoS_2 peaks were

decreased significantly and specifically, the (002) peak at 2θ = 14.4° became very low on the unsupported CoMo sulfide. It means that a much smaller size of (002) phase of MoS_2 is generated and Co or Ni is in place of the phase of MoS_2, specifically on the (002) phase. It results in fewer stacked layers and fracture of MoS_2, which is also observed in HRTEM analysis as shown in **Figure 3-10**. On the sulfides with promoters, the diffractions of Ni and Co sulfides were detected due to high loading amount of these metals and they are crystallized Ni_3S_4 and Co_9S_8. These metal (Ni and Co) sulfide particles might help hydrogen adsorb and dissociate. The H species are mobile enough in the conditions of catalysis to attack the MoS_2 particles and create coordinative unsaturation at the edges **[3-11].**

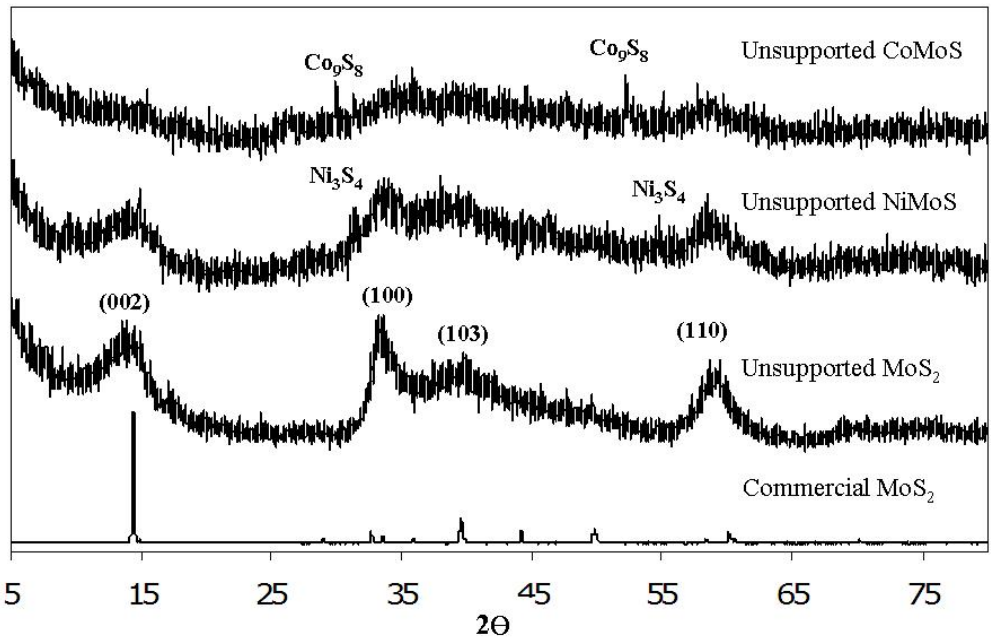

Figure 3-9. XRD patterns of unsupported Mo based sulfide catalysts.

Figure 3-10 shows the HRTEM images of the unsupported Mo sulfides with/without Ni promoter. Unsupported Mo sulfide showed well organized long and

multi-layered stacking of MoS_2. In addition of Ni promoter, however, it is clearly observed the increase of curvature of MoS_2 slabs and the decrease of slab length. Therefore, the HRTEM results coincide with the results of XRD analysis. In the absence of promoters, MoS_2 form large crystallized particles during the hydrothermal synthesis methods. However, the growth of crystallized particles is suppressed when the promoters are incorporated with them.

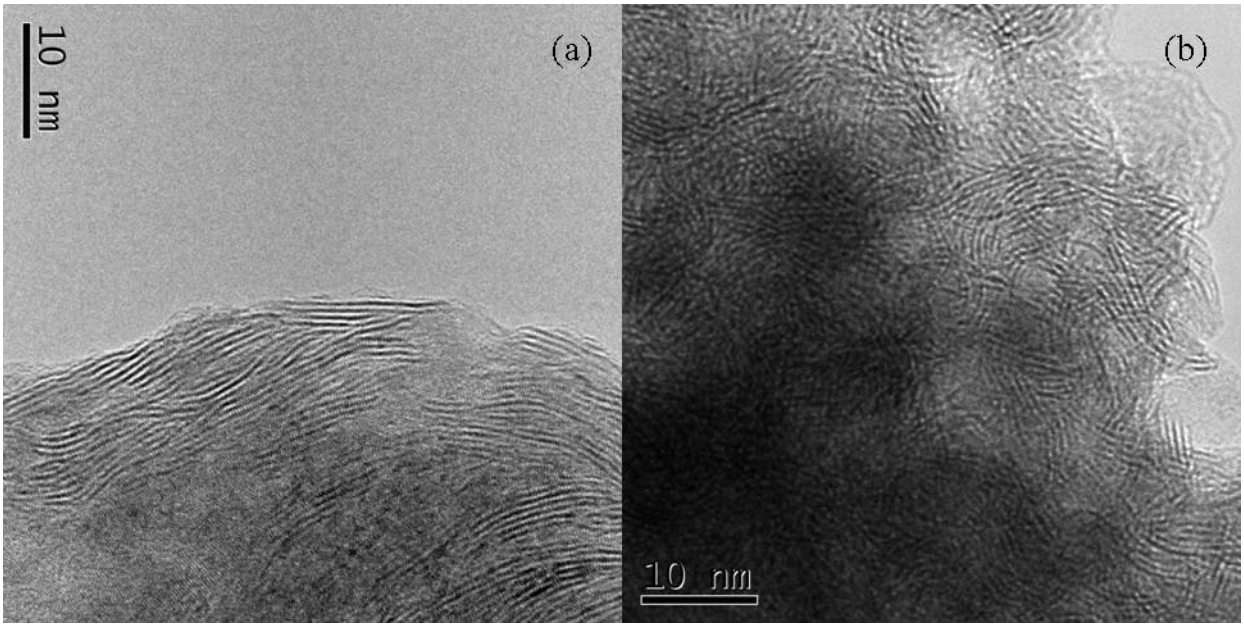

Figure 3-10. HRTEM images of unsupported (a) Mo and (b) NiMo sulfide catalysts.

3.1.3. Summary

3.1.3.1. Adsorptive desulfurization and denitrogenation of LCO

1) GC-PFPD analysis showed that the LCO contains wide range of sulfur compounds from BT (benzothiophene) and alkyl-BTs to alkyl-DBTs (dibenzothiophenes) in molecular size. Major compounds are C_2-BT, specifically 2,3-DMBT and 4-MDBT.

2) Based on the analysis of LCO treated by adsorption and hytrotreating by GC-PFPD, the adsorptive desulfurization on activated carbon prefer to remove sulfur compounds in DBT range due to the adsorbent's excellent adsorption properties for heavy and alkylated sulfur compounds. Hydrotreating favors to remove relatively light sulfur compounds in BT ranges because these sulfur compounds are generally more reactive than heavy sulfur compounds in DBT range, particularly 4,6-DMDBT. Therefore, adsorptive desulfurization and denitrogenation followed by hydrotreating improved considerably the removal of sulfur compounds in LCO.

3.1.3.2. Development of unsupported Mo sulfide catalysts for HDS

1) The unsupported Mo sulfide catalysts with Ni and Co promoters synthesized by hydrothermal method have much higher activity of simultaneous DBT and 4,6-DMDBT HDS than sulfided commercial HDS catalysts (Cr424 and Cr344). Based on the kinetic results, the unsupported NiMo and CoMo sulfides have much higher activity for DDS pathway as well as for HYD pathway than the commercial catalysts.
2) The unsupported Mo sulfide has higher 4,6-DMDBT conversion than DBT conversion at the conditions employed in this study, unlike other conventional HDS catalysts. However, the desulfurized activity of the catalyst was higher on DBT and 4,6-DMDBT and it is because the HDS activity mostly comes from high HDY activity. The addition of promoters (Ni and Co) on the Mo sulfide improved significantly DDS activity and, as well, HDY activity.
3) In the effects of promoters, the large amounts of Ni and Co were added on the unsupported Mo sulfides as compared with conventional supported NiMo and CoMo

catalysts. Therefore, some of promoters were not coordinated with Mo sulfides and their sulfide phases were observed by XRD analysis. These may result in the decrease of surface area and pore volume. However, the addition of promoters generates the increase of curvature of MoS_2 slabs and the decrease of slab length on the basis of XRD and HRTEM analysis because Ni and Co may be placed inside or edge of MoS_2 structure and prevent the growth (or aggregation) of crystallite size. These results provide more active phase for simultaneous HDS of DBT and 4,6-DMDBT.

3.1.4. Future work

1) The activated carbon will be modified to improve the capacity and selectivity of sulfur and nitrogen to other aromatic compounds and contaminants after investigation of fuel composition (nitrogen compounds) of light cycle oil (LCO). Further quantitative analysis of LCO and LCO treated by adsorption and hydrotreating will be conducted with Antek total sulfur and nitrogen analyzer and GC-PFPD/TSD.
2) Adsorptive denitrogenation of the blended LCO with RCO will be performed on activated carbon and modified carbon adsorbents at the same adsorption conditions performed in this study and the hydrodesulfurization of the blend fuels (LCO and RCO) treated by adsorption will also be performed.
3) Newly developed unsupported Mo sulfide catalysts with promoters will be modified further with additive or different preparation method. Hydrotreating will be conducted on these catalysts and noble metal (Pd, Pt and Pd/Pt) catalysts reported previously with different pretreatment (presulfidation, reduction and etc.).

Subtask 3.2. Saturation of Two-Ring Aromatics

As a part of the DOE refinery integration project, this sub-task aims at saturating aromatics for high-quality diesel and distillate fuels. High aromatics content in distillate fuels is undesirable since it lowers the fuel quality and contributes to the formation of environmentally harmful emissions. In general, lower aromatics content leads to increase thermal stability, improve combustion characteristics and less soot formation. The conventional method of dearomatization is by aromatics saturation (hydrogenation) and, typically, sulfided $CoMo/Al_2O_3$ or $NiMo/Al_2O_3$ catalysts are employed. However, these catalysts are most active at higher temperatures where equilibrium limitations may prevent complete hydrogenation. Noble-metal catalysts are active at lower temperatures, where equilibrium limitations can be overcome. However, sulfur-tolerance is a major obstacle to their commercial application.

To meet the fuel performance and compositional specifications for diesel fuel, it is necessary for both RCO and LCO to be hydrogenated. This work focuses on the development of increasingly sulfur-tolerant, noble-metal catalysts for the low-temperature hydrotreating and dearomatization (LTHDA) of distillate fuels for the production of ultra-clean and low-aromatic diesel fuels. In this reporting period, the influence of zeolite support type, silica coating of catalysts and hybrid catalysts were examined. It is expected that the contact of sulfur molecules with noble metal particles on zeolite surface can be eliminated by silica coating on catalyst surface; meanwhile, the noble metal particles inside the zeolite pores may be still accessible to hydrogen molecules. Therefore, we can observe the performance of metal particles inside the zeolite pore excluding the catalytic activity on catalyst surface. Hybrid catalyst is

prepared in order to verify the catalyst design concept proposed by Song **[3-12, 3-13]** and compared the activity and resistance to sulfur poisoning with other uniform catalyst.

3.2.1 Experimental

3.2.1.1 Catalyst preparation

Zeolite supports were obtained from Zeolyst International (formerly PQ Corporation). All zeolite supports were first calcined in air flow (~60 mL/min) for 4 hours at 450ºC, with a heating rate of approximately 1.5ºC/min, before catalyst preparation. Thus, any supports received in the NH_4^+ form were converted to the H^+ form. Properties of catalyst supports used in this work were summarized in **Table 3-3**. As zeolite was the sodium from, it needed pretreatment for ion exchange before calcination. A zeolite was dispersed in 1 M ammonium chloride solution. The zeolite and supernatant solution were then agitated by continuous shaking at room temperature for 3 h to come to equilibrium and then separated by vacuum filtration. The zeolite was rinsed with de-ionized water to remove excess ammonium solution. This procedure was repeated 3 times for zeolite to change to ammonium form thoroughly. The ammonium ion exchanged zeolite was dried in an oven at 50ºC and calcined as the same way described above.

Table 3-3. Properties of zeolite supports as received.

Support Type	Support Code	SiO_2/Al_2O_3 Ratio	Surface Area (m^2/g)	Pore size (Å)	Cation Form
Mordenite	CBV30A	38	512	7.0×6.5 (L) 5.7×2.6 (M) 4.8×3.4 (S)	NH_4^+
Y Zeolite	CBV720	30	780	11.2×11.2 (L) 7.4×7.4 (S)	H^+
A Zeolite	Advera 401	1.0	425	4.1×4.1	Na^+

All catalysts were prepared by incipient wetness impregnation (IWI) technique. The pore volume of a given support was determined by measuring the volume of water added dropwise to a known weight of the support until the support changed appearance from dry to slightly liquid. The appropriate amount of metal precursor, calculated for the desired metal loading, was dissolved in a total volume of water (and HCl) equivalent to the pore volume for the support being impregnated.

All catalysts in this work were prepared with a metal loading of 2 wt%. The solution of precursor metal salt was then added dropwise to the support. After a few drops were added, the mixture was stirred thoroughly, then a few more drops were added and the mixture was stirred again. Impregnation continued in this manner until all of the metal solution was loaded on the support. After the impregnation was complete, the catalysts were dried at 110°C for at least 2 h and then calcined in air flow (~60 ml/min) at 450°C for 4 h at a ramping rate of approximately 1.5°C/min. The calcined catalysts were then palletized, crushed and sieved to a particle size of 18-35 U.S.A. Standard Testing Sieve Mesh (0.5–1.0 mm). The metal precursors used in this study were $PdCl_2$ (Sigma Aldrich). In order to dissolve $PdCl_2$ in water, it was necessary to add HCl to form soluble $PdCl_4^{2-}$ species. For all catalysts prepared, HCl was added in sufficient quantities to dissolve $PdCl_2$ (2.35 g of 37% HCl solution for 0.167 g of $PdCl_2$).

Pd/HA and Pd/CBV30A catalysts were modified with TEOS by sol-gel process to form the silica wall on the catalyst surface. Prepared catalyst (1.5 g) was mixed with 20ml of tetraethyl orthosilicate (TEOS, Aldrich, 98%) in a conical flask at room temperature with continual agitation for 12 h. The sample was settled using a centrifuge and the supernatant TEOS was decanted and then evaporated off in an oven at 80°C

overnight. The sample was then mixed with 2.5 ml of acetone in order to hydrolyze the remaining organo-silicate bonds and fix the coating and the acetone was then evaporated to dryness 3-14]. The Pd/HA-Pd/Y720 and Pd/HA-SiO_2-Pd/Y720 hybrid catalysts were prepared by physically mixing and co-grinding Pd/HA and Pd/Y720 or Silica coated Pd/HA and Pd/Y720, respectively, at the ratio of 1:1 by weight, and pressure molding of mixture to granules (18-35 mesh).

Table 3-4. The list of catalysts prepared in this study

Catalyst	Metal Loading (wt%)	Precursor Metal	Support (SiO_2/Al_2O_3 Ratio)	Notes
Pd/CBV720	2.0	$PdCl_2$	Y Zeolite (30)	
Pd/CBV30A	2.0	$PdCl_2$	Mordenite (38)	
Pd/HA	2.0	$PdCl_2$	A Zeolite (1.0)	
Pd/CBV30A-SiO_2	2.0	$PdCl_2$	Mordenite (38)	Coated with
Pd/HA-SiO_2	2.0	$PdCl_2$	A Zeolite (1.0)	TEOS
Pd/HA-Pd/CBV720	2.0	$PdCl_2$	A and Y zeolite	Mixed at the
Pd/HA-SiO2-Pd/CBV720	2.0	$PdCl_2$	A and Y zeolite	ratio of 1:1

3.2.1.2 Catalytic evaluation in hydrogenation experiments

Feed composition for hydrogenation experiments was approximately 20 wt% tetralin (Aldrich, 99%), 75 wt% hexadecane (Aldrich, 99+%), and 5 wt% nonane (Aldrich, 99+%), with 100ppm of sulfur added as benzothiophene (BT) (Aldrich, 99%).

The reaction was carried in a down flow reactor system. For each experiment, 0.5 g of catalyst particles (screened between18-35 meshes) were used. Catalyst particles were mixed with 3.0 g of α-Al_2O_3 particles as a diluent. The volume of catalytic bed in all experiments was around 9.65 ml. Before each experiment, catalysts were reduced *in situ* under a hydrogen flow of 100 ml/min and the pressure was maintained under 100 psi. The temperature was increased from room temperature to 225°C at a rate of 2°C/min. The temperature was maintained at 225°C for two hours prior to the introduction of

liquid feed. After the reduction step was complete, the pressure was increased to 600 psi and the hydrogen flow was reduced to 80 ml/min. Liquid feed was then introduced at a rate of 0.08 ml/min. This corresponds to a gas-to-liquid ratio (G/L) of approximately 1000 and a weight hourly space velocity (WHSV) of approximately 8 h^{-1}. After starting the HPLC pump to introduce liquid feedstock, the system was allowed to equilibrate for 1.5 h. Therefore, 90 min after the start of feedstock was designated as time-on-stream (TOS) equal to zero. Liquid samples were then collected at 30 min intervals until the experiment was terminated. The liquid products were analyzed using a Shimadzu GC-17a gas chromatograph coupled with a Shimadzu QP-5000 quadrupole mass spectrometer. The capillary column (30m x 0.25mm, Restek XTI-5) was coated with a 0.25μm stationary phase of 5% phenyl-95% methyl polysiloxane.

3.2.1.3 Catalyst characterization

In order to examine the characteristics of catalysts prepared, several different analysis techniques were employed. Surface morphology was explored by scanning electron microscopy (SEM) using a Hitachi S-3500N. Micromeritics AutoChem 2910 was used for temperature programmed reduction (TPR) and Temperature Programmed desorption (TPD). TPR is used to reveal the temperature at which the reduction occurs and TPD analysis of hydrogen can determines the type and strength of active metal sites available on the surface of a catalyst from measurement of the amount of gas desorbed at various temperatures.

3.2.2 Results and discussion

3.2.2.1 Hydrogenation of tetralin over Pd on various types of Zeolite

3.2.2.1.1 Effect of zeolite type

The results for conversion of tetralin over 2 wt% Pd on various types of zeolite (mordenite, Y and A zeolite) were compared and the trans- and cis- decalin composition were also shown below. Y zeolite supported catalyst exhibited the greatest sulfur tolerance among the catalysts tested. As shown in **Figure 3-11**, Pd/CBV30A and Pd/HA catalysts deactivated drastically and showed less than 30% tetralin conversion after 7 h. In case of Pd/HA, the catalytic activity disappeared at 5 h. On the other hand, the conversion of tetralin was maintained around 80% with the Pd/CBV720 catalyst after 7 h. As deactivation due to sulfur proceeds, the selectivity toward trans-decalin decreases and all trans- and cis- decalin compositions are converged on around 62% and 38%, respectively. It is expected that mordenite is more acidic (SiO_2/Al_2O_3:38) and would exhibit greater sulfur tolerance due to the imparting of electron deficiency on the Pd metal by the acid sites. However, Y zeolite shows higher tetralin conversion which can be explained with the type of pore structure and large BET surface area from the data of previous report.

(a) (b)

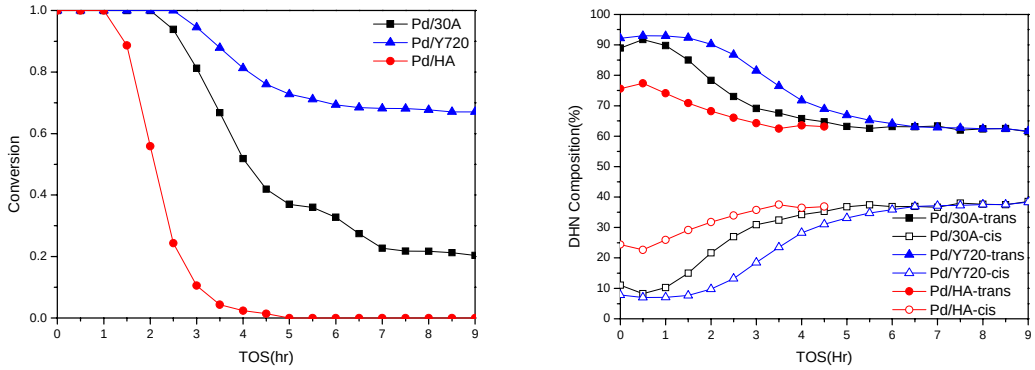

Figure 3-11. (a) Conversion vs. TOS for the hydrogenation of tetralin and **(b)** t-DHN, c-DHN selectivity for the hydrogenation of tetralin at 225 °C and 600 psig hydrogen pressure in the presence of 100 ppm sulfur as BT.

3.2.2.1.2 Effect of silica coating

Two Pd catalysts, Pd/CBV30A-SiO_2 and Pd/HA-SiO_2, were prepared by sol-gel method to examine the effects of internal pore on catalytic characteristics and performance. It was hypothesized that since the molecule size of tetraethyl orthosilicate (TEOS) is too large to enter the small pore of the zeolite, a silica wall might be formed not inside of zeolite pore but on its surface, allowing catalysts to perform inside pore opening but preventing outer surface reaction of zeolite.

The effect of silica coating was examined with two types of catalysts, Pd/CBV30A-SiO_2 and Pd/HA-SiO_2 and presented in **Figure 3-12** and **Figure 3-13**, respectively. For comparison, each result was plotted together with non silica coated catalysts. As seen in **Figure 3-12**, Pd/CBV30A-SiO_2 did not maintain tetralin conversion but drastically decreased. It can be explained that TEOS might coat outside of the large

pore opening and reduce the pore size, but the assumption was unclear and needed to be examined by means of further characterization technique. This problem was dealt with temperature programmed reduction profile in section 3.2.2.2.2 in order to investigate the reduction status of catalysts.

(a) (b)

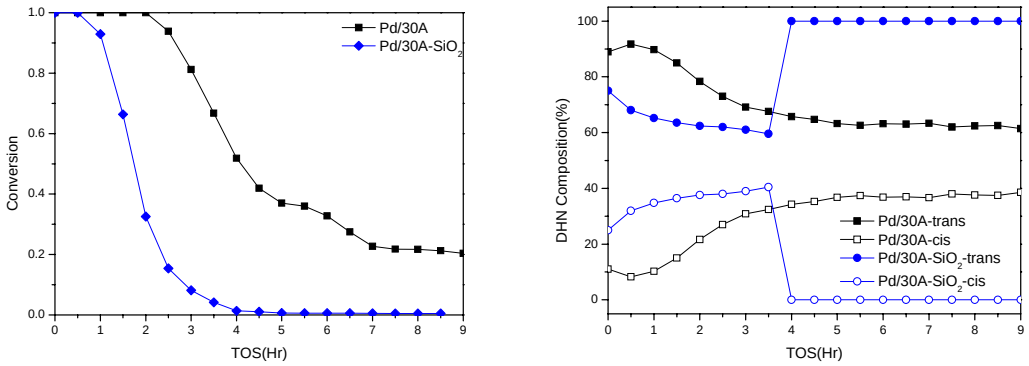

Figure 3-12. (a) Conversion vs. TOS for the hydrogenation of tetralin and **(b)** t-DHN, c-DHN selectivity for the hydrogenation of tetralin over Pd/CBV30A and Pd/CBV30A-SiO_2 at 225 °C and 600 psig hydrogen pressure in the presence of 100 ppm sulfur as BT.

From **Figure 3-13**, the results of tetralin conversion with Pd/HA and its coated catalysts were remarkably similar. As hypothesized, silica coating was successfully formed and the pore opening of zeolite remained allowing hydrogen molecules to enter but barring bulky organic sulfur compound like benzothiophene. However, inorganic sulfur, H_2S deactivated the novel metal inside pore and reduced tetralin conversion. There is a distinctive trend of trans-decalin selectivity over two silica coated catalysts. After the tetralin conversion drastically decreased, 100% of trans-decalin selectivity was shown. Since it was reported that SiO_2 wall does not have catalytic activity, it is an indication

that coated wall might influence the surface structure of pore opening, but there are no supporting results. Therefore, the effect of silica coating remains to be determined.

(a) (b)

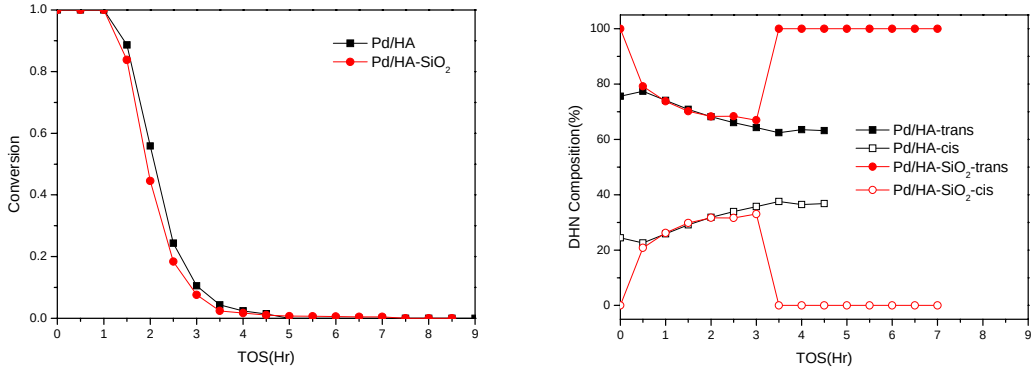

Figure 3-13. Figure 1 (a) Conversion vs. TOS for the hydrogenation of tetralin and **(b)** t-DHN, c-DHN selectivity for the hydrogenation of tetralin over Pd/HA and Pd/HA-SiO_2 at 225°C and 600 psig hydrogen pressure in the presence of 100 ppm S as BT.

Figure 3-14 shows the comparison between Pd/HA-SiO_2 and Pd/CBV30A-SiO_2. It is difficult to speculate why coated catalysts showed similar trend of conversion and decalin selectivity. When the catalytic activity decreases, the productivity of trans-decalin suddenly increased to 100%, and cis-decalin disappeared.

The effect of the Me/(Me+Mo) atomic ratio (Me=Co or Ni) on the HDS activity of both NiMo and CoMo catalyst is shown in **Figure 3-7**. The effect of Ni promoter was reported in previous year and compared with that of Co promoter in this study. For both series of catalysts, the HDS activity increased with increasing amount of Co or Ni, but it reached a maximum at the 0.5 of Me/(Me+Mo) ratio and then decreased at higher ratio. Higher addition of promoters may help to generate more active phase on the catalysts

because of better incorporation with the crystallites of Mo sulfide in small cluster. In this study, therefore, it is certainly observed the significant synergetic effect of Ni and Co promoters on the unsupported Mo sulfide catalysts for simultaneous HDS of DBT and 4,6-DMDBT as shown in **Figure 3-7**.

(a) (b)

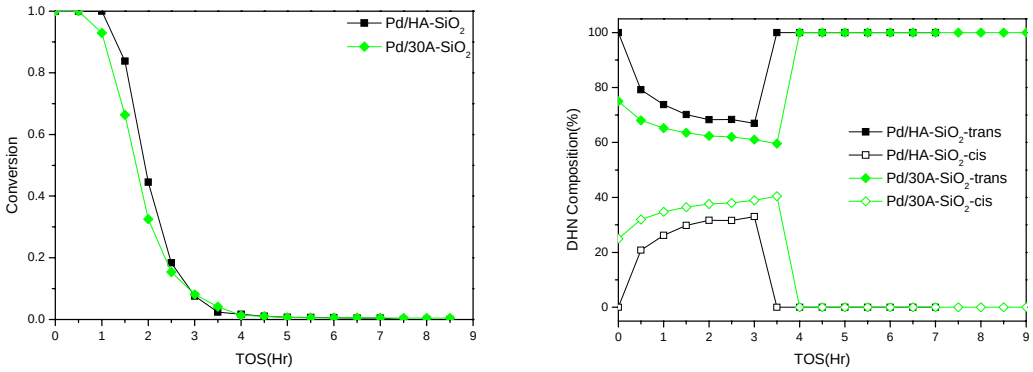

Figure 3-14. (a) Conversion vs. TOS for the hydrogenation of tetralin and (b) t-DHN, c-DHN selectivity for the hydrogenation of tetralin over Pd/CBV30A-SiO_2 and Pd/HA-SiO_2 at 225°C and 600 psig hydrogen pressure in the presence of 100 ppm sulfur as BT.

3.2.2.1.3 Effect of hybrid catalysts

Hybrid catalysts are prepared in order to verify the catalyst design concept proposed by Song **[3-12, 3-13]**. The Pd/CBV720 catalyst has a uniform pore size distribution and is used as a reference to compare the catalytic activity. **Figure 3-15** and **Figure 3-16** shows the reaction conversion and selectivity of decalin over Pd/HA, Pd/CBV720, Pd/HA-Pd/CBV720 hybrid catalyst and Pd/CBV720, silica coated Pd/HA catalyst, Pd/HA-SiO_2-Pd/CBV720 hybrid catalyst, respectively. Even though it was reported that Pd/HA-Pd/Y zeolite is more sulfur resistant, Pd/CBV720 has higher

conversion than other catalysts in this research. However, these results are not enough evidence to prove the design concept. As the mixing ratio is fixed to 1:1, the amount of Pd/CBV720 might not be sufficient to show significant results for the concept of hybrid catalyst. The effect of hybrid catalysts needs to be further examined by increasing the ratio of Pd/CBV catalyst.

(a) (b)

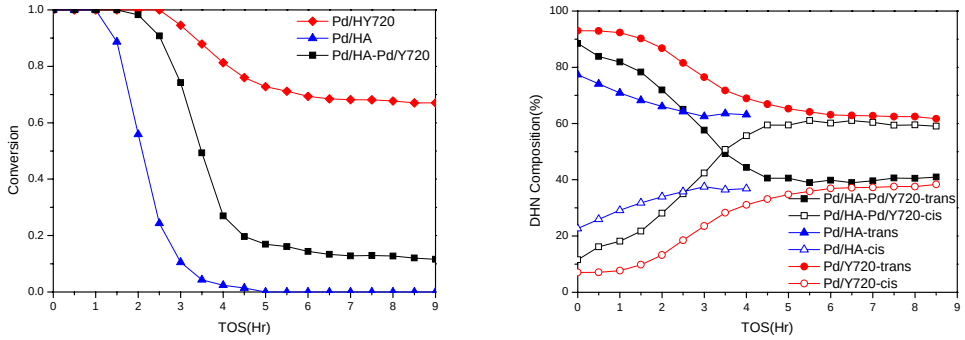

Figure 3-15. Figure 2 (a) Conversion vs. TOS for the hydrogenation of tetralin and **(b)** t-DHN, c-DHN selectivity for the hydrogenation of tetralin over Pd/CBV30A-SiO_2 and Pd/HA-SiO_2 at 225 °C and 600 psig hydrogen pressure in the presence of 100 ppm sulfur as BT.

(a) (b)

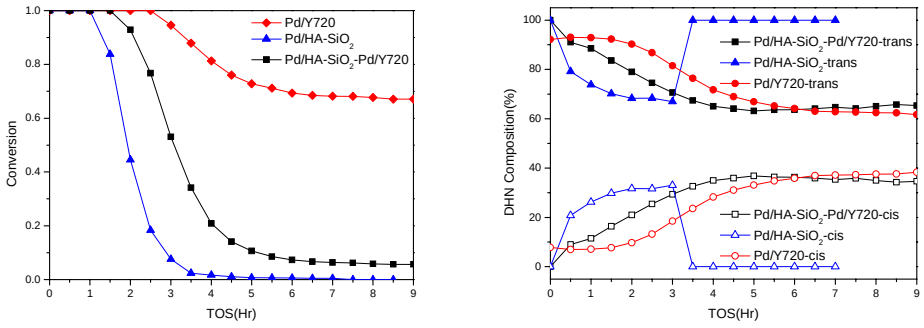

Figure 3-16. Figure 3 (a) Conversion vs. TOS for the hydrogenation of tetralin and **(b)** t-DHN, c-DHN selectivity for the hydrogenation of tetralin over Pd/CBV30A-SiO_2 and Pd/HA-SiO_2 at 225 °C and 600 psig hydrogen pressure in the presence of 100 ppm sulfur as BT.

Figure 3-17 shows the comparison between Pd/HA-SiO_2-Pd/CBV720 and Pd/HA-Pd/CBV720. Compared to other catalysts, including Pd/HA-SiO_2-Pd/CBV720 hybrid catalyst which has high trans-decalin selectivity, Pd/HA-Pd/CBV720 hybrid catalyst shows high cis-decalin selectivity. As mentioned before, it should be also further studied for finding the optimal ratio of hybrid catalysts.

(a) (b)

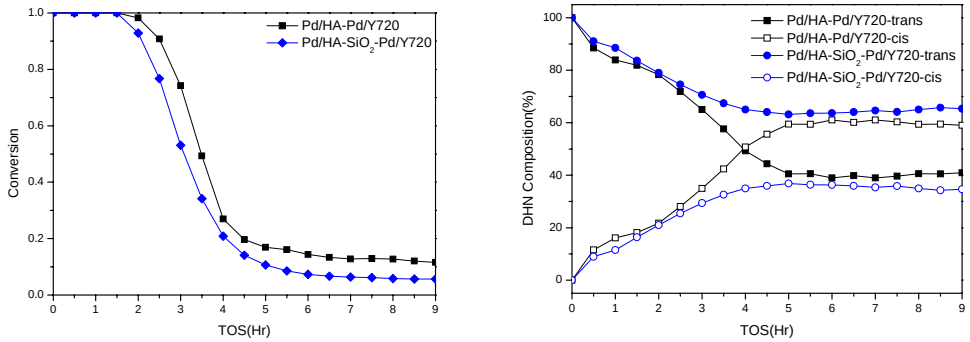

Figure 3-17. Figure 4 (a) Conversion vs. TOS for the hydrogenation of tetralin and **(b)** t-DHN, c-DHN selectivity for the hydrogenation of tetralin over Pd/CBV30A-SiO_2 and Pd/HA-SiO_2 at 225 °C and 600 psig hydrogen pressure in the presence of 100 ppm sulfur as BT.

3.2.2.2 Characterization

3.2.2.2.1 SEM image of catalysts prepared

Figure 3-18, **Figure 3-19** and **Figure 3- 20** show SEM images of catalysts prepared, zeolite examined before Pd impregnation, Pd impregnated zeolite and silica coated zeolite, respectively. As shown in these figures, it is supposed that no significant morphological change was occurred during catalyst preparation and coating procedure. The shapes of HA zeolite particle and its derivatives looked like regular hexahedrons

with edge lengths between 30-35 μm. Y zeolite CBV720 was composed of small even particles, which sizes were 3-7 μm. The crystallites of Mordenite CBV30A and its derivatives were uneven and small particles with various sizes (1-8μm) aggregated and formed large particles. These small sized particles of Mordenite and Y zeolite which increase contact area might cause high catalytic activity. Compared to these zeolites, HA zeolite might have mass transfer (diffusion) limitation caused from its large particle size.

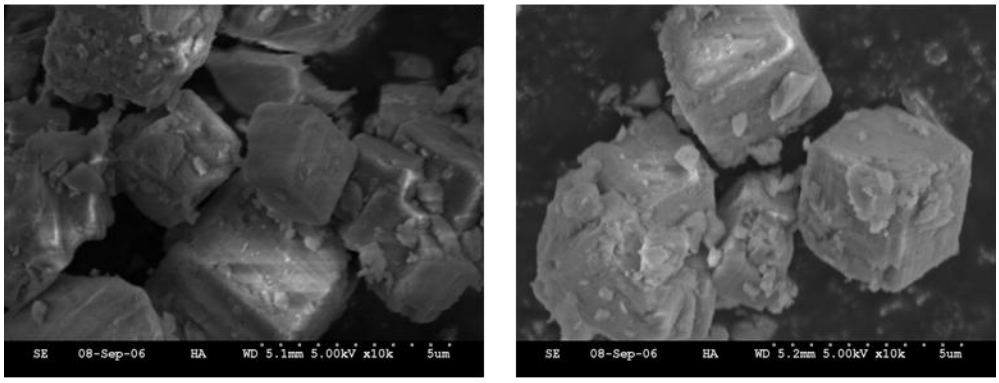

(a)HA (zeolite A)

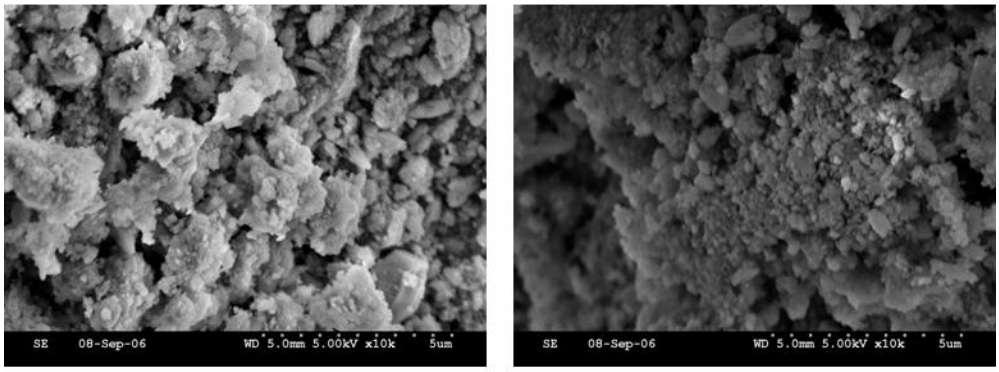

(b) CBV30A (Mordenite)

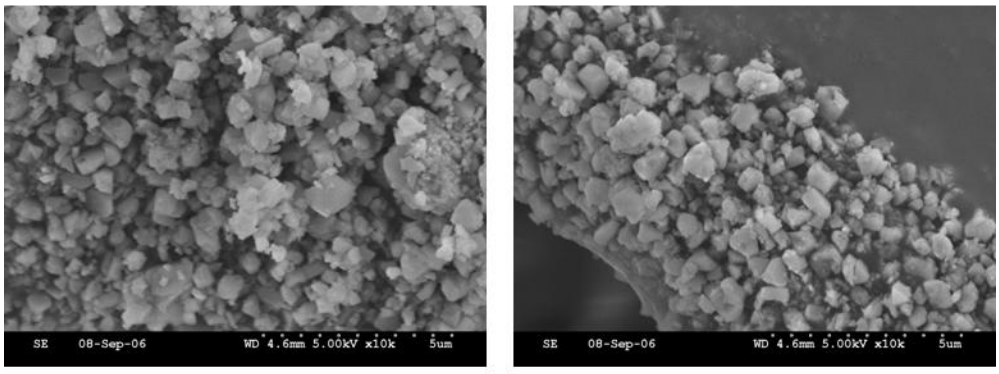

(c) CBV720 (zeolite Y)

Figure 3-18. SEM images of zeolite used in this research (a) HA (zeolite A), (b) CBV30A (Mordenite), and (c) CBV720 (zeolite Y).

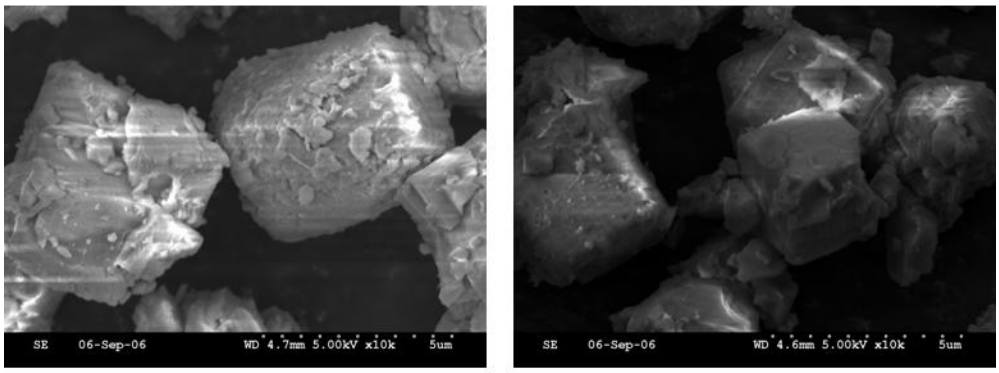

(a) 2wt% of Pd on HA (Pd/HA catalyst)

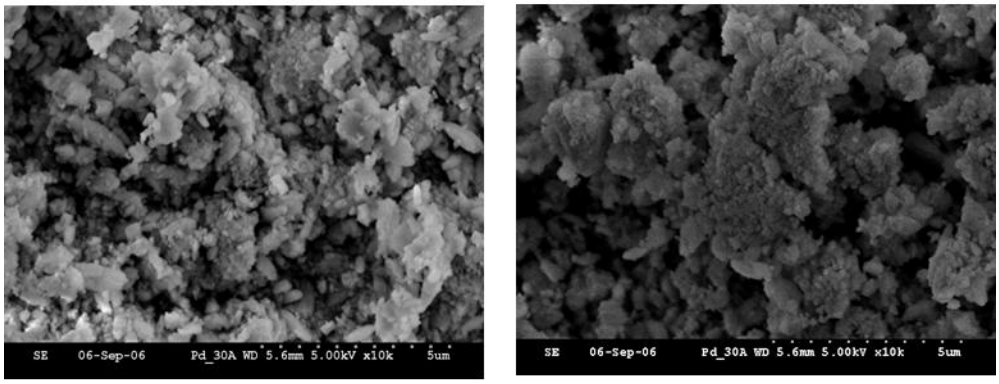

(b) 2wt% Pd on CBV30A (Pd/30A catalyst)

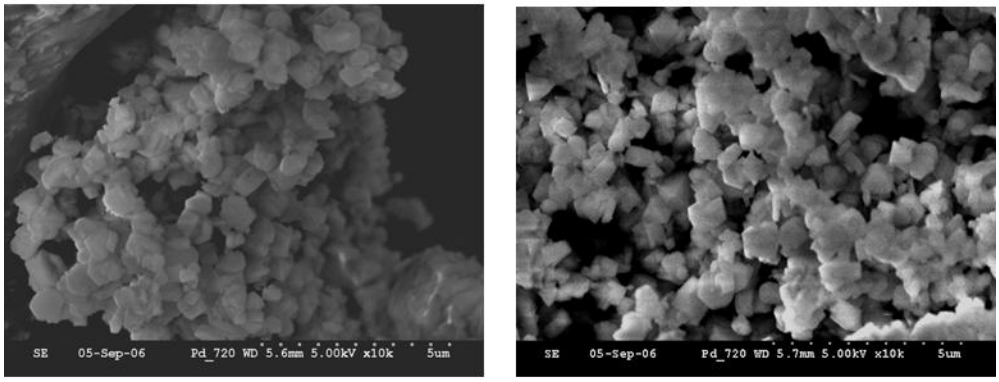

(c) 2wt% Pd on CBV720 (Pd/Y720 catalyst)

Figure 3-19. SEM image of catalysts prepared in this research, (a) 2wt% of Pd on HA (Pd/HA catalyst), (b) 2wt% Pd on CBV30A (Pd/30A catalyst), (c) 2wt% Pd on CBV720 (Pd/Y720 catalyst).

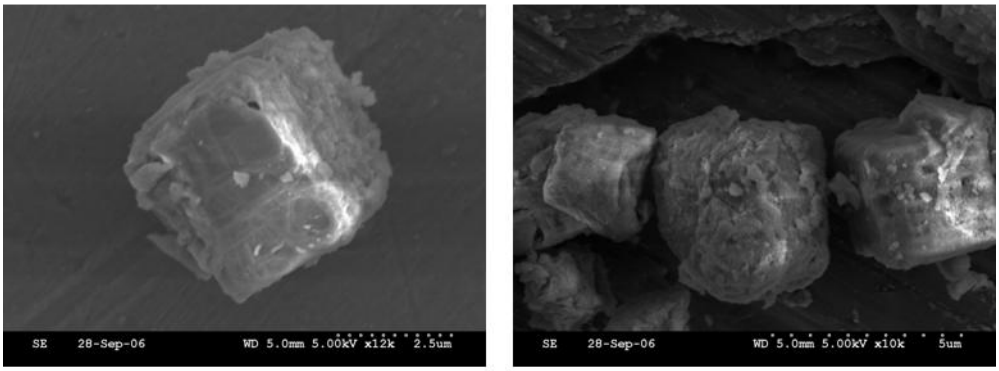

(a)Pd/HA-SiO_2

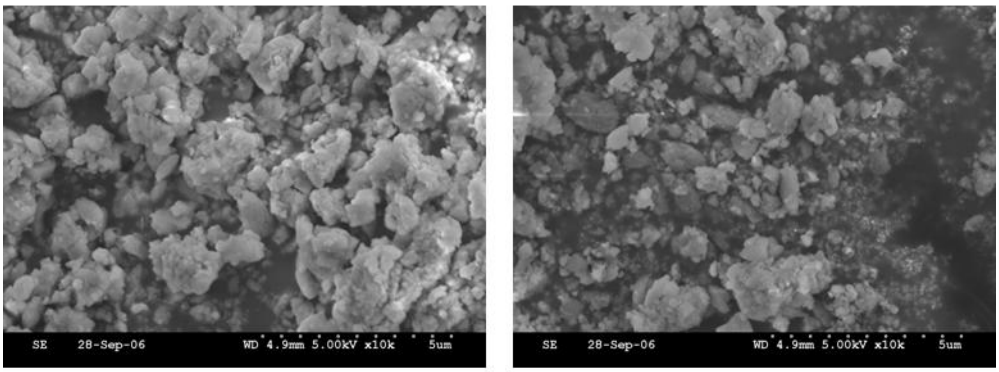

(b)Pd/CBV30A-SiO_2

Figure 3- 20. SEM image of catalysts coated with TEOS in this research, (a)Pd/HA-SiO_2 and (b)Pd/CBV30A-SiO_2.

3.2.2.2.2 Temperature programmed reduction of catalysts

Figure 3-21 shows the temperature programmed reduction profiles of catalysts prepared in this study. The positive sharp peak of Pd/30A and Pd/HA at the low temperature (70^oC) is caused by H_2 evolution from Pd hydride decomposition. TPR results of Pd/Y720 only shows one single negative peak. The negative broad peaks are contributed by H_2 consumption due to the reduction of Pd^{2+} ions to Pd^o atoms. **Figure 3-21** also shows that the negative peak of silica coated Pd/30A is shifted to right, which

means it is harder to fully reduce to Pd^o form at the reduction temperature in the flow reactor.

(a)

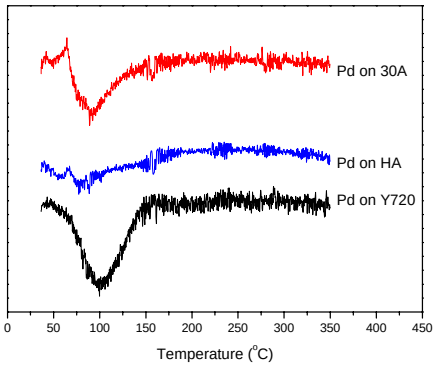

(b)

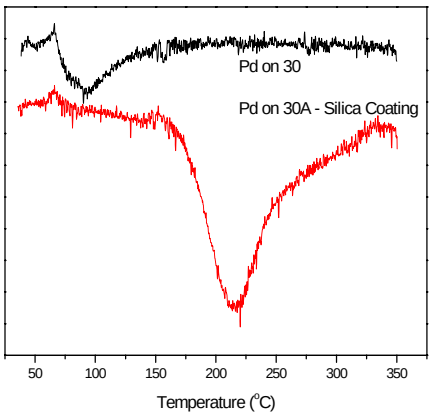

(c)

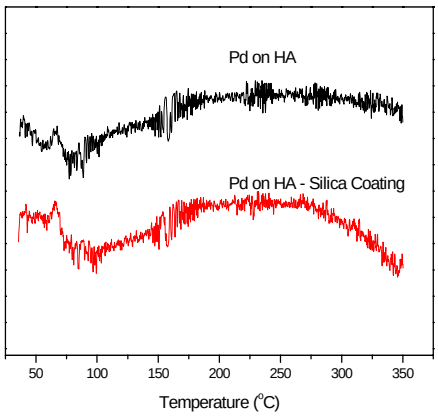

Figure 3-21. Temperature programmed reduction profile of catalysts prepared (a) Pd on CoA, Ha, Y720, (b) Pd on 30A and 30A-Silica coating, and (c) Pd on HA, and HA-Silica Coating.

3.2.2.2.3 Temperature programmed desorption of catalysts

Figure 3-22 exhibits the result for TPD of hydrogen over various zeolite supported palladium catalysts. They are almost the same in terms of peak trend except

that the desorption peak in Pd/CBV30A appears at higher temperature than the others. This implies that the hydrogen adsorbed in Pd/CBV30A is more difficult to remove than other catalysts.

(a) (b)

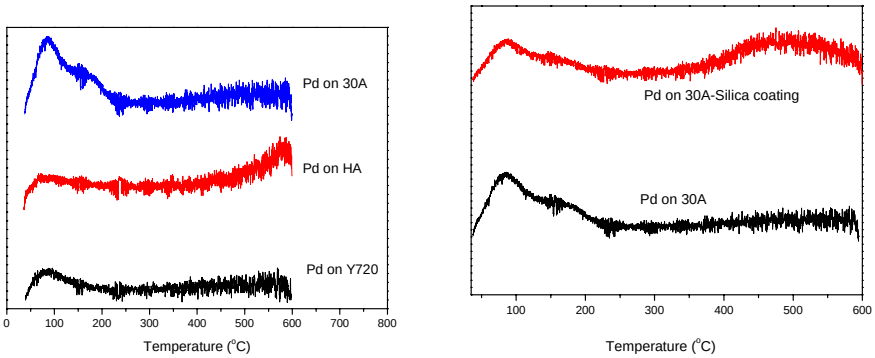

(c)

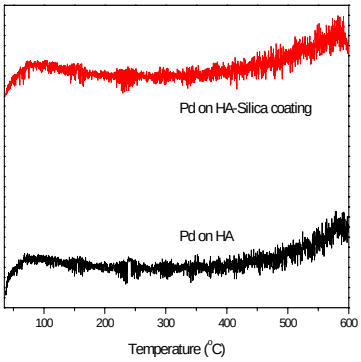

Figure 3-22. Temperature programmed desorption profile of catalysts prepared (a) Pd on CoA, Ha, Y720, (b) Pd on 30A and 30A-Silica coating, and (c) Pd on HA, and HA-Silica Coating.

3.2.3 Summary

Based on experiments on various catalysts for the hydrogenation of tetralin at 225°C and 600 psig of hydrogen pressure, in the presence of sulfur, and also on the characterization of the catalysts prepared for this study, the following conclusions can be made:

1) Y-zeolite supported catalysts exhibit higher sulfur tolerance than any of the other supports tested under the reaction conditions and methods of catalyst preparation employed in this study.
2) The silica wall made from TEOS was well coated onto the catalyst surface and didn't affect the catalytic conversion of Pd on HA catalyst. However, the coated Pd on CBV30A catalyst needs a higher reduction temperature.
3) The selectivity of trans- and cis-Decalin on all catalysts prepared converged into 62% and 38%, respectively. However, Pd/HA-Pd/CBV720 hybrid catalyst showed high cis-decalin selectivity. On the other hand, 100% of trans-decalin selectivity was observed after catalysts deactivated at the test of silica coated catalysts, which remains to be further examined.
4) There was no discernable morphological change observed during the preparation of catalyst. The size of HA zeolite particle and the catalysts prepared from it is around 5 times bigger than Y zeolite CBV720 and Mordenite CBV30A, which might cause mass transfer (diffusion) limitation and low catalytic conversion.
5) The hybrid catalyst should be further studied by changing the ratio of catalysts.

Subtask 3.3. Value-Added Chemicals from Naphthalene and Biphenyl

The shape-selective alkylation of naphthalene is carried out to develop 2,6-dialkylnaphthalene, which is one of monomers for highly value-added chemicals for making advanced polymer materials such as liquid crystalline polymers (LCPs). LCPs have outstanding mechanical properties at high temperature, excellent chemical resistance, and good weatherability. However, the key challenge lies in the selection of materials for shape-selective catalysis for the formation of 2,6-dialkylnaphthalne (2,6 DMN). This year, we developed new catalytic materials such as microporous aluminophosphate (AlPOs) and their modified acidic versions with different metals, ZSM-5 and Fe-ZSM-5. The new materials were developed by a classical hydrothermal synthesis and new and convenient dry-gel conversion method. The ZSM 5 was modified with iron using the impregnation method. The developed materials will be evaluated for alkylation of 2-methylnaphthalene and biphenyl.

3.3.1. Synthesis of magnesium containing AlPO-11 by dry-gel conversion method

Aluminophosphate molecular sieves are a new class of microporous crystalline materials. In 1982, Wilson et al. first reported the synthesis of AlPOs molecular sieves by using a hydrothermal synthesis method **[3-15].** Microporous materials such as zeolites and aluminophosphate molecular sieves ($AlPO_4$-n) are widely used in catalysis and separations, and are being developed for applications in membranes, sensors, optics, etc. **[3-16].** AlPO-11 is one of the microporous aluminophosphate materials developed by Flanigen et al. in 1982 **[3-17]**. It has a three dimensional structure with orthorhombic symmetry **[3-18]**. These materials are characterized by a 1-dimensional channel system

parallel to the c-axis with elliptical 10-membered ring with pore dimension of 0.39 x 0.63 nm **[3-19]**. The magnesium substituted MAPO-11, which has the acidic version of AEL structure might exhibit shape-selective catalysis of methylation of naphthalene.

Recently, new crystallization methods, such as microwave technique **[3-20]** and dry-gel conversion technique **[3-21, 3-22]** have been developed in zeolite synthesis in order to reduce the crystallization time and consumption of structure directing agent, respectively. The different aluminosilicate **[3-22, 3-23]**, boron-substituted aluminosilicate **[3-24],** titanium-substituted aluminosilicate **[3-25, 3-26],** and aluminophosphates such as AlPO-5, AlPO-11, SAPO-5 **[3-27]**, MAPO-36 **[3-28],** MAPO-5 **[3-29, 3-20]** and series of alkaline earth metal-substituted MAPO-5 (M: Mg, Ca, Sr and Ba) **[3-31]** molecular sieves have been synthesized by DGC method. The method has the following advantages over the hydrothermal crystallization method: allows nearly complete conversion, reduces the consumption of structure-directing agents, and involves minimization of waste disposal and reduction of reactor volume **[3-21]**. The uniform crystals with smaller particle size and also improvement of catalytic activity can be obtained by this method **[3-32, 3-33]**. Moreover, there are some examples in which dry-gel conditions are useful or convenient to form particular phase and properties **[3-22, 3-23, 3-28, 3-33]**.

In this study, we first report the synthesis of MAPO-11 by DGC method. The crystallization behavior and properties of MAPO-11 was investigated in different synthesis methods. Catalytic performance was studied for alkylation of naphthalene and biphenyl.

3.3.1.1 Synthesis

The syntheses of Mg-containing AEL were carried out by HTS and DGC methods. DGC method is divided into two inter related techniques: steam assisted conversion (SAC) and vapor-phase transport (VPT). Here, we verified HTS, SAC and VPT methods for the synthesis of MAPO-11. A typical gel composition was as follows: $1.0Al_2O_3$-0.10MgO-$1.0P_2O_5$-1.0DPN-$40H_2O$.

In a typical procedure of HTS, aluminum isopropoxide (8.33 g, 20.0 mmol) was mixed in water (7.72 g). To this suspension, 85% phosphoric acid (4.62 g, 20.0 mmol) diluted in water (3.00 g) was added dropwise over a period of 0.5 h with constant magnetic stirring. To the resulting mixture, a solution of magnesium acetate (0.43 g, 2.0 mmol, with 3.0 g water) was added dropwise over a period of 0.5 h and the stirring was further continued for 0.5 h. Finally n-dipropylamine (n-DPA) (2.023 g, 20.0 mmol) was added dropwise to the mixture and stirred for another 1 h. The homogeneous hydrogel was charged into a 125-ml Teflon-lined autoclave and statically heated at 175 °C for 24 h.

In the SAC method, hydrogel was prepared in the same manner as that of HTS method. The hydrogel was dried at 80 ºC in a heating mentle to remove water. When the gel became thick and viscous, it was homogenized manually using a Teflon-rod until it dried. The drying period varied ~ 1.0 h with the gel composition. A white solid formed material was then ground to a fine powder, and finally transferred in a small Teflon cup (25 mm x 25 mm i.d.). This cup was placed in a 125-ml Teflon-lined autoclave with the support of a Teflon holder. A small amount (0.3 g per 1.0 g of dry gel) of water was placed at the bottom of the autoclave in such a manner that the external bulk water never

came into the direct contact with the dry-gel. The crystallization was carried out in steam in an oven with autogenous pressure.

In VPT method, the initial gel was prepared and dried without the addition of SDA, and the SDA was finally mixed with the external bulk water and taken as the source of water-organic vapor in the bottom of the autoclave.

After the crystallization, in all cases, the products were washed with distilled water, separated by filtration, and dried at 100ºC overnight. The as-synthesized samples were calcined in a muffle furnace in a flow of air with a rate of 80 ml/min as follows: the temperature was raised from room temperature to 550ºC over 8 h, and kept at this temperature for another 6 h, and finally cooled to room temperature in ambient condition.

3.3.2. Modification of ZSM 5 using iron

Iron-modified ZSM-5 catalysts were prepared by modifying the HZSM-5 with iron (III) fluoride ($FeF_3 \cdot 3H_2O$) and ammonium hydrogen fluoride (NH_4HF_2) at a temperature of 92°C. The ZSM 5 was first converted to the HZSM 5 form from the ammoniated form by calcining in a muffle furnace at a temperature of 550°C for 6 h. The temperature ramp is 1.52°C/min. The ZSM-5 (Zeolyst International) with SiO_2/Al_2O_3 ratio of 50 (CBV5524G) was used. Four samples were prepared by this method and used for catalytic testing of the methylation of 2-methylnaphthalene. These catalysts were characterized by the temperature programmed desorption (NH_3 – TPD). The carbon content in the spent catalyst samples was also analyzed using the Leco Carbon Analyzer.

3.3.2.1 Catalyst preparation

In this modification procedure, about 15 g of HZSM 5 (50) was mixed in 150 g of deionized water and was placed in a stirrer for an hour in an oil bath at 92°C. Slurry of $FeF_3 \cdot 3H_2O$ and NH_4HF_3 was made in 100 g of deionised water. This salt slurry was added to the ZSM 5 –water slurry mixture drop by drop in one hour. The solution was then stirred at total reflux for 24 h at 92°C. The resultant solution was then washed, filtered by a vacuum filter and then dried in an oven at 110°C for 12 h. This mixture was powdered and then calcined in a muffle furnace for 6 h at a temperature of 550°C at a temperature ramp of 1.52°C/min. The calcined catalysts were then pelletized, crushed and sieved to a particle size of 18-35 U.S.A. Standard Testing Sieve Mesh (0.5–1.0 mm). **Table 3-5** shows the concentration of $FeF_3.3H_2O$ and NH_4HF_3 in each sample.

Table 3-5. The notation of Fe/ZSM-5 catalysts and concentration of $FeF_3.3H_2O$ and NH_4HF_2.

S.No	Name of the Catalyst	Amount of $FeF_3.3H_2O$(g)	Amount of NH_4HF_2(g)
1	Fe ZSM 5 1	0.129	0.102
2	Fe ZSM 5 2	0.258	0.204
3	Fe ZSM 5 3	0.555	0.417
4	Fe ZSM 5 4	0.813	0.615

3.3.2.2. Catalyst characterization and evaluation

The relative acidity of these catalysts was characterized using XRD and NH_3-TPD. Catalytic testing was carried out in a down-flow fixed bed reactor system. In a typical run, 0.3 g of catalyst (10-18 mesh) was loaded in reactor tube (Pyrex, I.D.: ½ inch) and placed in the furnace center. The catalyst was activated at 450°C for 1 h under the inert N_2 gas flow (20 ml/min). Then the temperature was cooled down to the reaction temperature. Reactant dissolved in mesitylene solvent (2-MN:methanol:mesitylene=1:5:5

mol ratio) was fed into a reactor through a HPLC pump at the flow rate of 1.98 ml/min together with 20 ml/min of carrier N_2 gas flow. The reaction product was collected at 1 h intervals. Both the reactants and products were analyzed by HP 5890 gas chromatography (GC) with a β-Dex 120 capillary column (60m, 0.25 mm I.D. column with 0.25 micrometer coating film thickness).

Approximately 0.05 g of the spent catalyst was used in determining the extent of the carbon deposition on the sample during the reaction. Temperature-programmed oxidation (TPO) consists of exposing the sample containing carbonaceous deposits to a flowing O_2 gas /O_2-inert gas mixture stream in a furnace while increasing the temperature of the furnace from a minimum of 100°C to a maximum of 900°C. A constant heating rate of 30°C/min was used in the TPO experiments with a holding period of 3 min at 900°C. A constant O_2 flow rate of 750 ml/min was used in all the analyses. Carbon in the sample, placed in a quartz boat, is oxidized by reacting with O_2. A downstream CuO catalyst bed ensures that any CO produced during the reaction is converted to CO_2. A calibrated IR cell measures the amount of total CO_2 produced by the oxidation of the deposit as a function of furnace temperature. Thus, a profile of CO_2 evolution (also designated as a TPO profile) normalized by the geometric area of the sample substrate gives the amount of carbon in the deposit (in $\mu g/cm^2$) as well as information on the *oxidation reactivity* of the carbonaceous deposit.

3.3.3. Results and discussion

3.3.3.1. Synthesis and evaluation of MAPO-11 for 2-MN with methanol

The synthesis conditions and the products obtained by HTS, VPT and SAC

methods with different gel compositions are listed in **Table 3-6**. **Figure 3-23**, **3-24** and **3-25** show XRD patterns of as-synthesized molecular sieves obtained by HTS, VPT and SAC methods, respectively. The crystallization was carried out at 175^{o}C for 24 h for all samples.

Table 3-6. Synthesis of AlPO-11 (AEL) and Mg-containing AFI

Entry No.	Method[a]	Gel composition					Temp.	Time	Product
		Al_2O_3	P_2O_5	MgO	DPA	H_2O	(° C)	(h)	
1	HTS	1	1	-	1.0	40	175	24	AEL
2	HTS	1	1	0.025	1.0	40	175	24	AEL
3	HTS	1	1	0.05	1.0	40	175	24	AEL
4	HTS	1	1	0.10	1.0	40	175	24	AEL+ trace imp.
5	SAC	1	1	-	1.0	40	175	24	AEL
6	SAC	1	1	0.025	1.0	40	175	24	AEL
7	SAC	1	1	0.05	1.0	40	175	24	AEL
8	SAC	1	1	0.10	1.0	40	175	24	AEL
9	VPT	1	1	-	1.0	40	175	24	AEL+ trace imp.
10	VPT	1	1	0.025	1.0	40	175	24	AEL+ trace imp.
11	VPT	1	1	0.05	1.0	40	175	24	AEL+ trace imp.
12	VPT	1	1	0.10	1.0	40	175	24	AEL
13	VPT	1	1	0.05	0.5	40	175	24	AEL+imp.
14	VPT	1	1	0.05	1.5	40	175	24	AEL+imp.
15	SAC	1	1	0.05	0.5	40	175	24	AEL
16	SAC	1	1	0.05	1.5	40	175	24	AEL
17	SAC	1	1	0.05	1.0	40	175	6	AEL+amorphous
18	SAC	1	1	0.05	1.0	40	175	12	AEL
19	SAC	1	1	0.05	1.0	40	175	48	AEL

[a]HTS= hydrothermal synthesis, SAC=steam-assisted conversion, VPT= vapor-phase transport;

From XRD results, it has been observed that the pure AEL phase was only obtained by the SAC method under the present conditions. In the HTS method, product was contaminated with trace amount of impurities at the highest concentration. This means, beyond the ratio of Mg/Al_2=0.05, magnesium may not enter into the framework of AlPO-11. However, in VPT method, product was contaminated in the lower Mg/Al_2 ratio (0.0~0.05), even synthesis was done by identical conditions. At further increase of the Mg/Al2 ratio from 0.05 to 1.0, the pure AEL phase was formed. This result indicated

that the pH of the synthesis media might be affected for formation of pure AEL phase. In the VPT method, amine solution was diluted with magnesium acetate salt at higher concentration, which may helpful for formation of pure AEL phase. The maximum concentration of magnesium can be loaded by SAC method. The high quality Mg-containing AEL can be synthesized by SAC method. Based on thes results, SAC method has been chosen for further study for optimization of synthesis parameters.

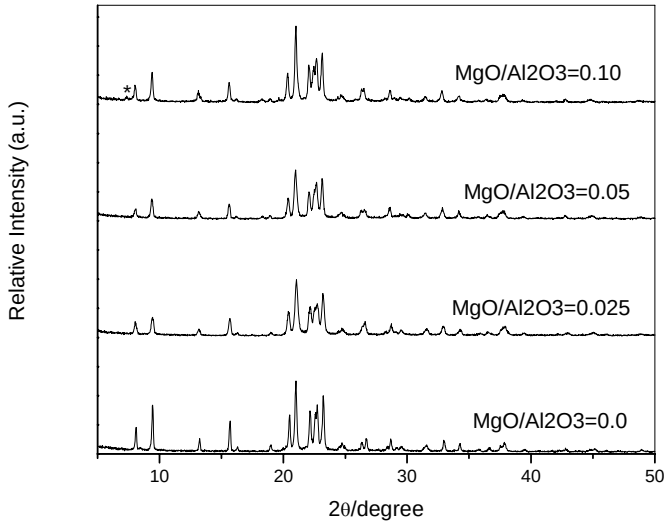

Figure 3-23. XRD pattern of MAPO-11 obtained by HTS (Table-1; Entry 1-4); *-impurities.

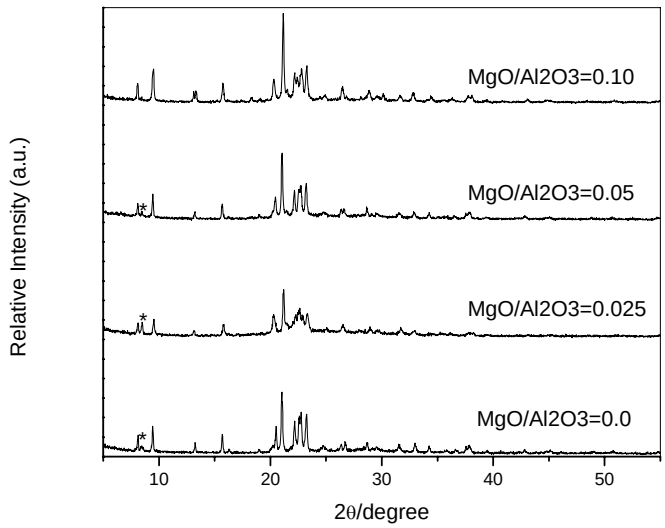

Figure 3-24. XRD pattern of MAPO-11 obtained by VPT (**Table 3-6**); *-impurities.

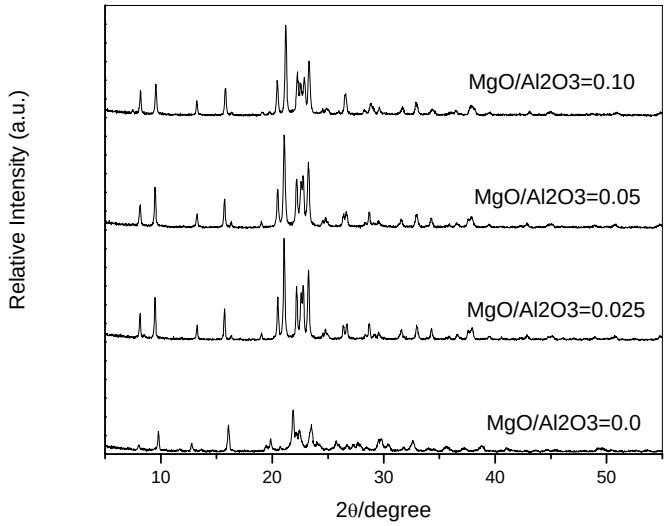

Figure 3-25. XRD pattern of MAPO-11 obtained by SAC (**Table 3-6**)

Effect of SDA amount on the synthesis of MAPO-11 by SAC method (Mg/Al_2=0.05) has been studied. Pure MAPO-11 was crystallized in all the ratio of SDA/Al_2 from 0.5~2.0. The phase and crystallinity of the sample does not affect with the variation of structure-directing agent by SAC method. One possibility is most of the SDA was evaporated along with water during drying the gel. As a result, with increasing the SDA concentration, phase and crystallinity are not affected. These results indicated that a minimum amount of SDA is sufficient for phase formation of AEL by SAC method.

Effect of crystallization time was varied from 6~48 h. It has been observed that within 6 h AEL phase appeared and further increased over the of time 6 to 12 h, which enhanced the crystallinity; the complete AEL phase was observed. The highest intensity was observed during 12-24 h. Prolonged crystallization time of 48 h did not change the phase and crystallinity. It should be noted that the yield of MAPO-11 by SAC is higher than that of HTS method. The range of yield is 77.0~87.0% obtained by SAC method whereas 63.0% obtained by HTS method.

Figure 3-26 shows the NH_3-TPD patterns of MAPO-11 with the variation of Mg/Al2 ratio. AlPO-11 showed an ammonia desorption peak only at around 200°C (so called *l*-peak), which is due to strongly physisorbed ammonia mainly on the external surface. However, Mg-containg samples show both the l-peak and a higher temperature desorption peak at 300-500°C (so called *h*-peak). The higher temperature desorption peak was due to the acidity of MAPO-11 by isomorphous substitution of Al^{3+} with Mg^{2+}. The acid amount corresponding to the h-peak proportionally increased with increasing Mg/Al_2 ratio. However, the highest Mg/Al_2 (0.1) did not give a proportional increase of the acid amount. This difference suggested that some Mg does not act as acidic sites, and the Mg

is likely at the external surface. This result correlated with the XRD pattern at highest ratio.

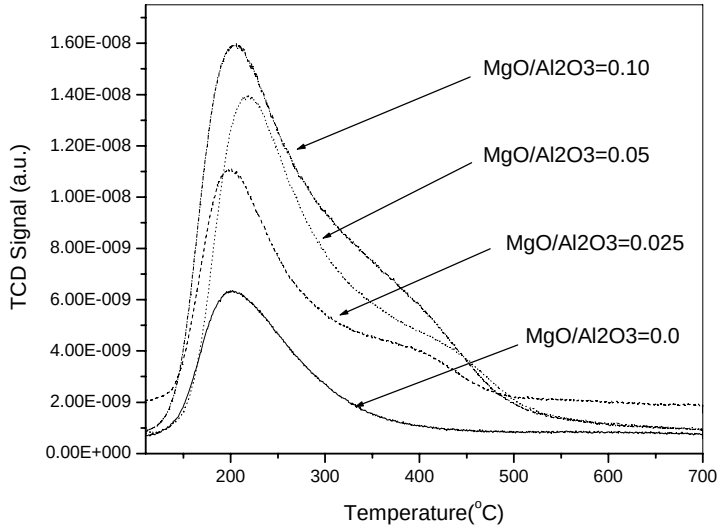

Figure 3-26. NH_3-TPD profiles of AlPO4-11 and MAPO-11 with dofferent Mg/Al2 ratio obtained by HTS method (Table-1; Entry-1-4).

Figure 3-27 shows the catalytic performance of MAPO-11 for methylation of naphthalene in different Mg/Al_2 ratio. It has been observed that highest catalytic activity was shown at Mg/Al_2=0.05 at 250°C. This result indicates that catalytic activity does not directly relate with acid concentration only.

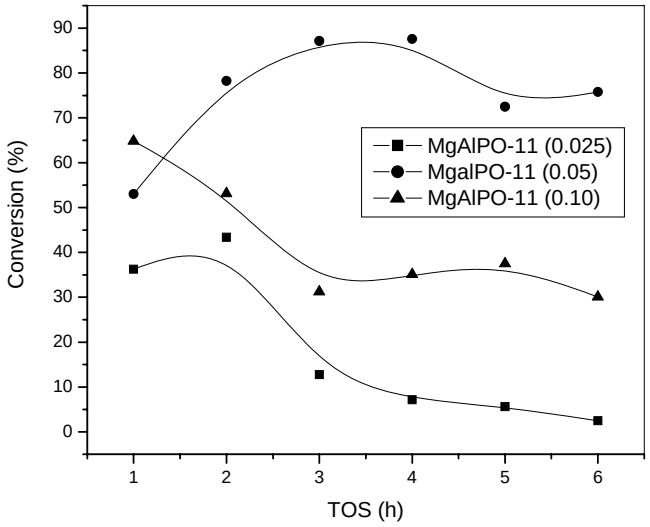

Figure 3-27. Catalytic activity of 2-MN with methanol over MAPO-11 (Condition: Temperature=250°C; WHSV=6.0 h^{-1}).

3.3.4.2. Synthesis of Fe-ZSM-5 and evaluation for 2-MN with methanol

Figure 3-28 shows the NH_3-TPD patterns of FeZSM 5 with the variation of Fe/Al ratio. The profile shows two peaks. The peaks around the 200 to 250°C correspond to the weak acid sites which are due to strongly physisorbed ammonia mainly on the external surface. Those at a higher temperature around 450°C correspond to the strong acid sites. The higher temperature desorption peak might be due to acidity of Fe ZSM 5 by isomorphous substitution of Al^{3+} with Fe^{3+}. The acid amount corresponding to the strong acid sites in the sample FeZSM 5 2 is the highest and decreases for the other three samples. **Figure 3-28** and **3-29** show TPD profiles of freshly synthesized FeZSM 5 samples and spent ZSM 5 samples.

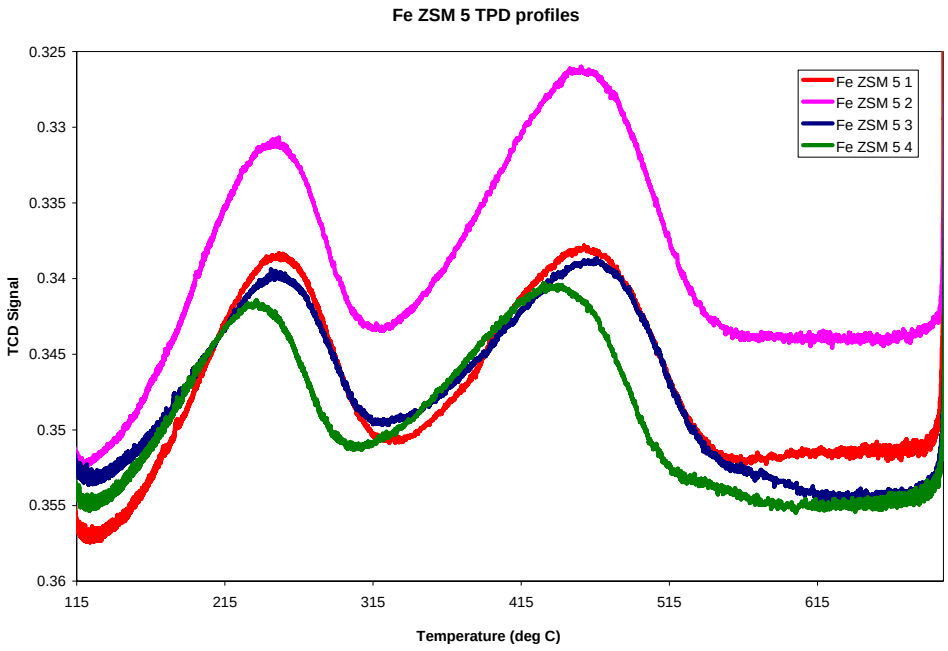

Figure 3-28. Comparision of NH_3 – TPD profiles of Fe ZSM 5 1, Fe ZSM 5 2 , Fe ZSM 5 3 and Fe ZSM 5 4 fresh catalysts.

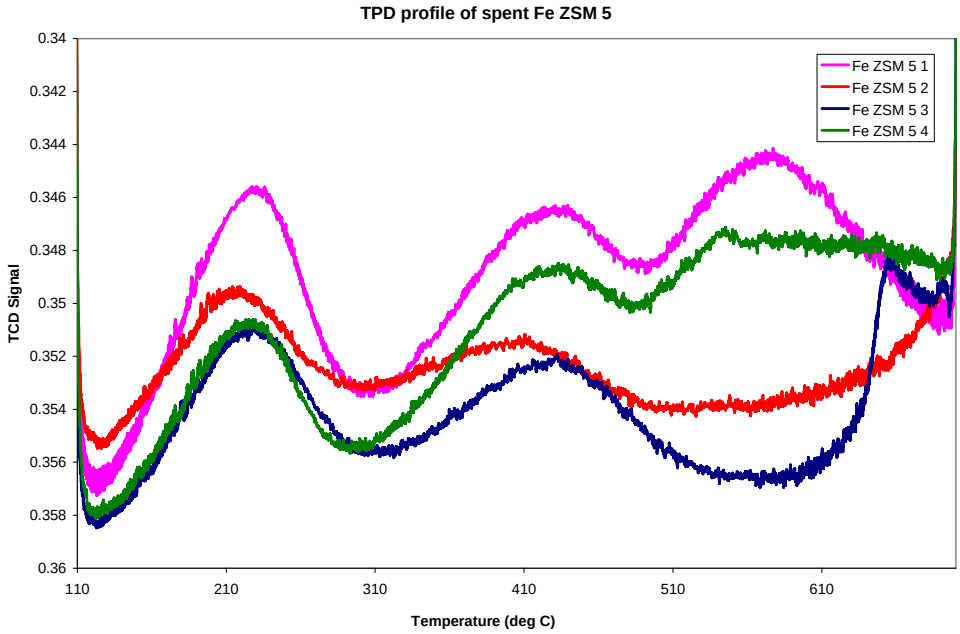

Figure 3-29. Fe ZSM 5 1, Fe ZSM 5 2, Fe ZSM 5 3, Fe ZSM 5 4 spent catalysts after reaction at 300º C.

In the above figure, we can see that in addition to the weak acid and strong acid peaks, we can see a third peak at about 550ºC. This peak may be a Lewis acid peak formed due to the dehydroxylation of the catalyst at higher temperatures

Figure 3-30 shows the catalytic testing of the four samples. The catalytic conversion of the four catalysts is compared in the following figure.

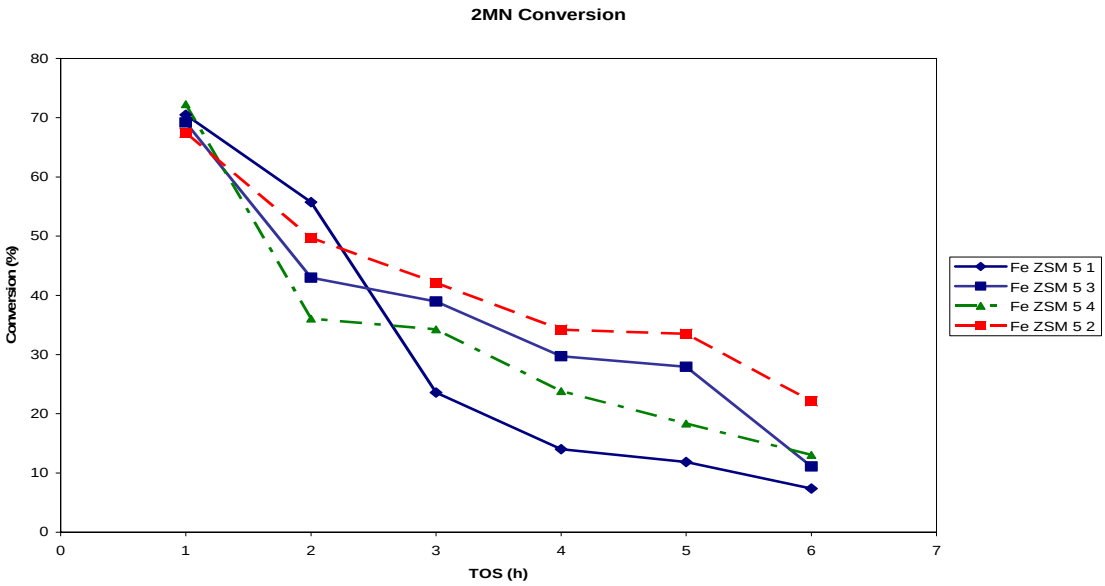

Figure 3-30. Comparison of the Conversion of 2-MN over Fe ZSM 5 catalysts. Reaction conditions: temperature: 300 ^{o}C; Feed (2-MN:methanol: mesitylene=1:5:5 mol ratio): 1.98 ml/hr; Catalyst: 0.3 gram; Gas flow: 20 ml/min.

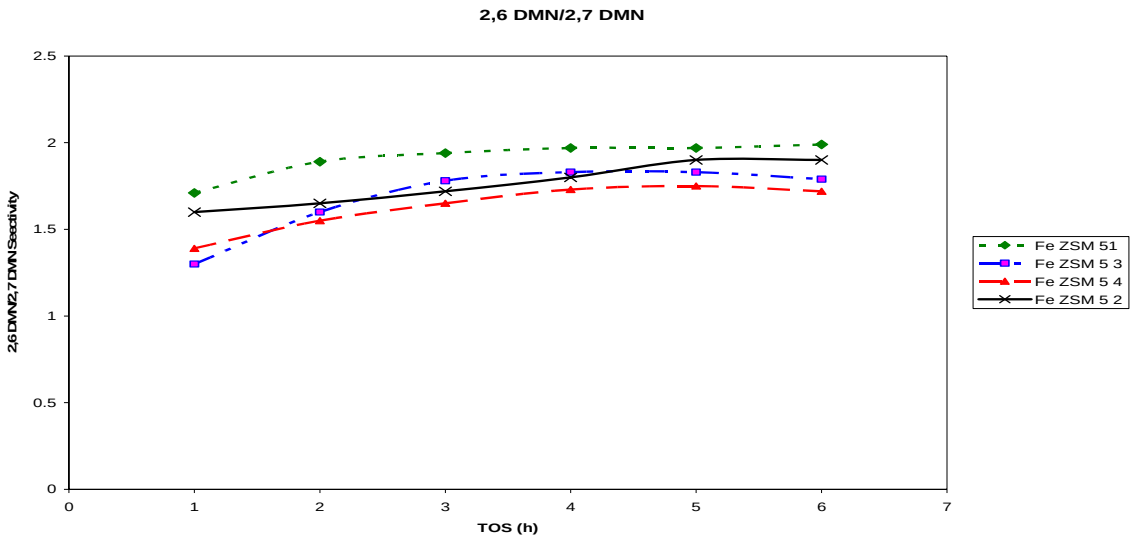

Figure 3-31. Fig 4. Comparison of the selectivity of 2,6DMN/2,7 DMN ZSM 5 catalysts. Reaction conditions: temperature: 300 ^{o}C; Feed (2-MN:methanol: mesitylene=1:5:5 mol ratio): 1.98 ml/hr; Catalyst: 0.3 gram; Gas flow: 20 ml/min.

From the above graph, we can observe that the highest conversion over all was obtained for the Fe ZSM 5 2 (Fe/Al = ¼)

From the above graph, we can observe that the 2,6/2,7 selectivity was the highest in the Fe ZSM 5 1 (Fe/Al = 1/8) followed by Fe ZSM 5 2 (Fe/Al = 1/4) and then by the Fe ZSM 5 3 (Fe/Al = ½) and Fe ZSM 5 4 (Fe/ Al = ¾).

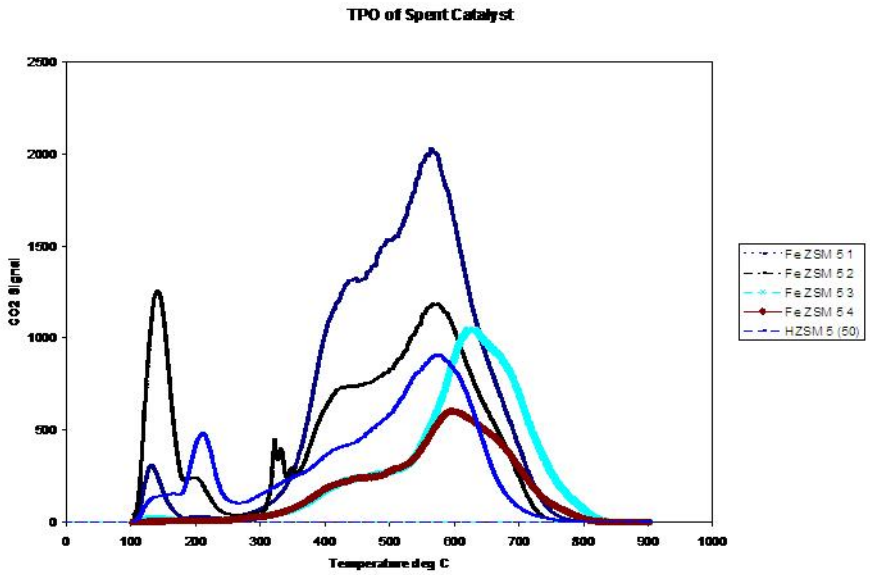

Figure 3- 32. TPO profiles of Spent Fe ZSM 5

The above figure shows the TPO profiles of the catalyst samples. TPO profiles may give multiple CO_2 evolution peaks in the range of 100°– 900°. The peaks around 200°C to 300°C are due to the liquid absorption on the sample. It is considered that CO_2 evolution at relatively low temperatures (typically below 500°C) represents high oxidation reactivity. High oxidation reactivity can, in turn, be related to relatively high H content of the deposits and/or a low degree of structural order present in the carbonaceous solids. In contrast, the CO_2 peaks evolving at higher temperatures (typically above 500°C) suggest the presence of a higher degree of structural order in the carbonaceous solids based on their lower oxidation reactivity. In this case, most of the peaks are near about in the range of 500˚C.

3. 3.4. Summary

1) MAPO-11 was successfully synthesized by a dry-gel conversion method and SAC method was the best for synthesis of pure MAPO-11 among the studied. The pure MAPO-11 was able to be synthesized within 12 h by SAC method. NH_3-TPD results clearly indicated Mg was incorporated into the neutral framework of AlPO-11 and this caused that the MAPO-11 had enough acidic sites for methylation of 2-methylnaphthalene.
2) Among the four Fe ZSM 5 catalysts, Fe ZSM 5 2 (Fe/Al = 1/4) catalyst turns out to be the best in terms of catalytic activity. However, the ratio of 2,6/2,7-DMN selectivity was the highest in the order of Fe ZSM 5 1 (Fe/Al = 1/8) > Fe ZSM 5 2 (Fe/Al = 1/4) > Fe ZSM 5 3 (Fe/Al = 1/2) > Fe ZSM 5 4 (Fe/ Al = 3/4). The formation of coke decreases from Fe ZSM 5 1 to Fe ZSM 5 4.

3. 3.5. Future work

Future work will focus on the continuous development of different types of high-quality catalyst with different structure. The detailed characterization of synthesized materials will be done by NH_3-TPD, SEM, TEM, and BET surface area/pore size distribution. Detailed catalytic performance of developed materials will be studied and will be compared with commercial catalyst. Also, the type of carbon compounds on the catalyst will be analyzed by using the GC-MS. The regenerability of the catalyst will also be examined.

Task 4. Evaluation of Coal-Based Fuel Products

(Prepared by Ronald T. Wincek, Sharon Falcone Miller, and Bruce G. Miller)

The objective of the Task 4 activities is to evaluate the effect of introducing coal into an existing petroleum refinery on the fuel oil product. To accomplish this, the combustion performance and trace element emissions of two fuel oils produced from either refined chemical oil (RCO) or a blend of RCO and light cycle oil (LCO) were measured in Penn State's watertube research boiler. The fuel oils were produced by different methods. The first fuel oil (sample X610) was derived by hydrotreating followed by fractionation of a 1:1 blend of RCO and LCO. The second fuel oil (sample X1333) was derived from the bottoms fractionated out of the RCO. The combustion performance and trace element emissions for the fuel oils produced by further refining of either the RCO or LCO-RCO blend were then compared with that from a commercial/petroleum-based No. 6 fuel oil. The testing was performed to determine if differences in the combustion behavior or emissions of the two fuel oils would result from variations in the API gravity, viscosity, or changes in composition including trace elements present in either fuel oil.

Subtask 4.1. Fuel Oil Analysis

The RCO/LCO-derived fuel oils and the No. 6 fuel oil used in the combustion and emissions tests were analyzed by a series of ASTM procedures and the results are shown in **Table 4-1**. **Table 4-1** also contains the analysis of previously tested No. 6 and co-processed fuel oils for comparison **[4-1]**. Analyses were selected that could be used to

compare the co-processed fuel oil with a petroleum-based commercial fuel oil. Specifically, they are used to: 1) ensure that the samples meet standardized fuel oil specifications **[4-2]**; 2) determine the quantity of trace elements in the co-processed fuel oil; and 3) classify the co-processed fuel oil per established specifications **[4-2]**.

The characteristics of the co-processed fuel oil (sample X610) tested in this reporting period differ from the co-processed fuel oil tested previously (sample EI-176). For example, the API gravity is lower than that measured for the sample tested in 2005.

Table 4-1. Analysis of No. 6 Fuel Oil and Co-Processed Fuel Oil

Characteristic Year Tested Sample No:	Method	No. 6 Fuel Oil (2004-2005)	Co-Processed Fuel Oil (2005) EI-176	Co-Processed Fuel Oil (2006) X610	No. 6 Fuel Oil (2006)	RCO Bottoms (2006) X1333
Specific Gravity, 60/60°F	ASTM D 1298-97 e2	0.975	0.972	1.015	0.970	1.093[b]
API Gravity, 60/60°F,	ASTM D 1298-97 e2	13.6	14.1	7.9	14.4	ND[a]
Viscosity @ 100°F, ssu	ASTM D 445-03	3,195	165	23	ND	ND
Viscosity @ 130°F, ssu	ASTM D 445-03	990	46	16	ND	ND
Viscosity @ 210°F, ssu	ASTM D 445-03	138	ND	8	ND	22
Total Sulfur, wt.%	ASTM D 4239-04a	0.93	0.02	0.06	1.8	0.54
Water, vol.%	ASTM D 1796-97 (2002)	0	0	0	0	ND
Sediment, vol.%	ASTM D 1796-97 (2002)	0	0	0	0	ND
Ash, wt.%	ASTM D 482-03	0.06	<0.02	0.02	0.2	0.03
Higher Heating Value, Btu/lb	ASTM D 240-02	18,714	18,376	17,890	18,437	16,823
Higher Heating Value, Btu/gal	ASTM D 240-02	152,272	149,046	151,540	149,249	153,452
Total Carbon, wt.%	ASTM D 5373-02	87.12	90.17	89.1	86.4	90.3
Total Hydrogen, wt.%	ASTM D 5373-02	11.44	9.55	7.65	11.3	5.10
Total Nitrogen, wt.%	ASTM D 5373-02	0.22	0.2	0.12	0.3	0.35

[a] Analysis not determined
[b] Analysis performed using a graduated cylinder.

It is also lower than the API gravity typically reported for No. 6 fuel oil (12°API gravity) **[4-2**]. A small difference of approximately 700 Btu per gallon was noted in the heating values of the co-processed fuel oils. However, these heating values are typical of those reported for No. 6 fuel oils (*i.e.*, 150,000 Btu/gal) **[4-2]**. Viscosity for the X610 co-processed fuel oil was not only less than the EI-176 co-processed fuel oil, but significantly lower than viscosities measured for each of the baseline No. 6 fuel oils tested. Two additional properties that exhibited significant deviation from a No. 6 fuel oil sample were ash and sulfur content. The sulfur content of the co-processed fuel oil was 0.06%, which is less than that typically reported in No. 1 fuel oil (*i.e.*, kerosene) and No. 2 fuel oil (home heating fuel). The ash content of 0.02% is typical of fuel oil grades No. 1, 2, and 4.

The properties measured for the RCO bottoms also differ from those typically reported for No. 6 fuel oil. The specific gravity measured for this fuel oil exceeded that of each baseline No.6 fuel oil. This measurement was made using a graduated cylinder and not a hydrometer as specified in ASTM Method D 1298-97 e2. The graduated cylinder was used because of the semi-solid nature of this fuel oil at 60^{o}F. The semisolid behavior not only contributes to a greater specific gravity, but also prevented a viscosity measurement at temperatures below 200^{o}F, the temperature at which the solid fraction melted. The viscosity measured at 210^{o}F, however, was significantly lower than that measured for the No. 6 fuel oil used as a baseline in 2004-2005. The sulfur content of the RCO bottoms, while noticeably greater than that measured in either co-processed fuel oil, still falls midway between typical sulfur values of No. 4 (*i.e.,* 0.48 wt.% sulfur) and No. 5

fuel oil (*i.e.,* 0.70 wt.% sulfur). The lack of hydrotreating and dilution by the LCO yields higher sulfur in this type of fuel oil.

Subtask 4.2. Fuel Atomization

In Subtask 4.2, the fuel oils were to undergo atomization tests at the conditions (*i.e.*, temperature and atomization pressures) they will be tested in the watertube boiler. This subtask was contingent upon the quantity of co-processed fuel oil that will be available for testing. The combustion/emissions characterization will take priority over atomization tests should there be a limited quantity of co-processed fuel oil available. Atomization tests were not performed on the co-processed fuel oil in Year 3 due to the limited quantity available. Because there was an insufficient quantity of co-processed fuel oil available in Year 3, viscosity measurements as a function of temperature were used to determine oil preheat conditions that will result in similar atomization characteristics as No. 6 fuel oil.

Subtask 4.3. Watertube Boiler Combustion Tests

In Subtask 4.3, combustion tests were performed firing the co-processed test fuel in Penn State's watertube boiler under conditions similar to the commercial heavy fuel oil testing in previous years. During the tests, gaseous emissions (CO, SO_2, NO_x, CO_2, and O_2) were monitored using continuous emissions monitors per EPA protocol, trace element and mercury (both total and speciated) emissions were measured using a combined EPA Method 29/Ontario Hydro sampling method, and boiler efficiencies were determined using two ASTM methods (*i.e.*, Heat Loss and Input/Output).

The gaseous emissions will be measured and boiler efficiencies determined to quantify any differences in combustion performance between the commercial fuel oil and the co-processed fuel oils. Similarly, testing for trace elements and mercury speciation were performed to determine if trace metals have been concentrated in the fuel oil fraction during the modified refining process and to determine if mercury from the coal is contained in the heavy fuel fraction. This is especially important with the recent mercury legislation for coal-fired boilers (discussed below in more detail) as well as concerns regarding metals such as vanadium and arsenic in fuels. Mercury is a very volatile metal and tends to be in the vapor phase in coal-fired boilers but it is not known at this time which refinery stream mercury will end up in or in what concentration.

4.3.1 Description of the Research Boiler and Ancillary Equipment

Penn State's research boiler and ancillary equipment are shown in **Figure 4-1**. The 1,000 lb saturated steam (@ 150 psig)/h boiler is an A-Frame watertube boiler, designed and built by Cleaver Brooks. The combustion chamber is a 3x3x7 ft ($63ft^3$) chamber with a maximum heat release rate of 42,000 Btu/ft^3-h. It contains 288 ft^2 of heating surface and the maximum firing rate is two million Btu/h (60 Hp).

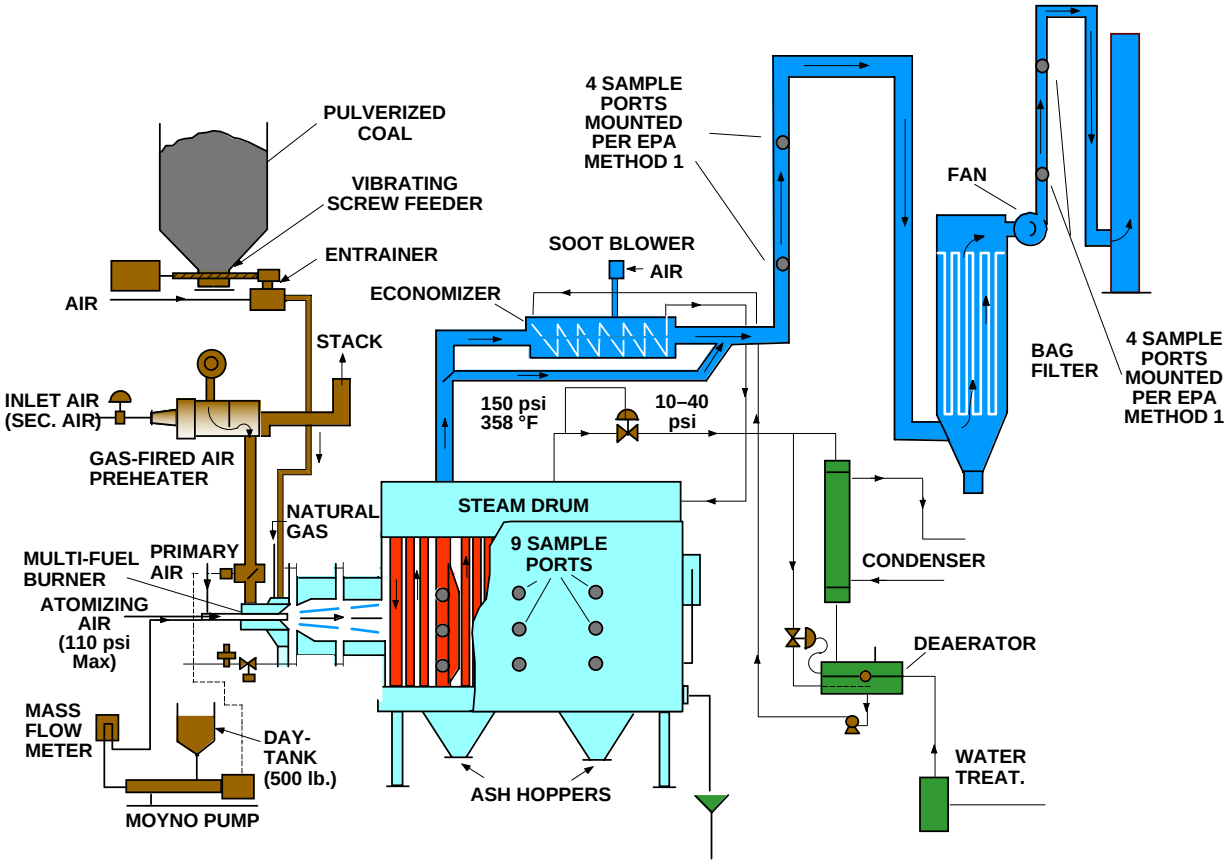

Figure 4-1. Schematic diagram of the research boiler system.

The boiler is equipped with eighteen side ports for gaseous and particulate sampling. Fourteen of the ports have diameters of 3 inches and four have diameters of 4 inches. The combustion gases split into two convective sections, one on each side of the radiant combustion chamber. There are access doors into each of the convective sections. There are also two ash hoppers under each convective section and a doorway giving access into the radiant combustion chamber.

During testing, the steam pressure is maintained constant at 100 psig by a back-pressure regulator. The steam flow rate is measured at the outlet of the steam drum by a

steam flow meter before passing through a condenser. The condensed steam then flows into a feedwater tank before returning to the boiler.

To promote and enhance combustion, a ceramic burner throat extends the combustion chamber by two feet. This ceramic section, termed a quarl, is preheated by natural gas prior to introducing the fuel oil. The quarl aids in the support of the fuel's ignition by storing some of the radiant heat energy released by the flame.

Similar to the No. 6 fuel oil, the co-processed fuel oil was preheated and transported to the fuel oil gun for introduction into the boiler. High-pressure steam was also taken from the boiler's main steam drum and fed into the oil gun providing the energy to atomize the oil. A Micro Motion Mass Flow Meter monitored the oil and atomizing steam flow rates, while the fuel oil temperature was recorded by a thermocouple located at the inlet to the oil gun. A diagram of the feed system is shown in **Figure 4-2**.

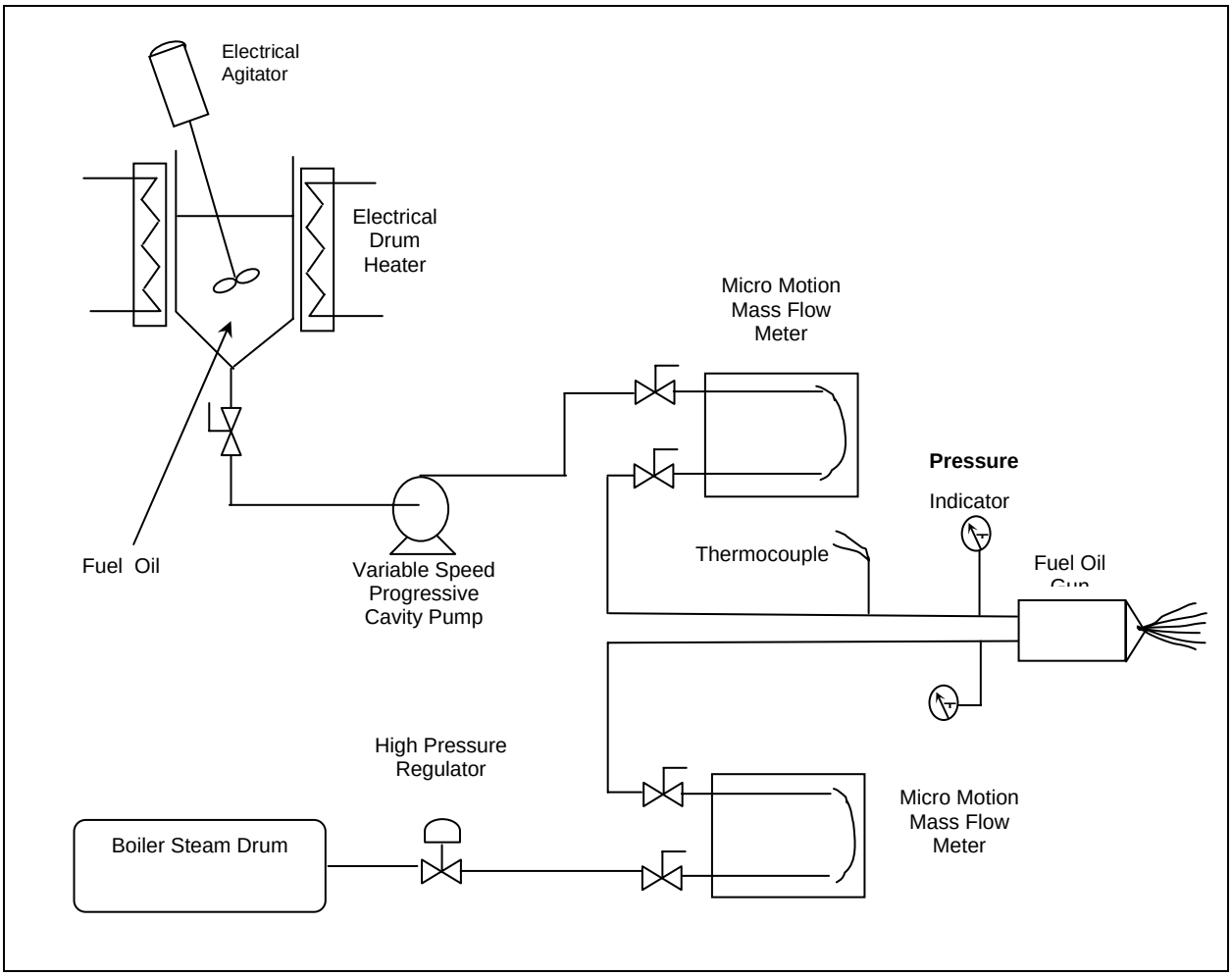

Figure 4-2. Flow diagram of the fuel oil feed system.

A commercially available oil gun was used with combustion testing of both the baseline No. 6 fuel oil and the RCO/LCO fuel oils. This was a type-T oil gun manufactured by Faber Burner Company in Lock Haven, Pennsylvania. A diagram of the Faber oil gun is provided in **Figure 4-3**.

A type SLC internal-mix atomizer was connected to the outlet end of the oil gun and was drilled out to an angle of 30°. This spray angle was chosen to prevent impingement of the oil droplets on the refractory-lined burner throat (quarl) during the combustion testing. It is also important that the spray angle be chosen such that the fuel droplets are entrained in the swirling combustion air stream. This ensures that the

droplets are brought in contact with oxygen in the preheated air as well as the hot recirculated products of combustion.

A gas-fired combustion air preheater supplies over 300,000 Btu/h to preheat up to 1,200 lb/h of air to 350°F. The preheated combustion air (primary air) was passed through a conventional swirl ring several inches before the gas distribution ring, both of which are 8 inches in diameter. A small portion of unheated primary air was fed through an annulus gap surrounding the nozzle. Preheated secondary air was introduced into the quarl tangentially through two headers that were balanced for uniform flow. The percentages of air introduced as cooling, primary, and secondary used in this study were approximately 2, 75, and 23, respectively.

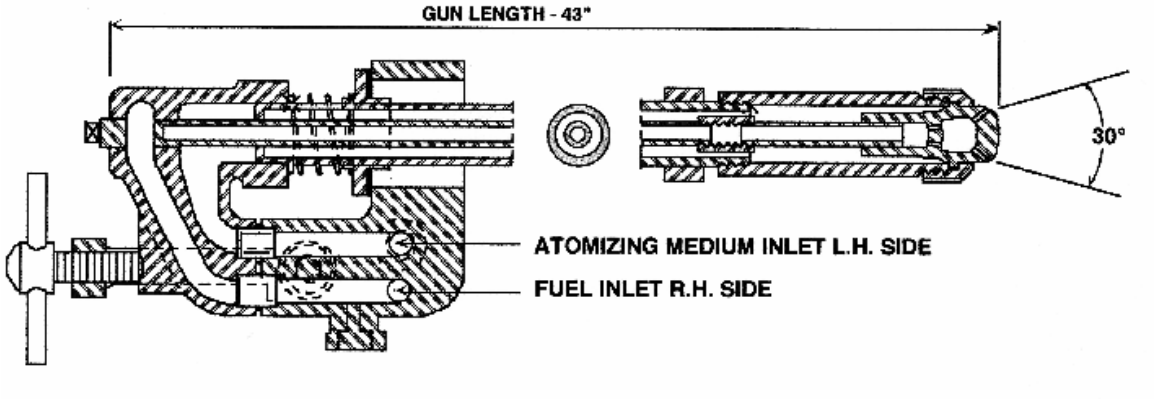

Figure 4-3. Schematic diagram of the Faber oil gun.

The flue gas composition (O_2, CO_2, CO, NO_x, and SO_2) was monitored using a continuous emissions monitoring system. After leaving the boiler, the combustion products passed through an economizer and a baghouse for the removal of particulate matter. Additional sampling ports have been added to the inlet and outlet ducting of the

baghouse per EPA Method 1. All instrumentation readings were recorded by a microcomputer data acquisition system.

4.3.2 Fuel Oil Combustion Test Results

Two combustion performance tests burning the baseline No. 6 fuel oil and one test burning each of the RCO/LCO derived fuel oils were performed on the research boiler during this reporting period. With the exception of the RCO bottoms testing, the operating conditions (*i.e.*, atomizing steam pressure, firing rate, *etc*.) for these tests were similar to those used for the baseline and co-processed fuel oil testing performed previously **[4-1]**. A mechanical problem with the fuel oil pump during the RCO bottoms testing resulted in a lower firing rate and higher excess air levels. A summary of the average operating conditions and combustion data for all tests performed in **Task 4** is provided in **Table 4-2.**

At the beginning of each test, the quarl was heated to a temperature of approximately 1,200°F burning natural gas. The boiler was then switched to firing the desired fuel oil. While burning fuel oil, the system was allowed to stabilize after the transition from natural gas. After steady-state operation was achieved, sampling of the boiler's emissions and the logging of the operating conditions were started.

With the exception of the co-processed fuel oil, each fuel oil was heated prior to being delivered to the oil gun. Heating the fuel oils desreases their viscosity, thus improving their atomization quality. Viscosity, measured as function of temperature, was used in determining the required preheat temperature for each fuel. The baseline No. 6 fuel oils were heated to a temperature of 200 – 210°F. This resulted in a viscosity of

approximately 138 standard saybolt units (ssu). Targeting a similar viscosity in each of the RCO/LCO-derived fuel oils, no heating of the co-processed fuel oil was required because of its low viscosity at ambient temperature. The temperature required for the RCO bottoms was not determined from viscosity data, but by the temperature at which

Table 4-2. Summary of Average Boiler Operating Conditions

Fuel Type	Baseline Fuel Oil	Baseline Fuel Oil	Baseline Fuel Oil	Baseline Fuel Oil	Co-processed Fuel Oil	Co-processed Fuel Oil	Baseline Fuel Oil	Baseline Fuel Oil	RCO Bottoms
Test Date	06/16/04	07/07/04	07/07/04	05/24/05	05/24/05	08/02/06	08/07/06	08/07/06	08/14/06
Test Duration (h)	6.0	7.0	5.5	1.75	1.25	2.5	3.5	2.0	2.0
Flows									
Fuel Feed Rate (lb/h)	79.8	79.8	79.8	79.5	82.8	83.7	81.4	81.0	67.2
Firing Rate (MMBtu/h)	1.49	1.49	1.49	1.45	1.52	1.50	1.49	1.49	1.13
Total Combustion Air (lb/h)	1,502	1,581	1,543	1,248	1,290	1,364	1,314	1,308	932
Cooling Air (lb/h)	24	24	24	24	24	25	25	25	25
Primary Air (lb/h)	1,135	1,183	1,176	1,022	1,055	1,176	1,128	1,118	742
Secondary Air (lb/h)	343	374	343	202	211	163	161	165	165
Steam Production (lb/h)	1,080	1,070	1,099	1,063	1,098	1,152	1,153	1,164	794
Atomizing Steam (lb/h)	71	75	74	75	74	70	72	71	80
Temperatures (^{o}F)									
Primary Air	356	349	352	346	348	340	345	344	347
Secondary Air	618	582	599	661	668	692	689	691	551
Quarl Top	1,208	1,361	1,306	1,299	1,347	1,246	1,255	1,254	1,169
Fuel Oil	208	211	206	199	134	111	199	213	198
Flue Gas Composition (dry)									
O_2 (%)	3.8	4.0	3.9	3.9	3.9	4.1	4.0	4.0	5.1
CO @ 3% O_2 (ppm)	148	138	123	87	45	175	45	51	84
CO_2 @ 3% O_2 (%)	14.8	13.4	13.9	13.7	13.8	14.4	13.7	13.8	15.3
SO_2 @ 3% O_2 (ppm)	553	302	306	545	42	13.5	929	933	338
NO_x @ 3% O_2 (ppm)	539	582	NA	308	87	198	356	364	575
Boiler Efficiency (%)	72.3	71.8	73.3	71.0	71.6	70.4	70.3	71.2	62.3

the semisolid sample melted into a liquid. This temperature was approximately 200°F. **Figure 4-4** shows an open drum of the RCO bottoms prior to heating.

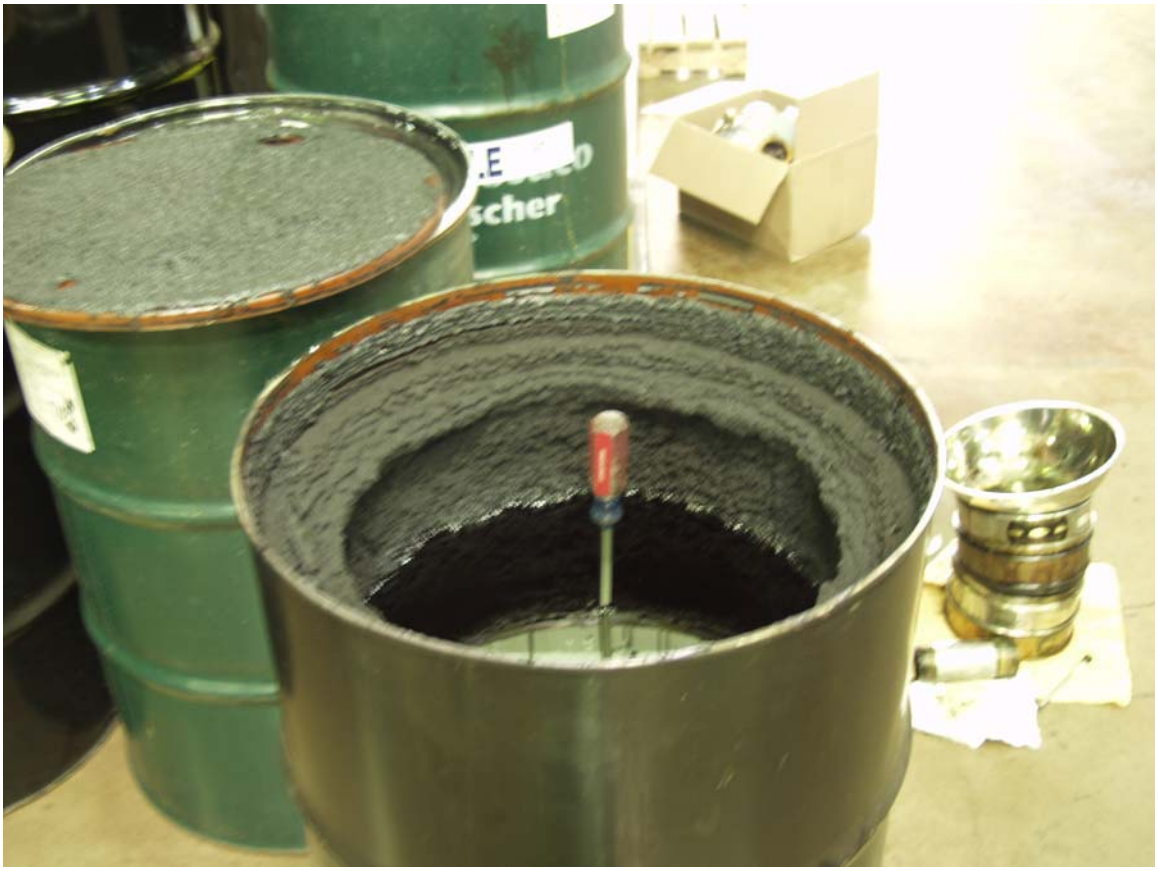

Figure 4-4. Drum of RCO Bottoms prior to heating.

Similar excess oxygen levels (approximately 4.0%) were maintained in the flue gas for all tests with the exception of the RCO bottoms testing. The percent oxygen for this test steadily rose throughout the test period. This increase resulted from a gradual drop in the fuel oil's flow rate. After the test was completed, it was noted that the fuel oil

had reacted with the rubber lining inside the progressive cavity oil pump resulting in decreased pumping efficiency.

The emissions measured by the CEMs for each test were corrected to a basis of 3% oxygen and are plotted in **Figures 4-5 – 4-8.** The most noticeable difference between the emissions produced from burning the RCO/LCO-derived fuel oils and the baseline No. 6 fuel oils is the large reduction in both the sulfur dioxide (SO_2) and oxides of nitrogen (NO_x). The reduction in the sulfur dioxide levels observed burning the RCO/LCO-derived fuel oils is attributed to the lower sulfur content of these fuel oils compared to the baseline No. 6 fuel oil. As reported in **Table 4-1**, the weight percent of sulfur in the No. 6, co-processed, and RCO bottoms fuel oils is 1.8, 0.06 and 0.54 wt.%, respectively.

Although numerous researchers have shown fuel NO_x to be an important mechanism in NO_x formation from fuel oil with a strong correlation between the percent nitrogen in the fuel oil versus NO_x formation, there appears to be no such correlation in the various fuel oils tested **[4-3]**. This may suggest that the differences can be attributed to a more dominant mechanism of thermal NO_x formation within the oil flames. The decrease in NO_x emissions when firing the co-processed fuel oil must reflect a decrease in thermal NO_x, which may have resulted from preheating the co-processed fuel oil to a lower temperature. Although the RCO bottoms fuel oil contains the greatest amount of fuel-bound nitrogen, its believed that the higher NO_x emissions from this fuel oil can be attributed to a greater availability of oxygen resulting from higher excess air levels.

The thermal efficiency of the watertube boiler was determined for each test in accordance with the input-output method as described in the ASME Power Test Codes

for Steam Generating Units – Section 4.1 **[4-4]**. The efficiency for this method is expressed by the following equation:

$$\text{Boiler Efficiency (\%)} = \frac{\text{Output}}{\text{Input}} = \frac{\text{Heat adsorbed by working fluids}}{\text{Heat in fuel + heat credits}} \times 100$$

The results of these calculations are reported in **Table 4-2**.

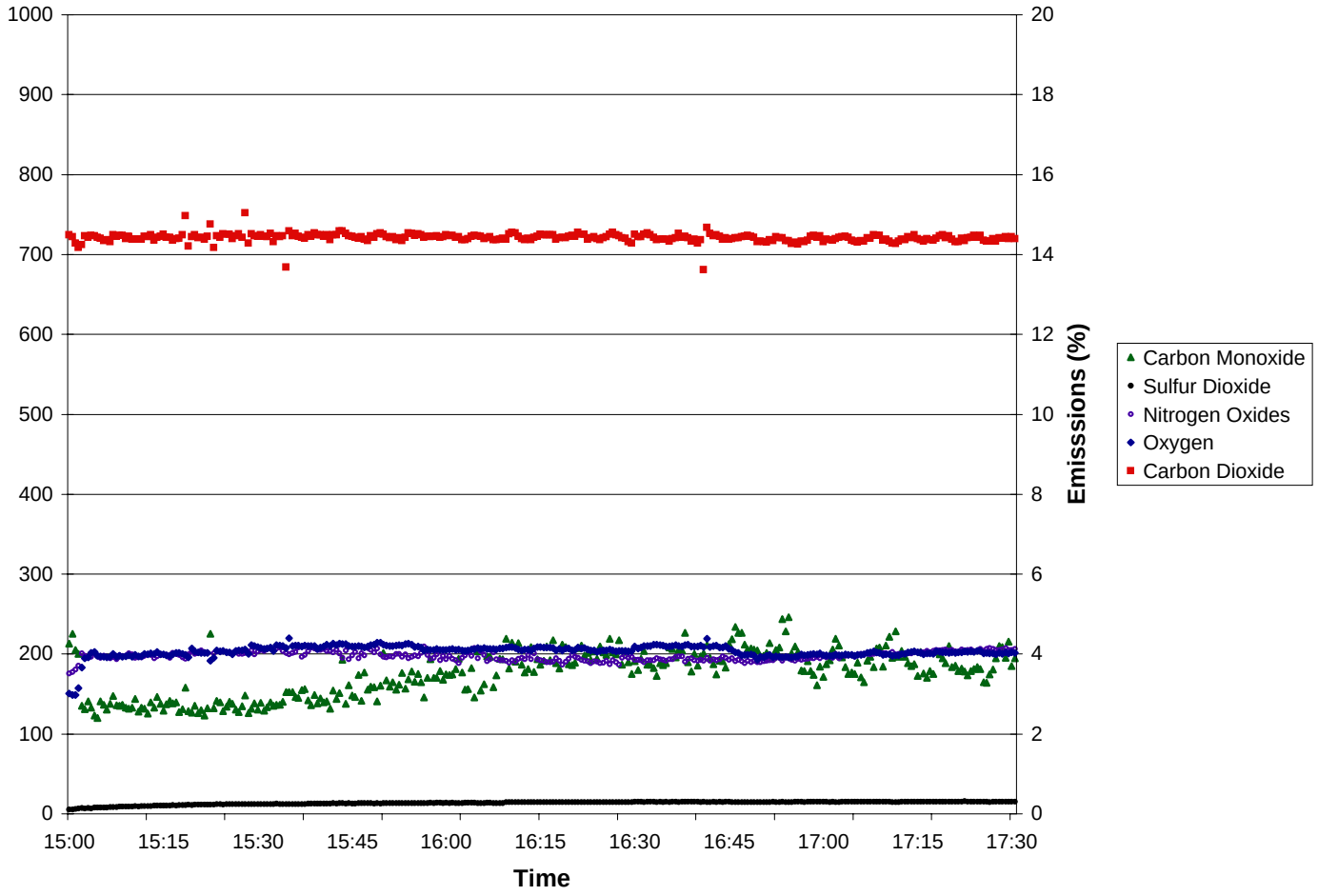

Figure 4-5. Emissions (on a 3% O_2 basis) as a function of time for RCO/LCO co-processed fuel oil testing on August 2, 2006.

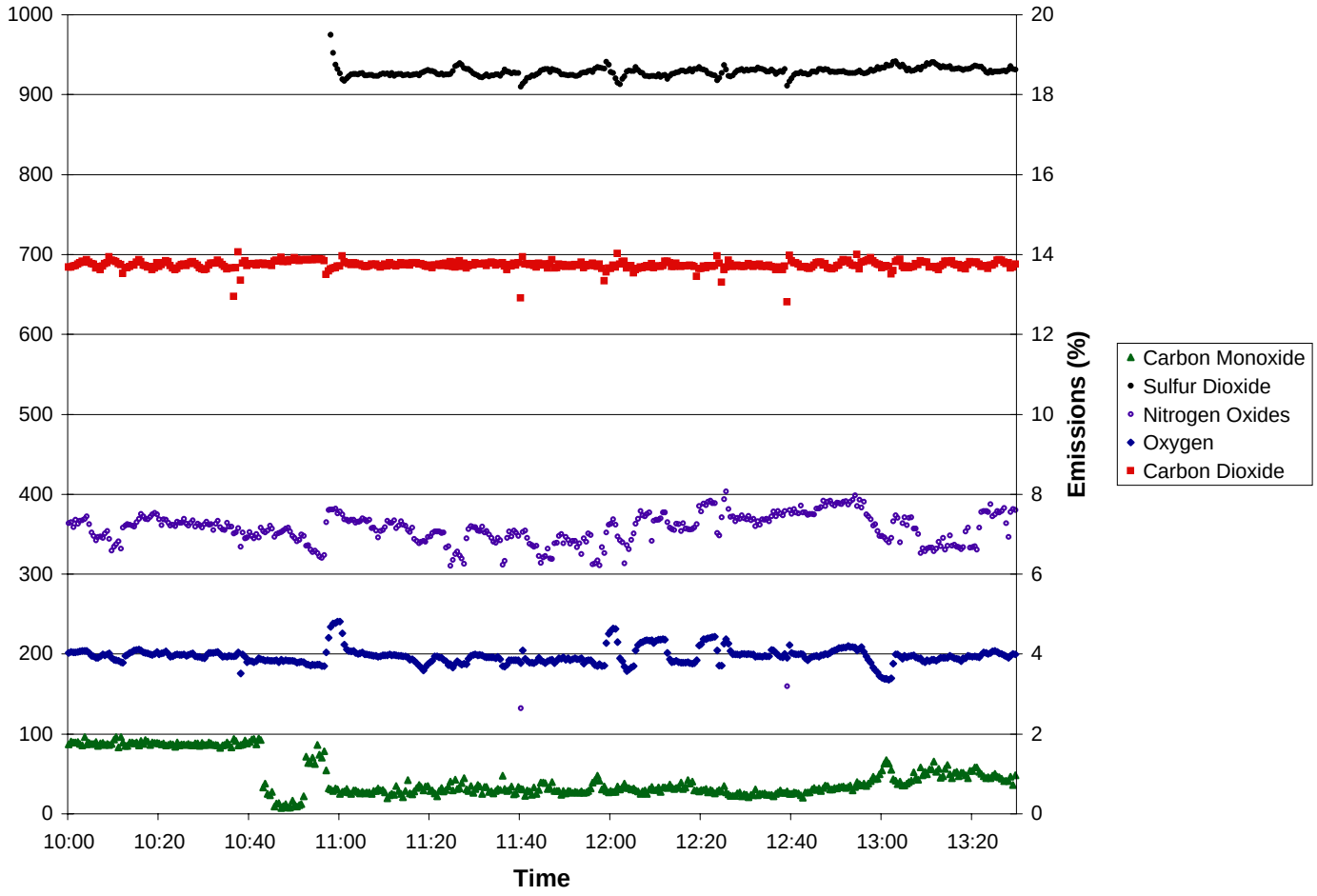

Figure 4-6. Emissions (on a 3% O_2 basis) as a function of time for No. 6 fuel oil testing on August 7, 2006.

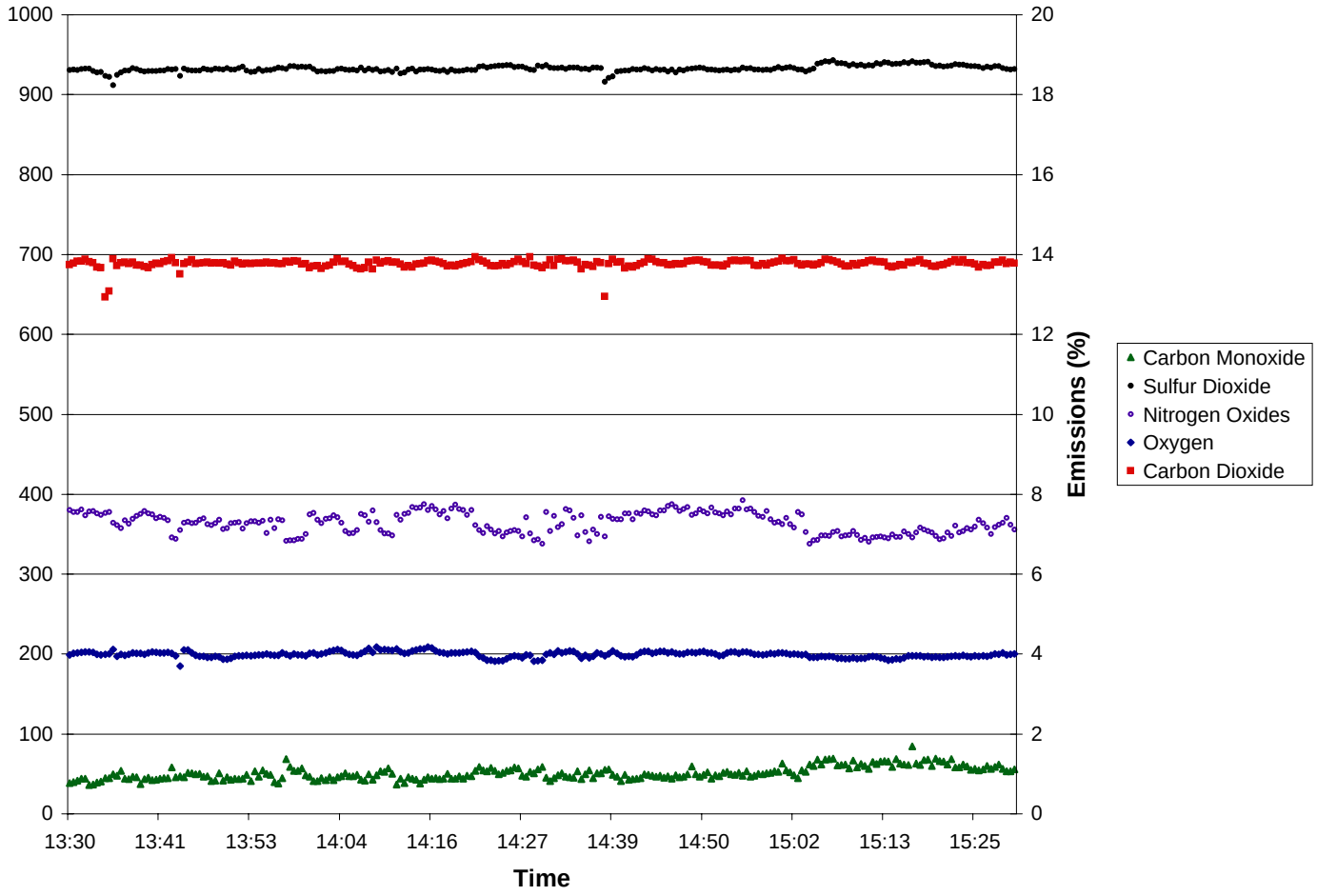

Figure 4-7. Emissions (on a 3% O_2 basis) as a function of time for No. 6 fuel oil testing on August 7, 2006.

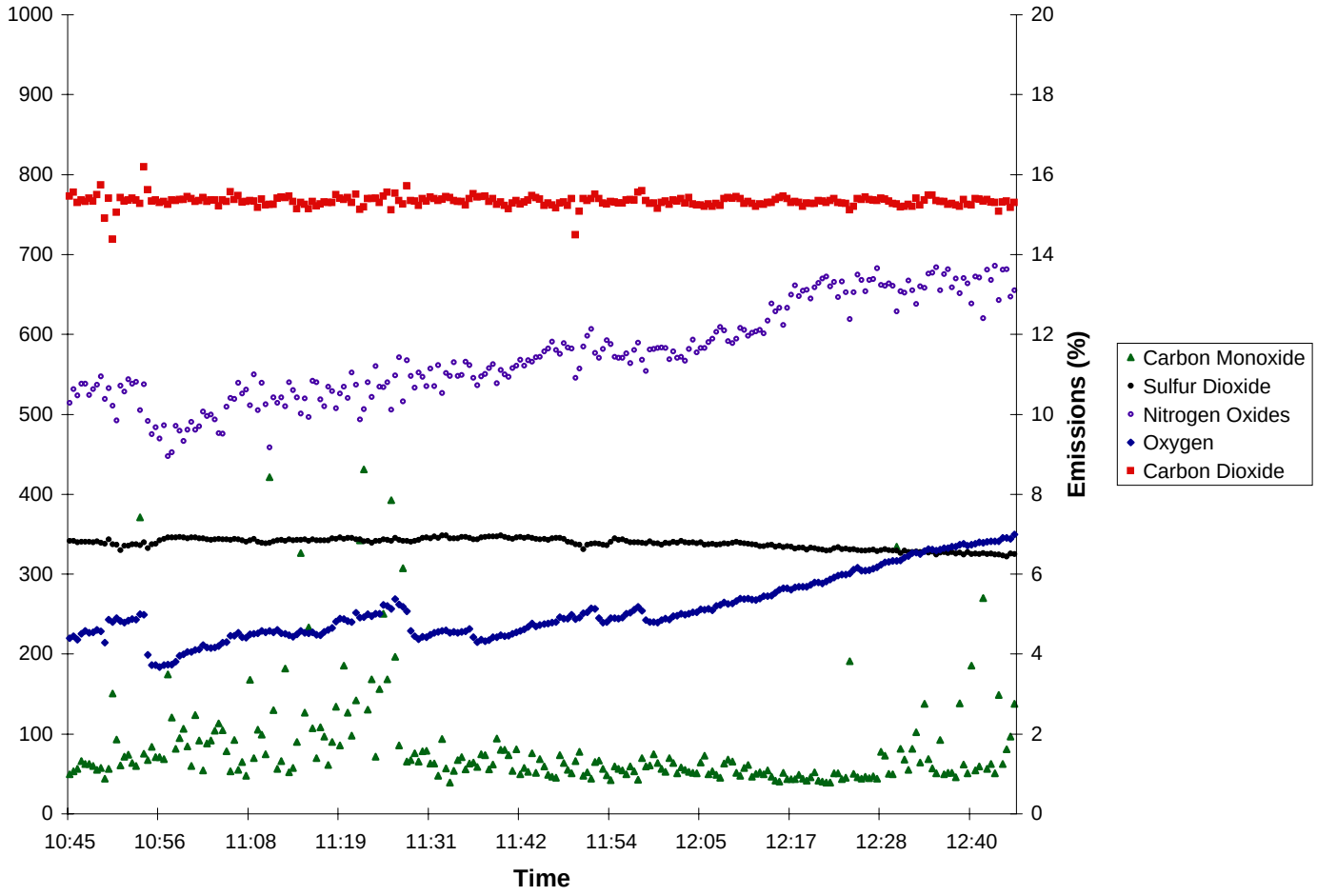

Figure 4-8. Emissions (on a 3% O_2 basis) as a function of time for RCO bottoms testing on August 14, 2006.

The efficiency for the six tests performed burning the baseline No. 6 fuel oil varied between 70.3 and 73.3%, while the efficiency determined when burning the co-processed fuel oil on 05/24/05 and 08/02/06 was 71.6% and 70.4%, respectively. The efficiency determined for the RCO bottoms testing was lower because of the reduced firing rate (1.13 MM Btu/h). Since the efficiency for the co-processed fuel oils lie within the spread of efficiencies determined for the baseline fuel oil, there appears to be no differences in boiler performance between the fuel oils. The detailed thermal efficiency calculations are provided in **Appendix 4-A**.

4.3.3 Emission Testing of Co-Processed Fuel Oil

Trace metal emissions sampling was performed during combustion testing of the baseline No. 6 fuel oil (conducted on 08/07/06), sample X610 (conducted on 08/02/06), and the X1333 sample (conducted on 08/14/06) using the PSU Method, which is a combination of the procedures outlined in the EPA Method 29 (Determination of Metals Emissions from Stationary Sources to measure trace elements in the gas and particulate phases of the flue gases generated during coal combustion) and Ontario Hydro Mercury Speciation Methods **[4-5, 4-6]**. The results are being evaluated and will be reported in the next semiannual report along with a comparison to previous metals emissions testing.

Task 5. Pitch and Coke Material (G. Mitchell, C. Clifford, O. Gul, M. Escallon, Y. Suriyapraphadilok, J. Griffith)

Progress was made during the past five months in evaluating the quality of carbon products (coke and pitch materials) made in our laboratory-scale delayed coker using a blend of decant oil and a cleaned frother cell effluent sample of the Pittsburgh seam coal discussed in the Annual Report 2005 **[5-1]**. In particular, our efforts have been directed at generating coke and pitch products that may be suitable for anode-grade quality coke used by the aluminum industry. In addition, preliminary laboratory-scale work has been completed on the heat treatment of various hydrotreated decant oils coked alone and with coal. Basically, this work represents an extension of an investigation into the influence of hydrotreatment on the properties of liquid products and will explore what influence hydrotreatment might have on carbon product quality. The following is a summary of the research that has been completed during this performance period.

Subtask 5.1 Sample Procurement and Preparation

Subtask 5.1.1 Experimental

During this report period a new coal from A.T. Massey's Marfork Cleaning Plant in Raleigh County, WV was procured for the preparation of an ultra-clean sample for co-coking. This coal cleaning plant was the source of the Powellton and Eagle seam coals that figured in the early development of co-coking using tubing bomb reactors **[5-1, 5-2]** and was the source for the Powellton/Eagle blend (EI-106) used in early shake-down runs #16-42 for the laboratory delayed coking unit. As with the Pittsburgh seam **[5-3]**, two types of samples were obtained from the Marfork facility; a run-of-mine sample designated DECS-36 and a larger sample of fines for further cleaning obtained from the output of the Jameson cell circuit. The cleaning plant generates a coal product sold as a

metallurgical coking coal and on the day of sampling ((7-20-06) was processing a mixed feed from five different mines that included four different coal seams. The exact concentration of each seam was unknown, but included the Eagle seam from the River Fork mine, the #2 Gas seam (locally called the Upper Powellton) from the White Queen Mine, the Powellton from the River Fork Mine, and the Lower Cedar Grove seam from the Marsh Fork and Slip Ridge Mines. Because of the uncertainty regarding the origin of the coal the sample will be discussed as the "Marfork Product".

The run-of-mine sample was taken with a full-cut automatic sampler from the belt leading to clean coal storage. Sampling was performed over about a 45 min period yielding about 155 kg of 1.3 x 0 cm coal that was divided into two 113 L drums that were seals, sparged with argon and sealed under a positive pressure for shipment back to Penn State. These samples were air dried overnight, crushed to pass 6.3 mm (-1/4 inch) and split in half. One half was sealed in foil mutilaminate bags at 6.3 mm, whereas the other half was crushed to pass -0.85 mm (-20 mesh) and seal in bags under argon and refrigerated. A 2.3 kg bags has been sent to Standard Laboratories for complete analysis to become part of the Penn State Coal Sample Bank and Database.

The Jameson cell is a contact dependent flotation device that combines air and pulp (fine coal particles) under pressure which is let down through an orifice plate called a downcomer. The resulting high velocity plunging jet of liquid shears the surrounding air, creating a vacuum that causes air to be entrained into the feed and broken up into very fine bubbles creating a dense foam with a high void fraction. The smaller mean bubble size and greater shear intensity means that when the bubbles are released from the pulp and washed with a counter-current flow of water a high purity coal concentrate can

be collected. At Marfork, the Jameson effluent is directed to a filter press that removes moisture from about 80% to 20% and the resultant cake is transferred by belt to a storage building where our sample was collected. Over a 90 minute period eleven 76 L drums and two 208 L drums containing about 760 kg of fines were collected.

Subtask 5.1.2 Results and Discussion

To determine the nature of the Jameson Cell sample, a Davis sampler was used to obtain core samples from each of the smaller drums to build a composite sample of about 0.8 kg. This sample was dried in an oven at 104ºC overnight, homogenized and prepared for proximate analysis, petrographic analysis and the remainder was wet-sieved to determine the amount of sample >150 μm (>100 mesh), <150 μm x >45 μm (<100 x >325 mesh) and the amount <45 μm (<325 mesh). The whole Jameson sample contained 21.9% moisture and yielded 7.4% ash. Wet sieving revealed that 17% of the Jameson effluent was >150 μm and 50% of the sample passed 45 μm. The <150 μm x >45 μm fraction, which was the particle size fraction employed in co-coking the Pittsburgh seam product, amounted to 33% and is the particle size fraction of initial interest for co-coking. As shown in **Table 5-1**, both the >150 μm and <150 x >325 μm fractions have similarly lower ash yield than the whole product or the <45 μm fraction (not shown) which was 11.45% and comparably higher vitrinite content than the run-of-mine product (DECS-36). Based upon our experience with the Pittsburgh seam frother cell effluent **[5-3]** which provided about 3.1% recovery of <1.0% ash yield material after floating the collected particle size fraction at a specific gravity of 1.280 g/mL, we should be able to recover at least 15 kg of ultra-clean coal from the Marfork Jameson cell effluent.

Table 5-1 Comparison of the Clean Coal Jameson Cell Effluent with the Run-of-Mine Marfork Product Coal

Analytical Procedure	Marfork Product DECS-36	Marfork Jameson +100 mesh	Marfork Jameson -100 x +325 Mesh	Marfork Jameson -100 x +325 Interim
Proximate Analysis: (dry)				
Fixed Carbon, %	64.05	66.77	66.29	66.53
Volatile Matter, %	29.19	30.26	30.25	29.42
Ash, %	6.76	2.97	3.46	4.05
Gieseler Plastometer:				
Softening Temperature, (C)	384	nd	nd	386
Fluid Temperature Range (C)	108	nd	nd	103
Maximum Fluidity (ddpm)	30,000	nd	nd	18,498
Temperature at Maximum (C)	448	nd	nd	449
Organic Petrography:				
Total Vitrinite, %	73.8	84.7	86.5	83.4
Total Liptinite, %	5.3	3.0	2.8	2.5
Total Inertinite, %	20.9	12.3	10.7	14.1

Processing of the bulk Jameson cell effluent sample was begun August 21st using the Derrick Model K Vibrating Screen Machine our combination vibrating/wet sieving apparatus. As with the Pittsburgh seam frother effluent, the Marfork Jameson cell sample was processed through two nested 58"l x 17.5"w screens with opening of 150 µm and 45µm that were adjusted to 15º from horizontal and vibrated at 3600 cycles per minute. A high-pressure spray of water was maintained across the entire width of the screens and the >150 µm and 150 µm x 45 µm products were collected. The higher ash <45 µm material was not collected. Many problems were encountered during two weeks of operation and only about half of the Jameson cell effluent has currently been processed. Preliminary evaluation of the <150 µm >45 µm product has been conducted and the results are displayed in **Table 5-1**. As seen, it appears that the interim product quality is not as good as was derived from manual wet sieving because the ash yield is higher and the concentration of vitrinite lower. However, some of this may have to do with

sampling as the Davis sampler mainly collected the material that had settled in the storage drum and missed some of the lighter fraction that was still suspended in water. Processing of the remaining Jameson cell sample will begin directly and will probably include reprocessing of the >150 μm fraction that was collected, because it may contain a significant amount of our size fraction product.

Subtask 5.1.3 Conclusions

Progress has been made towards acquiring and processing of an ultra-clean coal for our next delayed coker series using a metallurgical coal product from the Marfork cleaning plant. Analysis of the run-of-mine sample suggests that the product is of superior quality that will become wholly thermoplastic under the experimental conditions and therefore should co-coke with the decant oil being employed in this research study. Whether the Jameson cell effluent can be sized and cleaned to a raw product with less than a percent of ash yield with sufficiently low iron and silica levels to result in a coke product of high quality is to be determined in the next reporting period.

Subtask 5.2 Deeply Hydrotreated Decant Oil Reactions: Characterization of petroleum cokes generated from tubing bomb

Introduction and hypothesis

The research being discussed in this section of the report concerns the development of a correlation between the chemical composition of the feedstocks and the quality of coke obtained from small scale tubing bomb reactors. The chosen feedstock was a decant oil that has been hydrotreated to different levels, giving origin to three versions of hydrotreated decant oil. In general, hydrotreatment resulted in the saturation

of aromatic rings, producing hydroaromatics and naphthenic compounds (cycloalkanes), and a reduction in heteroatom concentration. A variety of analytical techniques has been employed to establish the chemical composition of the original decant oil and three hydrotreated versions. The small amount of coke material generated from the tubing bomb reactors imposes some limitation on the methods of characterization that can be brought to bear. Typically, cokes having a more needle-like textural character, those used for the production of ultra high power (UHP) electrodes, are considered premium carbons, whereas those of more isotropic character are unacceptable. Even though, structure is not the only decisive factor in determine a given coke's use, it can be used as an initial criterion for the selection of a particular coke for a given application **[5-4]**.

The structure of petroleum cokes in general, and needle cokes in particular, is commonly described in terms of anisotropy where the most needle-like cokes are considered the most anisotropic **[5-5]**. In general, two methods have been employed to determine the anisotropy of the cokes **[5-6 – 5-8]**:

1. Anisotropy determination via polarized light microscopy **[5-9, 5-10]**.
2. Bacon anisotropy based on X-ray diffraction **[5-6, 5-9]**

Only the first method has been completed during this reporting period and will be discussed. The second method will be carried out in the future to corroborate or to extend the results found by optical microscopy **[5-6]**. Microscopy techniques have the disadvantage in that the observations tend to be subjective and are limited to the resolution of the optical microscope; however, the combination of both techniques will give a more complete description of the anisotropic or isotropic character of the coke **[5-11]**.

Besides structure, other techniques can be used to characterize the coke **[5-4]**:

- **Strength and/or hardness**; performed on green or calcined coke.

Without a strong green coke particle, electrodes of adequate strength and thermal shock/stress characteristics to perform adequately cannot be produced **[5-4]**.

- ***Density***

The real or helium density is important because it gives an indication of the efficiency of the calcination process. Generally, values of 3.18-3.31 kg/m^3 are desirable. Lower values tend to indicate a porous, poorly formed coke which will require extra coal-tar pitch binder to process properly, as the binder penetrates too deeply into the pores; coke may have a closed pore structure and again not interact with pitch **[5-4]**.

- ***Coefficient of thermal expansion CTE***

Low CTE values ($1\text{-}4x10^{-7}$ cm/cm/°C) are observed for anisotropic or needle-type coke, while high values ($20\text{-}40x10^{-7}$ cm/cm/°C) are observed for isotropic or shot-type coke **[5-13]**. The CTE is principally governed by the uni-axial orientation of graphite lamellae in the filler coke, which is evaluated by microscopy examination of optical anisotropy and bacon anisotropy based on X-ray diffraction **[5-8]**. A correlation between the Bacon anisotropy factor derived from X-ray diffraction measurements can be used to predict the coefficient of thermal expansion. Thus, the X-ray technique can be employed to give an indication of the quality of a coke more readily than would be the case if a full assessment was made on the graphite artifacts **[5-7]**. CTE values will not be carried out in this research because the amount of sample is insufficient to perform the analysis.

- ***Sulfur content***

Higher sulfur levels generally lead to increased puffing and hence, degradation of properties **[5-4]**. It is expected that cokes derived from hydrotreated decant oils have lower sulfur content and hence, eliminating puffing problems when compared to the coke derived from the unhydrotreated decant oil.

Table **Table 5-2** shows a range of properties by which calcined petroleum needle coke are classified, including CTE, real density and sulfur.

Table 5-2 Typical calcined petroleum needle coke properties **[5-12]**

Property	Units	Super premium	Premium	Intermediate	Regular
CTE (30-100°C) coefficient of thermal expansion	m/m/°C x 10^{-6}	<0.25	<0.4	<0.7	<1.8
Real density	g/cm^3	>2.12	>2.11	>2.10	>2.04
Sulfur	Wt %	<0.7	<0.7	<0.7	<2.0

- ***Coke source***

The observed structure of a well-ordered needle coke can be greatly influenced by the type of feedstock used to produce coke **[5-4]**. Different feedstocks include decant oils, vacuum resid, coal-tar pitches, among others. The coke properties related to source have been studied by different authors **[5-13 – 5-15]** and some of these properties are provided in **Table 5-3** for comparison.

Table 5-3 Graphite electrodes properties made from delayed coke **[5-12]**

Green coke properties	Vacuum resid	Pyrolysis tar	Decant oil
Volatile matter, %	7.8	5.5	6.2
Sulfur, %	1.6	0.2	1.2
Graphite properties			
Density (g/cm^3)	1.65	1.55	1.55
CTE x 10^6 / °C	1.83	0.64	0.17

- ***Coke processing, coking, calcination.***

As covered by other authors **[5-15, 5-16]**, processing conditions (temperature and pressure) have a profound influence on coke quality. Calcination rate also plays an important role **[5-4]**. Calcination rates in excess of 50°C per minute are not recommended for calcining cokes of either premium or regular quality. Such cokes are used in the production of electrodes for the electric arc steel furnace. Calcination heating rates in excess of 50°C per minute appear to be acceptable for cokes used in the manufacture of less thermally and mechanically severe applications, such as aluminum anodes. Slower calcination rates are necessary to produce the most optimum properties in anisotropic cokes **[5-17]**.

The intent of the current work is to correlate the coke structure with the coke source material or feedstock used to generate the coke (i.e. decant oil and hydrotreated versions). Analysis of the coke structure using optical microscopy and XRD and combined with other analyses will provide information about the end-use of the coke derived from the different petroleum feedstocks. So far, the microscope analysis has been completed; however, this method alone is not enough to determine the end use of the coke. XRD experiments will be carried out as well as other properties such as density and sulfur content.

Hypothesis

There are two conditions to obtain a premium coke or needle coke **[5-13, 5-18]**:

- Formation of bulk mesophase. Growth and coalescence of anisotropic spheres
- Rearrangement of these anisotropic regions into an oriented flow texture.

With regarding to the first condition, it has been reported that the formation of bulk mesophase is influenced by the viscosity **[5-13]**. Low viscosity favors the formation of bulk mesophase while high viscosity constrains mesophase growth and coalescence.

In relation to the second condition, it has been reported that highly aromatic feedstocks develop bulk mesophase, but lacks gas evolution that results in the orientation of mesophase into a flow texture **[5-19]**. Consequently, in feedstocks with a high concentration of naphthenic compounds, the dehydrogenation and dealkylation reactions that generate gases may control the orientation of the bulk mesophase **[5-19]**.

Since the two factors mentioned above are necessary in obtaining of a premium coke, our experiments were designed to study the influence of feedstock composition, reaction pressure and reaction time on coke quality. These conditions will affect the two parameters that influence mesophase growth and orientation, viscosity and naphthenic hydrogen composition, based on the follow hypotheses:

1. *It is hypothesized that higher pressure might favor better anisotropic development of bulk mesophase; because when working under high pressure lower molecular weight compounds are retained in the medium which would tend to decrease viscosity* **[5-20]**.

In order to prove or disapprove the hypothesis, coking experiments were carried out at two different pressures: autogenous (68-102 atm) and atmospheric pressure. Mochida et al. **[5-21]** reported a model in which the viscosity changes during the liquid-phase carbonization were monitored by varying time and temperature. The model proposed by

Mochida et al., helps to explain the importance of viscosity in the development of mesophase and hence, in the coke quality.

- A higher pressure was favorable for the better anisotropic development of bulk mesophase; the thinking being that the retained volatile matter may moderate carbonization reactions through dissolution and/or hydrogen transfer thus keeping a lower viscosity of the carbonizing system for a smooth coalescence of mesophase spheres **[5-20]**. Under high pressure, the lower molecular weight compounds would be retained in the medium and decrease viscosity **[5-18]**.
- Under low pressure (i.e. atmospheric pressure), lower molecular weight molecules would leave the system and contribute to an increased viscosity of the medium. A higher viscosity would be expected to hinder mesophase formation **[5-18]**.

The method used to monitor mesophase growth was by measuring the size of the isochromatic units in cokes generated from a particular feedstock under autogenous and atmospheric pressure using optical microscope. For instance, a high percentage of small isochromatic units would be evidence of poor mesophase growth.

2. It is hypothesized that, the formation of bulk mesophase will be developed to a greater extent and the anisotropic spheres would be arranged into an oriented flow texture when using hydrotreated decant oil because of the presence of naphthenic hydrogen.

The carbonization that lead to the formation of premium coke (needle coke) consist of two important steps: the formation of bulk mesophase through the growth and coalescence of anisotropic spheres and its rearrangement into an oriented flow texture by gas evolution before solidification into a bulk carbon **[5-22]**. Feedstocks having extensive aromatization lack gas evolution characteristics at the solidification stage,

although the bulk mesophase of low viscosity is developed due to the relatively low reactivity of highly aromatic compounds **[5-15, 5-22]**. Consequently, employing decant oil hydrotreated at different levels and resulting in a greater concentration of naphthenic hydrogen, may provide the gas evolution characteristics needed for orientation of the bulk mesophase before solidification.

Subtask 5.2.1 Experimental

Decant oil

A commercial decant oil obtained from United Refining Co, Warren, PA was supplied to PARC Technical Services, Inc., Harmarville, PA for hydrotreatment under the conditions shown in **Table 5-4**. The reduction in sulfur and nitrogen shows the effectiveness of the hydrotreatment.

Table 5-4 Hydrotreatment conditions

Feedstock fa[a]	Former designation	Pressure psig	Temperature, °F / °C	LHSV[b] h^{-1}	S[c]	N[d]
0.71	DO107	---	---	---	2.99	0.22
0.67	DO135	600	675 / 357	0.74	0.44	0.17
0.64	DO134	600	624 / 329	0.75	0.94	0.24
0.62	DO138	1200	734 / 390	0.51	0.02	0.12

a aromaticity

b Liquid hour space velocity below the calculations are shown to find fa

c sulfur (wt %)

d nitrogen (wt %)

The decant oils were designated by PARC as DO107, DO134, DO135 and DO138; however, this designation has been changed. Hereafter, the aromaticity calculated based on results from ^{1}H NMR and elemental analysis will be substituted for

the decant oil's designation. The chemical shift for functional groups has been reported elsewhere **[5-23]** and is shown in the table below. The conditions for determining ^{1}H were as follows, through the integration of the peaks in the spectrum.

Chemical Shift (ppm)	Symbol
6.2-9.2	H_{AR}
1.7-4.4	H α
1.0-1.7	H β
0.7-1.0	H γ

$H_{AR}^* = H_{AR} / H_{TOTAL}$; $H_\alpha^* = H_\alpha / H_{TOTAL}$; $H_\beta^* = H_\beta / H_{TOTAL}$; $H_\chi^* = H_\chi / H_{TOTAL}$ **[5-24]**

$$Ho^* = \frac{H\beta}{x} - \frac{H\gamma}{y}$$

$$fa = \frac{\frac{C}{H} - \frac{H\alpha^*}{x} - \frac{Ho^*}{y}}{\frac{C}{H}}$$

$$\frac{H_{AR}}{C_{AR}} = \frac{\frac{H\alpha^*}{x} - H_{AR}^* - \frac{O}{H}}{\frac{C}{H} - \frac{H\alpha^*}{x} - \frac{Ho^*}{y}} \qquad \textbf{[5-25]}$$

$\frac{H_{AR}}{C_{AR}}$ is an indicative of the presence of hydroaromatics and cycloalkanes

Nuclear Magnetic Resonance – NMR

This equipment is a liquid-state NMR spectrometer with imaging capabilities. The samples were analyzed on a Bruker AMX 360 NMR operating at 9.4 Tesla and a 70° tip angle. The NMR was carried out on the decant oil and its hydrotreated versions. The samples were dissolved in $CDCl_3$ for analyses.

CHN Elemental Analysis

The LECO 600 CHN analyzer was used to measure total carbon, hydrogen and nitrogen contents in solid and liquid samples. The amount of oxygen was obtained by difference.

Gas Chromatography / Mass Spectrometry (GC/MS)

This analysis was carried out for the original decant oil and its hydrotreated versions. All the samples injected into the GC/MS were prepared as follows: approximately 0.02-0.03 grams of the decant oil was diluted in approximately 1 gram of dichloromethane. The injection volume was 1.0 μL.

Preparative Liquid Chromatography - PLC and GC/MS

It is important to point out that Preparative Liquid Chromatography is a semi-quantitative method. The methodology followed was the same reported by Karam et al **[5-26]**. In this procedure, 300 mg of decant oil was dissolved in a minimal amount of THF and stirred with 2g of silica gel. The slurry was placed at the top of a glass column, which previously was packed with silica gel. Different solvents were added to the column in order to elute different fractions: hexane (to obtain saturated hydrocarbons and monoaromatic hydrocarbons), 11.5% v/v benzene in hexane (to obtain diaromatic hydrocarbons), 32% v/v benzene in hexane (to obtain triaromatic hydrocarbons), 3:4:3 v/v benzene/acetone/CH_2Cl_2 (to obtain resins), 2:8 v/v acetone/THF (to obtain asphalthenes) and methanol (to obtain asphaltols). Fractions were obtained by

monitoring color change under UV light. Solvents were evaporated from each fraction at ambient temperature and the weight recorded. Each fraction was analyzed by GC/MS. Although using color change is subjective, the approach provides comparative information on the composition of the different groups of hydrocarbons that might influence coke texture and structure.

Coking Experiments

The original decant oil and its hydrotreated versions were subjected to heat treatment using a tubing bomb apparatus. Five-gram samples of feedstock were loaded into individual 25-mL vertical microautoclave reactor (commonly referred to as a tubing bomb) and immersed in a sand bath held at 465°C for reaction times of 6, 12 and 18 h under two different pressures: autogenous and atmospheric. **Figure 5-1** shows a schematic of the tubing bomb. The reactors were constructed of 316 stainless steel tubing and fitted with Swagelok weld-on fittings on both ends. The experiments were run in duplicate. The coking took place under autogenous pressure which reached as high as 1000 psig at the reaction temperature. After the desired reaction time, the reactor was quenched with cold water. The coke was recovered by Soxhlet extraction with pentane and THF. The change in conditions was done to observe the influence of reaction time and pressure on the different feedstocks by monitoring the correspondent coke texture by optical microscopy.

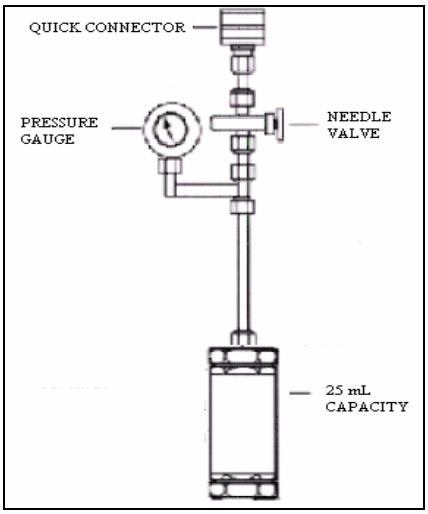

Figure 5-1 Tubing bomb

To run the experiments under atmospheric pressure, the same equipment was used with a slight modification; the Swagelok weld-on tube fitting (female) was coupled to the Swagelok weld-on tube fitting (male) and the needle valve was open. This slight modification allowed for the release of volatile components (gases and liquids) in a controllable manner during the experiments and guaranteed a working pressure of 1 atm.

Microscope Analysis

THF-extracted residue was divided in half, embedded in a cold-setting epoxy resin, placed under vacuum and then in a centrifuge to force a density/particle size gradient. After hardening, samples were cut in half longitudinally and mounted in 25 mm diameter molds. The hardened samples were polished for reflected light microscopy using a series of grit papers (400 and 600 grit) and alumina polishing slurries (0.3 mm and 0.05 mm). The carbon material was evaluated in white light using an oil immersion objective at a total magnification of 625 X in polarized or cross-polarized light. Point count analysis was performed by traversing the sample based upon a 0.4 x 0.4 mm grid

and identifying the textural elements under a crosshair held in the microscope eyepiece. A total of 1000 counts was accumulated, 500 from each of two polished mounts.

Five different textural elements as described below were identified in cokes derived from the different experiments **[5-27, 5-28]**.

Isotropic – a relatively low reflecting, dark gray carbon material derived from decant oil that displays little or no optical activity under polarized light.

Mosaic – a higher reflecting carbon textural element identified from decant oil materials that displays optical anisotropy and is characterized by isochromatic units of < 10 μm.

Small Domain – an anisotropic carbon texture exclusively derived from decant oil and that exhibits isochromatic units of 10-60 μm.

Domain – an anisotropic carbon derived from decant oil and having isochromatic units of greater than 60 μm.

Flow Domain – is an aligned anisotropic texture exhibiting elongated isochromatic areas of greater than 60 μm in length and >10 μm wide.

Subtask 5.2.2. Results and Discussion

Feedstock Composition: Table 5-5 shows the composition of the decant oils (DO) by GC/MS. The feedstock with fa=0.71 corresponds to the original decant oils so-called here after "original decant oil" while decant oils with fa 0.67, 0.64 and 0.62 correspond to the hydrotreated versions; fa=0.62 being the most hydrotreated.

It can be observed from **Tables 5-5 and 5-6** that the original decant oil was composed mostly of tri-aromatic (75 %) compounds, while the hydrotreated decant oils included less tri-aromatic and an increasing presence of di-aromatic compounds. **Table**

5-5 indicates that the most hydrotreated decant oil had increased amounts of decalins and/or cycloalkanes.

Table 5-5 shows the weight percentage in wt of the compounds present in the decant oil on a semi-quantitative basis.

Table 5-5 Composition of DO by GC/MS

Decant oil / fa	**0.71**	**0.67**	**0.64**	**0.62**
paraffins	0.43	0.42	1.07	2.05
saturated cyclics	0.99	3.73	1.98	14.40
alkyl benzenes	7.00	17.02	24.85	11.42
Indenes	0.10	6.92	2.77	4.19
Naphthalenes	3.24	2.95	5.61	4.16
Tetralins	0.00	2.98	6.53	6.81
Decalins	0.00	0.00	0.00	6.69
Polycyclic compounds	88.24	65.99	57.19	50.28

Table 5-6 Preparative liquid chromatography (PLC) and GC/MS

fa	**0.71**	**0.67**	**0.64**	**0.62**
Alkanes	4-5	5-7	4-5	>10
	straight-chain alkanes	straight-chain alkanes	straight-chain alkanes	straight-chain alkanes
				cycloalkanes
mono-Ar	<1	3-5	3-5	10-20
di-Ar	<5	15-25	16-25	6-15
tri-Ar	70-75	50-60	50-60	50-60
tetra and penta - Ar	<5	7-15	7-15	Not observed
polar compounds	10-15	<5	<5	<5

From the results given above it can be concluded that the four feedstocks have different chemical composition largely owing to differences in the presence of hydroaromatics and cycloalkanes which suggest that most hydrotreated feedstock have higher amounts of naphthenic hydrogen.

Coke Characterization - textures of cokes from decant oils (optical microscope)

Autogenous Pressure

To be more concise, optical textures have been grouped as large, intermediate and small isochromatic units in this report. The plots have been designed with two y axes (reaction time in hours and optical texture as a volume percentage) to be compared with the x axis of aromatic hydrogen to aromatic carbon ratio (Har/Car).

Larger isochromatic units: domain and flow domain – Autogenous pressure

The largest isochromatic units, which are flow domain and domain, have been combined as shown in **Figure 5-2**.

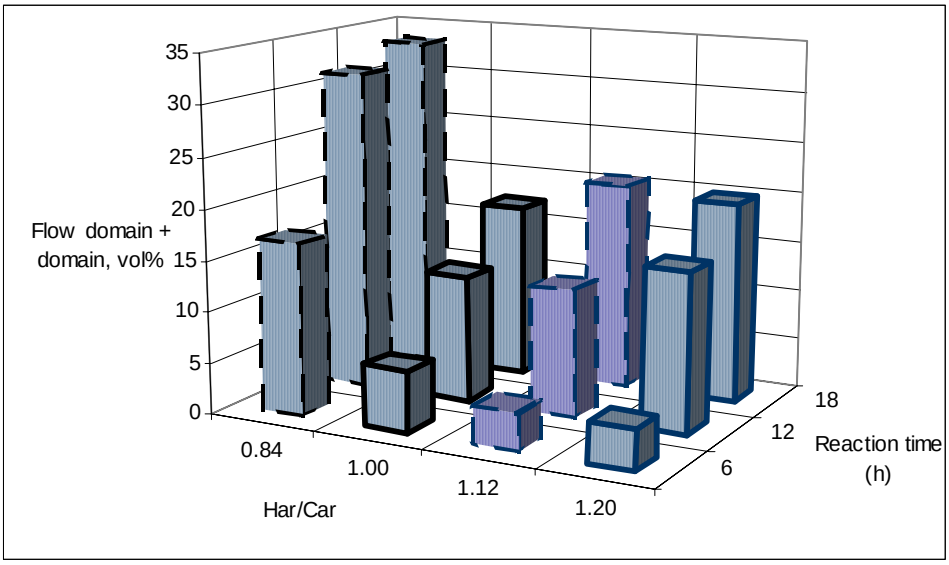

Figure 5-2 Variation of flow domain and domain with reaction time and feedstock chemical composition (Har/Car) – Autogenous pressure

It has been reported that the larger and the more elongated the isochromatic units, the better the quality of the coke **[5-29]**. As observed in **Figure 5-2**, flow domain and domain percentages, called hereafter "total domains" were greater in concentration after

18h for all decant oils. This suggests that at longer reaction times mesophase continued to grow larger and coalesce into more elongated regions.

A higher percentage of total domains were found for the original decant oil (which has lower Har/Car ratio - 0.84) when compared to the hydrotreated decant oils having higher Har/Car ratios. This may be a result of an increased presence of hydrogen in the hydrotreated decant oils decreasing the viscosity of the medium by delaying the coking formation. Naphthene rings such as tetralins, mainly serve as donor solvent that interfere with the formation of condensed aromatic structures **[5-30]**. Hydrogen transfer is a major termination mechanism with no increase of molecular size to suppress the radical reaction, therefore delaying the carbonization reaction **[5-15]**.

To some extent, having a low-viscosity medium may improve the mesophase growth since the mesogen spheres have extended freedom of motion to coalesce. However, in the current situation it appeared that this process has been delayed and suggests that the lower viscosity actually inhibited coalescence of the mesogen molecules. This phenomenon occurred under autogenous pressure, in which low-molecular weight compounds were retained in the system decreasing the viscosity of the medium **[5-18]**.

Medium size isochromatic units

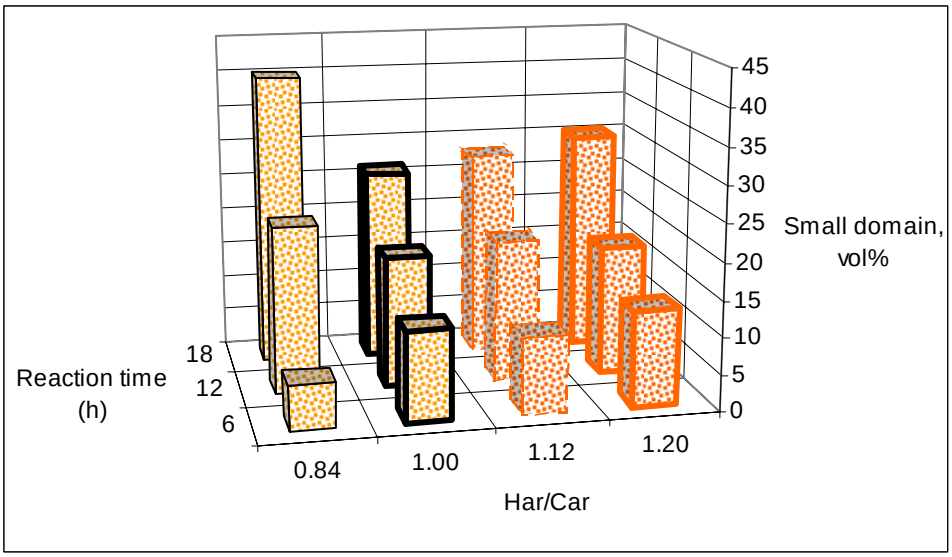

Figure 5-3 Variation of small domain % with reaction time and feedstock chemistry (Har/Car) – autogenous pressure

The percentage of small domains increased as reaction time was increased in all the feedstocks (**Figure 5-3**). At 18h reaction time, the feedstock that commanded the higher percentage of small domain was the original decant oil.

Small size isochromatic unit

The smallest isochromatic units are mosaic and isotropic, although strictly speaking isotropic texture does not exhibit any optical activity when viewed under the microscope. Due to the resolution of the optical microscope (0.5 microns), any mesophase formed below 0.5 microns goes undetected, meaning that the isotropic structure might have some submicron mesophase **[5-31]**. In spite of having some submicron mesophase, the isotropic structure exhibits the least mesophase growth when compared to the other structures (mosaic, small domain, domain and flow domain).

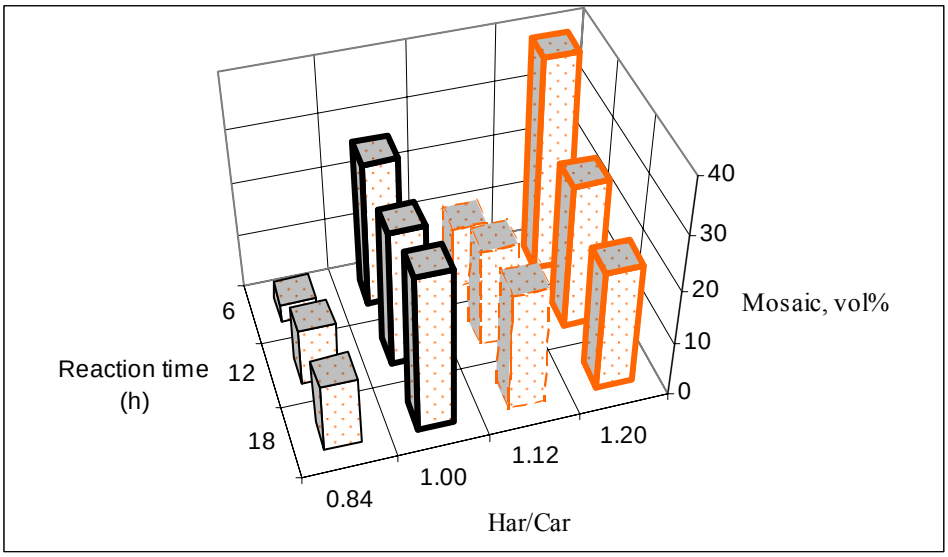

Figure 5-4 Variation of mosaic with reaction time and feedstock chemical composition (Har/Car) – Autogenous pressure

Figure 5-4 shows that the mosaic texture percentage decreased with increasing reaction time. Cokes derived from the original decant oil have the lowest percentage of mosaic texture compared to the cokes derived from the hydrotreated versions.

Figure 5-5 shows the decreasing concentration of the isotropic texture with increasing reaction time. The original decant oil exhibited the lowest percentage of isotropic texture at 18 hours when compared to the percentage of the hydrotreated decant oils.

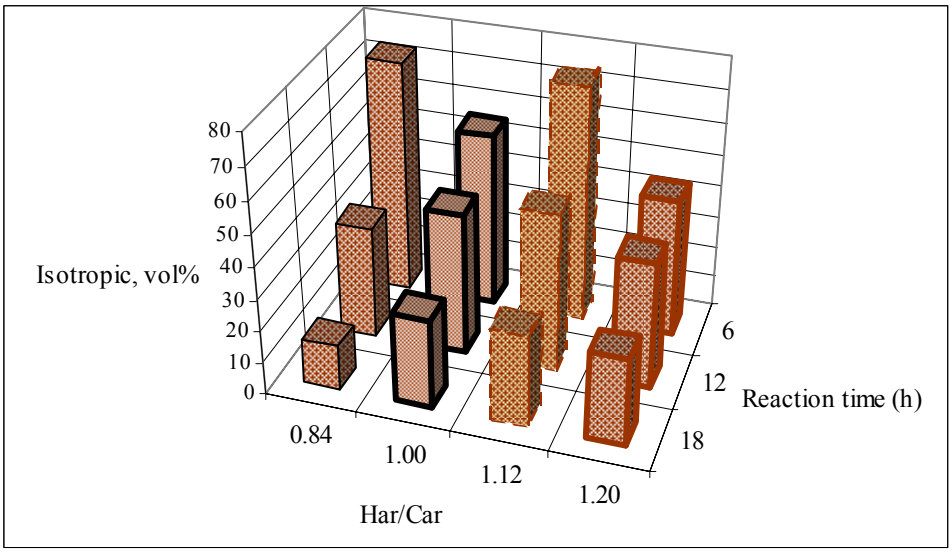

Figure 5-5 Variation of isotropic carbon with reaction time and feedstock chemical composition (Har/Car) – Autogenous pressure

Because the original decant oil contained higher amounts of polycyclic aromatics and lower percentages of alkanes, cycloalkanes and hydroaromatics when compared to the hydrotreated decant oils, the resulting pyrolysis process was dominated by condensation reactions rather than cracking, thus leading to a carbon of larger isochromatic units. As the level of hydrotreatment increased among the other decant oils, a greater amount of gas must have been generated, but was retained in the system under autogenous pressure. Entrainment of gas in the bulk mesophase may have lead to the development of a fine mosaic texture **[5-18]**.

Atmospheric Pressure

Larger isochromatic units: domain and flow domain

Figure 5-6 shows the distribution of total domains for decant oils reacted under atmospheric pressure. The concentration of total domains was highest after 18h reactions time except for the decant oil Har/Car 1.00 for which total domain percentage were

comparable at 12 and 18h. The highest total domain percentages was obtained in cokes generated from the most hydrotreated decant oils (Har/Car = 1.12 and 1.20) which was opposite to the results found from reaction under autogenous pressure. Under atmospheric pressure, the lighter molecular weight fractions were removed from the system as they were formed **[5-18]**. Based on the concentration of total domains, it would seem that the main advantage of increasing levels of hydrotreatment was that gas evolved from the system after the formation of bulk mesophase and resulted in the orientation of the isochromatic units into flow textures.

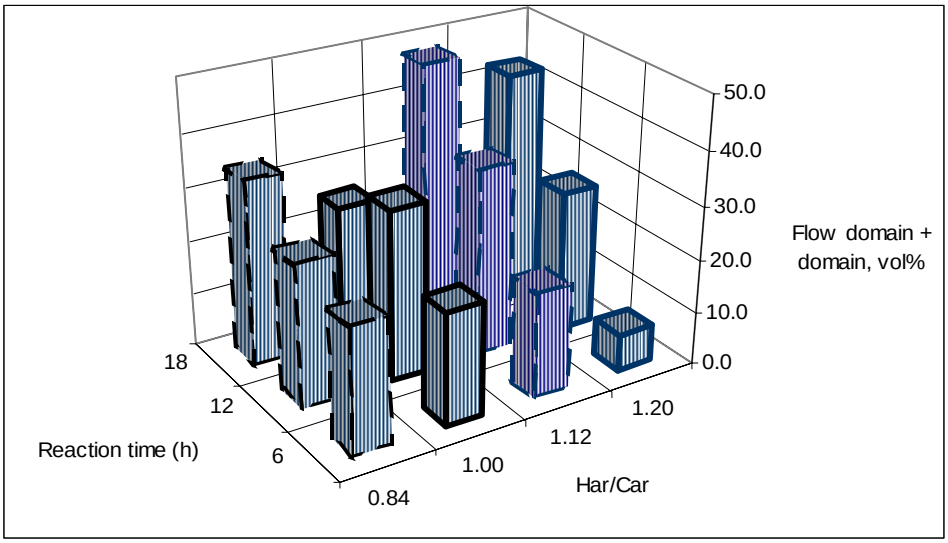

Figure 5-6 Variation of flow domain and domain with reaction time and feedstock chemistry (Har/Car) – Atmospheric pressure

Medium size isochromatic units

Figure 5-7 shows that the small domain textures increased in concentration from 6 to 12h and was nearly constant from 12h to 18h for all the decant oils except for the least hydrotreated decant oil (Har/Car 1.00).

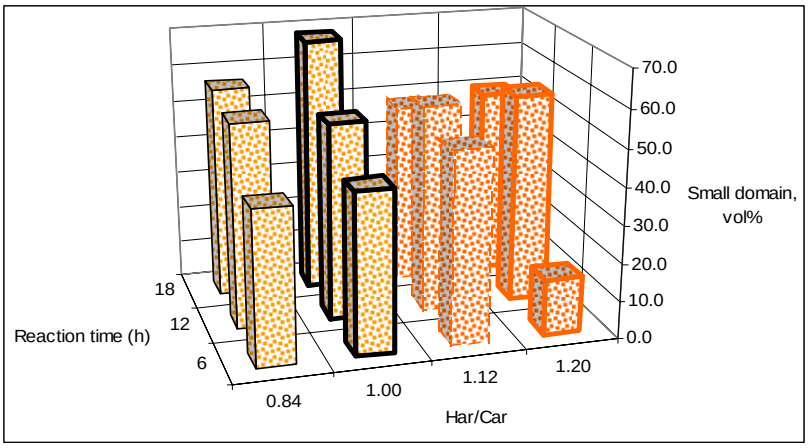

Figure 5-7 Variation of small domain with reaction time and feedstock chemical composition (Har/Car) – Atmospheric pressure

Small size isochromatic unit

Figure 5-8 and **5-9** show that the concentration of mosaic and isotropic textures decreased as reaction time increased under atmospheric pressure and were significantly lower than that generated under autogenous pressure with. Although the loss of lower molecular weight components may lead to higher viscosity, more bulk mesophase of larger size texture was generated which may be direct related to the presence of naphthenic hydrogen.

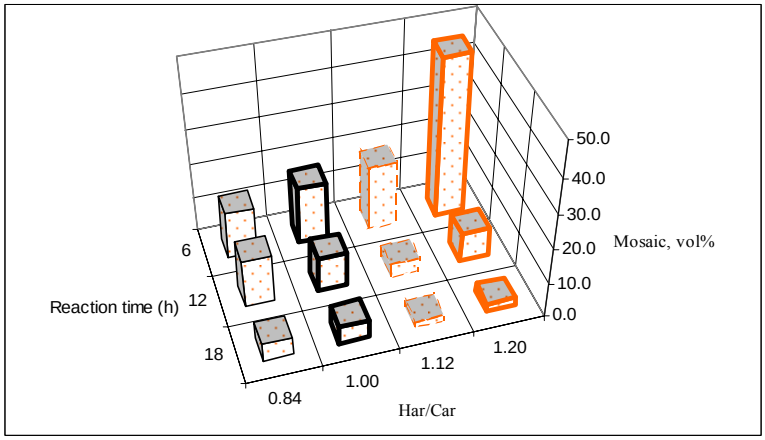

Figure 5-8 Variation of mosaic with reaction time and feedstock chemical composition (Har/Car) – Atmospheric pressure

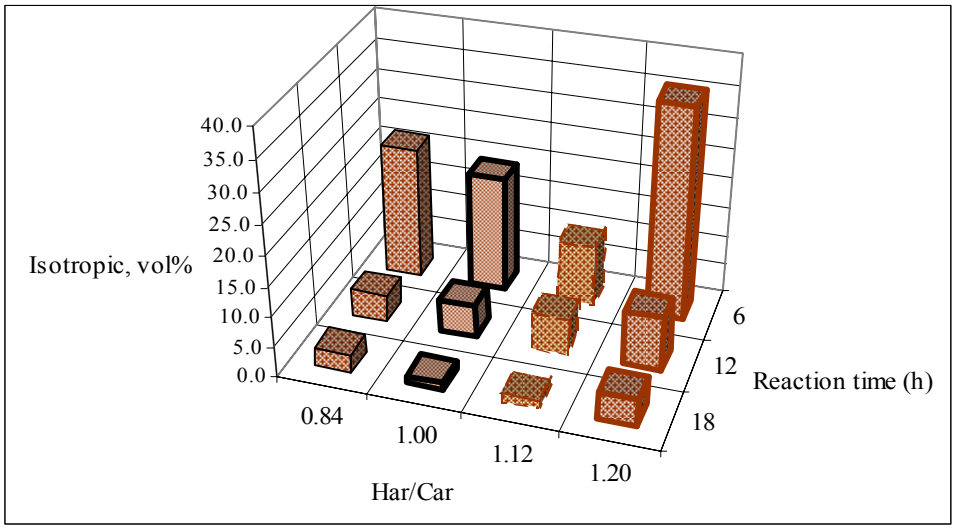

Figure 5-9 Variation of isotropic carbon with reaction time and feedstock chemical composition (Har/Car) – Atmospheric pressure

Comparison coke textures generated under different pressures at 18 h

It has been shown that larger isochromatic units were formed at 18h; a condition more comparable with industrial delayed coking. To obtain a better understanding of the influence of pressure and chemical composition on textural developments in cokes, the results for the 18 h reactions generated under autogenous and atmospheric pressure are compared.

Larger isochromatic units: total domains

Figure 5-10 shows that total domains were found in higher concentration under atmospheric pressure than autogenous from the most hydrotreated decant oils, whereas the original decant oil values were comparable. This suggests that the optimum pressure, and hence, the optimum viscosity depends on the chemical composition of the feedstock. The formation of total domains was slightly favored under high pressures in cokes

derived from high-polycondensed aromatic feedstock (original decant oil). On the other hand, a lower pressure favored the development of larger oriented coke textures when the decant oil has a higher concentration of hydroaromatic and naphthenic compounds.

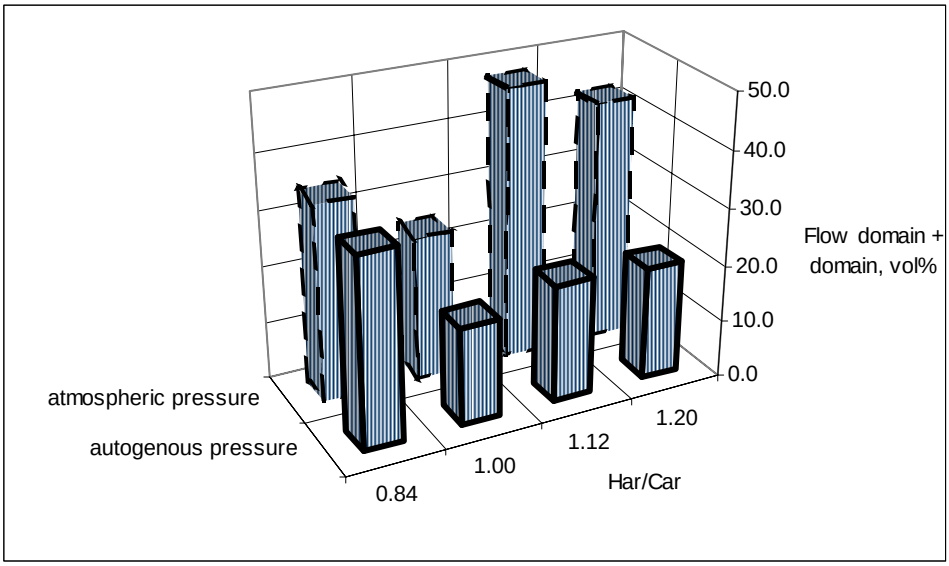

Figure 5-10 Comparison of total domains for the different feedstocks under atmospheric and autogenous pressure at 18h reaction time

Medium size isochromatic units

Figure 5-11 shows that the concentrations of small domain were maximized for all of the feedstocks under atmospheric pressure at 18h reaction time.

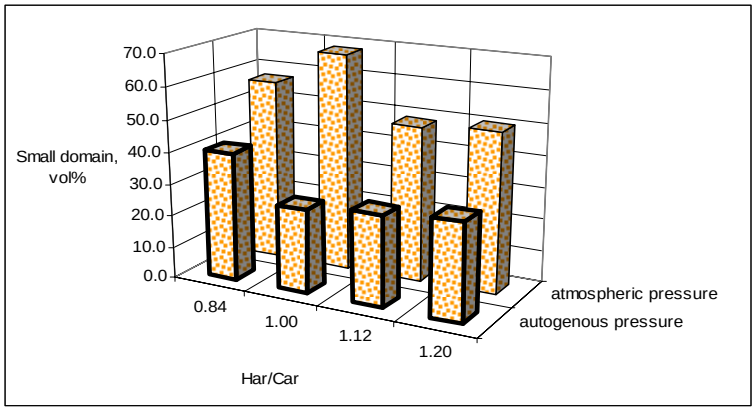

Figure 5-11 Comparison of small domain for the different feedstocks under atmospheric and autogenous pressure at 18 h reaction time

Small size isochromatic unit

The high content of small size isochromatic units (mosaic and isotropic) is an indicative of a poor mesophase growth. **Figure 5-12** and **Figure 5-13** show that a much lower percentage of mosaic and isotropic were present at atmospheric pressure when compared to the percentages under autogenous pressure. In all the decant oils, atmospheric pressure was responsible for an improved grow and coalescence of mesophase.

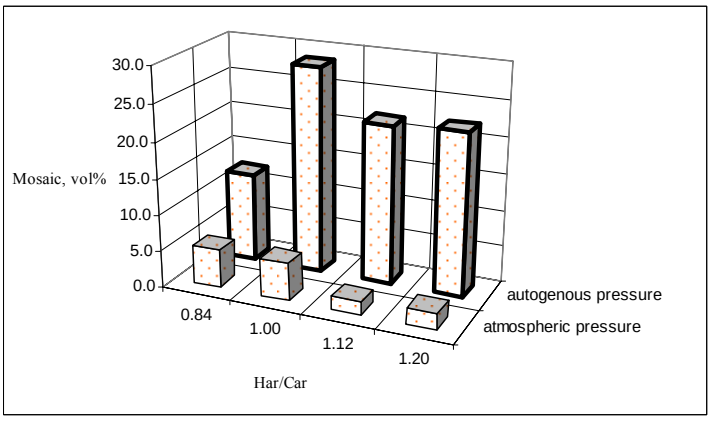

Figure 5-12 Comparison of mosaic for the different feedstocks under atmospheric and autogenous pressure at 18 h reaction time

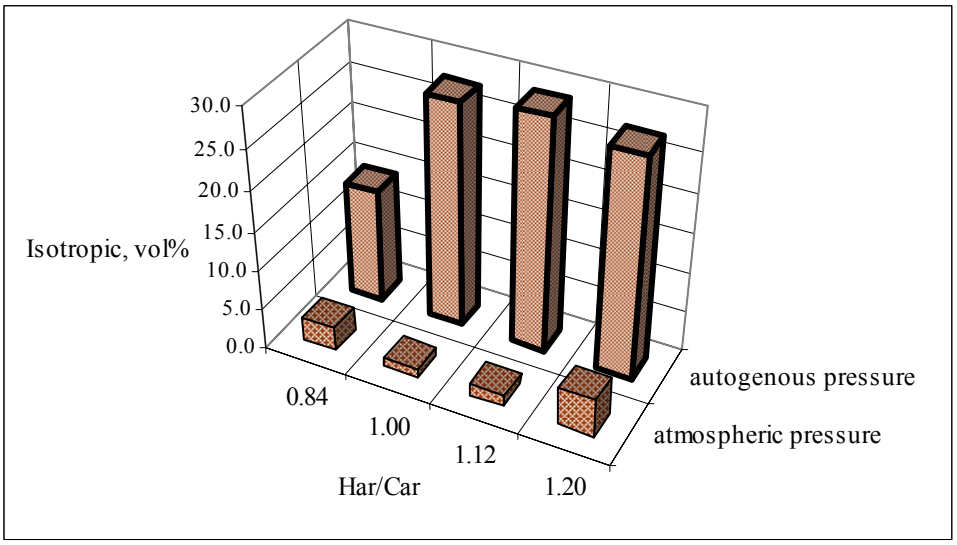

Figure 5-13 Comparison of isotropic carbon for the different feedstocks under atmospheric and autogenous pressure at 18 h reaction time

Subtask 5.2.3 Conclusions

Composition of the feedstock

- The decant oils employed in this study were different in chemical composition. The original feedstock was mostly tri-aromatic while the hydrotreated versions have a larger composition, tri-, di- and mono- aromatics. The most hydrotreated feedstock commanded the higher percentage of naphthenic compounds and hydroaromatics; the mild hydrotreated feedstocks had some cycloalkanes and hydroaromatics. The differentiation in the feedstock's chemical composition provided a means of comparing the influence of chemical composition on the quality of the coke.

Optical microscopy

- The reaction time that commands the higher percentage of larger isochromatic units and lower percentages of smaller isochromatic units was 18 h. This suggests

that a higher reaction time was necessary for the growth and coalescence of the mesophase.

- Under autogenous pressure, the decant oil that performed better in terms of the formation of a high quality coke was the original decant oil. With increasing hydrotreatment and the presence of naphthenic hydrogen, although perhaps causing a decreased viscosity, apparently inhibited the growth and coalescence of the mesophase.
- Under atmospheric pressure, the decant oils that performed better toward the formation of a high quality coke were those that were more deeply hydrotreated. Even though the presence of naphthenic hydrogen might cause decreased viscosity in a closed system, the steady loss of low-molecular-weight compounds in an open system seemed to exert more control on system viscosity. Consequently, the net viscosity increase has had a more profound influence on the formation of larger isochromatic units.
- When comparing the isochromatic units formed under autogenous and atmospheric pressure at 18 h, the best condition to generate a high quality coke was under atmospheric pressure. However, significant levels of hydrotreatment not only reduced the level of heteroatoms in the decant oil, but were shown to improve coke quality, as well.

Future work

- Substantiate the improved anisotropic percentage found by using optical microscopy by measuring Bacon's anisotropy from XRD analysis.

- Carry out other analysis such as density and sulfur content on the green and calcined coke.

Subtask 5.3 Co-Coking of Coal and Heavy Petroleum Stream

Subtask 5.3.1 Co-Coking Of Hydrotreated Decant Oil/Coal Blends In A Laboratory Scale Coking Unit: Characterization Of Feedstock And Distillates From Vacuum Distillation

Subtask 5.3.1.1 Experimental

Materials

A commercial petroleum-based decant oil (EI-107) obtained from United Refining Corporation of the type used for making premium needle coke was used in this study. This decant oil was hydrotreated to different levels of severity at PARC using a NiMo Syncat-37 catalyst. Hydrotreatment conditions and related information can be found elsewhere **[5-32]**. Hydrotreated decant oils were labeled as EI-133, EI-134, EI-135, EI-136, EI-137 and EI-138. The degree of hydrotreatment increases with increasing EI number. The coal used in this study (EI-106) was a 50/50 blend of the Powellton and Eagle seams, both very similar coals of high volatile A bituminous rank. Proximate and ultimate analyses, fluidity and organic petrography results for these feedstocks are shown in **Table 5-7**. Ash and sulfur yields of the original decant oil (EI-107) were found to be 0.22% and 2.99%, respectively.

Apparatus

The pilot-scale delayed coker at The Energy Institute is used to provide reliable

Table 5--7 Proximate and Ultimate Analysis of the Feeds Used in this Study

	Coal	Decant Oil
Proximate analysis [a]	EI-106	EI-107
Ash (%)	8.12	0.22
Volatile matter (%)	27.27	-
Fixed carbon (%)	64.61	-
Ultimate analysis [a]		
Carbon (%)	80.92	89.59
Hydrogen (%)	4.55	7.32
Nitrogen (%)	1.28	0.22
Sulfur (%)	0.88	2.99
Oxygen (by diff.) (%)	4.25	
Fluidity Data [b]		
Fluid Temperature Range (°C)	88	na
Maximum Fluidity (ddpm)	7,002	na
Softening Temperature (°C)	397	na
Organic Petrography, vol%		
Total Vitrinte (vol. %)	86.5	na
Total Liptinite (vol. %)	1.4	na
Total Inertinite (vol. %)	12.1	na

[a] values reported on a dry basis [b] Determined using a Gieseler plastometer

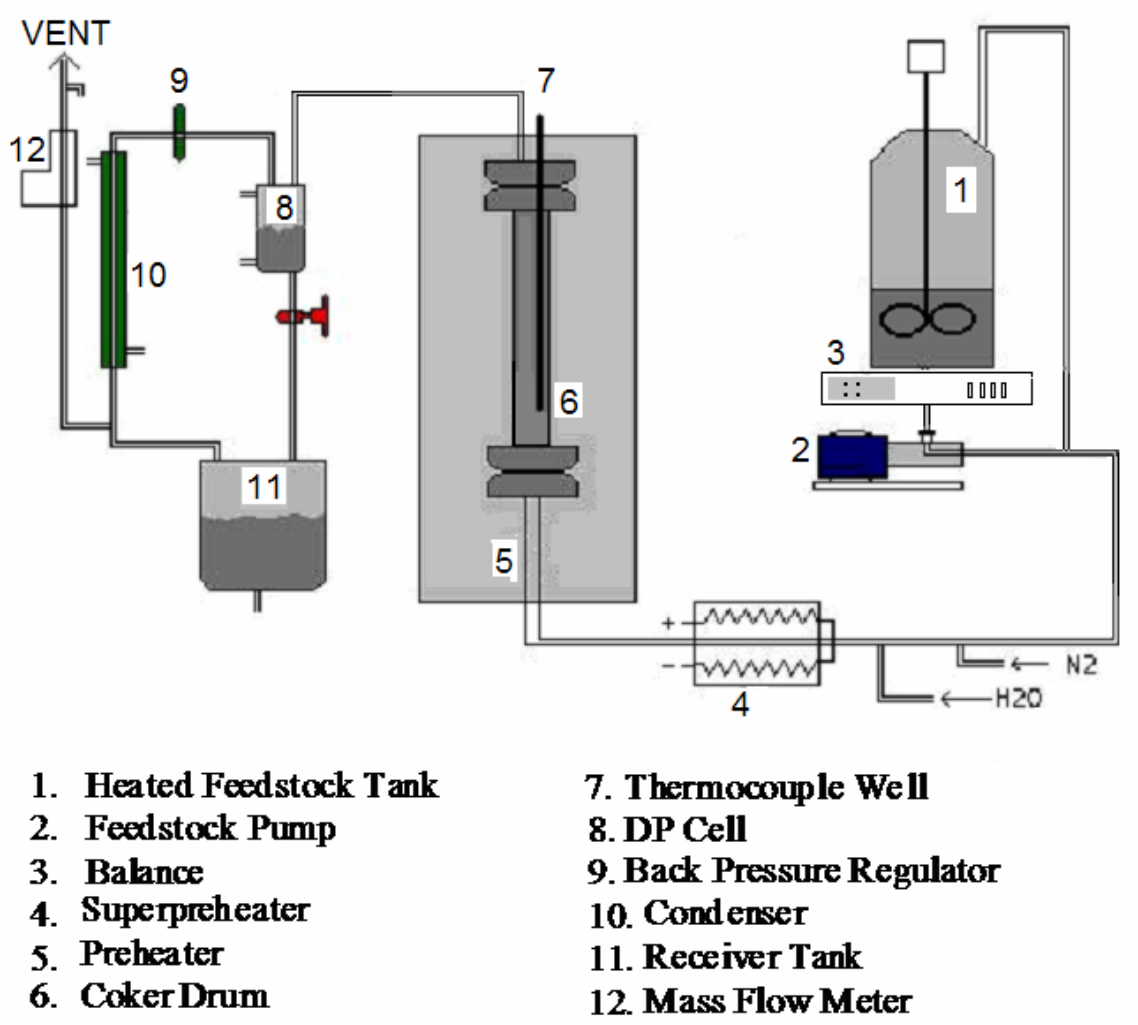

Figure 5-14 A schematic of pilot-scale delayed coker (5.3.1.2)

continuous delayed coking for 4-6 hours to provide acceptable quantities of liquid and coke products for evaluation. The unit is capable of operating under most delayed coking process conditions. The system pressure, temperature and flow rates are monitored by a number of computer-controlled devices, and data from these devices is recorded throughout the run. The slurry feed rate in these experiments was continuous and constant and was measured gravimetrically with time. Some of our earlier results from this PSLC were published recently **[5-33]** and previous work has shown good

reproducibility in terms of product distribution of delayed coker and vacuum fractionation distillates **[5-34]**.

As shown in **Figure 5-14**, the apparatus consisted of a stirred and heated feed tank that was maintained at 66 ºC during the current experimental program. This was connected to a 0.635 cm (1/4 in.) o.d. line that carried feedstocks from the feed pump. Feed materials were pumped to the superpreheater (part 4 in **Figure 5-14**) through a 0.953 cm (3/8 in.) o.d. line that was heated to 120 ºC using heating tape. The preheater (part 5 in **Figure 5-14**) consists of a 2.5 cm o.d. x 51 cm stainless steel tube fitted directly to the bottom of the reactor. The temperature gradient through this 51 cm preheater was on the order of 200 °C, with an outlet temperature of 420-460 °C. The pilot-scale laboratory coker (PSLC) consisted of a 7.5 cm i.d. x 102.5 cm cylindrical reactor unit (coker drum) having an internal volume of approximately 4.5 L. Vaporous materials (liquid and gaseous products) are vented at the top of the reactor drum and collected for evaluation and analysis.

Reaction Procedures

The following operating conditions were used: coke drum inlet temperature 465 °C, coke drum pressure 25 psig, slurry feed rate 16.7 g/min, and feed introduction to the coker for 360 min. At the conclusion of each experiment, the coke drum was maintained at temperature for an additional 360 min to ensure carbonization of nonvolatile components. Additional information about the pilot-scale laboratory coker and associated equipment has been discussed elsewhere **[5-34]**.

In the co-coking experiments, a slurry of coal and decant oil was fed into the coker where the volatile components of the coal and oil were vaporized and subsequently

condensed. The vented reactor system allowed for flash vaporization of the volatiles and subsequent carbonization of the heavy petroleum fraction and coal. In the delayed coking process, feedstock is pumped (16.7 g/min) into the coker drum where reactions between the coke and the liquid lead to the formation of light desirable liquids and carbonaceous solid.

The feed was initially charged to a feedstock vessel that was heated to 66 ºC and continuously mixed throughout the co-coking experiment to achieve and maintain homogeneity. The vessel was placed on a balance for monitoring the feeding rate. The feed was incrementally heated along the feed line to the preheater. Feed was heated in the lines prior to the preheater to about ~220 °C and, then, to about ~440 °C in the preheater before being introduced in to the vertical coker drum. Thermocouples attached at different positions along the coke drum were used to measure and to control the temperature during the experiment. Light hydrocarbons vapor exited from the top of coker drum and pass through a series of condensers. Gases were passed through a mass flow meter and were either collected for analysis or vented.

In the experiments reported here, the liquid products from the reaction were passed through a series of condensers and valves that facilitated their isolation. At the conclusion of the experiment, the mass of the liquid condensate and the carbonaceous solid removed from the coke drum and weighed; gas was determined by difference.

Analytical Procedures

Gas chromatography/mass spectroscopy (GC/MS) analysis, using a Shimadzu QP5000 spectrometer, was performed on liquid samples to determine their chemical

composition. The temperature was held at 40 °C for 5 min, programmed from 40 to 270 °C at 6 °C/min, and then held at 270 °C for an additional 20 min. An XTI-5 (Restek; 30 m x 0.25 mm x 0.25 μm) column was used for the GC/MS analyses. Simulated distillation gas chromatography was performed on liquid samples to determine the refinery boiling range distribution in accordance with the ASTM 2887 method by using an HP 5890 GC-FID fitted with an MXT-500 simulated distillation column (Restek; 10 m, 0.53 mm i.d., and 2.65 μm). The carrier gas flow rate was adjusted to 13 mL/min for sim-dist analysis, and SimDis Expert 6.3 software was used to calculate the percentage of fractions.

Finally, the distillate liquids from each co-coking experiment were vacuum distilled into refinery cuts corresponding to gasoline, jet fuel, diesel, and fuel oil. These fractions were characterized in detail using GC/MS.

Subtask 5.3.1.2. Results and Discussion

Characterization of feedstocks

The coal used in this study was a Powellton/Eagle blend of high volatile A bituminous coals. The petroleum-based decant oil (EI-107) used in this study represents a typical decant oil. Decant oil was hydrotreated at PARC Technical Services (Harmarville) to provide a series of samples of decant oils with different levels of hydrotreating severity. These materials were characterized using a variety of analytical techniques. This information was used to correlate decant oil structure and composition with the quality and yield of the liquid products produced by co-coking with coal.

The objective of this study was to compare the results of the co-coking of the different severity hydrotreated-decant oil and a coal. In co-coking experiments, the coal was used at 20 wt% and the slurry was continuously heated (66 °C) and stirred to ensure homogeneity of the slurry during introduction to the coking reactor. The rate of feed material was maintained at 16.7 g/mL.

Un-hydrotreated original decant oil (EI-107) and hydrotreated versions of original decant oil (EI-133 to EI-138) were analyzed using GC/MS and the compositions of the oils were grouped as the following: paraffins, saturated cyclics, alkyl benzenes, indanes, naphthalenes, tetralins, decalins and polycyclic compounds (Tri-ring +). The GC/MS results in area percentages of these materials are shown in **Table 5-8**.

EI-107 almost completely consisted of aromatic components. As noted in **Table 5-8**, hydrotreatment resulted in increased amounts of paraffins, saturated cyclics, alkyl benzenes, indanes, naphthalenes, tetralins, decalins but decreased amounts of polycyclic compounds in the liquid. One can conclude that as the hydrotreating severity increased, tri-ring + molecules were hydrogenated and converted into small molecules such as naphthalenes, indanes, and benzenes, and as a result of thermal hydrocracking, the amount of tri-ring + compounds was decreased. Hydrogenated homologous of naphthalenes (tetralins & decalins) also were observed in increasing amounts in hydrotreated decant oils as a result of hydrotreatment. The lowest severity hydrotreated decant oil, EI-133, had no decalins, the lowest amount of saturated cyclics, and the highest amount of tri-ring + compounds, while the highest severity hydrotreated decant oil, EI-138, had the highest amounts of saturated cyclics, tetralins, decalins and the

Table 5-8. Percent distribution of the product fractions of original hydrotreated-decant oils*.

Group Classification	Decant Oils						
	EI-107 (Original Decant Oil)	EI-133	EI-134	EI-135	EI-136	EI-137	EI-138
Paraffins	0.4	0.0	1.1	0.4	0.0	3.7	2.1
Saturated cyclics	1.0	1.3	2.0	3.7	3.9	6.7	14.4
Benzenes	7.0	21.0	24.9	17.0	24.6	13.3	11.4
Indanes	0.1	0.1	2.8	6.9	5.6	2.3	4.2
Naphthalenes	3.2	4.0	5.6	3.0	2.6	8.9	4.2
Tetralins	0.0	4.5	6.5	3.0	1.6	6.2	6.8
Decalins	0.0	0.0	0.0	0.0	0.0	6.3	6.7
Tri-ring +	88.2	69.1	57.2	66.0	61.7	52.6	50.3

*: Percent distributions belong to the ratio of GC-MS peak areas

lowest amount of tri-ring + compounds. GC/MS observations were consistent with the hydrotreatment levels of decant oils.

Product recovery

The six co-coking experiments (Runs #27-32) used feedstocks in an 80:20 ratio of hydrotreated decant oil to coal, and the severity of hydrotreatment increased with increasing run number. The decant oils used were EI-133 to EI-138, as stated above, with EI-138 (run 32) having the greatest degree of hydrotreating. Conditions and product yields from each of the co-coking runs are summarized in **Table 5-9** as well as in reference **[5-32]**.

The conditions applied were nearly the same for all of co-coking experiments, e.g., amount of fed material, feed rate and temperatures used. Using similar conditions for each of the experiments, the yields of coke, liquid, and gas were 15.9-24.4 %, 71.0-76.2 %, and 2.2-8.0 %, respectively. Based on our previous work, adding coal to the decant oil resulted in a higher coke yield **[5-33]**. A typical product distribution for a delayed co-coking operation was found as 65% liquids, 30% coke and 5% gas [**5-33]**. Generally, increasing the level of hydrotreatment of decant oil resulted in a lower coke and a higher liquid yields. The process was found to be reproducible in terms of the yields of green coke and liquids isolated from experiments **[5-34]**.

Table 5-9. Conditions and product distributions for co-coking experiments **[5-32]**

	Run # 27	Run # 28	Run # 29	Run # 30	Run # 31	Run # 32
Conditions	DO/Coal 80/20 DO=EI-133 C= EI-106	DO/Coal 80/20 DO=EI-134 C= EI-106	DO/Coal 80/20 DO=EI-135 C= EI-106	DO/Coal 80/20 DO=EI-136 C= EI-106	DO/Coal 80/20 DO=EI-137 C= EI-106	DO/Coal 80/20 DO=EI-138 C= EI-106
Feedstock, hours	6	6	6	6	6	6
Hold at 500 °C, hrs	6	6	6	6	6	6
Feed rate, g/min	16.7	16.7	16.7	16.7	16.7	16.7
Preheater inlet, °C	230	236	227	223	225	224
Preheater outlet, °C	456	440	443	445	439	425
Coke drum inlet, °C	470	470	460	462	468	472
Coke drum lower/middle, °C	472	471	470	470	473	468
Coke drum top, °C	474	472	474	473	478	472
Material Fed to Reactor (g)	6093	5948	5752	6229	6076	5926
Product						
Coke (g)	1099	1453	1079	990	1130	1068
Liquid (g)	4366	4220	4157	4727	4532	4513
Gas (by difference) (g)	486	128	383	369	283	232
Preheater content (g)	142	147	133	143	131	113
Coke + Liquid product (g)	5465	5673	5236	5717	5662	5581
Liquid / Coke	3.97	2.90	3.85	4.77	4.01	4.23
Coke (wt%)	18.0	24.4	18.8	15.9	18.6	18.0
Liquid product (wt%)	71.7	71.0	72.3	75.9	74.6	76.2
Gas (wt%)	8.0	2.2	6.7	5.9	4.7	3.9

Product distributions of distillates

The concept of co-coking stemmed from the need to produce coal-based liquids that would ultimately be converted into thermally stable jet fuel, while relying on domestic fossil fuel resources. With the introduction of coal to the process stream, it was assumed that the volatile constituents of coal may be produced along with the volatiles from the petroleum feed and subsequently fractionated. Previous studies have determined that the compounds present in jet fuel that are derived from coal account for improved thermal stability **[5-35 – 5-42]**.

The liquid products from six co-coking studies were analyzed to determine the proportion of materials in each of the refinery cut boiling ranges. The collected overhead liquids from each co-coking experiment were distilled into conventional refinery boiling ranges by vacuum distillation; boiling point distribution of the liquid products was determined. Vacuum distillation was carried out using approximately 1200 g of the liquid products from the co-coking runs. Each fraction was cut and collected according to the given cut-point temperatures given below at a measured system pressure.

The following boiling point ranges for the liquid products from the fractionation of co-coking overhead liquid were used in this study: gasoline (Initial Boiling Point to 180 °C), jet fuel (180 - 270 °C), diesel (270 - 332 °C) and fuel oil (332 - Final Boiling Point). It has been hypothesized that the yields of products in the given boiling range depends on the degree of hydrotreating of the decant oil feedstock.

GC/MS analyses have been performed to assess compositional changes of gasoline, jet fuel and diesel fractions of overhead liquids of the co-coking experiments. Evaluations of GC/MS analyses results were performed according to the same evaluation

technique for the original hydrotreated decant oils as described above. The compositions of the gasoline, jet fuel and diesel were grouped as the following: paraffins, saturated cyclics, indanes, alkyl benzenes, naphthalenes, tetralins, and polycyclic compounds. GC/MS analyses results of gasoline, jet fuel and diesel fractions are given in **Tables 5-10 – 5-12**, respectively.

Gasoline fractions consisted mainly of paraffins, saturated cyclics and benzenes and small quantities of indanes, tetralins and decalins. No polycyclic aromatic hydrocarbon (tri-ring +) was observed in gasoline fractions (**Table 5-10**). These analyses showed that the amounts of saturated species, e.g., saturated cyclics (from ~25% to ~40%) and decalins (from 0% to 4%) increased as hydrotreatment severity increased; in contrast, the amounts of paraffins (from ~40% to ~20%) decreased. Alkylated benzenes were observed in lower quantities in Runs # 29 and 30 (~28%).

GC/MS analyses showed that the jet fuel fractions were composed of paraffins, saturated cyclics, benzenes, and lower quantities of naphthalenes, tetralins, decalins and very little (~2%) indanes (**Table 5-11**). No tri-ring + compounds were identified in jet fuel fraction. As observed in gasoline fractions, saturated cyclic species were observed in higher quantities as the hydrotreatment level of decant oil increased. These results are consistent with the hydrotreatment levels of decant oil and increased quantity of saturated cyclic species provide an advantage to jet fuel against to thermal cracking at elevated temperatures.

Diesel fraction GC/MS analyses showed that these fractions consisted mainly of highly-alkylated benzenes, naphthalenes and tri-ring + structures (**Table 5-12**). An obvious increasing trend was observed for the saturated cyclics (~5% →~23%), but

decreasing trends were observed for indanes (~6% →~1%) and naphthalenes (~23% →~8%) as the hydrotreatment level increased (from run # 27 to #32). In gasoline and jet fuel fractions saturated cyclic compounds were generally alkyl substituted cyclohexanes, but in the diesel fraction, these saturated cyclic structures also contained saturated higher-ring species. In the diesel fractions, either no decalins were observed (for the first four co-coking experiments (Run # 27-30)), or very small amount of decalins (~1%) were observed (in the other two co-coking runs (Run # 31 and 32)).

Our earlier decant oil/coal co-coking studies showed that both decant oil light fraction and coal-derived light hydrocarbons were co-distilled **[5-34]**. In these six co-coking experiments, the only changing parameter was the hydrotreatment severity of decant oil used. The effect of hydrotreatment level of decant oil can be seen in each of the vacuum fraction, such as an increase of hydrogenated species (saturated cyclics, decalins, etc.) and a decrease of aromatics (naphthalenes, benzenes, etc.). From the data, it appears that the light fraction of hydrogenated decant oil significantly contributed to the overhead liquids and determined the composition of fractionated liquid more drastically. It has been hypothesized that the yields of products in the given boiling range depends on the degree of hydrotreating of the decant oil feedstock.

Table 5-10. Percent distribution of the product fractions of gasoline obtained from vacuum distillation of co-coking overhead liquid.

Group Classification	Run 27 (EI-133)	Run 28 (EI-134)	Run 29 (EI-135)	Run 30 (EI-136)	Run 31 (EI-137)	Run 32 (EI-138)
Paraffins	38.9	37.8	40.1	35.1	23.4	21.6
Saturated cyclics	25.6	23.5	29.7	38.0	42.3	38.1
Benzenes	35.5	37.7	28.7	26.7	32.6	35.4
Indanes	0.0	0.1	0.1	0.0	0.0	0.5
Naphthalenes	0.0	0.4	0.3	0.0	0.0	0.0
Tetralins	0.0	0.5	0.5	0.1	0.1	0.3
Decalins	0.0	0.0	0.5	0.1	1.7	4.1
Tri-ring +	0.0	0.0	0.0	0.0	0.0	0.0

Table 5-11 Percent distribution of the product fractions of jet fuels obtained from vacuum distillation of co-coking overhead liquid.

Group Classification	Run 27 (EI-133)	Run 28 (EI-134)	Run 29 (EI-135)	Run 30 (EI-136)	Run 31 (EI-137)	Run 32 (EI-138)
Paraffins	33.8	27.6	26.8	29.4	21.6	20.0
Saturated cyclics	12.5	18.3	17.3	21.7	31.0	35.8
Benzenes	32.2	26.7	29.5	27.9	18.5	20.9
Indanes	0.8	3.7	2.0	1.3	0.6	1.5
Naphthalenes	11.5	13.7	14.0	11.5	9.6	6.5
Tetralins	8.8	9.5	8.8	6.0	10.0	9.9
Decalins	0.5	0.6	1.6	2.2	8.7	5.6
Tri-ring +	0.0	0.0	0.0	0.0	0.0	0.0

Table 5-12. Percent distribution of the product fractions of diesel fuels obtained from vacuum distillation of co-coking overhead liquid.

Group Classification	Run 27 (EI-133)	Run 28 (EI-134)	Run 29 (EI-135)	Run 30 (EI-136)	Run 31 (EI-137)	Run 32 (EI-138)
Paraffins	5.2	4.3	2.3	2.3	2.7	9.1
Saturated cyclics	4.9	4.5	4.4	7.9	10.4	23.4
Benzenes	39.9	47.4	56.2	60.0	43.1	40.1
Indanes	5.5	4.5	0.5	3.5	0.9	0.8
Naphthalenes	23.2	12.2	15.8	11.0	11.8	8.4
Tetralins	2.5	1.2	0.3	0.6	0.3	0.6
Decalins	0.0	0.0	0.0	0.0	1.0	0.5
Tri-ring +	19.0	25.9	20.6	14.7	29.8	17.2

Subtask 5.3.1.3. Conclusions

Increased hydrotreating severity resulted in decreased tri-ring + molecules and increased smaller molecules (e.g., naphthalenes, indanes, benzenes) and hydrogenated species of these smaller molecules (e.g., tetralins, decalins, saturated cyclics). Use of the pilot-scale laboratory coker provides sufficient quantities of distillate liquids so as to provide distillable product from co-coking reactions. Vacuum distillation of the collected distillate liquids from co-coking experiments was performed to provide gasoline, jet fuel, diesel, and fuel oil products. The boiling point distributions and chemical compositions in the co-coking experiments were found to be relatively dependent on hydrotreatment levels of decant oil. An increase in saturated cyclics, tetralins and decalins, but a decrease in paraffins, benzenes, and naphthalenes in the co-coking experiments, was measured by GC/MS as the hydrotreatment severity increased. No tri-ring + compounds were identified in gasoline and jet fuel fractions. The data support hydrotreatment of the decant oil as a means of providing a potentially thermal stable jet fuel **[5-43]** via increasing the saturated cyclics and decalins contents of jet fuel fraction. Our earlier results also showed **[5-32]** that coal introduction to the delayed coker increased the aromatic content of delayed coker distillate liquid. Further hydrotreatment/hydrogenation of this liquid having more aromatic could provide thermally stable jet fuel.

Subtask 5.3.2 Production of Coal Tar from Coal Extraction

Refined Chemical Oil (RCO) is a distillate produced from the refining of coal tar (a by-product of metallurgical coke industry) and it represents around 10% of the coal tar yield. RCO consists mainly of a mixture of naphthalene (70%), indene and their derivatives. It is of special interest to current research at Penn State as it is blended with

Light Cycle Oil (LCO) derived from the catalytic cracking of petroleum, for further processing. Upon hydroprocessing, the blend can be converted to process streams containing a high concentration of two-ring aromatic compounds (tetralin and decalin) that can then be used to formulate a thermally stable jet fuel. Unfortunately, under current environmental regulations it is unlikely that new by-product coke ovens will be built in the United States and the older remaining facilities are in danger of being closed. Therefore, a stable supply of RCO for the future is questionable.

With this in mind, it is important to consider alternative ways of producing RCO from coal in a very inexpensive process. Direct coal liquefaction would not be considered as an option, because there is no indication that this process would be economically competitive with petroleum processes. In order for a new process to be economic, it should be able to be integrated into a refinery. Therefore, it should use operating units, chemical reagents and/or solvents that are used or produced in a refinery. In this sense, the processes expected to be used are those that do not require expensive chemical reagents (in particular catalysts and consumption of hydrogen) and do not consume high quantities of energy. The processes that could possibly produce useful two-ring compounds from coal and meet these criteria are some form of solvent extraction of coal.

Because our objective is to use coal-derived materials in blends with LCO, it was decided to try LCO as the solvent for the extraction. This would save the steps of stripping the solvent off the extract, blending the extract with LCO, and recycling the solvent. Our initial aim was to produce an extract using a 1:1 LCO/Coal blend that could be sent to a hydrotreating and hydrogenation process up-stream in the refinery to end

with the production of the highly thermal stable jet fuel. In the research performed during this reporting period and discussed below, a variety of coal-extraction processing schemes were evaluated to meet these goals.

Subtask 5.3.2.1 Experimental

Samples

A variety of coals were obtained from Argonne National Laboratory Premium Coal Sample Bank as well as the Penn State Coal Sample Bank to cover a broad distribution of rank and thermoplastic properties. The coals used in this work were ground to –60 mesh (250 μm) and their ultimate and proximate analyses are given in **Table 5-13**. The LCO used as a solvent to extract organic components from these coals was obtained from United Refining Company, Warren PA. The properties of this solvent are listed in **Table 5-14**.

Table 5-13 Coal properties

	Pittsburgh	Powellton	Blind Canyon	Illinois # 6	Upper Freeport	Splash Dam
ASTM Rank	hvAb	hvAb	hvAb	hvCb	mvb	mvb
Proximate Analysis (dry)						
Ash, %	10.25	5.00	5.84	13.39	13.18	3.89
Volatile Matter, %	36.02	29.90	44.50	40.83	27.45	30.13
Fixed Carbon, %	53.73	65.10	49.66	45.78	59.37	65.98
Ultimate Analysis (dry)						
Carbon, %	83.32	87.60	81.28	76.26	85.5	87.83
Hydrogen, %	5.69	5.80	6.24	5.30	4.7	5.36
Nitrogen, %	1.37	1.60	1.55	1.32	1.55	1.57
Sulfur, %	1.25	0.90	0.42	6.38	2.32	0.82
Oxygen, %	8.37	4.10	10.50	10.74	7.5	4.42
Thermoplastic Properties (Gieseler Plastometer & Free Swelling Index)						
Initial Softening Temperature, ºC	387	385	400	366	373	383
Maximum Fluidity Temperature, ºC	440	448	419	410	450	458
Solidification Temperature, ºC	477	488	438	444	497	500
Fluid Temperature Range, ºC	90	103	38	78	124	117
Maximum Fluidity (ddpm)	20002	30000	3	49	30000	28188
Free-swelling index	7.5	7.5	2	3	8.5	8

Table 5-14 LCO properties

Properties		
API Gravity @ 60 °F, ASTM D-287	10.3	
Specific Gravity (gr/mL), ASTM D-1298	0.9979	
Sulfur (wt %), ASTM D-5453	1.92	
Nitrogen (ppm), ASTM D-5762	535	
Distillation (° C)	ASTM D-86	ASTM D-2887
IBP	220	146
10	266	249
20	277	271
30	286	279
50	296	301
70	313	324
80	324	341
90	336	359
FBP	354	396

Thermal Extraction

Single-stage extraction at room temperature filtration

Figure 5-15 shows a schematic of the 165-mL stirred batch reactor initially used to carry out the extraction experiments. The reactor has a fitted impeller, which gives good mixing of the LCO/coal dispersion during the reaction. The reaction conditions were 350 °C, 100 psi and 1 hour reaction time. Coals were dried in a vacuum oven at 100 °C at 30 mmHg overnight and cooled for one hour in a desiccator. The appropriate amount of LCO and coal were loaded in the reactor. The reactor was sealed and then placed in the heater. The sealed reactor was purged three times with 1000 psi (7 MPa) of ultra-high-purity N_2 (UHP, 99.999%) and finally pressurized to a 100 psi of N_2.

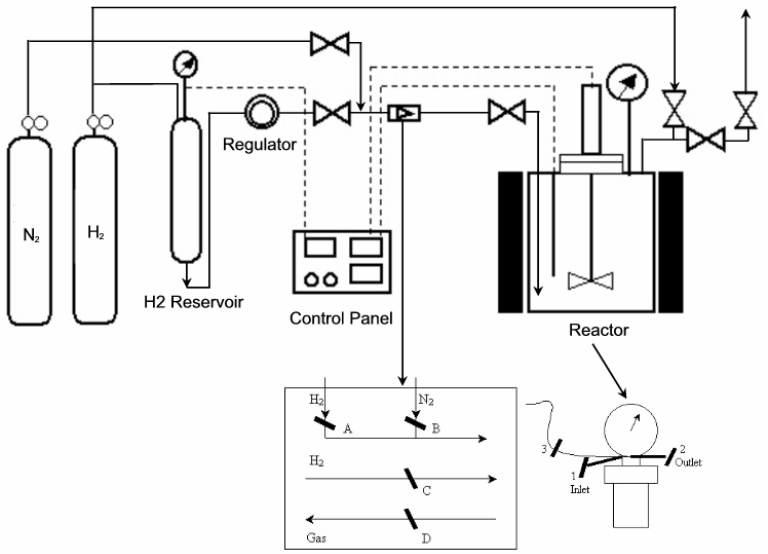

Figure 5-15 Schematic single-stage extraction at room temperature filtration reactor

When the temperature reached 70-80 °C below the reaction temperature, the stirrer was started and set at 1500 rpm. After the reaction, the reactor was brought to room temperature by immersing it in a cold water bath for 1 hour.

The LCO/coal dispersion was filtered using a Millipore filter (fine porosity) with a previously weighed PTFE filter. The reactor and the solid were washed with dichloromethane (DCM) until the supernatant became almost colorless. The resulting solid material, which is called the "residue" hereafter, was quantitatively transferred to a previously weighed Petri dish and then dried in a vacuum oven at 110 °C and 30 mmHg for at least 4 hours, cooled to room temperature in a desiccator for an hour and then weighed. This was repeated until a constant weight was obtained. The resulting solution, which is called the "extract" hereafter, was rotary evaporated in a water bath at 60 °C until all the dichloromethane was removed. In order to eliminate any remaining dichloromethane, the solution was held overnight in a vacuum oven without heating and then weighed. This was repeated until the loss of weight was less than 200 mg.

The extraction yields were calculated from the weight of initial amount of coal and residue on a dry ash-free basis according to Equation 1.

$$\text{Extraction Yield} = \frac{1 - \frac{\text{residue weight (gr)}}{\text{coal weight (gr)}}}{1 - \frac{\text{ash (wt \%, db)}}{100}} \times 100 \quad (1)$$

The extract yields were calculated with respect to the initial amount of coal according to Equation 2 and with respect to the initial amount of LCO according to Equation 3.

$$\text{Extract Yield}_{\text{coal}} = \frac{\text{extract weight (gr)} - \text{LCO weight (gr)}}{\text{coal weight (gr)} \times (1 - \frac{\text{ash (wt \%, db)}}{100})} \times 100 \quad (2)$$

$$\text{Extract Yield}_{\text{LCO}} = \frac{\text{extract weight (gr)} - \text{LCO weight (gr)}}{\text{LCO weight (gr)}} \times 100 \quad (3)$$

Single-stage extraction at high temperature filtration

Figure 5-16 shows a schematic of the high temperature extraction/filtration device. Initially coal extractions were carried out using a 1 L stirred autoclave (single-stage extraction) under typical reaction conditions of 350 °C, 100 psi and 1 hour reaction time. The coal/solvent slurries were prepared using different coal/solvent ratios. After the reaction, the reactants flowed down to a filter system for hot liquid/solid separation. The filtration system in the extraction device consists of a 47 mm stainless steel autoclave funnel holding a 0.45 μm PTFE filter.

The filtration system containing the remaining solid material can be separated from the extraction device. The funnel and solids were washed with dichloromethane (DCM) until the supernatant became almost colorless. The solid residue was dried in a vacuum oven at 110 °C and 30 mmHg for at least 4 hours, cooled to room temperature in a desiccator for an hour and then weighed. This was repeated until a constant weight was obtained.

Coal conversion was calculated using ash as a tracer according to Equation 4.

$$\text{Coal Conversion } \% = 100\left[1 - \frac{A_0(100 - A')}{A'(100 - A_0)}\right] \quad (4)$$

Where A'= ASTM ash of the dry residue and A_0= ASTM ash of the dry coal.

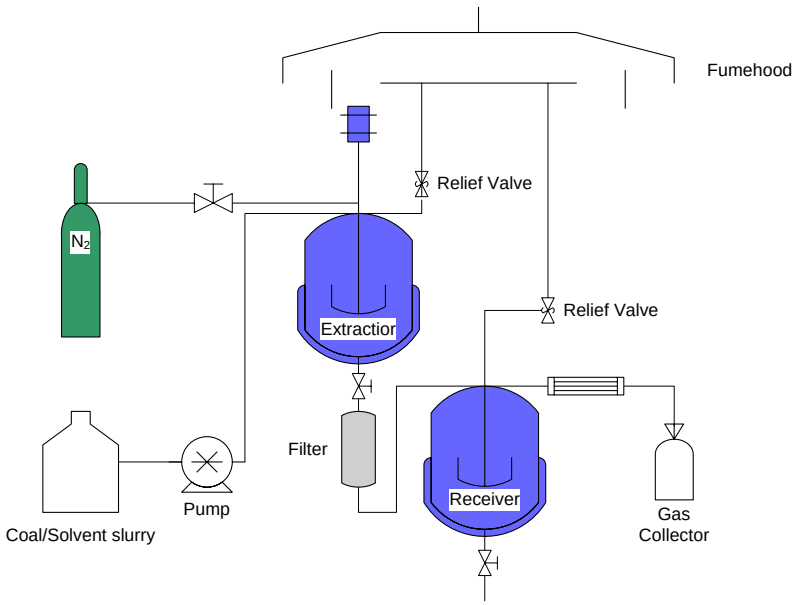

Figure 5-16. Schematic of the single-stage extraction at high temperature filtration device

Multi-stage extraction in a flow reactor

Figure 5-17 shows a schematic of a flow reactor designed to carry out multi-stage extraction of coal. Coals were dried in a vacuum oven at 100 °C and 30 mmHg overnight and cooled for one hour in a desiccator. The three extraction cells were loaded with 3 gr of coal each. The system was purged three times with 1000 psi (7 MPa) of ultra-high-purity N_2 (UHP, 99.999%) and finally pressurized to 100 psi of N_2. The LCO was continuously flowed to the system by means of the HPLC pump using a rate of 1 mL/min and was preheated at 300 °C before entering in the extraction cells that were heated to 350 °C. After 1 hour of reaction time the HPLC pump and the furnace were turned off and allowed to cool down.

The remaining solid materials from each extraction cell were separately filtered using a previously weighed Millipore apparatus and a 0.45 μm PTFE filter. The cells and

the solid were washed with dichloromethane (DCM) until the supernatant became almost colorless. The resulting residues were quantitatively transferred to a previously weighed Petri dish and then dried in a vacuum oven at 110 °C and 30 mmHg for at least 4 hours, cooled to room temperature in a desiccator for an hour and then weighed. This was repeated until a constant weight was obtained.

Coal conversion was calculated on a dry ash-free basis according to Equation 5.

$$\text{Coal Conversion (wt \% daf)} = \frac{\text{feed coal (daf) - residue (daf)}}{\text{feed coal (daf)}} \times 100 \quad (5)$$

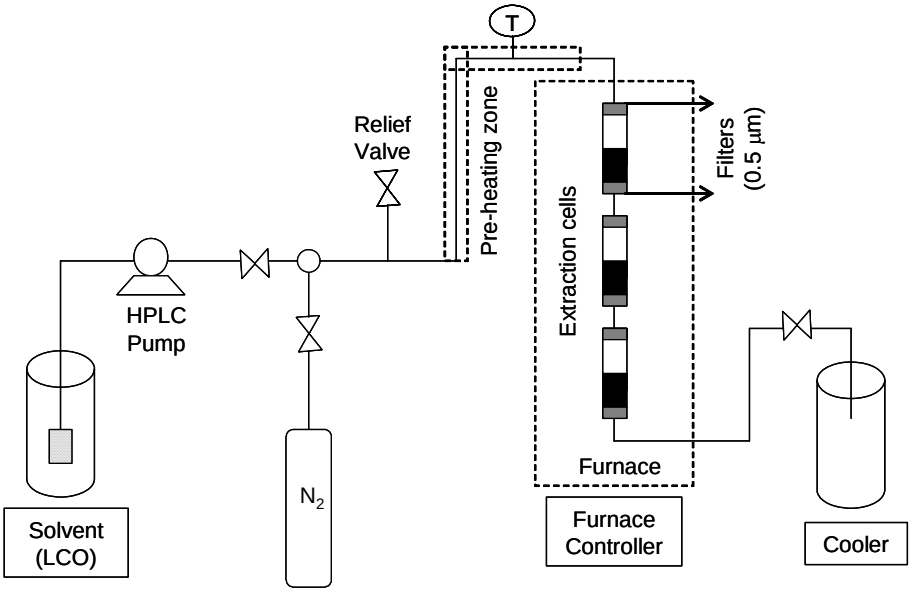

Figure 5-17. Schematic of the multi-stage extraction in a flow reactor.

Analyses

Fractionation of LCO and LCO/Pittsburgh extract

To characterize the material extracted from coal, the original LCO and the extract obtained from the Pittsburgh coal at 350 °C and LCO/coal 10:1 ratio were fractionated using preparative liquid chromatography. This method, known as PLC-8, was used to separate samples into eight discrete fractions with chemical identity very well defined **[5-**

44] and has been used before to characterize the hydrocarbon products from coal processing **[5-45]**.

In this procedure 300 mg of sample were dissolved in a minimal amount of THF, stirred with 2 g of Silica gel (Merck, grade 10181, 35-70 mesh) pre-activated for 4 hours at 180 °C and then the solvent was evaporated. The separation was carried out in triplicate using three 50 cm (L) x 11 mm (I.D.) glass columns fitted with a teflon stopcock that were slurry packed. A plug of glass wool on the end was used to support the solid adsorbent. The slurry was packed by first adding the pre-activated Silica gel (18 g) a little at a time to hexane (60 mL) in a beaker, swirling the beaker and placing the slurry into a draining column previously filled about 1/3 full with hexane that was mechanically agitated. The sample-coated silica gel was placed on the top of the column. The elution was performed with the mobile phases and the volume listed in **Table 5-15.** The flow rate at the column outlet was maintained at 1.2 mL/min. The separation was followed by collecting fractions of 10 mL in 20 mL vials previously weighted. The solvents were evaporated to constant weight in a vacuum oven and then weighed; the material mass in the vial was determined by difference.

GC-MS Analyses

The GC-MS analyses were conducted on a Shimadzu GC174 coupled with a Shimadzu QP-5000 MS detector. The column used was a Restek XTI5 (5% diphenyl/95% dimethylsiloxane) and the starting temperature is 40 °C, hold for 4 min, then heated up in stages to 150°C with a heating rate of 6 °C/min and then from 150 to 290 °C with a rate of 4 °C/min and held for 10 min. The initial and final pressures in the column were 48.9 and 144 kPa, respectively.

Table 5-15. Fractionation of samples by PLC.

Fraction	Fraction eluted	Eluent	Volume (mL)	Vials
F1	Saturated Hydrocarbon	Hexane	40	1-4
F2	Monoaromatic Hydrocarbon	Hexane	27	5-7
F3	Diaromatic Hydrocarbon	11.5% v/v benzene in hexane	36	8-11
F4	Triaromatic Hydrocarbon	32% v/v benzene in hexane	24	12-14
F5	Polynuclear Aromatic Hydrocarbon	32% v/v benzene in hexane	25	15-17
F6	Resins	3:4:3 v/v benzene/acetone/CH_2Cl_2	65	18-23
F7	Asphaltenes	2:8 v/v acetone/THF	60	24-29
F8	Asphaltols	Methanol	65	30-35

Proximate Analyses

The proximate analyses were carried out using a LECO MAC-400 analyzer. This instrument measures moisture, volatile matter and ash yields by determining the weight lost after having been heated under different atmospheric and thermal conditions. The fixed carbon is a calculated value determined as the difference from 100 of the measured values (moisture, volatile matter and ash).

Subtask 5.3.2.2 Results and Discussion

Single-stage extraction at room temperature filtration

The extraction and extract yields at 350 °C and different LCO/coal ratio are shown in **Figure 5-18**. The extraction yields are in the range of 30 to 50 wt %. These

results are comparable to the results reported by Takanohashi et al. **[5-47]** using LCO and crude methyl-naphthalene oil at 360 °C to extract bituminous and sub-bituminous coals to produce an ashless coal (hypercoal). In this work extraction yields between 34-42 wt % were obtained. In the current investigation, the highest extraction yields were found using a LCO/coal ratio of 10:1, which suggests that the greater the amount of LCO available in the process, the better extraction and extract yields. Under these conditions and as shown in **Figure 5-18** the extraction yields were 39 wt % for Pittsburgh, 29 wt % for Powellton, 51 wt % for Illinois#6, 36 wt % for Upper Freeport and 46 wt % for Blind Canyon.

Takanohashi et al.**[5-47 - 5-50]** have reported that the high extraction yields obtained with industrial, non-polar and non-hydrogen donor solvents like LCO may be the result of heat-induced structural relaxation followed by solubilization of coal component in the solvent. This means that there is not a strong interaction between LCO and coal that would make it possible to break the bonds that keep the coal network structure intact. Instead, it appears that the LCO acts to disperse the components derived from the coal bulk during the onset of the softening process. **Figure 5-19** shows that under the thermal conditions employed, there is a very strong relationship between coal rank (volatile matter) and extraction yields. This result seems to confirm that LCO can act as an effective vehicle to move material out of the coal network during the extraction process.

Another way to evaluate extract yields would be to calculate them with respect to the initial amount of coal and LCO. The extract yield with respect to the initial amount of LCO provides a measure of the amount of material dispersed from coal into the LCO.

If we call the material extracted RCO, then a RCO/LCO ratio can be determined. **Figure 5-18** shows that these extract yields ranged between 3 to 7 wt % and that the LCO/Blind Canyon extraction gave the best extraction yields since the resultant blend raised almost 1/9 RCO/LCO.

The results presented here suggest that even when extraction yields were high enough, the high LCO/coal ratios (10:1) used produced a RCO/LCO blend that was still too concentrated with respect to LCO and too diluted with respect to RCO. It was not possible to employ a RCO/LCO 50/50 blend in a coal extraction process conducted in one single-stage. Presumably, greater extraction yields would be obtained from a multi-stage extraction process. However, the greatest level of extraction and extract yields were obtained in this study at 350 °C, 10:1 LCO/coal ratio, 1 hour reaction time and 100 psi N_2. Conditions such as these, at relatively low severity, may be the basis for an economic extraction process.

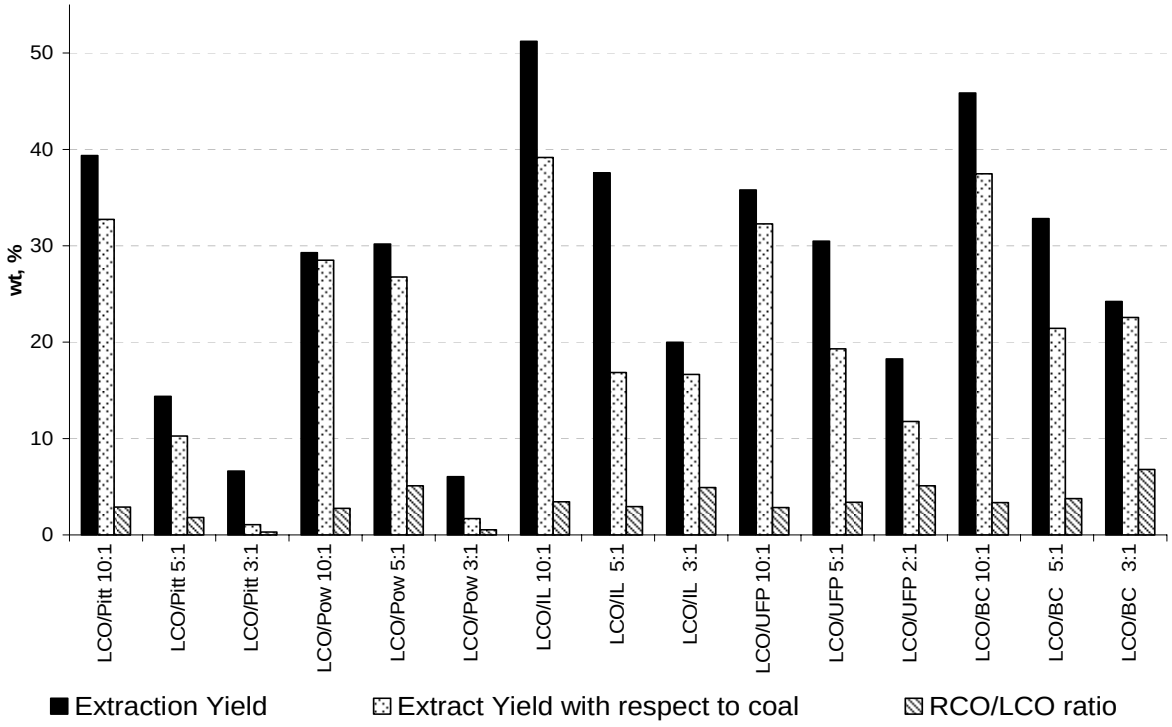

Figure 5-18 Extractions yields for LCO/coal extraction of bituminous coals at 350 °C.

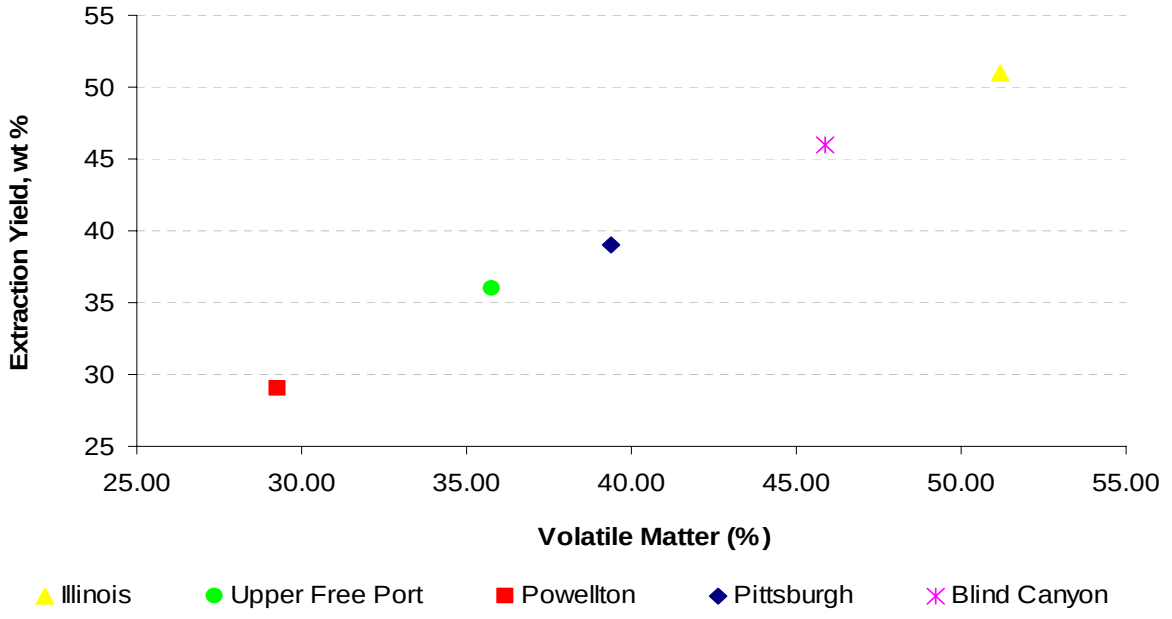

Figure 5-19 Correlation between the extraction yields and the coal volatile matter.

A combination of preparative liquid chromatography and GC/MS were used to determine the chemical nature of materials that may have been extracted from the Pittsburgh seam coal. **Figure 5-20** shows the results obtained from preparative liquid chromatography. In the fraction 5 (F-5) of the LCO/Pittsburgh extract, a material was detected that was not present in the original LCO used to make the extraction. GC-MS analyses of at least one vial for each fraction obtained from this separation were studied.

The GC-MS analyses are shown in **Figure 5-21**. Fraction 1 (F-1) of the LCO and the LCO/Pittsburgh extract were very similar in that they contained mainly saturated hydrocarbons in the range of C_{13}-C_{23}. Fraction 2 (F-2) of the LCO and the LCO/Pittsburgh extract were also very similar and these contain only monoaromatic hydrocarbons with long side chains (C_9-C_{15}). Fraction 3 (F-3) of LCO and LCO/Pittsburgh extract were still very similar, but they were more complex than the two previous fractions. The major constituents of these fractions were basically naphthalene and alkyl-naphthalenes, although indans and tetralins were also found in very low concentrations. To this point fractionation was very selective in the kind of compound concentrated in each one of these fractions.

In fractions 4 (F-4) the GC-MS analyses begins to show some differences between the sample coming from LCO and the sample coming from LCO/Pittsburgh extract. These fractions contained a mixture of diaromatic and triaromatic compounds. The chromatogram corresponding to the fraction of LCO showed that the concentration of diaromatic compounds appeared to decrease as the concentration of triaromatic compounds increased. In the case of the chromatogram corresponding to the fraction of LCO/Pittsburgh extract the concentration of diaromatic compounds was still very high.

Fraction 5 (F-5) of the LCO/Pittsburgh extract appeared to contain material extracted from coal. Comparison of the chromatograms of LCO and LCO/Pittsburgh extract showed that the concentration of organic material was higher in the LCO/Pittsburgh extract. The presence of naphthalene, biphenyl, fluorene, benzothiophene, dibenzothiphene, phenanthrene and anthracene in extracts from coal also have been reported by other researchers **[5-51 - 5-55]**.

Fraction 6 (F-6) from LCO/Pittsburgh contained mainly oxygen and nitrogen containing compounds that were not present in the original LCO. Fractions 7 and 8 (F-7 and F-8) from LCO/Pittsburgh were similar to Fraction 6 (chromatogram are not shown here). More details about the characterization of these fraction can be found elsewhere **[5-56].**

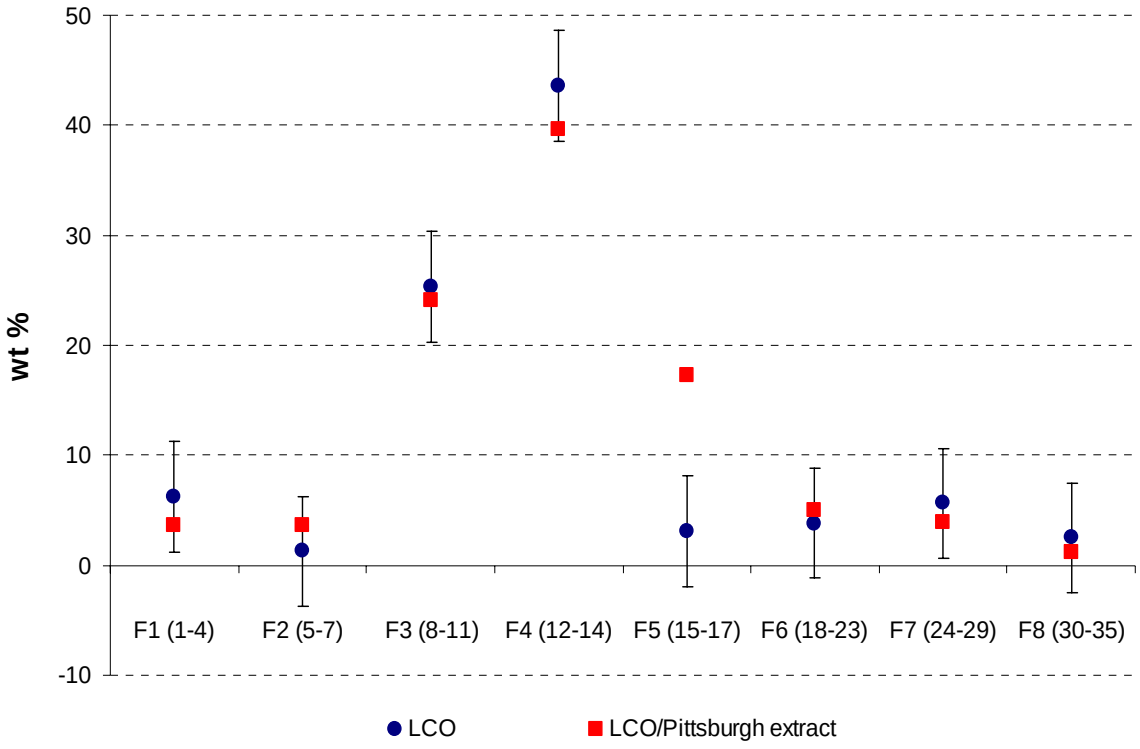

Figure 5-20 Results of the fractionation of LCO and Pittsburgh coal extract obtained from preparative liquid chromatography.

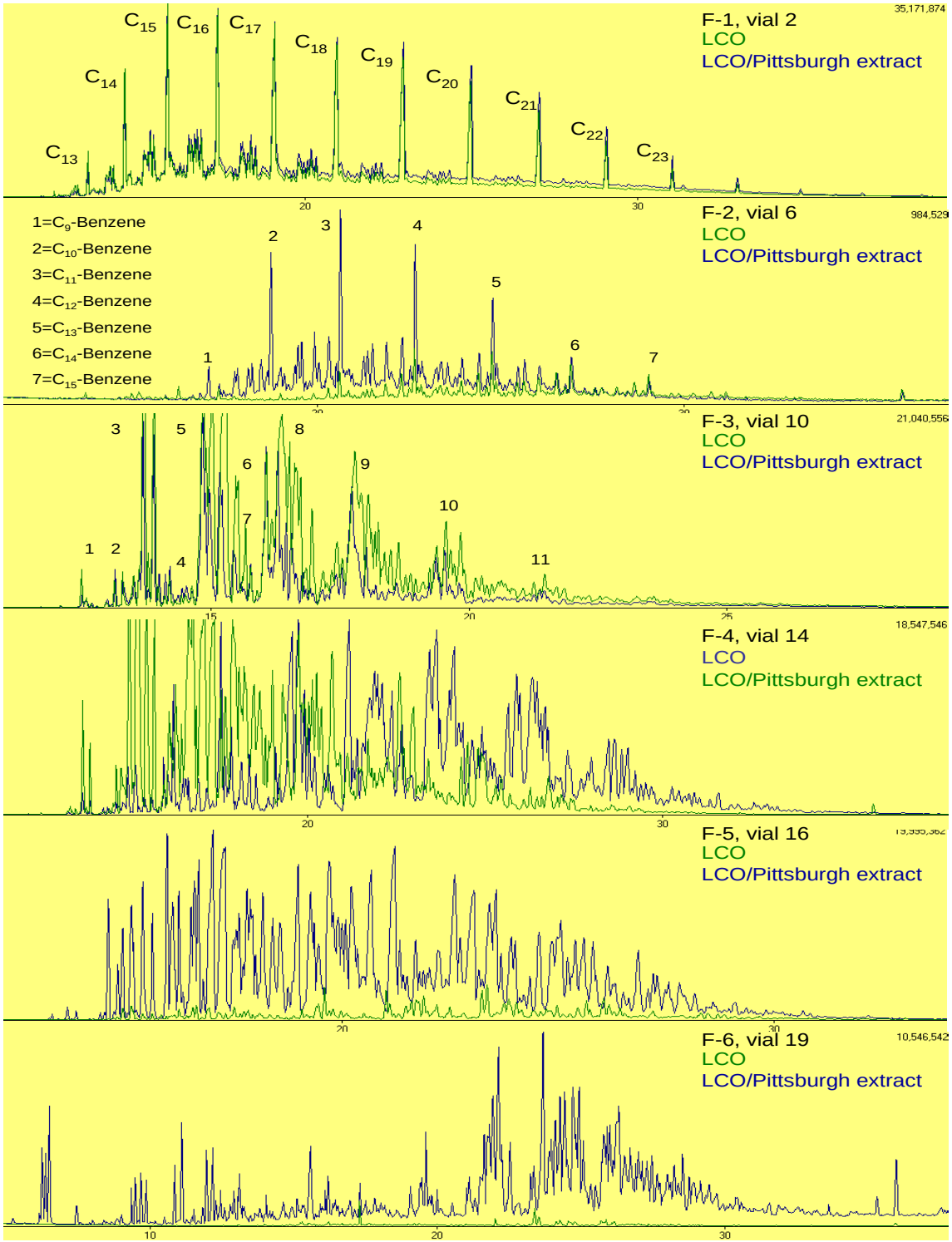

Figure 5-21 GC-MS results from the fractionation of LCO and Pittsburgh coal extract obtained from preparative liquid chromatography.

Single-stage extraction at high temperature filtration

Results of coal conversion using single-stage extraction at high temperature filtration are shown in **Table 5-16**. Coal conversion was found to be in the range of 36-59 % wt. and, as expected, was higher for the hvAb coals than for the mvb coal. Also, it was observed that conversion yields were higher for this series of experiments than those obtained in previous results that did not employ hot filtration. Using high temperature filtration allowed the extraction of the heavy material that was soluble at high temperature which in consequence increased the coal conversion **[5-57-5-59]**.

Table 5-16. Coal conversion for single-stage extraction at high temperature filtration.

Coal Seam	Coal Conversion, % wt
Pittsburgh	52
Powellton	54
Blind Canyon	59
Illinois # 6	55
Splash Dam	36

Figure 5-22 shows the result of the proximate analysis for the original coals and their residues. From the comparison of the volatile matter of the original coal and the residue from the extraction, it can be observed that the volatile matter decreased in the residue as a consequence of the loss of organic matter that have been extracted with LCO and resulted in an increase in the ash yield and fixed carbon.

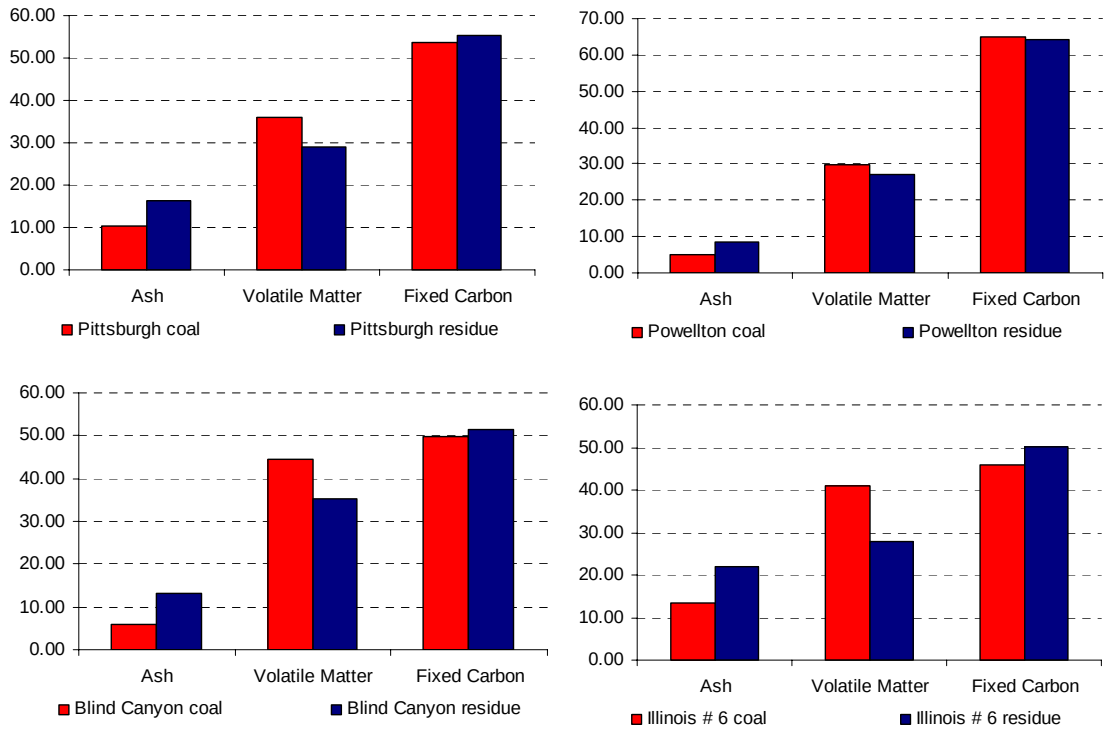

Figure 5-22 Proximate analysis of original coal and residue.

Figure 5-23 shows the result of the MALDI analysis of the extract. It can be observed that in all the extracts, except for the LCO/Blind Canyon extract, there was a higher concentration of the material with molecular weight ranging 200-400 mass/charge. It is suspect that this material was mainly composed of aromatic units with 4-6 fused rings, but further characterization needs to be done.

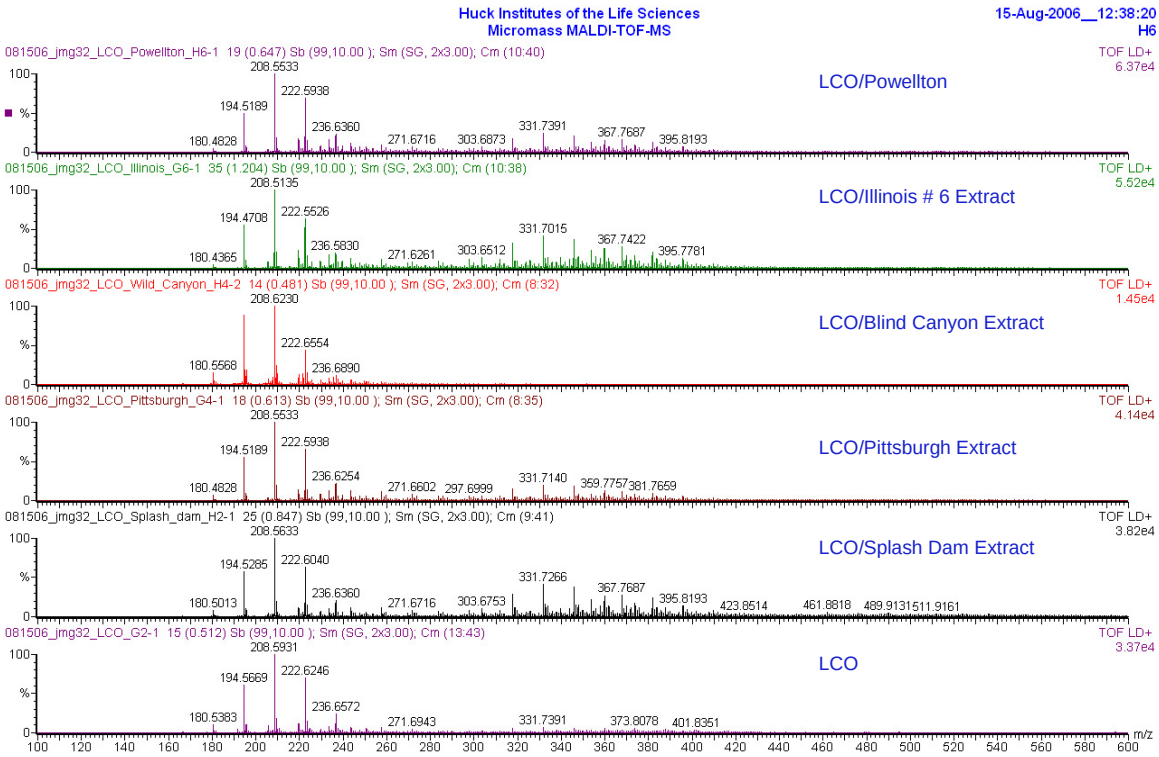

Figure 5-23 Result of the MALDI analysis of the extract.

Multi-stage extraction in a flow reactor

The results of coal conversion from the extraction of Pittsburgh seam coal in the flow reactor system are shown in **Table 5-17**. Conversion of Pittsburgh coal from the three cells was found to be between 64-74 wt%, which represents a significant increase with respect to conversion reached using the single-stage systems. It has been reported by others **5-57-5-59],** that hot filtration increases coal conversion because it permits extraction of the coal fraction soluble at high temperature. In the multi-stage system investigated here a steady increase in conversion was observed from cell 1 to 3. One possible explanation for increased conversion is that the RCO enrichment of the LCO has a positive influence in extraction process.

Unfortunately, we have been unable to run more experiments in the flow reactor system because the porous metal filter used in this reactor becomes plugged. During our second trial system pressure reached a very high level and was consider unsafe to continue. As these porous metal filters are very expensive, we will consider another type of filter and are currently in the process of constructing a new multi-stage reactor that will begin operation in the next two months. Future research will include the mass balance and coal conversion for the extraction process for bituminous coals using LCO and DO (decant oil) as solvents.

Table 5-17. Results of Pittsburgh extraction using a flow reactor system.

Cell	Feed coal (gr)	Residue (gr)	Coal Conversion wt, %
1	3.085	1.316	63.891
2	3.120	1.125	71.245
3	3.093	1.046	73.740

Subtask 5.3.3 Solubility Prediction of Coals in Some Petroleum Streams

Solvent extraction of coal can be used to produce useful two-ring compounds from coal in an inexpensive process without involving catalysts or hydrogen consumption. In brief, this research has been dealing with the solvent extraction of bituminous coals using Light Cycle Oil (LCO) to produce a blend suitable for the JP-900 formulation **[5-56, 5-60]**. The co-coking process, also being investigated in this project, involves the simultaneous thermal treatment of a bituminous coal and a petroleum product such as Decant Oil (DO) to obtain a coal-based liquid suitable for the JP-900

formulation as well as a potentially high-value carbonaceous product **[5-61-5-64].** Both processes involve the solubilization of bituminous coals in a petroleum stream, i.e. LCO or DO. The coal solubilization in these non-pure solvents has yet to be studied. If either of these processes are going to be scaled-up, it would be important to predict the coal solubility in a given petroleum stream.

The solubilization of bituminous coals in pure solvents has been studied using polymer chemistry **[5-65].** It is very well known that the term "solubility parameter (δ)", proposed by Hildebrand and designate as $\delta = (\Delta E_{vap} / V)^{1/2}$, controls the mixing process. A given bituminous coal will be miscible in a solvent that has a similar δ-value **[5-66].**

Solubility parameters have been widely reported for pure solvents **[5-67, 5-68]**; however, these values have not been reported for blends. There are two ways to calculate the solubility parameters of a blend:

1. If the composition of a mixture is known and the solubility parameters of the components are known, the solubility parameter of the mixture can be found by taking the volume average.
2. The other method is by using the van Krevelen approach **[5-69, 5-70]** which involves an additive scheme for calculating solubility parameters. For this method the carbon functional group distribution, which can be obtained using ^{13}C NMR, is required to calculate the solubility.

Since the components present in the LCO and DO are not known, the second approach will be carried out. These parameters will be compared with the solubility parameters of the coals used in co-coking and coal extraction to predict the solvent–coal

interaction. Because the solubility parameters of the coals have not been reported in the literature, they will be calculated using coal swelling techniques **[5-71, 5-72]**.

Subtask 5.3.3.1 Experimental

Samples

The LCO and DO used were obtained from United Refining Company, Warren PA. The properties of these solvents are listed in **Table 5-18.**

Table 5-18 Properties of petroleum streams.

Properties	LCO	DO
API Gravity @ 60 °F, ASTM D-287	10.3	-
Specific Gravity (gr/mL), ASTM D-1298	0.9979	1.1100
Sulfur (wt %), ASTM D-5453	1.92	-
Nitrogen (ppm), ASTM D-5762	535	-
Distillation (° C), ASTM D-2887		-
IBP	146	
10	249	349.0
30	279	393.4
50	301	413.3
70	324	438.3
90	359	481.2
FBP	396	

^{13}C-NMR Analyses

NMR analyses where conducted in a liquid-state NMR spectrometer with imaging capabilities. The samples were analyzed on a Bruker AMX 360 NMR operating at 9.4 Tesla and a 70° tip angle. LCO and DO were dissolved in $CDCl_3$ for analyses.

The regions for the integration of the spectra were defined according to the information in chemical shift table for ^{13}C. A detailed interpretation was applied following the peak integration method suggested by Rodriguez et al. **[5-67]** and a modification was made regrouping the main functional groups found according to those given in **Table 5-19**.

Table 5-19 ^{13}C NMR assignments for functional groups of interest.

Assignment	Band TMS (ppm)
CH3-	11.0-22.5
CH2-	22.5-37.0
-CH-	37.0-60.0
$C=C_{AR}$	108.0-138.0

Solubility Parameter Estimation

Assuming that there are no nitrogen bases in these solvents and that the carbon functional group distribution can be obtained by ^{13}C-NMR, the van Krevelen additive scheme can be used to calculate the solubility parameters. This technique has been used to calculate solubility parameters of kerogens and it is thought to work for petroleum streams. In this scheme van Krevelen states that the molar attraction constants (F) are additive and related to the solubility parameter by:

$$\delta = \sum_{i} \mathbf{F_i} / \mathbf{V}$$

The percentages of each functional group were calculated by integrating the ^{13}C-NMR spectra according to the chemical shift reported in **Table 5-19**. The molar attraction constants and the molar volume for each functional group are listed in **Table 5-**

20. Each percentage was multiplied by F and the individual contributions were added to calculate:

$$\sum_i \%\,C \times F_i$$

The same procedure was followed to calculate:

$$\sum_i \%\,C \times Vr_i$$

Table 5-20 Molar attraction constants (at 25 °C) according to Hoy **[5-63]**

Group	% C		F_{Hoy} $(cal.cm^3)^{1/2}/mol$	V_r (cm^3/mol)
	LCO	DO		
—CH_3	18.84	13.40	148.3	22.8
CH_2	11.81	9.92	131.5	16.45
CH	2.02	5.09	86.0	9.85
Car—	67.33	71.59	98.1	6.13

Subtask 5.3.3.2 Results and Discussion

The solubility parameters were calculated for LCO and DO and are reported in **Table 5-21**. For discussion purpose, the solubility parameters calculated here were compared with some pure solvents. The LCO and DO solubility parameters were far from n-pentane, benzene and methanol, but were similar to those reported for naphthalene and bi-phenyl **[5-61, 5-68]**.

The chemical composition for LCO was about 75% di-aromatic and for the DO was about 85% tri-aromatic. The solubility parameter of a di-aromatic (d for 2-methyl-naphthalene 9.86 $cal^{1/2}cm^{-3/2}$) was in the range of the calculated solubility parameter of LCO. For decant oil, the solubility parameter of anthracene was not found to make the comparison. The calculation of the solubility parameter of the coals used in the current research (Pittsburgh and Powellton/Eagle) will be carried out in the next report period.

Table 5-21 Solubility parameters.

	LCO	**DO**
$\sum_i \%\times F_i$	11126	10753
$\sum_i \%\times Vr_i$	1056	958
$\delta=\sum_i \%\times F_i / \sum_i \%\times Vr_i$	10.53	11.23

Subtask 5.3.3.3 Conclusion

The solubility parameter was calculated for DO and LCO using ^{13}C NMR. This has been our first attempt to calculate the solubility parameters of petroleum streams using the molar attraction constants reported by Hoy **[5-63]**. The values are within the expected range.

Subtask 5.4 Analysis of Co-Coke

There was only minor activity in the area of analyzing co-coke during this reporting period, because our efforts were directed at acquiring and preparing a new coal for additional co-coking experiments. Most of the work completed under this subtask will be discussed in subtask 5.6 as it was performed in support of characterization and testing of carbon artifacts. However, in an attempt to characterize and to quantify the relative anisotropy of green and calcined cokes a technique involving the measurement of bireflectance using optical microscopy was evaluated. Preliminary results and their implications are discussed.

Subtask 5.4.1 Experimental

Background

The measurement of reflectance values is routinely employed for the evaluation of coal rank and as an indicator of organic maturity in petroleum exploration, but has only been used rarely to characterize the thermal characteristics of cokes and carbons. The reason for this has more to do with the theory upon which the analysis technique is based than the ease of making the measurement. In general, reflectance readings are taken from a polished surface of some unique component or phase within the specimen being evaluated by directing a small amount of reflected incident and filtered light to a photomultiplier where the photon energy is amplified to an electrical current. The photoelectric system (current) is calibrated within the range of the unknown specimen using a series of isotropic glass standards of known reflectance (or index of refraction). Unfortunately the apparent ease of making these measurements is confounded by

characteristics of the materials from which the measurements are made. For example, materials that are translucent, transparent or highly absorbing contribute incident light from refraction and internal reflection and therefore provide reflectance values that are not unique to the material or reproducible. Consequently, the measurement of reflectance values is restricted to materials that are optically opaque.

Another restriction to this technique involves the crystalline nature of the materials being measured. An isotropic opaque mineral has a single index of refraction, which means that a measured property (like reflectance, heat transfer, electrical conductivity, etc) will provide roughly the same value in any orientation, whereas an anisotropic mineral may have two (uniaxial) or more (biaxial) indices of refraction. Therefore, anisotropic materials can provide two or more unique reflectance values if the material is perfectly oriented and can provide an infinite number of resultant values between the end members.

Application and use of reflectance analysis in the coal and petroleum exploration industry where measurements are made on non-crystalline materials (vitrinite and humic organic matter) is predicated on the assumption and confirmed by measurement that these materials act like uniaxial negative crystals. Consequently, these organic materials possess two unique values of reflectance corresponding to a maximum and minimum value. Davis **[5-73]** considered the measurement of reflectance values from different sections of oriented vitrinite and suggested that it would be possible to obtain a unique maximum reflectance value from any randomly oriented particle of coal by rotation of that particle under polarized light. However, a true minimum value corresponding to the second axial direction of the pseudo-crystal could only be obtained in one orientation; all

other values of minimum reflectance would be intermediate values resultant between a true maximum and a true minimum. Maximum vitrinite or huminite reflectance provides a unique and reproducible value that is the underpinning of ASTM and ISO standards used in the industry. Never-the-less, the measurement of maximum (Rmax) and apparent minimum (Rmin) reflectance values have been used to describe the relatively anisotropy of natural organic materials. Generally, as the rank or maturity of organic matter increases both of these values increase, but the minimum reflectance increases at a lower rate. Thus, bireflectance (B_i = Rmax – Rmin) increases with increasing rank or maturity and is considered to be a measure of anisotropy.

It is commonly held that maximum reflectance and bireflectance continue to increase at a uniform rate even at very high rank (meta-anthracite to graphite), but this is incorrect. From studies of artificial coalification **[5-74]** there is evidence that between 600-700ºC and above 4.0% maximum reflectance that the refractive index begins to decrease. This corresponds to a point where the adsorption index, maximum reflectance and the bireflectance begin to rise strongly. Typically, bireflectance increases because of an increase in Rmax, as well as a large decrease in the Rmin value (which probably reflects the decrease in refractive index). These observations suggest a significant change in the crystalline nature of the carbonaceous material, but even so bireflectance should still be a valid method of determining the relative level of anisotropy.

Samples and Preparation

A variety of samples were selected for this investigation that included both green and calcined cokes from co-coke made with cleaned Pittsburgh seam FCE used by Alcoa,

as well as cokes removed from four different sections (bottom to top) of coker Run #14 that employed 80:20 ratio of Seadrift decant oil and the Powellton/Eagle coal (see section 5.6.1 for details of sectioning). Samples of the Run #14 sections were pulverized to pass 0.85 mm and were calcined for one hour at 1300 ºC, whereas the bulk composite sample from the Pittsburgh seam co-coke was crushed to pass 30 mm and calcined at 1275 ºC. Representative samples of the Pittsburgh seam co-coke were further crushed to 1.19 mm for microscopy, while the Run #14 sections were maintained at 0.85 mm. Both green and calcined coke samples were placed in a cold setting epoxy resin, vacuum impregnated and spun in a centrifuge to create a density gradient of particles. After the epoxy hardened, the cylindrical samples were cut in half longitudinally to expose the gradient and re-embedded in epoxy so that the gradient surface could be ground and polished for microscopy. Samples were desiccated overnight before reflectance analyses were performed.

Reflectance Technique

Measurement of reflectance values was performed using a Leitz MPV2 photometer system under oil immersion at 625 X magnification and polarized light. Because of the very high reflectance values of the green and calcined coke specimens being evaluated, individual readings were made using a calibrated neutral density filter (10% transmittance) inserted into the light path to bring the light intensity into the range maximum stability of the photomultiplier (0.5 – 1.8 v). Readings were made on specific isochromatic units of greater than 30 μm that possessed anisotropic properties. (Note: Because of their orientation some isochromatic units did not exhibit complete extinction

when rotated in polarized light and these regions were avoided.) The region of interest was placed under the 3.2 μm measuring spot, the light passed through a filter of 546 nm ±5 nm to the photomultiplier, the particle (stage) was rotated 360º and the maximum and minimum voltage was recorded as their percentage reflectance values. Fifty particles were measured in this manner and the mean maximum and mean apparent minimum values were calculated after adjustment of the raw values for the neutral density filter transmittance.

Subtask 5.4.2 Results and Discussion

Mean values of maximum and apparent minimum reflectance and bireflectance are given in **Table 5-22** along with the determined standard deviations for both green and calcined cokes selected for this investigation. Because of the interrelationship between the Run #14 sections, their mean values and standard deviations are reported for comparison with the composite samples of the Pittsburgh seam co-coke that was returned from A.J. Edmond.

Maximum reflectance values obtained from the green coke for the different sections of Run #14 showed a small, but significant decrease from the bottom of the reactor (section #1) to the top (section #4). This probably results from the relatively lower coking time experienced by coke formed at the top of the reactor as the coker was being filled over a six hour period. It also corresponds to the relatively higher volatile matter yield found previously for sections removed from the top of the reactor **[5-75]**. Apparent minimum values were less affected by the shorted coking time and were uniformly low. However, because of the decreasing maximum reflectance the

bireflectance values similarly decreased as a result of decreasing coking time. The maximum reflectance and bireflectance values of the Pittsburgh composite sample were comparable to those values obtained from the lower sections of Run #14, and may have been more uniform as all of the runs (#50-61) that contributed to the composite were soaked at 500 ºC for 24 hours **(3)**.

Table 5-22 Mean Reflectance Values Determined from Isochromatic Areas >30 Microns for Sections of PSU Coker Run #14 and the Pittsburgh Co-coking Composite

Sample Id.	Type Of Coke	Maximum, R_{max}	Stand. Dev., σ	Minimum, R_{min}	Stand. Dev., σ	Bireflectance, B_i
Run #14, Section #1	Green	6.62	0.27	0.56	0.29	6.06
	Calcined	17.05	1.04	1.47	0.43	15.58
Run #14, Section #2	Green	6.57	0.32	0.66	0.55	5.91
	Calcined	16.45	1.49	1.66	1.24	14.79
Run #14, Section #3	Green	6.02	0.28	0.56	0.38	5.46
	Calcined	16.59	1.13	1.67	0.79	14.92
Run #14, Section #4	Green	5.45	0.25	0.46	0.20	4.99
	Calcined	16.62	1.46	1.60	0.46	15.02
Mean Values Run #14	**Green**	**6.16**	**0.55**	**0.56**	**0.08**	**5.60**
	Calcined	**16.68**	**0.26**	**1.60**	**0.09**	**15.08**
Pittsburgh Composite Co-coke, AJE	Green	6.63	0.45	0.57	0.24	6.10
	Calcined	16.12	1.22	1.65	0.78	14.47

Calcination had a marked influence on the maximum reflectance and bireflectance of the cokes and resulted in a 2.7 times increase in those values. Although reflectance values were slightly lower for the Pittsburgh composite co-coke which may reflect the lower temperature of calcination and greater particle size (thermal gradient issues), the standard deviation suggested that these differences were insignificant. Furthermore, the calcination process apparently eliminates the small reflectance differences observed from different sections of the reactor; meaning that, once a mesophase has formed and coalesced into relatively large isochromatic regions, the solidified carbon may follow the

same path in forming a graphitic product. However, this does not mean that other physical properties may be influenced negatively. The release of a greater amount of trapped volatile matter may affect the strength and porosity of the resulting coke.

5.4.3 Conclusions

The relative uniformity of reflectance and bireflectance properties of predominately petroleum-derived isochromatic units from different section of the delayed coker compared with a large composite sample, suggested that processing conditions (temperature and soaking time) had an initial impact on anisotropy which was mitigated when the cokes were heated further (calcination). As a technique for the measurement of carbon anisotropy, determination of bireflectance could have some limited application. However, as a measure of the relative anisotropy of bulk carbon that could be compared with x-ray diffraction properties (d-spacing or crystallite stacking), density, the coefficient of thermal expansion, etc., much more work would need to be performed. The evaluation performed in this study was limited to one type of isochromatic region that represented less than perhaps 50% of the total mass; it may be the properties of the remaining 50% that are of more importance to bulk carbon quality.

5.5 Analysis of Co-Coking Binder Pitch

As discussed in the Semi-Annual Report 2006 **[5-76]** the liquid product from the co-coking Run #50 was further distilled to yield a pitch material, namely CCP-2. It was reported that CCP-2 was too light to be used as a binder for an aluminum production. Two methods of heat treatment were used to produce more condensed aromatic-fused-

ring compounds: heat soaking and oxidation. The aim of this research was to prepare new co-coking pitch samples having a mass distribution close to that of the standard coal tar pitch (SCTP) and petroleum pitch (PP).

5.5.1 Materials and Experimental

The material for generating co-coking pitch was obtained by using a laboratory-scale vacuum distillation apparatus. The distillates from co-coking were placed in a round-bottom flask, which was connected to a riser and condenser assembly. The temperature of the boiling liquid was measured by a thermocouple. A cold trap kept in liquid nitrogen was used to collect any light product not condensed in the collection flask. After the pressure was reduced to 5 mmHg using a rotary-vane vacuum pump, the heating mantle was switched on. The temperature was increased and distillates collected until the desired cut-point temperature was reached. A 360°C cut-point was chosen to obtain a final product of 360°C-FBP (Final Boling Point) remaining in the round-bottom flask. From a GC/MS analysis (the spectra not shown in this report), this fraction did not contain any aliphatic compounds and should be a good starting material to obtain good binder pitch samples.

There are two main methods of producing heavy compounds from petroleum fractions: heat soaking and oxidation (or polymerization with oxygen) **[5-77]**. These methods combined with distillation and solvent extraction have been widely used to produce petroleum pitch **[5-77].**

The 360°C-FBP fraction of co-coking liquid Run #50 was heat soaked and oxidized with the conditions described in

Table **5-23 and 5-24**, respectively. Five grams of the sample were placed in a 20 mL reactor. UHP N_2, and O_2 were used to purge and pressurize the sample in the heat soaking and oxidation experiments, respectively. A pressure gauge was attached to each reactor to monitor the pressure before, during and after the reactions. All reactor parts that contained the reacting material were totally immersed in a fluidized-sand bath which was equipped with a temperature controller. After the reaction, the reactor was quenched in water. All the original samples and their derived materials were characterized by Laser Desorption Mass Spectrometry (LDMS) to determine the mass distribution.

Table 5-23 Heat soaking conditions of co-coking liquid distillate Run#50.

Sample #	Cut Temperatures of Original	Heat Soaking Conditions		
		Temp. (°C)	Time (hr)	P_{ini} (psig)
HT13, 16	360°C-FBP	475	0.5	0
HT02, 14, 17	360°C-FBP	475	1	0
HT15, 18	360°C-FBP	475	2	0
HT19, 22	360°C-FBP	440	3	0
HT20, 23	360°C-FBP	440	6	0
HT21, 24	360°C-FBP	440	10	0
HT25, 28	360°C-FBP	460	1.5	0
HT26, 29	360°C-FBP	460	3	0
HT27, 30	360°C-FBP	460	5	0

Table 5-24 Oxidation conditions of co-coking liquid distillate Run#50.

Sample #	Cut Temperatures of Original	Oxidation Conditions		
		Temp. (°C)	Time (hr)	P_{ini} (psig)
OX31, 34	360°C-FBP	150	2	300
OX32, 35	360°C-FBP	150	4	300
OX33, 36	360°C-FBP	150	6	300
OX37, 40	360°C-FBP	200	2	300
OX38, 41	360°C-FBP	200	4	300
OX39, 42	360°C-FBP	200	6	300
OX43, 46	360°C-FBP	250	2	300
OX44, 47	360°C-FBP	250	4	300
OX45, 48	360°C-FBP	250	6	300

Laser Desorption Mass Spectrometry (LDMS)

Laser Desorption mass spectra were obtained using a Micromass MALDI-L/R. The samples were analyzed by the Huck Institute, Department of Chemistry, Penn State. No matrix assistance was used on any samples. A 20 mg whole pitch was dissolved in 1 mL toluene and sonicate for 1 hour. The pitch solution was deposited on a sample cell and dried before insertion in the mass spectrometer ion source.

5.5.2 Results and Discussion

Error! Reference source not found. shows the LDMS spectra of the original 360°C-FBP fraction and its heat treated products as compared to those of SCTP-2 and PP-1. Consider the materials ranging from 175-350 dalton as a group of monomer (see Error! Reference source not found.**(c)**). After heat soaked and oxidized the 360°C-FBP fraction, di-, tri-mers and so on were formed (see **Figure 5-24(d)** and **Figure 5-24(e)**).

Varying temperatures and reaction times give the same mass ranges of these oligomers, but different yields of each fraction.

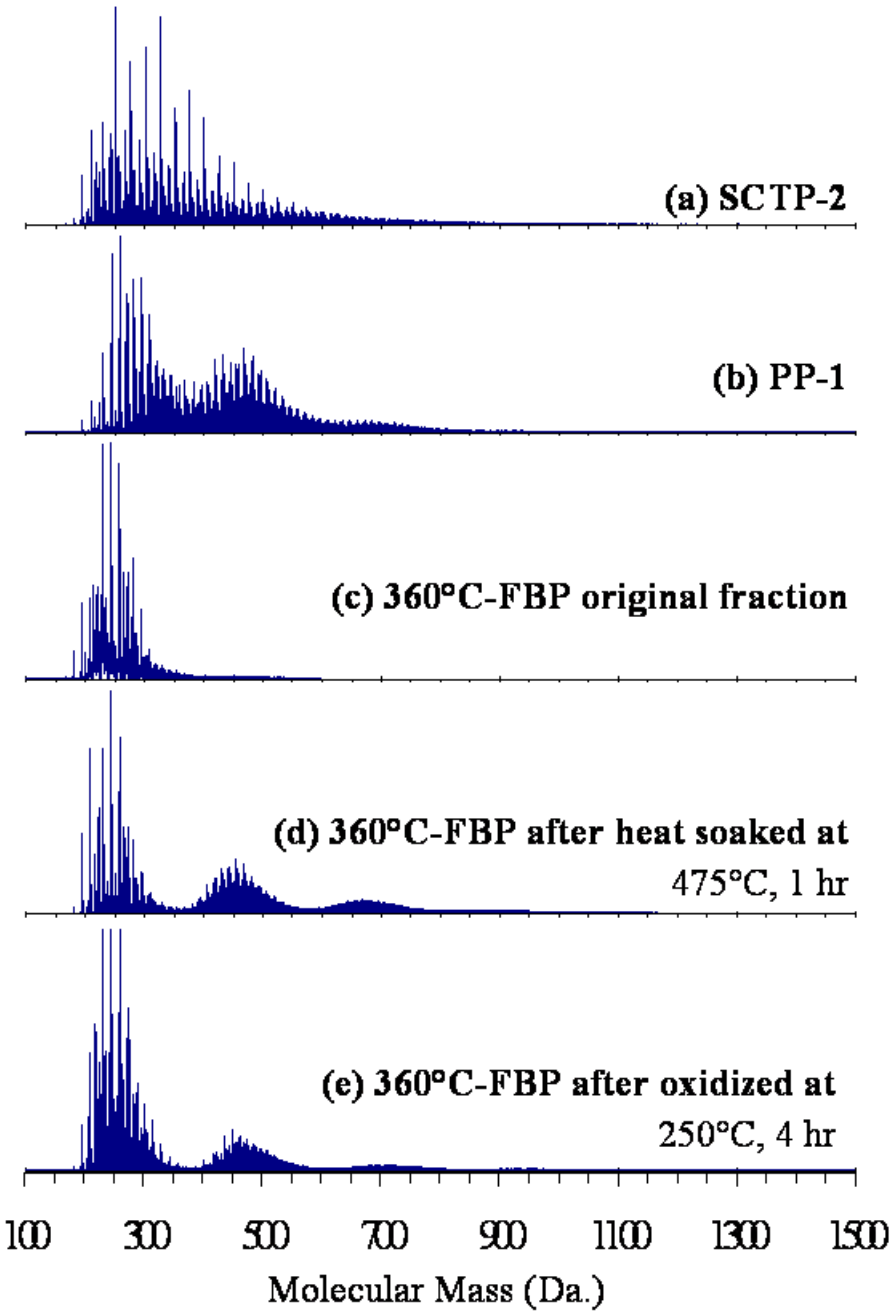

Figure 5-24LDMS spectra of (a) SCTP-2; (b) PP-1; (c) 360°C-FBP original fraction; (d) 360°C-FBP after heat soaked at 475°C, 1 hr; and (e) 360°C-FBP after oxidized at 250°C, 4 hr.

Number and weight average of the heat-soaked and oxidized materials are compared with its original, SCTP-2 and PP-1 as shown in **Figure 5-25 and Figure 5-26**, respectively. In the heat soaked products (see **Figure 5-25**), as the reaction time increased, more heavy compounds were formed as indicated by an increase in average molecular weight. The same trend was observed for the oxidized products at 250°C (see **Figure 5-26**). However, the oxidized products at 150 and 200°C did not follow this trend as shown in **Figure 5-26**. A number of careful experiments will be done in the future to investigate the cause of these results.

It is of interest to observe a similar behavior in the PP-1 spectra as shown in **5-24(b)**. It was reported that petroleum pitch was obtained by using a proper blend of the heat treatment products and heavy petroleum fractions **[5-77]**. With a careful selection of the co-coking liquid fractions, it is promising that the heat-treatment can be performed to obtain a suitable mass range which would give good binder pitch properties.

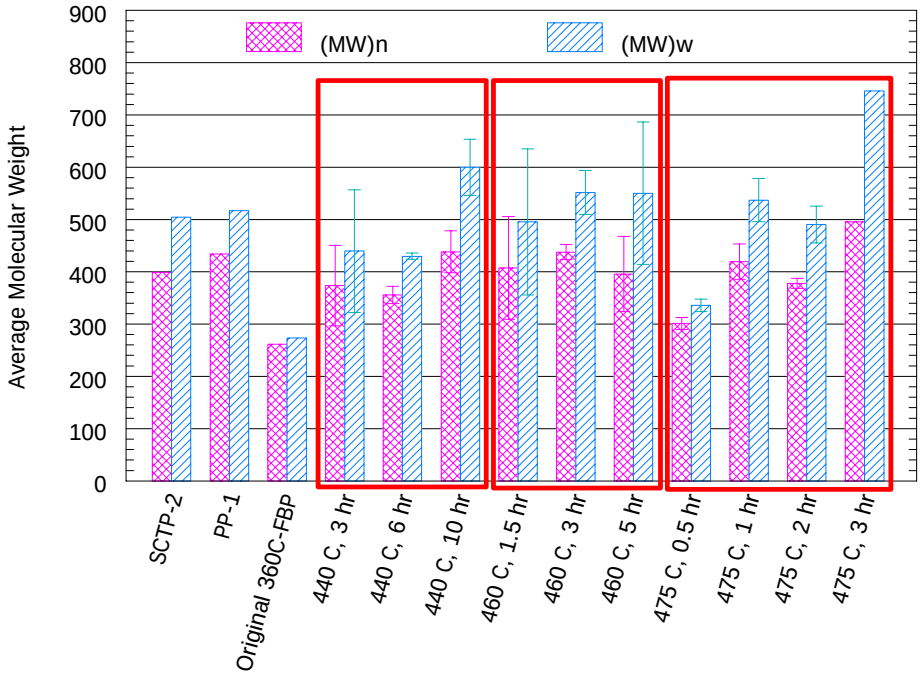

Figure 5-25 Number average, $(MW)_n$, and weight average, $(MW)_w$ of the heat soaked products derived from Run#50 360°C –FBP fraction. A comparison was made with SCTP-2 and PP-1.

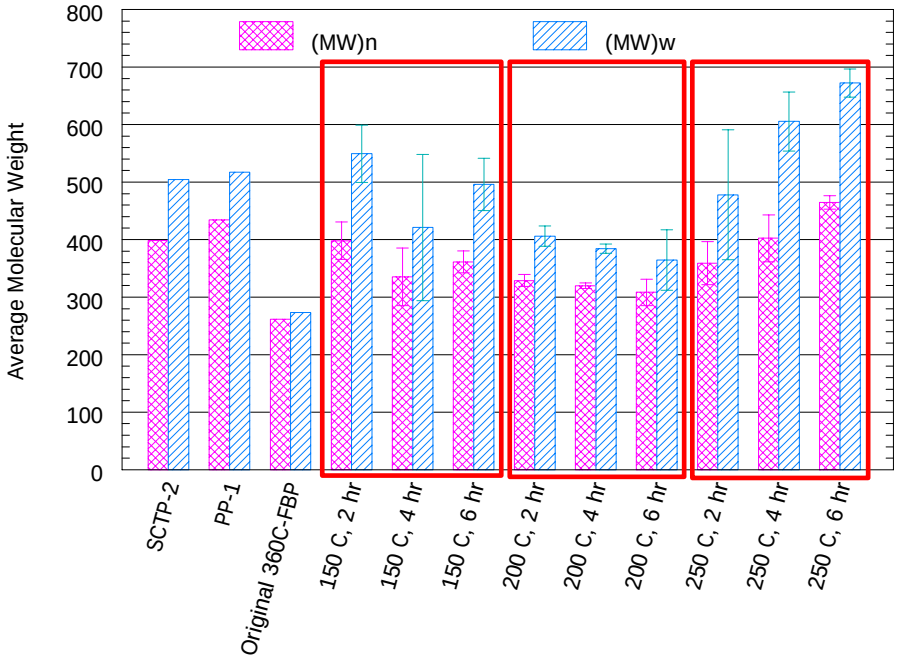

Figure 5-26 Number average, $(MW)_n$, and weight average, $(MW)_w$ of the oxidized products derived from Run#50 360°C-FBP fraction. A comparison was made with SCTP-2 and PP-1.

5.5.3 Conclusions and Future Work

Heat soaking and oxidation were performed on the Run#50 360°C-FBP fraction. Oligomers were formed as a result of heat treatment. Careful selections of the co-coking liquid fractions and heat treatment conditions will be done to obtain suitable mass range. Distillation and/or solvent extraction will be used to remove unwanted materials in order to obtain good properties binder pitch.

5.6 Manufacture and Testing of Carbon Artifacts

Coke samples generated in the Penn State Laboratory Delayed Coker and produced from coking of decant oil alone and from co-coking of decant oil with coal were evaluated by different methods to establish their quality. Two approaches were followed: In the first case, coke samples were sectioned at various levels above the reactor inlet, crushed to -20 mesh and then subjected to different analysis. Although the reason for sectioning has been discussed elsewhere **[5-78]**, the technique has revealed the heterogeneous distribution of carbon textures within the coke being produced. In the second case, the total coke artifact removed from the reactor was homogenized by crushing them to -20 mesh and then subjected them to different analysis. These two approaches will provide information about our operating unit so that homogenization issues during processing can be addressed and will provide information on the potential commercial aspects of coke quality. Progress made during this reporting period on each of these approaches is discussed separately below.

5.6.1 Evaluation of Different Sections of Coke Samples

5.6.1.1 Experimental

Coke Samples

The whole coke artifact generated from Runs #13, #14, #35, #44 were cut into three or four (depends to the height of the coke artifact) different 4-5 cm thick sections from the bottom of the coke (or coker inlet). Separately, these sections were crushed and grounded to pass a 0.85 mm, 20 mesh Tyler sieve. The height of the each section above the inlet for each run and the nomenclature used for green and calcined coke is given in **Table 5-25**.

Table 5-25 Nomenclature of Coke Samples

Nomenclature	Explanation
13s1gc and 13s1cc	Section 1, 2-6 cm from bottom, (Run #13), Green coke (gc) and calcined coke (cc)
13s2gc and 13s2cc	Section 2, 7-12 cm from bottom, (Run #13), Green coke (gc) and calcined coke (cc)
13s3gc and 13s3cc	Section 3, 13-18 cm from bottom, (Run #13), Green coke (gc) and calcined coke (cc)
14s1gc and 14s1cc	Section 1, 2-6 cm from bottom, (Run #14), Green coke (gc) and calcined coke (cc)
14s2gc and 14s2cc	Section 2, 7-12 cm from bottom, (Run #14), Green coke (gc) and calcined coke (cc)
14s3gc and 14s3cc	Section 3, 19-24 cm from bottom, (Run #14), Green coke (gc) and calcined coke (cc)
14s4gc and 14s4cc	Section 4, 31-36 cm from bottom, (Run #14), Green coke (gc) and calcined coke (cc)
35s1gc and 35s1cc	Section 1, 2-6 cm from bottom, (Run #35), Green coke (gc) and calcined coke (cc)
35s2gc and 35s2cc	Section 2, 13-18 cm from bottom, (Run #35), Green coke (gc) and calcined coke (cc)
35s3gc and 35s3cc	Section 3, 25-29 cm from bottom, (Run #35), Green coke (gc) and calcined coke (cc)
44s1gc and 44s1cc	Section 1, 2-6 cm from bottom, (Run #44), Green coke (gc) and calcined coke (cc)
44s2gc and 44s2cc	Section 2, 13-18 cm from bottom, (Run #44), Green coke (gc) and calcined coke (cc)
44s3gc and 44s3cc	Section 3, 24-30 cm from bottom, (Run #44), Green coke (gc) and calcined coke (cc)

Calcination Conditions

Calcination experiments were carried out in a Centorr Vacuum Industry 45 furnace, which operates in either a vacuum or argon atmosphere. The samples were weighed to 10-15 g and placed in graphite crucibles with lids, provided by POCO Graphite and placed in the hot zone of the cold furnace. The environment of the hot zone was purged by pulling a vacuum, and then backfilling with ultra-high purity argon three times to ensure an inert atmosphere. Following this purge, the samples were heated to 1300ºC at a heating rate of 20ºC/min and held at the maximum temperature for one hour (in a flow of argon). Following heat treatment, the furnace was cooled in a flow of argon. After the furnace reached to room temperature, the flow of argon was stopped and the coke samples were removed from the furnace for further analysis. The weights of coke samples before and after calcinations were recorded.

Green and Calcined Coke Properties

The ash yields were determined using a MAC 400 Proximate Analyzer (ASTM 05.06 D5142) and the real densities of green and calcined cokes were determined by helium pycnometer (using ASTM 05.02 D2638 method). These results are summarized in **Table 5-26**. Because of the potentially large number of samples generated by sectioning the four different coker runs, one or two of the cokes (Runs #14 and #35) were initially selected for detailed evaluation. Major and some trace elements were determined using ICP spectrochemcial analysis (Run #14). Polarized light microscopy was used to define and illustrate a variety of coke textures only for the green and calcined coke from Run #14. X-ray diffraction was used to evaluate the degree of structural

anisotropy in green and calcined cokes for green and calcined cokes from Runs #14 and #35. X-ray diffraction data were acquired using a Phillips X'Pert MPD with CuKα radiation. Continuous type scans were made from 5º to 95º with a step size of 0.02º. Time per step was 10 s. To calculate the L_c and d spacing, Jade+ Version 7.1 software was used. The [002] peak was used to calculate the d spacing using the Bragg equation and L_c was calculated using the Scherrer equation **[5-79]**.

Optical Microscopy

Characterization of two green (14s1gc and 14s4gc) and two calcined coke (14s1cc and 14s4cc) samples were done using optical microscopy. The products were embedded in a cold-setting epoxy resin and then polished. Evaluation was performed in reflected polarized white light with oil immersion objectives at 625x magnification using a Zeiss Universal research microscope. Point-count analysis was performed by traversing the sample on a 0.4 mm x 0.4 mm grid and using a classification scheme modified from Oya et al. **[5-80]** by Eser **[5-81]** for petroleum-derived semi-coke and from ASTM 05.06 D5061 for metallurgical coke derived from coal. A total of 1000 counts was accumulated, 500 from each of two polished mounts and the results for each component are reported as a volume percentage in **Table 5-28**.

5.6.1.2 Results and Discussion

Conditions and product distribution for the coking experiments are provided in **Table 5-26**. Product distribution shows that the coking of decant oil only and co-coking of decant oil and coal generated a considerable amounts of solids which encouraged us to investigate the potential end-use of product. Previous results showed that the coke

artifacts obtained from co-coking experiments were not "homogenous" **[5-82]**. In fact, the remnants of coal appeared to be concentrated in the lower half and toward the center of the coke artifact. In previous coke evaluation one-centimeter thick sections were cut from different levels of coke artifacts. However, in this evaluation 4-5 centimeter thick sections were removed to provide a more representative sampling of the coke artifact.

Weight Loss during Calcination

Figure 5-27 summarizes the percentage weight loss during calcination experiments. In all cases, the volatility of coke samples was increased by adding coal to the system. The weight loss in different section for the samples produced from coking of decant oil only was nearly the same, but was found to be more variable with the addition of coal. Because of the highly aromatic nature of coal, devolatilization appeared to lag behind that of decant oil. Consequently, those sections of the coke having a higher concentration of coal remnants tended to have higher volatile matter yields.

Table 5-26 Conditions and Product Distributions for Coking and Co-coking Experiments

Conditions	**DO=Seadrift**	**DO=Seadrift/Coal Powellton/Eagle**	**DO107/Coal Pittsburgh Seam**	**DO107/Coal Pittsburgh Seam**
Run #	**13**	**14**	**35**	**44**
Feedstock, hours	6	6	51/2	6
Hold at 500ºC, hours	0	6	6	24 (550ºC)
Feed rate, g/min	16.7	16.7	16.7	16.7
Preheater inlet, ºC	181	87	227	120
Preheater outlet, ºC	417	419	443	425
Coke drum inlet, ºC	446	474	470	470
Coke drum middle, ºC	493	481	471	471
Coke drum top, ºC	458	466	470	475
Product Distributions:				
% Coke	14.27	31.67	30.24	26.81
% Liquid	79.63	65.84	60.35	58.74
%Gas (by difference)	6.10	2.44	9.41	14.45

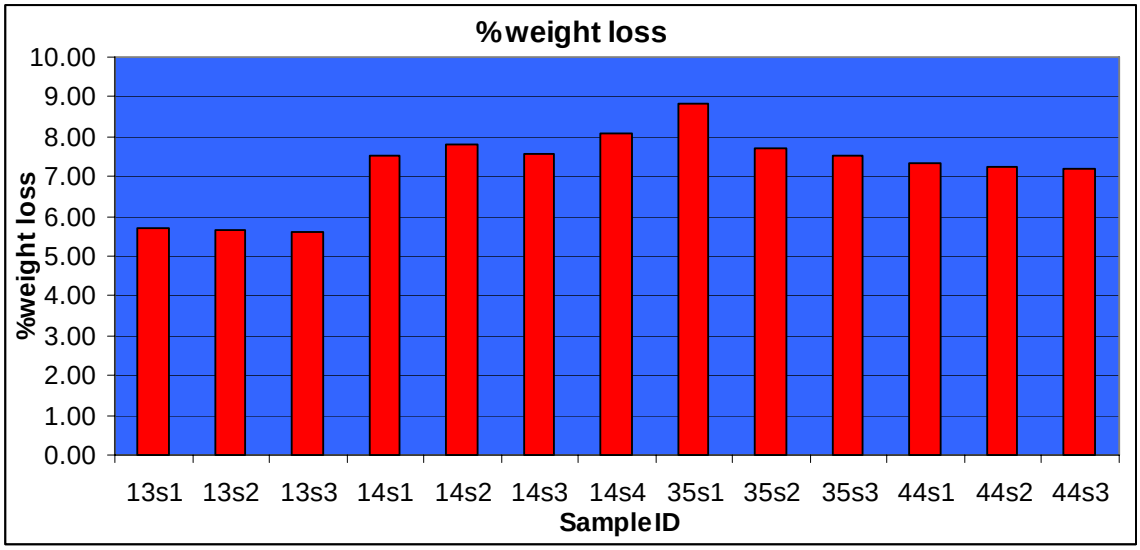

Figure 5-27 Percent Weight Loss during Calcination.

Ash Contents, Petrographic Analysis and Density Measurements:

According to the ash yields (**Table 5-27**) and petrographic analyses (**Table 5-28**) of the first and fourth sections of coke artifact produced from co-coking of Seardrift decant oil and Powellton/Eagle coal (Run #14), there was not a great difference of coal distribution at different heights of coke in this particular coke artifact. However, comparison of ash yields of all sections showed that there was a significant increase in coal remnant in the second section (7-12 cm) and a considerable decrease in the third section. Unfortunately, petrographic analyses have not been completed for all green and calcined coke sections, but it is expected that they will confirm the variability shown from the ash analyses. Although the green cokes contained about 44-47% coal-derived carbon textures, there was a significant shift in the textures derived from vitrinite. The section closer to the inlet had more vitrinite-enhanced textures, whereas the one furthest away (14s4gc) had more non-enhanced vitrinite. This trend suggests less interaction

between decant oil and thermoplastic coal in the upper part of the reactor. Most of the anisotropic carbon textures derived from the decant oil (48-49%) were generally less than 60 μm The influence of calcination on the carbon textural distribution was minor. Both green cokes (14s1gc and 14s4gc) contain minor amounts of isotropic carbon coming from the coal fraction and none from the petroleum fraction, which during calcinations appear to be converted to anisotropic structures. In both sections calcination resulted in a minor increase in flow domain, decrease in small domain and domain units and an increase in mosaic textures.

In contrast, coke samples from Run #35 and from Run # 44 exhibited large differences of coal distribution at different heights of coke which was most apparent in the coke sample studied from Run #35. The ash yield of the first section of green coke sample was 4.53, however values of 0.73 and 0.12 were obtained in second and third sections, respectively. This difference was less noticeable for coke samples produced from Run #44, but still the coal remnants concentrated at the bottom of the coke artifact.

Table 5-27 Ash Contents and Real Densities of Coke Samples

Sample ID	Ash Content (%)	Real Densities (g/ml)
13s1gc	0.54	1.441
13s2gc	0.18	1.443
13s3gc	0.54	1.486
13s1cc	0.27	2.165
13s2cc	0.27	2.163
13s3cc	0.13	-
14s1gc	6.76	1.513
14s2gc	8.25	1.489
14s3gc	5.72	1.465
14s4gc	6.23	1.452
14s1cc	6.95	2.128
14s2cc	8.63	2.095
14s3cc	5.76	2.108
14s4cc	6.60	2.099
35s1gc	4.53	1.48
35s2gc	0.73	1.44
35s3gc	0.12	1.42
35s1cc	4.50	2.08
35s2cc	0.60	2.14
35s3cc	0.35	2.18
44s1gc	5.61	1.61
44s2gc	-	1.57
44s3gc	-	1.52
44s1cc	5.94	2.08
44s2cc	4.11	2.12
44s3cc	2.83	2.12

Table 5-28 Petrographic Analysis of Two Green and Two Calcined Coke Samples

Optical textures	14s1gc	14s1cc	14s4gc	14s4cc
Coal derived (total)	**43.9**	**50.3**	**46.6**	**42.6**
Enhanced vitrinite derived	23.7	29.7	8.9	8.9
Non-enhanced vitrinite derived	10.3	11.2	29.2	26.9
Inert-derived	9.3	8.6	7.6	5.8
Isotropic vitrinite	0.1	0.0	0.1	0.0
Mineral matter	0.5	0.8	0.8	1.0
Petroleum derived (total)	**56.1**	**49.7**	**53.4**	**57.4**
Isotropic petroleum derived	0.0	0.0	0.0	0.0
Mosaic, <10µm	16.0	18.2	9.9	16.8
Small domain, 10-60µm	33.5	28.7	38.8	36.8
Domain, >60µm	6.5	2.3	3.6	1.2
Flow Domain, >60µm L, <10µm W	0.1	0.5	1.1	2.6

Table 5-29 The general specifications for anode grade coke

Properties	**Raw Coke**	**Calcined coke**
Moisture, %wt	**8-10**	**<0.30**
Hydrogen, %wt	**----**	**<0.10**
Ash, %wt	**<0.40**	**<0.40**
Sulfur, %wt	**<3.5**	**<3.0**
V, wppm	**<300**	**<250**
Ni, wppm	**<200**	**<200**
Si, wppm	**<250**	**<200**
Fe, wppm	**<300**	**<300**
Real Density, g/cc	**------**	**2.05-2.08**

Density values for all calcined coke samples were found to be higher than the specifications for both anode grade and electrode grade cokes (**Table 5-29**). Real density of green petroleum coke should be in the range of 1.3-1.4. Therefore, it should come as

no surprise that co-coke has a higher density, as it contains the remnants of mineral matter. But after calcinations anode grade coke was usually calcined around 2.05 to 2.08 g/ml (**Table 5-29**). Calcined needle coke for graphite electrodes can reach real densities of 2.13 g/ml **[6]**. After calcination all of our coke samples meet density specifications for anode grade coke, and some meet the density specifications for graphite electrode grade coke, too. Calcinations temperature are typically higher for needle type cokes used to make graphite electrodes and so by increasing the calcinations temperature coke densities would probably meet that specification, as well.

The density of green cokes decreased with increased height above the inlet which probably reflects the greater duration of coking time for the material near the bottom of the reactor and the fact that all of the feed material passes through this section. At the conclusion of the experiment (6 hrs) and the pump is turned off, the feedstock settles into the distributary channels in the bottom half of the reactor where heating was continued for 6 additional hours. For this reason the duration of coking for coke in the bottom of the reactor was not the same as that for the upper part cokes. The same conclusion can be made for calcined coke, except that the second section contained a high concentration of coal remnants.

Table 5-30 summarizes an evaluation of major and some trace elements for both green and calcined cokes samples from Run #14. According to the data in **Table 5-30,** Si, Al, and Fe constitute the main elements found in both sections. These quantities were much higher than the amounts allowable in both anode- and graphite- grade cokes. However, the coal used in this particular test (Powellton) was not deeply cleaned as was suggested by the evaluation of ash yield given in **Table 5-27**.

Table 5-30 An Evaluation of Major and Some Trace Elements

Oxides (%)	14s1gc	14s1cc	14s4gc	14s4cc
Al_2O_3	19.5	18.9	18.8	19.4
BaO	0.05	0.05	0.06	0.05
CaO	0.37	0.4	0.41	0.4
Fe_2O_3	2.02	1.92	2.34	2.27
K_2O	1.97	1.1	1.11	1.24
MgO	0.75	0.78	0.96	0.83
MnO	0.05	0.02	0.02	0.02
Na_2O	0.99	0.92	0.92	1.03
P_2O_5	0.05	0.07	<0.05	<0.05
SiO_2	72.2	72.2	72.8	72.1
SrO_2	0.19	0.07	0.08	0.08
TiO_2	1.5	1.59	2.03	1.98
Total	99.6	98.0	99.6	99.4

Table 5-31 summarizes X-ray analysis of all calcined coke samples produced from Runs #14 and #35. **Figures 5-28** and **5-29** compares the X-ray patterns for calcined and green cokes (second and forth sections) produced from Run #14. The 'signature peaks' for the ideal graphite (hexagonal) are those observed at 26.381º representing [002], the peak at 44.391º representing [101] direction, and the 42.221º which represents the [100] direction. Because of the interference of mineral matter inherent in coal, the peaks around 40-50 were difficult to resolve. **Figure 5-28** clearly shows that for calcined cokes the [002] peak was sharper than for the green cokes. In both cases, the [002] peak includes peak from amorphous phase and from graphite structure **[5-79]**, but clearly the intensity of amorphous phase peak decreased during the calcination process. There are no distinct correlations between coal remnant concentration and the d-spacing or crystallite stacking height (Lc).

Table 5-31 X-Ray results of some calcined coke samples

	d-Spacing, Å	Lc
14s1cc	3.440	34
14s2cc	3.4271	34
14s3cc	3.4391	34
14s4cc	3.4173	34
35s1cc	3.4520	36
35s2cc	3.4668	36
35s3cc	3.4725	37

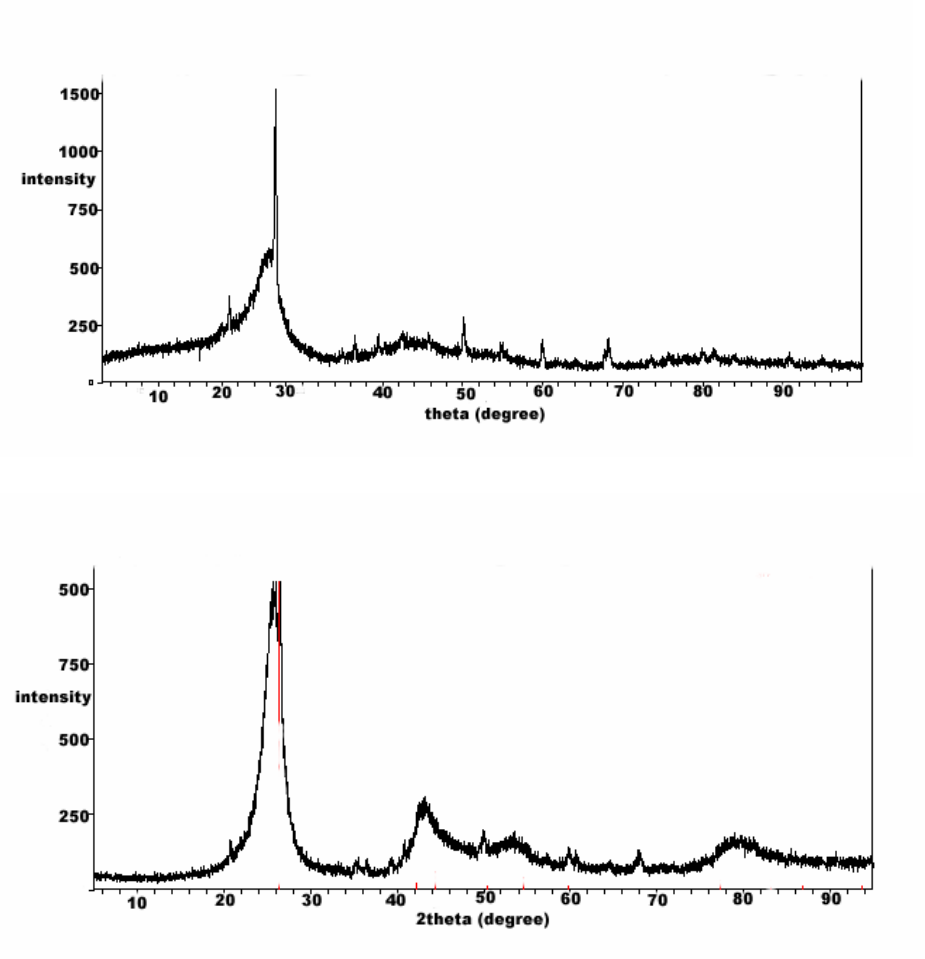

Figure 5-28 The X-ray diffraction profiles for second section coke sample (Run #14) before (top) and after (bottom) calcination.

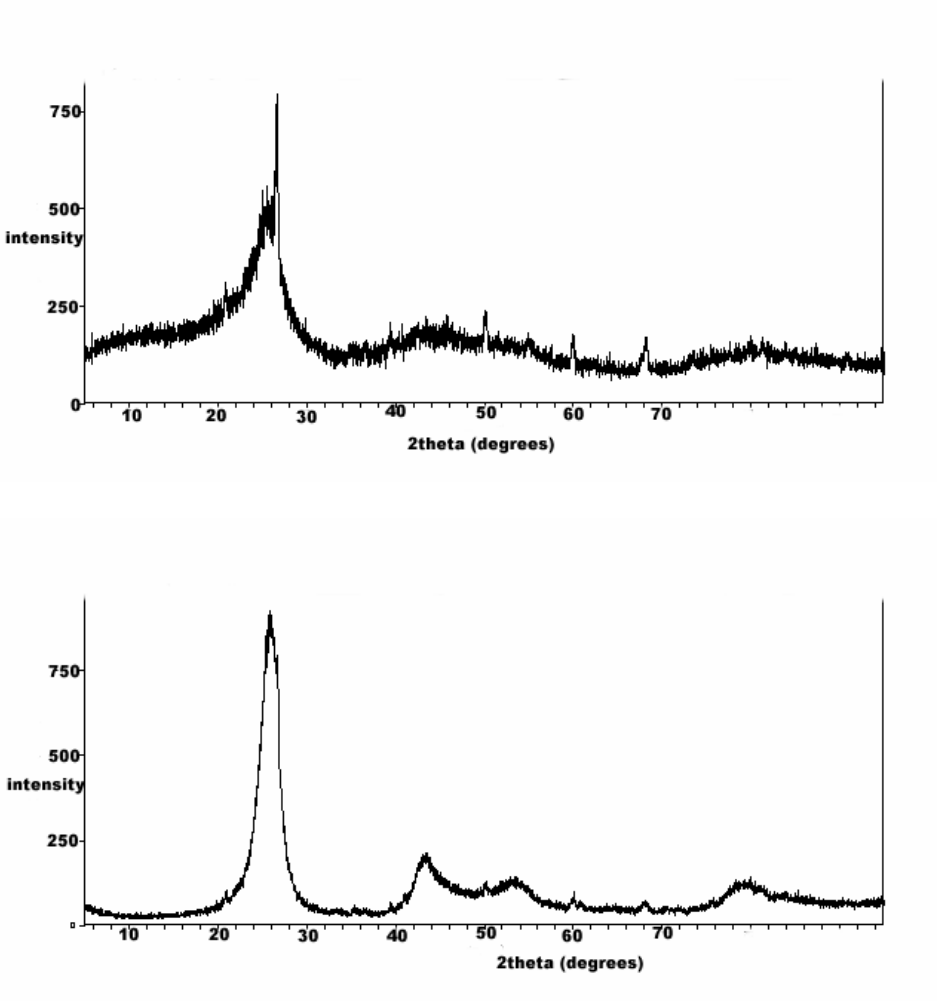

Figure 5-29 The X-ray diffraction profiles for fourth section coke sample (Run #14) before (top) and after (bottom) calcination.

5.6.2 Evaluation of Whole Crushed Coke Samples

5.6.2.1. Experimental

Materials

Whole-coke artifacts from Runs #12, #16, #20, #24, #36, #38, #39 and #48 were crushed and grounded to pass a 0.85 mm, 20 mesh Tyler sieve. After sieving, the 20 mesh coke samples were placed in special plastic bags and sealed under argon gas to protect them from deterioration. These cokes were selected for a variety of reasons, but

the principal aim was to evaluate the influence of different coals and decant oils on final coke properties. Most of these co-coking runs employed a 4:1 blend of decant oil and coal, except Run #36 which used a 70/30 % blend of decant oil and coal. Unfortunately, by increasing the percentage of coal in the blend caused pumping problems and therefore, probably represents the upper limit of coal concentration for our equipment. The nomenclature describing the green and calcined cokes is given in **Table 5-32** and the conditions and product distributions for each experiment are provided in **Table 5-33**.

Table 5-32 Nomenclature of Coke Samples

Run #	Nomenclature	Explanation
12	DOS	Seadrift decant oil
16	DOS/PE	Seadrift decant oil with Powellton Eagle coal
20	DO107/PE	United Refinery decant oil with Powellton Eagle coal
24	DO107/C	United Refinery decant oil with Canterbury coal
36	DO107/C (70/30)	United Refinery decant oil with Canterbury coal (70/30 ratio)
38	DO107	United Refinery decant oil
39	DO107	United Refinery decant oil
48	DO107	United Refinery decant oil
12	12gc and 12cc	Green coke and calcined coke, respectively, from Run # 12
16	16gc and 16cc	Green coke and calcined coke, respectively, from Run # 16
20	20gc and 20cc	Green coke and calcined coke, respectively, from Run # 20
24	24gc and 24cc	Green coke and calcined coke, respectively, from Run # 24
36	36gc and 36cc	Green coke and calcined coke, respectively, from Run # 36
38	38gc and 38cc	Green coke and calcined coke, respectively, from Run # 38
39	39gc and 39cc	Green coke and calcined coke, respectively, from Run # 39
48	48gc and 48cc	Green coke and calcined coke, respectively, from Run # 48

In addition, **Figures 5-30** and **5-31** briefly describe the interrelationship between experimental conditions for both Seadrift and United Decant oils and for both coals (Powellton/Eagle and Canterbury). Product distribution shows that the co-coking of

decant oil and coal generated a considerable amount of solids which encouraged us to investigate their potential end-use of product.

Regarding the different feed materials, **Table 5-34** compares some of the basic properties of the decant oils and coals employed in these selected runs. Both of the coals used were actually blends of multiple seams, where the EI-106 was a 50:50 blend of the Powellton and Eagle seams. These two high volatile A bituminous (hvAb) coals are nearly indistinguishable in their physical and chemical properties. However, the Canterbury coal (Lower Kittanning seam) was found to be a blend of two unspecified coals of different rank. The Canterbury coal was an early prospect sample obtained from

Table 5-33 Conditions and Product Distributions for Coking and Co-coking Experiments

Run #	**12**	**16**	**20**	**24**	**36**	**38**	**39**	**48**
Conditions	DO-S	DO-S/P	DO107/P	DO107/C	DO107/C (70/30)	DO107	DO107	DO107
feedstock (h)	6	6	6	6	5.5	6	6	6
hold at 500 °C (h)	5	5	6	0	6	6	24	24 (at 600°C)
feed rate (g/min)	16.7	16.7	16.7	16.7	16.7	16.7	16.7	16.7
preheater inlet (°C)	188	185	238	228	228	144	148	120
preheater outlet (°C)	440	432	425	437	436	447	446	462
coke drum inlet (°C)	487	nd	480	480	468	476	471	516
coke drum lower/middle (°C)	490	482	499	490	468	474	474	506
coke drum top (°C)	430	466	478	476	474	476	476	478
Product Distributions (%)								
% coke	6.85	33.09	26.79	29.42	37.53	19.81	22.23	14.17
% liquid product	70.86	67.65	68.85	57.92	51.75	70.80	70.54	77.21
% gas (by difference)	22.29	-	4.36	12.66	10.72	9.39	7.23	8.62

the Canterbury mine in western Pennsylvania that was determined by vitrinite reflectance to be a blend of 73% hvAb and 27% medium volatile bituminous (mvb) coals. When the froth flotation cell effluent product was evaluated, it was found to contain 91% hvAb and 9% mvb and owing to this variability the coal was rejected as a prospect for co-coking. Although neither coal was deeply cleaned to a low ash yield product, the as-received coals were used during process development runs in the (at the time) newly redesigned delayed coker.

Table 5-34 Properties of the Feed Materials

	Coals		**Decant Oils**	
Proximate analysis [a]	**Powellton/Eagle EI-106**	**Canterbury**	**Seadrift**	**EI-107**
Ash (%)	8.12	10.02	0.15	0.22
Volatile matter (%)	27.27	28.33	-	-
Fixed carbon (%)	64.61	61.65	-	-
Ultimate analysis [a]				
Carbon (%)	80.92	78.50	89.7	89.59
Hydrogen (%)	4.55	5.37	9.3	7.32
Nitrogen (%)	1.28	1.38	0.2	0.22
Sulfur (%)	0.88	1.72	0.8	2.99
Oxygen (by diff.) (%)	4.25	3.01	-	-
Fluidity Data [b]				
Fluid Temperature Range (°C)	88	110	na	na
Maximum Fluidity (ddpm)	7,002	27,469	na	na
Softening Temperature (°C)	397	381	na	na
Organic Petrography, vol%				
Total Vitrinte (vol. %)	86.5	87.0	na	na
Total Liptinite (vol. %)	1.4	2.6	na	na
Total Inertinite (vol.%)	12.1	10.4	na	na

[a] values reported on a dry basis
[b] Determined using a Gieseler plastometer

Calcination Conditions

All samples were calcined following the same method which was described in Section 5.6.1. The weights of coke samples before and after calcinations were recorded.

Green and Calcined Coke Properties

The ash yields and real densities of green and calcined coke samples were determined by the same procedure described in Section 5.6.1 and these results are summarized in **Table 5-35**. X-ray diffraction again was used to evaluate the degree of structural anisotropy in green and calcined cokes.

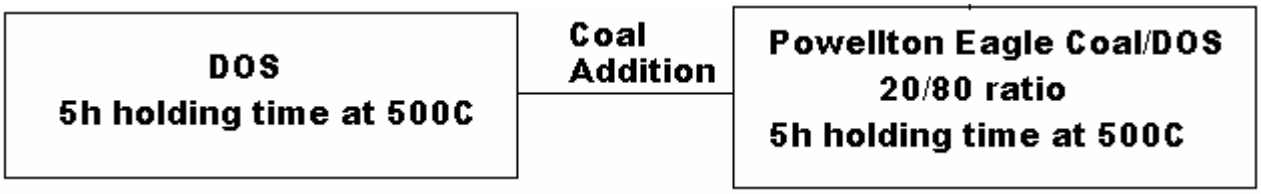

Figure 5-30 Schematic of experimental conditions for coking of Seadrift decant oil alone and co-coking of Seadrift decant oil with Powellton/Eagle coal.

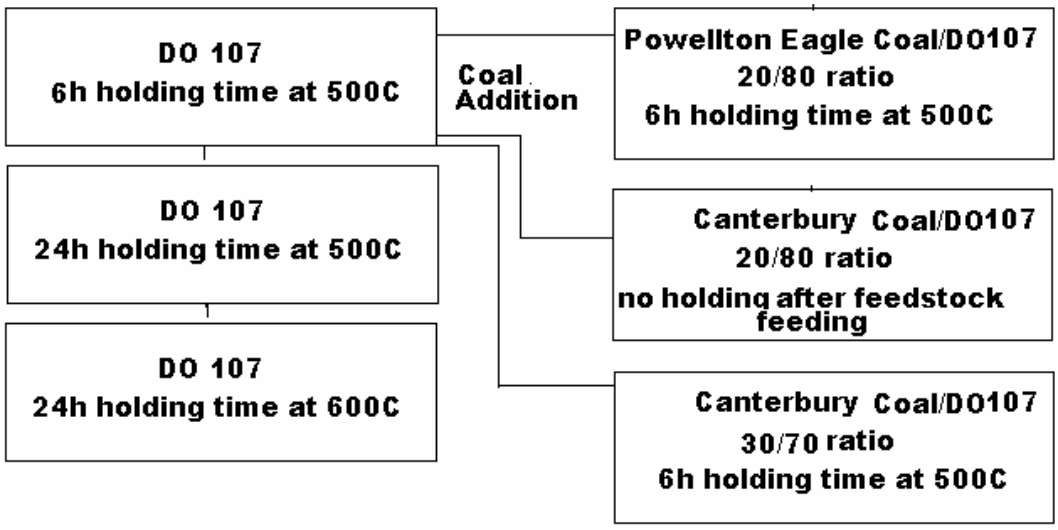

Figure 5-31 Schematic of experimental conditions for coking of United decant oil alone and co-coking of United decant oil with two different coals.

5.6.2.2. Results and Discussion

Experimental

Conditions and product distributions for coking and co-coking experiments are provided in **Table 5-33**. Product distributions show that liquids constituted the main product with yields in the range of ~50-78% depending on the feed material and experimental conditions employed. Those runs using decant oil alone generated more liquid and less coke compared with runs where coal was used. Use of 20 wt.% coal resulted in approximately twice the carbon yield, whereas increasing the coal ratio 30% resulted in about an 8% increase in coke yield and a 6 % decrease in the liquid yield (Run #24 and #36). Gas yields were low in most experiments except for when the Seadrift decant oil was coked alone (Run #12) and excluding Run #12 ranged from about 4.4 to 12.7 wt.%. Surprisingly, the two runs using Canterbury coal (Runs # 23 and #36) exhibited the highest gas make of this group of experiments.

Weight Loss during Calcination

Figure 5-32 summarizes the percentage weight loss during calcination experiments. The weight loss was almost the same for cokes produced from coking decant oil alone, regardless of decant oil used. In all cases, the apparent volatility of coke samples was found to be higher with the addition of coal to coking system. The highest weight loss was observed for the coke made with 20 wt.% Canterbury coal and probably resulted from the fact that it was not exposed to a 5 hour soak period at 500 ºC as were

the other coke artifacts (**Table 5-33**). Volatile matter release from coal occurs at a higher temperature because of its largely aromatic structure. As coal rank increases, the temperature of volatile matter release increases. Consequently, the presence of medium volatile coal in the Canterbury coal may have resulted in a slightly higher weight loss during calcinations compared to the runs using Powellton/Eagle coal (Runs #16 and #20).

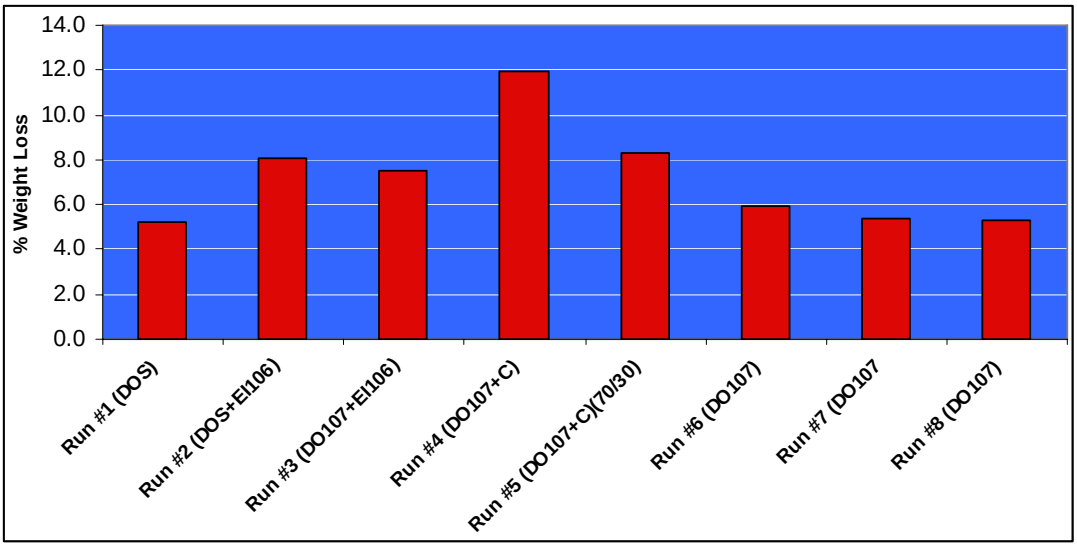

Figure 5-32 Percent Weight Loss during Calcination.

Ash Contents and Density Data for Green and Calcined Cokes

Table 5-35 summarizes the ash yields and density values for green and calcined coke samples. The densities for green and calcined cokes also are compared in **Figures 5-33** and **5-34**, respectively. As expected, the ash yields of coke samples obtained from decant oil only feeds were lower in all cases, whereas the addition of coal to coking system resulted in an increase of ash yields from the final cokes. Canterbury coal had the highest ash yield and, therefore, the coke samples had a high ash contents. Cokes made using the Powellton/Eagle coal were slightly lower in ash yield. As listed in **Table 5-29**,

the ash content of anode grade cokes should not exceed 0.4 wt% **[5-83]**. Graphite electrode manufacturers now demand that the needle coke ash content be below 0.3 wt% **[5-83]**. Therefore, these cokes would be well out of range of premium cokes and underscores the reason for deep cleaning the coals before coking.

The real densities of green coke samples were lower then those of calcined coke samples. Densities of green cokes derived from coking of decant oil alone were typically lower than those from co-coking runs, except for Run #48. In this particular run, the coke sample was held at 600°C for 24 hours. Densities of green cokes made with Powellton/Eagle coal were higher than those runs using Canterbury coal, even though the ash yields were significantly different.

Table 5-35 Ash Contents and Density Data for Green and Calcined Cokes

Sample	Ash %	Real Density (g/cm^3)
12gc (DOS)	0.43	1.4366
12cc (DOS)	0.44	2.1650
16gc (DOS+EI106)	5.36	1.4942
16cc (DOS+EI106)	5.50	2.1309
20gc (DO107+EI106)	5.62	1.5095
20cc (DO107+EI106)	5.78	2.1225
24gc (DO107+C)	6.44	1.4586
24cc (DO107+C)	7.27	2.0687
36gc (DO107+C) (70/30)	6.33	1.4776
36cc (DO107+C) (70/30)	7.11	2.0324
38gc (DO107)	nd	1.4279
38cc (DO107)	0.43	2.1674
39gc (DO107)	0.19	1.4501
39cc (DO107)	nd	2.1604
48gc (DO107)	0.22	1.6074
48cc (DO107)	nd	2.1632

The situation was different for calcined cokes. After calcination, coke samples obtained from coking of decant oil alone had higher real densities then the cokes derived

from co-coking experiments. Although green coke produced from coking of DO107 held 600°C for 24 hours (Run #48) had the highest real density among all other green cokes. After calcination, the real density of this sample was almost the same with real densities of other coke samples derived from coking decant oils alone. Density values for cokes made using Powellton/Eagle coal, although lower than those derived from decant oil feeds, were significantly higher than those derived from using the Canterbury coal. Increasing the ratio of coal in the blend caused a further decrease in the real density value (compare Runs #24 and #36). Results shown from the evaluation of segments

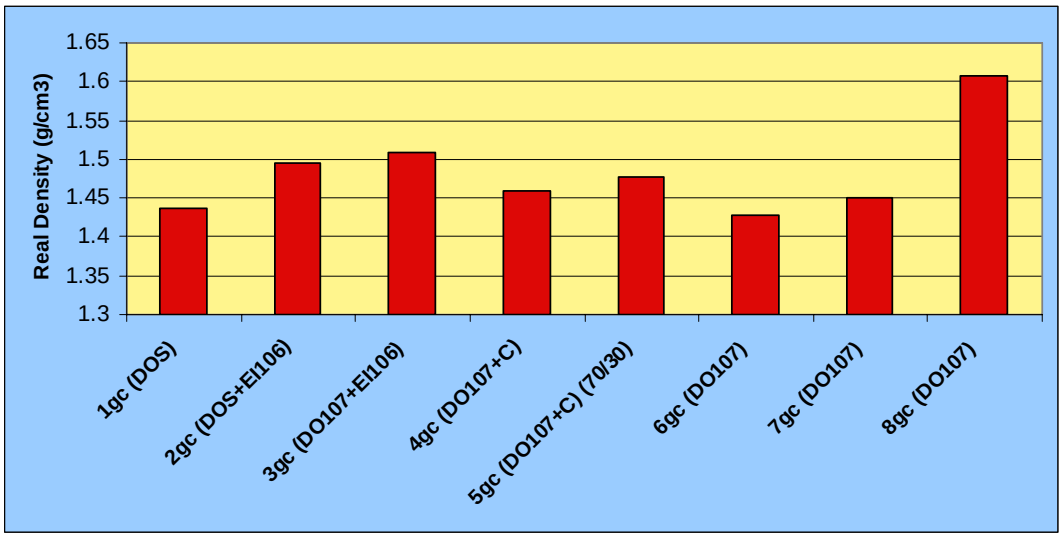

Figure 5-33 Densities of green (uncalcined) coke samples.

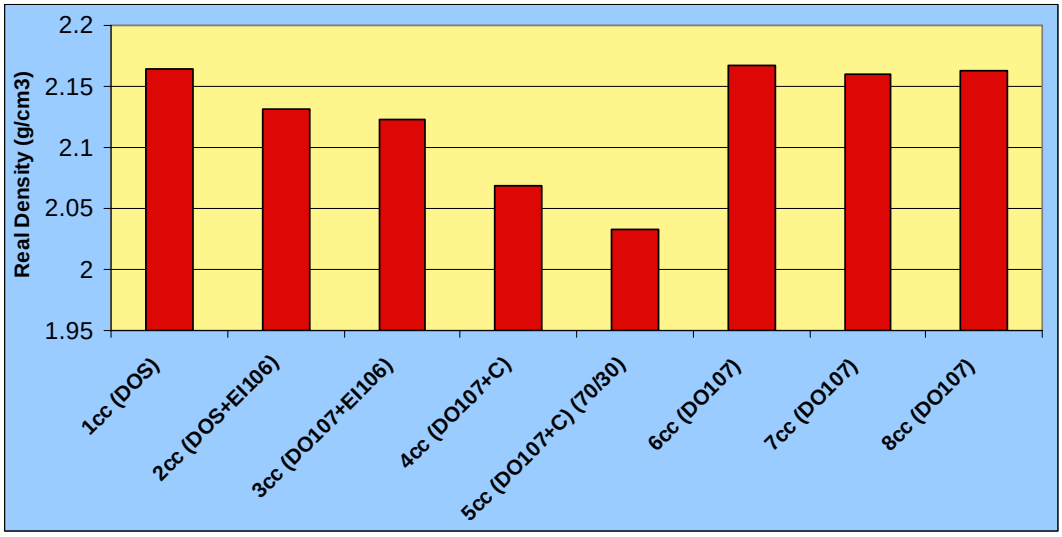

Figure 5-34 Densities of calcined coke samples

of coke artifacts (**section 5.6.1.2**) suggest that the presence of mineral matter influences density values. The conditions of calcinations can be used to adjust the real density of the final product. Anode grade coke densities are typically adjusted to around 2.05 to 2.08 g/ml, whereas those of needle coke for graphite electrodes are adjusted to meet a density of 2.13 g/ml. Except for Run #36 (a 70/30 DO to coal ratio), all calcined coke real densities were within the anode coke specification.

X-Ray results of calcined coke samples

Figures 5-35 – 5-38 show the X-ray diffraction patterns and **Table 5-36** summarizes d-spacing and crystallite stacking height derived from these patterns for all of calcined coke samples. The d-spacing represents the height between two adjacent layers of atoms in the z direction (vertical height), whereas Lc represents the average height of individual crystals of carbon in the c direction. Generally, as calcination or graphitization temperature increases d-spacing decreases and Lc increases. The

interplanar distance for graphite is 0.3348 Å **[5-79]**. As seen in **Table 5-36**, the d-spacing for all of the calcined cokes is significantly higher than for graphite, which would be expected from the low temperature of calcinization (1300 ºC) compared with grapitization (>2700 ºC). Furthermore, in all cases the addition of coal to the coking blend resulted in a decrease in d-spacing and the coke sample produced from blend of DO-107 and Canterbury coal in a ratio of 70/30 had the lowest d-spacing value. In comparison, the crystallite stacking height was fairly uniform for the sample set, but those derived from the calcined Canterbury cokes were the lowest. Generally, Seadrift decant oil had lower d-spacing and lower crystallite stacking height compared with those runs using the DO-107 decant oil from United Refining. Coke obtained from co-coking of Seadrift decant oil with Powellton/Eagle coal (EI106) had the same Lc value as coke obtained from coking of Seadrift decant oil alone (12cc and 16cc), but the reverse was found when comparing calcined coke obtained from coking of DO107 and Powellton/Eagle coal (20cc and 38cc). Whether run conditions have any significant impact on the crystallinity and anisotropy of calcined coke as measured by X-ray is difficult to say. For Runs #38 and #39 using Do-107 decant oil, increasing the hold time did not influence the Lc, but may have contributed to a decrease in d-spacing. Likewise, the increase the hold temperature from 500°C to 600°C between Runs #39 and #48 may have contributed to a decrease in d-spacing and an increase Lc.

Table 5-36 d-spacing and crystallite stacking height for of all calcined coke samples

Sample	**d-Spacing, Å**	**Lc (crystallite stacking height)**
12cc (DOS)	3.4489	35
16cc (DOS+EI106)	3.4455	35
20cc (DO107+EI106)	3.4361	37
24cc (DO107+C)	3.4283	33
36cc (DO107+C) (70/30)	3.4221	33
38cc (DO107)	3.4503	36
39cc (DO107)	3.4499	36
48cc (DO107)	3.4484	37

With regard to the diffraction patterns shown in **Figures 5-35 – 5-38**, as before the region 40-50º two-theta was difficult to resolve in the cokes made using coal owing to the presence of mineral matter.

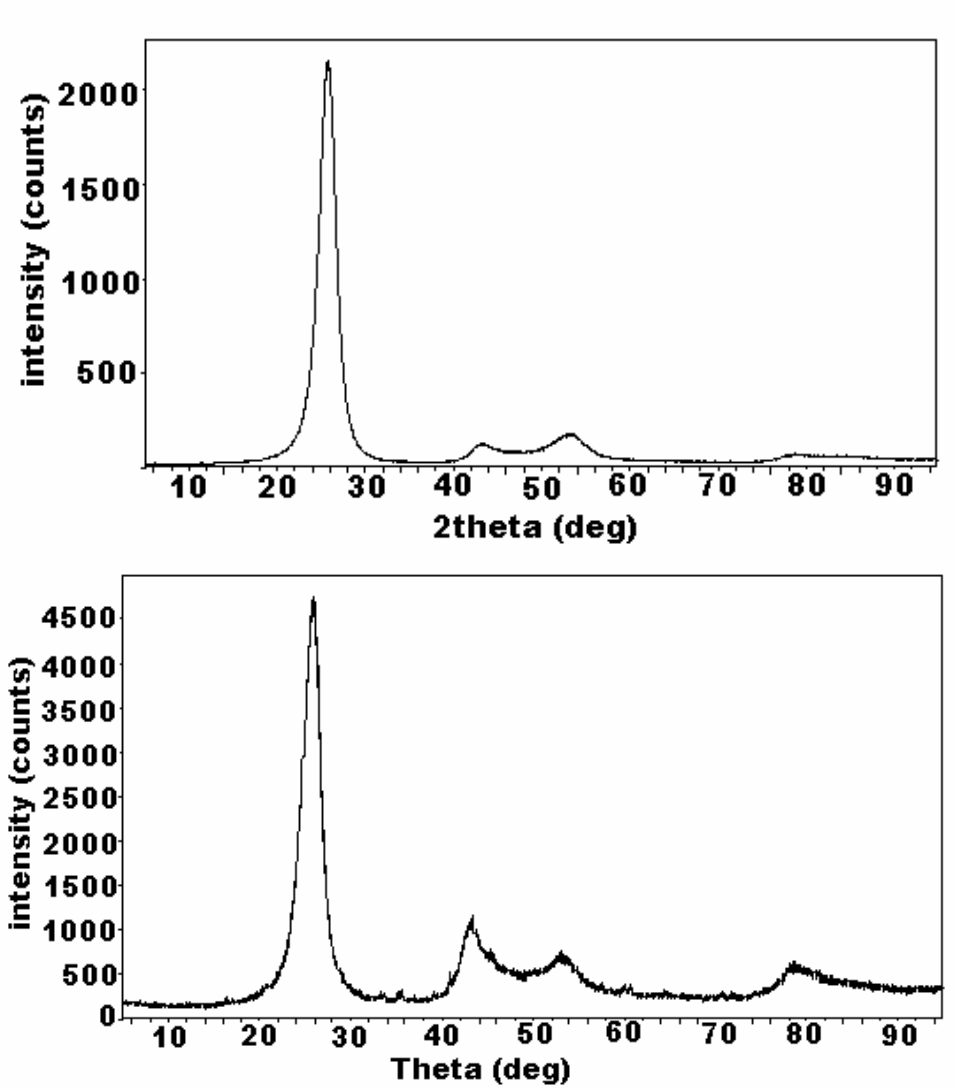

Figure 5-35 Diffractometric records of calcined coke samples (12cc (at the top) and 16cc (at the bottom)).

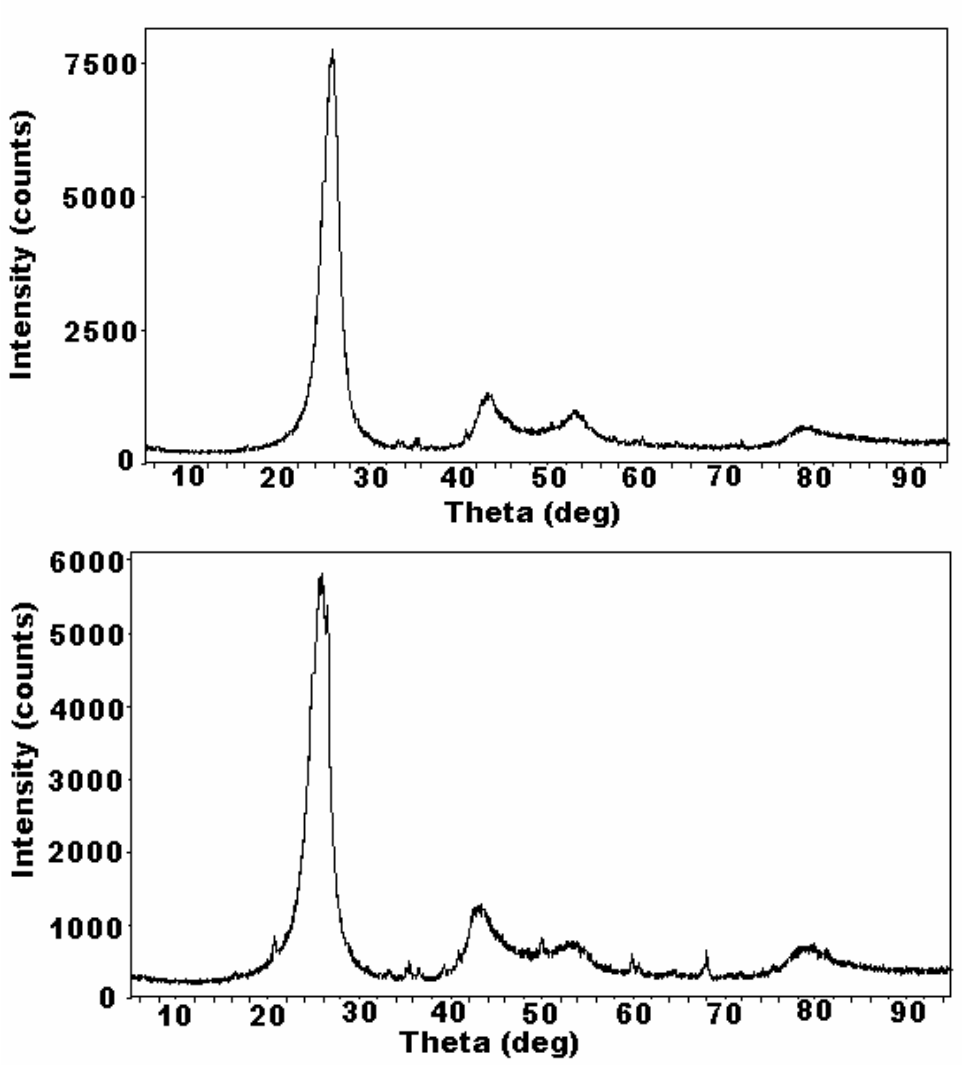

Figure 5-36 Diffractometric records of calcined coke samples (20cc (at the top) and 24cc (at the bottom)).

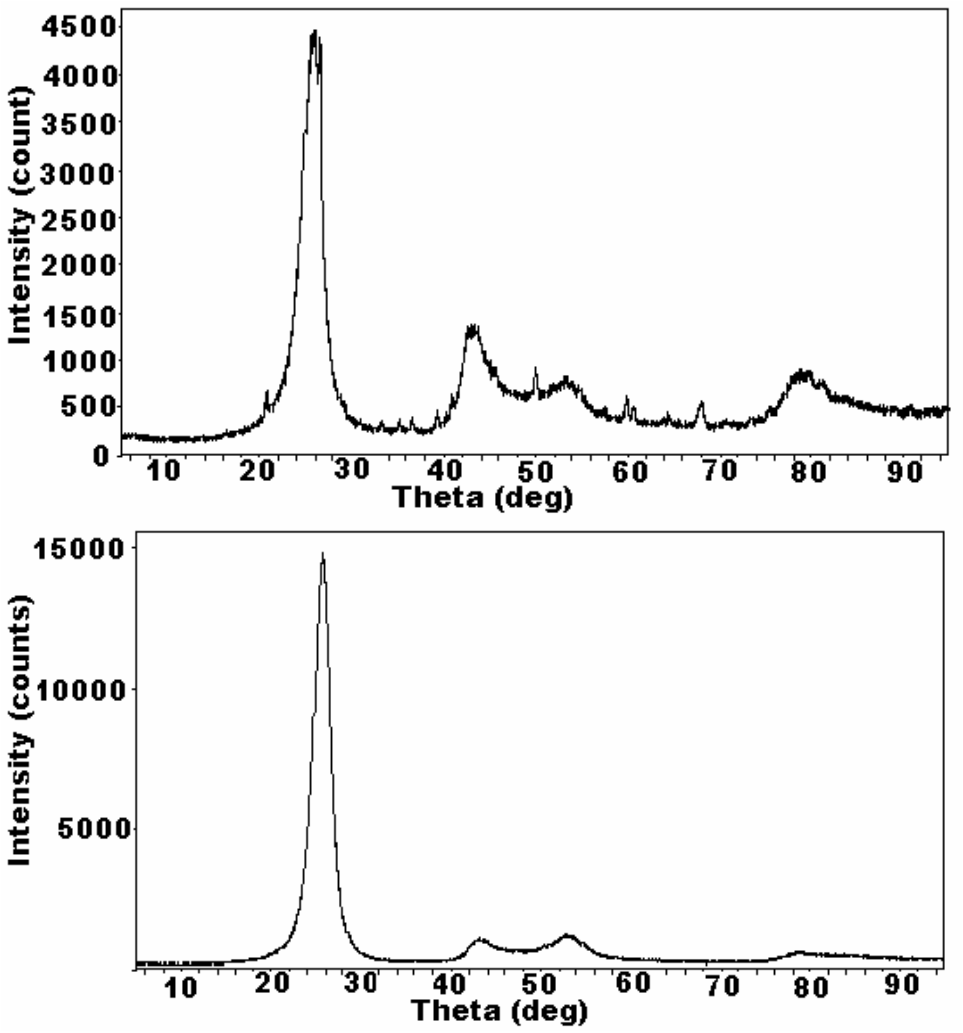

Figure 5-37 Diffractometric records of calcined coke samples (36cc (at the top) and 38cc (at the bottom)).

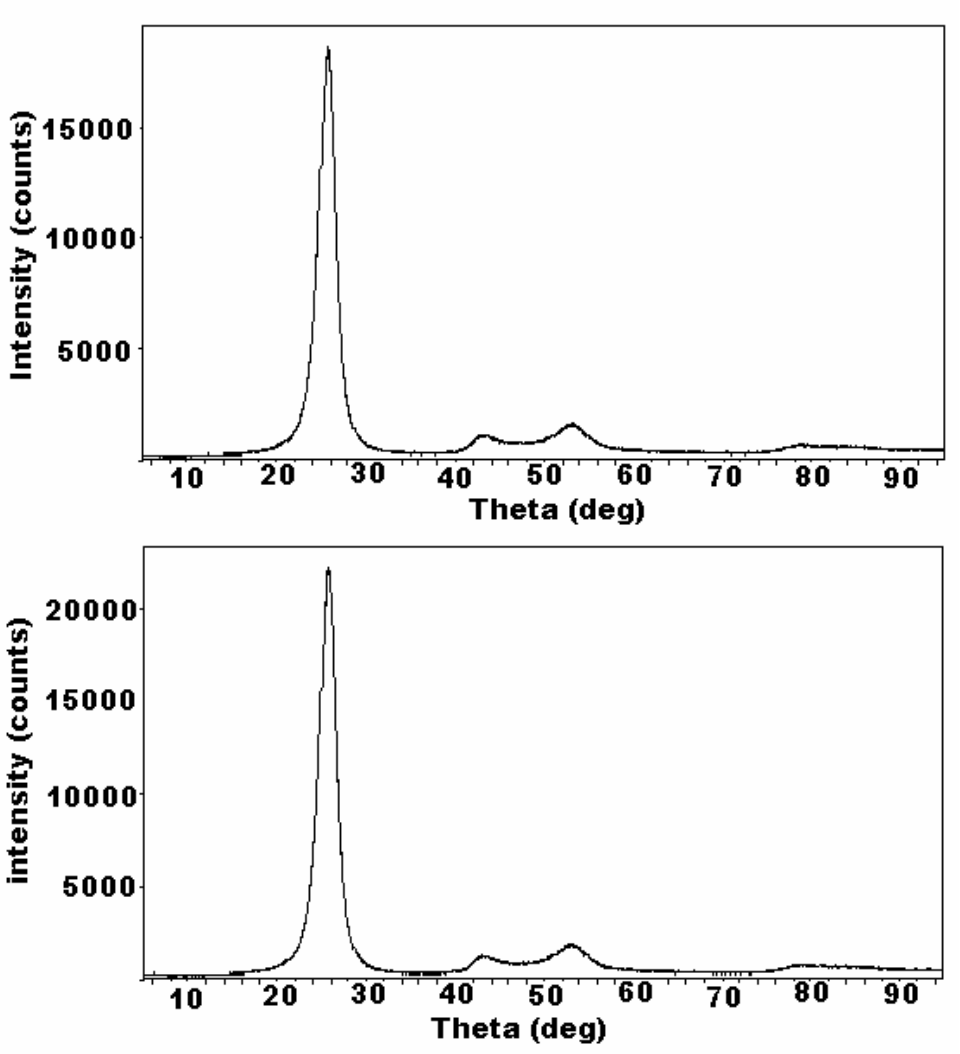

Figure 5-38 Diffractometric records of calcined coke samples (39cc (at the top) and 48cc (at the bottom)).

5.6.3 Conclusions

The main objective of this part of project is to evaluate cokes from co-coking of decant oil and coal. The results are summarized briefly:

Conclusion for the evaluation of different sections of coke samples

1) There is a variable distribution in coal-derived materials in these different sections.

2) Real densities meet the specifications for anode grade coke.

3) The concentrations of certain major elements (Si and Fe) of the calcined cokes were outside of the range suitable for anode or electrode grade coke.

4) The high ash content problem can only be solved by perparing better raw materials (i.e., a low ash yield coal).

Conclusion for the evaluation of whole crushed coke samples

1) Coking of Decant Oil Only: Two different decant oils were subjected to coking experiments and both behaved similarly during coking. Hold time and temperature have some effect to final carbon quality. Increasing holding temperature from 500ºC to 600ºC improved or increased carbon quality of the green coke, but upon calcinations no improvement was observed.

2) Addition of Coal to Coking Experiments: Although there were differences in conditions among the coker runs being studied some general observations can be made.

a) Weight loss during calcinations was greater for runs containing coal compared with runs where decant oil alone was employed. It is suspected that because coals devolatilize more completely at higher temperatures, the coal remnants retain more volatile matter that is released during calcinations at 1300 ºC.

b) Density values for green cokes made with coal were found to be higher than those from decant oil alone (except when held for 24 hours at 600 ºC), but upon calcination the reverse observation was found, i.e., decant oil alone > co-coke.

c) X-ray analysis of calcined cokes and the comparison of d-spacing and crystallite height (Lc) exhibited some minor differences which show that d-spacing and

Lc decreased with the addition of coal to the system, although this was a variable result depending upon the coal used.

d) Increasing the amount of coal in the blend with decant oil, in addition to causing operating problems, seemed to have a negative effect on the quality of the final carbon product.

REFERENCES

1-1 Schobert, H. H., Advanced Thermally Stable Coal-Based Jet Fuels, *Annual Progress Report,* AFOSR Grant F49620-99-1-0290, 2001-2002

1-2 Schobert, H. H., Advanced Thermally Stable Coal-Based Jet Fuels, *Annual Progress Report,* AFOSR Grant F49620-99-1-0290, 2000-2001

1-3 Schobert, H. H., Advanced Thermally Stable Coal-Based Jet Fuels, *Annual Progress Report,* AFOSR Grant F49620-99-1-0290, 1999-2000

1-4 Coleman, M. M., Fearnley, S. P., Kumar, S. and Sobkowiak, M., Fuel Stabilization, AFRL-PR-WP-TR-2000-2007, Final Report for 07/01/1995 – 12/31/1998, September 1999.

1-5 Song, C., Lai, W.-C., Schobert, H.H. Hydrogen-Transferring Pyrolysis of Long-Chain Alkanes and Thermal Stability Improvement of Jet Fuels by Hydrogen Donors. *Ind. Eng. Chem. Res.,* **1994**, 33 (3), 548-557

1-6 Lai, W.-C and Song, C., *Prepr. Pap.- Amer. Chem. Soc. Div. Fuel Chem.* **1996a** 41:524

1-7 Lai, W.-C and Song, C., *Fuel Processing Technology,* **1996b** 48:1

1-8 Selvaraj, L., Sobkowiak, M., Song, C., Stallman, J., Coleman, M. M. A Model System for the Study of Additives Designed to Enhance the Stability of Jet Fuels at Temperatures Above 400°C. *Energy & Fuels,* **1994**, 8 (4), 839-845.

1-9 Yoon, E.M., Selvaraj, L., Song, C., Stallman, J., Coleman, M. M., High Temperature Stabilizers for Jet Fuels and Similar Hydrocarbon Mixtures. 1. Comparative Studies of Hydrogen Donors. *Energy & Fuels,* **1996a**, 10 (3), 806-811.

1-10 Yoon, E.M., Selvaraj, L., Eser, S. and Coleman, M. M., High Temperature Stabilizers for Jet Fuels and Similar Hydrocarbon Mixtures. 2. Kinetic studies, *Energy & Fuels,* **1996a**, 10 (3), 812-815.

1-11 Andrésen, J.M., Strohm, J.J., Boyer, M.L., Song, C, Schobert, H.H. and Butnark, S., *Am. Chem. Soc. Div. Petrol. Chem. Prepr.,* **2001a**, 46(1), 208-209.

1-12 Andrésen, J.M., Strohm, J.J., Sun, L., Song, C. *Energy & Fuels,* **2001b**, 15(3), 714-723.

1-13 Badger, M. W., Fickinger, A. E.,Martin, S. C.,Mitchell, G. D. and Schobert, H. H., *Proc. 8th Austrlian Coal Science Conference,* **1998**, 245.

1-14 Badger, M. W., Fickinger, A. E., Mitchell, G. D., Adams, A. N. and Schobert, H. H., *Proc. 205th International Technical Conference on Coal Utilization and Fuel Systems (in press).*

1-15 Butnark, S., Badger, M.W. and Schobert, H.H., *Amer. Chem. Soc., Div. Fuel Chem. Prepr.,* **1999**, 44 (3), 662-665.

1-16 Butnark, S., Badger, M. W. and Schobert, H. H., *Prepr. Pap.- Amer. Chem. Soc. Div. Petrol. Chem.,* **2000** 45:493.

1-17 Fickinger, A. E., **2000**, M. S. Thesis, The Pennsylvania State University, University Park, PA.

1-18 Fickinger, A. E., Badger, M. W., Mitchell, G. D. and Schobert, H. H., , *Prepr. Pap.- Amer. Chem. Soc. Div. Fuel Chem*, **1999**, 44:106.

1-19 Fickinger, A. E., Badger, M. W., Mitchell, G. D. and Schobert, H. H., , *Prepr. Pap.- Amer. Chem. Soc. Div. Fuel Chem,* **2000**, 45:299.

1-20 Song, C., and Schobert, H. H., , *Prepr. Pap.- Amer. Chem. Soc. Div. Fuel Chem.,* **2000**, 45:819.

1-21 Butnark, S., Badger, M. W. and Schobert, H. H., Determining the Desired Chemical Composition for Thermally Stable Jet Fuel, *Amer. Chem. Soc., Div. Fuel Chem. Prepr.,* **2001**, 46 (2), 492-494.

1-22 Butnark, S., Badger, M. W. and Schobert, H. H. and Wilson, G. R., Selection of Prototype Thermally Stable Jet Fuels 3. Jet Fuel Boiling Range and its Affect on Pyrolytic Stability, *Prepr. Pap.- Amer. Chem. Soc. Div. Petrol. Chem.,* **2002**, 47(3), 201.

1-23 Schobert, H. H., Badger, M. W. and Santoro, R. J., Progress Toward Coal-Based JP-900, *Prepr. Pap.- Amer. Chem. Soc. Div. Petrol. Chem.,* **2002**, 47:192.

1-24 Wilson, G. R., Project Report on AFOSR-Subcontract for Advanced Thermally Stable Coal-Based Jet Fuels for the Pennsylvania State University, PARC Technical Services Inc., Pittsburgh, PA. August **2002**.

1-25 Rudnick, L. R., et al. "Refinery Integration of By-Products from Coal-Derived Jet Fuels", Year Annual Progress Report, Grant No. DE-FC26-03NT41828, November 17, **2005**.

2-1 Heywood, J. B. *Internal Combustion Engine Fundamentals*, McGraw-Hill: New York, 1988.

2-2 Yang, Y., J. P. Szybist, and A. L. Boehman, "Low Temperature Oxidation of Methylcyclohexane in an SI Engine," *Prepr. Pap.-Am. Chem. Soc., Div. Fuel Chem.* **2006,** *51(1),* 329-330.

2-3 Tanaka, S.; Ayala, F.; Keck, J. C.; Heywood, J. B., *Combustion and Flame* **2003,** 132, (1-2), 219-239.

2-4 Szybist, J., A.L. Boehman, D. C. Haworth, and H. Koga, "Premixed Ignition Behavior of Alternative Diesel Fuel-Relevant Compounds in a Motored Engine Experiment," Accepted for publication in *Combustion and Flame*, **2006**.

2-5 Boehman, A.L., J. Song, and M. Alam, "Impact of biodiesel blending on diesel soot and the regeneration of particulate filters." *Energy & Fuels*, **2005**. *19(5)*, 1857-1864.

2-6 Song, J., M. Alam, A.L. Boehman and U. Kim, "Examination of the oxidation behavior of biodiesel soot," *Combustion & Flame*, **2006**, 146:589-604.

2-7 Al-Qurashi, K. and A.L. Boehman, "The impacts of simulated exhaust gas recirculation on the oxidative reactivity of diesel soot," *Prepr. Pap.-Am. Chem. Soc., Div. Fuel Chem.* **2006,** *51(2),* 805-807.

2-8 Kirby, S.R., A. L. Boehman, and D. J. Clifford, "Evaluation of coal-based diesel products affect on fuel quality," *Prepr. Pap.-Am. Chem. Soc., Div. Fuel Chem.* **2005**, *50 (2)*, 732-733.

2-9 **The Institute of Petroleum**, *Modern Petroleum Technology*, 3rd ed.; London **1962**; p 609.

2-10 Westbrook K. C., Pitz J. W., and Curran J. H, "Chemical Kinetic Modeling Study of the Effects of Oxygenated Hydrocarbons on Soot Emissions from Diesel Engines," *Phys.Chem. A* **2006**, 110, 6912-6922.

2-11 Vala, M,. Eyler, R.J., Rearson, W., "Theoretical Study of Photo dissociation and Hydrogenation of Fluorene Cation," *J. Physics. Chem. A* **2001**, 105, 9388-9395.

2-12 Chen, H.X. and R.A. Dobbins, "Crystallogenesis of particles formed in hydrocarbon combustion," *Combustion Science and Technology*, **2000**. *159,* 109-128.

2-13 VanderWal, R., "Soot Nanostructure: Dependence upon Synthesis Condition," *Combustion and Flame*, **2004**, *136,* 129-140.

2-14 Tuinstra, F. and J.L. Koenig, "Raman Spectrum of Graphite." *Journal of Chemical Physics*, **1970**. *53(3),* 1126-1130.

2-15 Escribano, R., et al., "Raman spectroscopy of carbon-containing particles," *Vibrational Spectroscopy*, **2001**. *26(2)*, 179-186.

2-16 Liu, F.S., et al., "The chemical effects of carbon dioxide as an additive in an ethylene diffusion flame: Implications for soot and NOx formation," *Combustion and Flame*, **2001**, *125(1-2)*, 778-787.

2-17 Du, D. X., Axelbaum R. L., and Law, C. K., "The Influence of Carbon Dioxide and Oxygen as Additives on Soot Formation in Diffusion Flames," *23rd Symposium (International) on Combustion*/ The Combustion Institute, **1990**, 1501-1507.

2-18 Kim, C.H., et al., "Soot surface growth and oxidation in laminar diffusion flames at pressures of 0.1-1.0 at,". *Combustion and Flame*, **2004**. *136(1-2)*, 191-207.

3-1 Song, C. and Ma, X. *Appl. Catal. B:Env.*, 2003, 41, 207.

3-2 Lee, S.-W.; Ryu, J. W. and Min, W. *Catal. Surv. Asia* 2003, 7, 271.

3-3 Sano, Y.; Choi, K.-H.; Korai, Y. and Mochida, I. *Appl. Catal*. B 2004, 49, 219.

3-4 Oyama, S. T.; Wang, X.; Lee, Y.-K.; Bando, K. and Requejo, F. G., *J. Catal.* 2002, 210, 207.

3-5 Stinner, C.; Prins, R. and Weber, Th., *J. Catal*. 2001, 202, 187.

3-6 Oyama, S. T., *J. Catal*. 2003, 216, 343.

3-7 Sie, S. T., *Fuel Proc. Tech*. 1999, 61, 149.

3-8 Sano, Y.; Choi, K.-H.; Korai, Y. and Mochida, I. *Energy & Fuels* 2004, 18, 644.

3-9 J.H. Kim, X. Ma, C. Song, Y. Lee and S. T. Oyama, *Energy & Fuel*, 2005, 19, 353-364

3-10 Topsoe, H., Clausen, B. S., Topsoe, N. Y., Pedersen, E., Niemann, W., Müller, A., Bögge, H., and Lengeler, B., *J. Chem. Soc. Faraday Trans,* 1987, 83, 2157.

3-11 B. Delmon, *Surf. Rev. Lett*, 1995, 2, 1, 25-41.

3-12 Song, C. *Am. Chem. Soc. Div. Petrol. Chem. Prepr*., 1998, 43, 573.

3-13 Song, C. *CHEMTECH*, 1999, March, 26.

3-14 Johnson,C.D and Worrall, F. *Microporous and Mesoporous Materials* 2004, 73, 191.

3-15 S.T. Wilson, B.M. Lok, C.A. Messina, E.R. Cannan and E.M. Flanigen, J. Am. Chem. Soc. 104 (1982) 1146.

3-16 M.E. Davis, Nature 417 (2002) 813.

3-17 3. S.T. Wilson, B.M. Lok, E.M. Flanigen, US Pat. 4 310 440, (1982).

3-18 J.M. Bennett, Jr. Richardson, J.W. Pluth, J.V. Smith, Zeolite, 7, (1987) 160.

3-19 D.B. Akolekar, J. Mol. Catl. A: Chem., 104 (1995) 95.

3-20 S.H. Jhung, J-S. Chang, D.S. Kim, S-E. Park, Micropor. Mesopor. Mater. 71 (2004) 135.

3-21 M.H. Kim, H.X. Li, M.E. Davis, Micropor. Mater. 1 (1993) 191.

3-22 M. Matsukata, M. Ogura, T. Osaki, P.R.H.P. Rao, M. Nomura, E. Kikuchi., Topics in Catal. 9 (1999) 77.

3-23 Bandyophadhyay, R.K. Ahedi, Y. Kubota, M. Ogawa, Y. Goto, Y. Fukushima, and Y. Sugi, J. Mater. Chem. 11 (2001) 1869.

3-24 R. Bandyopadhyay, Y. Kubota, N. Sugimoto, Y. Fukushima, and Y. Sugi, Micropor. Mesopor. Mater. 32 (1999) 81.

3-25 T. Tatsumi and N. Jappar, J. Phys. Chem. B, 102 (1998) 7126.

3-26 A. Bhaumik and T. Tatsumi, Micropor. Mesopor. Mater. 34 (2000) 1.

3-27 R. Bandyopadhyay, M. Bandyopadhyay, Y. Kubota, Y. Sugi, J. Porous Mater. 9 (2002) 83.

3-28 S.K. Saha, Y.Kubota, Y. Sugi, Chem. Lett. 32(11) (2003) 1026.

3-29 S.K. Saha, S.B. Waghmode, Y.Kubota, Y. Sugi, Mater. Lett. 58 (2004) 2918.

3-30 S.B. Waghmode, S.K. Saha, Y.Kubota, Y. Sugi, J. Catl. 228 (2004) 192.

3-31 S.K. Saha, S.B. Waghmode, H. Maekawa, K. Kumora, Y.Kubota, Y. Sugi, Y.Oumi and T. Sano, Micropor. Mesopor. Mater. 81 (2005) 289.

3-32 T. Tatsumi, Q. Xia, N. Jappar, Chem. Lett. (1997) 677.

3-33 P.R.H.P. Rao, M. Matsukata, Chem. Commun. (1996) 1441.

4-1 Rudnick, L.R., A. Boehman, C. Song, B. Miller, and J. Andresen, "Refinery Integration of By-Products from Coal-Derived Jet Fuels Semiannual Progress Report for the Period March 18, 2004 to September 17, 2005," DE-FC26-03NT41828, October 18, 2005.

4-2 Singer, J.G. (editor), Combustion: Fossil Power Systems, Combustion Engineering, Inc., pp.2-28 – 2-31, 1981.

4-3 Habelt, W.W., "The Influence of Coal Oxygen to Coal Nitrogen Ratio on NO_x Formation," Presented at the 70th Annual AIChE Meeting, New York, November 13-17, 1977.

4-4 Steam Generating Units Power Test Codes, ASME PTC 4.1, The American Society of Mechanical Engineers, 1965 (with 1968 and 1969 addenda, reaffirmed 1973).

4-5 Federal Register, Title 40 CFR Parts 60 and 61, Standards of Performance for New Stationary Sources National Emission Standards for Hazardous Air Pollutants Addition of Method 29 to Appendix A of Part 60 and Amendments to Method 101A of Appendix B of Part 61, 18260-18279, 1996.

4-6 U.S. Environmental Protection Agency, Standard Test Method for Elemental, Oxidized, Particle-bound and Total Mercury in Flue Gas Generated from Coal-Fire Stationary Sources (Ontario-Hydro Method), /prelim/pre_003.pdf, May 12, 1999.

5-1 Fickinger, A.E., M.S. Thesis. Laboratory-scale coking of coal/petroleum mixtures, The Pennsylvania State University, **2000**.

5-2 Escallón, M.M., M.S. Thesis. Reaction of decant oil and bituminous coal at 465ºC in a laboratory scale coker, Pennsylvania State University, **2004**.

5-3 Burgess-Clifford, C.E., Boehman, A., Song, C., Miller, B., Mitchell, G., "Refinery Integration of By-Products from Coal-derived Jet Fuels," Semi-Annual Progress Report for Grant DE-FC26-03NT41828, May 17, **2006**.

5-4 Heintz, E.A. Influence of coke structure on the properties of the carbon-graphite artifact. Fuel, 64, 1192-1196. 1985.

5-5 Pysz, R.W., Hoff, L. and Heintz, E.A. Terminology for the structural evaluation of coke via scanning electron microscopy. Carbon 27, 6, 935-944. 1989.

5-6 Murty, H.N., Biederman, D.L., and Heintz, E.A. Kinetics of graphitization – II. Pre-exponential factors. Carbon, 7, 683-688. 1969.

5-7 Rumsey, J.C. and Pitt, G.J. Some techniques for the characterization of cokes and graphite. Fuel, 57, 155-161. 1978.

5-8 Mochida, I., Nakamo, S., Oyama, T., Nesumi, Y and Todo, Y. Puffing and CTE of carbon rods prepared from hydrodesulfurized petroleum needle coke. Carbon, 26, 5, 751-754. 1988.

5-9 Kenshun, S, Chengfang, W. and Jifu, L. Influence of microstructure on thermal expansion and graphitization of oil cokes. Fuel, 64, 174-177. 1985.

5-10 Kipling, J.J. and Shooter, P.V. Factors affecting the graphitization of carbon: evidence from polarized light microscopy. Carbon, 4, 1-4. 1966.

5-11 Heitz, E. A. The characterization of petroleum coke. Carbon, 34, 6, 699-709. 1996.

5-12 Casiello, G.L. and Chang J. Needle coke application and quality. Paper presented at the 1995 Carbon quality conference, Houston TX, Sept 26-28, p 1995, 21 pages.

5-13 Mochida,I.; Korai, Y. Carbonization in the tube bomb leading to needle coke: I. Cocarbonization of a petroleum vacuum residue and a FCC-decant oil into better needle coke. Carbon, 27(3), 359-365. 1989.

5-14 Mochida, I.; Toshima, H.; Korai, Y. Comparative evaluation of mesophase pitches derived from coal tar and FCC-DO.

5-15 Mochida, I.; Oyama, T.; Korai, Y.; Qing Fei, Y. Study of carbonization using a tube bomb: evaluation of lump needle coke, carbonization mechanism and optimization. Fuel, 67(9): 1171-1181. 1988.

5-16 Martinez-Escandell, M.; Torregosa, P.; Marsh, H.; Rodriguez-Reinoso, F., Santamaria-Ramirez, R.; Gomez-De-Salazar, C.; Romero-Palazon, E. Pyrolysis of petroleum residues: I. yields and product analyses. Carbon 37, 1567-1582. 1999.

5-17 Heintz, E. A. Effect of calcination rate on petroleum coke properties. Carbon, 33, 6, 817-820. 1995.

5-18 Makabe, M., Itoh, H., Ouchi, K. Mesophase formation of pitch under reduced pressure. Carbon 1976, 14, p 365.

5-19 Mochida, I., Fei, Y.Q., Korai, Y. Carbonization in the tube bomb leading to needle coke: III. Carbonization properties of several coal-tar pitches. Carbon, 1989, 27, 375-380.

5-20 Mochida, I.; Oyama, T.; Korai, Y. Improvements to needle-coke quality by pressure reductions from a tube reactor. Carbon, 26 (1); 57-60. 1988.

5-21 Mochida, I.; Korai, Y.; Wang, Y.-G.; Hong, S.-H. In Graphite and Precursors; Delhaes, P., Ed.; Gordon and Breach Science Publishers, 1979; 221-225.

5-22 Mochida, I., Fei, Y.Q., Furuno, T. Optimization of carbonization conditions for needle coke production from a low-sulphur petroleum vacuum residue. Journal of material science 23(1):298-304, 1988.

5-23 Zander, M. In Sciences of Carbon Materials; Marsh, H., Rodriguez-Reinoso, F., Eds. Universidad de Alicante, 2000, p 220.

5-24 Collin, P. J.; Tyler, R. J.; Wilson, M. A. ^{1}H n.m.r. study of tars from flash pyrolysis of three Australian coals *Fuel* 1980, *59*, 479-486.

5-25 Brown and Ladner, Fuel 1960, 39, 89.

5-26 Karam, H.S.; McNair, H.M.; Lancas, F.M. Characterization of Alternative Fuels by HPLC and GC-MS. LC-GC, 5, 1, 41-48. 1987.

5-27 Oya, A.; Quian, Z.; Marsh, H. Structural study of cokes using optical microscopy and X-ray diffraction. Fuel 1983, 62, 274-278.

5-28 Eser S. In Supercarbon: Synthesis, Properties and Applications; Yoshimura, S., Chang, R., eds Springer-Verlag, Berlin, 1998; 147.

5-29 Mochida, I., Korai, Y, and Oyama, T. Semi-quantitative correlation between optical anisotropy and CTE of needle-like coke grains. Carbon 1987, 25, 273-278.

5-30 Ishihara, A., Morita, S. and Kabe, T. Elucidation of hydrogen transfer mechanisms in coal liquefaction using a tritium tracer method. Fuel 74(1):63-69, 1995.

5-31 Marsh, H.; Martinez-Escandell, M.; Rodriguez-Reinoso, F. Review: Semicokes from pitch pyrolysis: mechanisms and kinetics. *Carbon* **1999**, *37*, 363-390.

5-32 Rudnick, L.R., Boehman, A., Song, C., Miller, B., Mithchell, G. Refinery Integration of By-Products from Caol-Derived Jet Fuels, Grant DE-FC26-03NT41828, Semi-Annual Progress Report, November 17, 2005.

5-33 Gül, Ö.; Rudnick, L.R.; Schobert, H.H. "Delayed Coking of Decant Oil and Coal in a Laboratory-Scale Coking Unit" Energy & Fuels, 2006, 4, 1647-1655.

5-34 Gül, Ö., Clifford,C.E.B., Rudnick, L.R. and Schobert, H.H. “Process repeatability of co-coking of coal and decant oil in a pilot-scale delayed coker” 2nd International Symposium on Hydrotreating/Hydrocracking Technologies, Division of Petroleum Chemistry, The 232nd ACS National Meeting, San Francisco, CA, September 10-14, 2006.

5-35 Gül, Ö., L. Rudnick, Schobert, H.H. "The Effect of Reaction Temperature and Fuel Treatment On Deposit Formation of Jet Fuels." Abstracts of Papers of The American Chemical Society 2005, 230: U1699-U1699.

5-36 Rudnick, L., Gül, Ö., Schobert, H.H. "Effects of chemical composition of coal derived jet fuels on carbon deposits." Abstracts of Papers of The American Chemical Society 2004, 228: U674-U674.

5-37 Strohm, J., S. Butnark, Keyser, T.L., Andresen, J.M., Badger, M., Schobert, H.H., Song, C. "Use Of Coal Pyrolysis Products for the Development of Thermally Stable Jet Fuels." Abstracts of Papers of The American Chemical Society 2002, 223: U564-U564.

5-38 Andresen, J., J. Strohm, Boyer, M.L., Song, C.S., Schobert, H.H., Butnark, S. "Thermal Stability of Hydrotreated Refined Chemical Oil Derived Jet Fuels In The Pyrolytic Regime." Abstracts of Papers of The American Chemical Society 2001, 221: U505-U505.

5-39 Fickinger, A., M. Badger, Mitchell, G.D., Schobert, H.H. "Co-Coking: An Alternative Process For Coal Derived Jet Fuel Production." Abstracts Of Papers Of The American Chemical Society 1999, 217: U811-U812.

5-40 Song, C., W. Lai, Schobert, H.H. "Hydrogen-Transferring Pyrolysis Of Long-Chain Alkanes And Thermal-Stability Improvement Of Jet Fuels By Hydrogen Donors." Industrial & Engineering Chemistry Research 1994, 33(3): 548-557.

5-41 Burgess, C. and Schobert, H. H. "Direct Coal-Liquefaction - A Potential Route To Thermally Stable Jet Fuel." Abstracts of Papers of the American Chemical Society 1993, 206: 29-Fuel.

5-42 Song, C., Eser, S., Schobert, H.H., Hatcher, P.G., "Pyrolytic Degradation Studies Of A Coal-Derived And A Petroleum-Derived Aviation Jet Fuel." Energy & Fuels 1993, 7(2): 234-243.

5-43 Gül, Ö.; Rudnick, L.R.; Schobert, H.H. “The Effect of Chemical Composition of Coal-Based Jet Fuels on the Deposit Tendency and Morphology”, Energy Fuels, 2006, 6, in Press.

5-44 F. M. Lanças, H. S. Karam and H. M. McNair, *LC-GC, magazine of liquid and gas chromatography* **1987**, *5*, 41-48.

5-45 C. Dariva, J. V. de Oliveira, M. G. R. Vale and E. B. Caramão, *Fuel* **1997**, *76*, 585-591.

5-46 K. Masaki, T. Yoshida, C. Li, T. Takanohashi and I. Saito, *Energy&Fuels* **2004**, *18*, 995-1000.

5-47 T. Yoshida, C. Li, T. Takanohashi, A. Matsumura, S. Sato and I. Saito, *Fuel Processing Technology* **2004**, *86*, 61-72.

5-48 T. Yoshida, T. Takanohashi and K. Katoh, *Fuel* **2000**, *79*, 399-404.

5-49 T. Yoshida, T. Takanohashi, K. Sakanishi and I. Saito, *Energy&Fuels* **2002**, *16*, 1006-1007.

5-50 T. Yoshida, T. Takanohashi, K. Sakanishi, I. Saito, M. Fujita and K. Mashimo, *Fuel* **2002**, *81*, 1463-1469.

5-51 C. Song and W.-C. Lai, *Fuel* **1995**, *10*, 1436-1451.

5-52 E. B. Caramão, L. M. F. Gomes, A. Bristoti and F. M. LanVas, *Fuel Science and Technology International* **1990**, *8*, 173-190.

5-53 F. M. Lanças and M. C. R. Peralba, *Fuel Science and Technology International* **1993**, *11*, 541-560.

5-54 F. M. Lanças and E. B. Caramão, *Fuel Science and Technology International* **1992**, *10*, 1197-1205.

5-55 F. M. Lanças and E. B. Caramão, *Fuel Science and Technology International* **1996**, *14*, 427-450.

5-56 J. M. Griffith, L. R. Rudnick and H. H. Schobert, *Preprints of ACS Division Petroleum Chemistry* **2006**, *51*, 231-237.

5-57 K. Miura, *Fuel Processing Technology* **2000**, *62*, 119-135.

5-58 K. Miura, K. Mae, H. Yoo Sock, R. Ashida and M. Morimoto, *Preprints of ACS Division Fuel Chemistry* **1999**, *45*, 652-656.

5-59 K. Miura, M. Shimada, K. Mae and H. Yoo Sock, *Fuel* **2001**, *80*, 1573-1582.

5-60 J. M. Griffith, C. E. Clifford Burgess, L. R. Rudnick and H. H. Schobert, *Preprints of ACS Division Fuel Chemistry* **2004**, *49*, 627-629.

5-61 M. M. Escallón in *Reaction of decant oil and bituminous coal at 465°C in a laboratory scale coker*, *Vol.* Pennsylvania State University, State College, **2004**, p. In press.

5-62 M. M. Escallón, P. Gafarova, G. D. Mitchell, O. Gul and H. H. Schobert, *Petroleum Chemistry Division Preprints* **2005**, *50*, 401-404.

5-63 M. M. Escallón, P. Gafarova, G. D. Mitchell, O. Gul, H. H. Schobert and L. Rudnick, *22nd Annual Meeting of the Society for Organic Petrology* (Lousville, Kentucky, USA) **2005**, pp. 52-55.

5-64 M. M. Escallon, R. Venkataraman, D. J. Clifford and H. H. Schobert, *Petroleum Chemistry Division Preprints* **2003**, *48*, 147-149.

5-65 J. H. Hildebrand, J. M. Prausnitz and R. L. Scott, *Regular and Related Solutions*, VNR, New York, **1970**, p. 228.

5-66 H.-P. Hombach, *Fuel* **1980**, *59*, 465-470.

5-67 J. W. Larsen, T. K. Green and J. Kovac, *Journal of Organic Chemistry* **1985**, *50*, 4729-4735.

5-68 E. M. Suuberg, Y. Otake, M. J. Langner, K. T. Leung and I. Milosavljevic, *Energy & Fuels* **1994**, *8*, 1247-1262.

5-69 D. W. van Krevelen, *Properties of Polymers. Correlations with chemical structure.*, Elsevier Publishing Company, New York, **1972**, p. 427.

5-70 P. C. Painter, J. Graf and M. M. Coleman, *Energy & Fuels* **1990**, *4*, 379-384.

5-71 T. K. Green, J. Kovac and J. W. Larsen, *Fuel* **1984**, *63*, 935-938.

5-72 Y. Otake and E. M. Suuberg, *Fuel* **1989**, *68*, 1609-1612.

5-73 Davis, A., 1978, Chapter 2: The Reflectance of Coal, in: Analytical Methods for Coal and Coal Products, (Ed. C.Karr, Jr.), Academic Press, New York, pp. 27-81.

5-74 Taylor, G.H. et al., 1998, Chapter 2: The Origin of Organic Matter in Sedimentary Rocks, in: Organic Petrology, Gebrüder Borntraegar, Berlin, pp. 116-126.

5-75 Burgess-Clifford, C.E., Boehman, A., Song, C., Miller, B., Mitchell, G., "Refinery Integration of By-Products from Coal-derived Jet Fuels," Semi-Annual Progress Report for Grant DE-FC26-03NT41828, May 17, **2006**.

5-76 Clifford, C.E.B., Boehman, A., Song, C., Miller, B., and Mitchell, G. (2006). Refinery Integration of By-Products from Coal-Derived Jet Fuels: Semi-Progress Report, The Energy Institute, PSU: University Park.

5-77 Newman, J.W., and Newman, K.L. (1997). A History of Pitch Technologies. In Introduction to Carbon Technologies, H. Marsh, Heintz, E. A., and Rodriguez-Reinoso, F., ed. (Secretariado de Publicaciones), pp. 269-328.

5-78 Clifford, C.E.B., Boehman, A., Song, C., Miller, B., and Mitchell, G. (2006). Refinery Integration of By-Products from Coal-Derived Jet Fuels: Semi-Progress Report, The Energy Institute, PSU: University Park.

5-79 Nitkiewicz, Z.; Pajak, L.; Konstanciak, A.; Balaga, Z. Archives of Metallurgy 2000, 45, 343-354

5-80 Oya, A.; Qian, Z.; Marsh, H. *Fuel* **1983**, *62*, 274.

5-81 Eser, S. In *Supercarbon: Synthesis, Properties and Applications*; Yoshimura, S., Chang, R. P. H., Eds.; Springer-Verlag: Berlin, **1998**; p 147.

5-82 Mitchell, G.D.; Rudnick, L.R.; Schobert, H.H., The Society for Organic Petrology Abstracts, September, **2005**, p. 92-94.

5-83 Ellis, P.J.; Paul, C. A. Tutorial: Petroleum Coke Calcining and Uses of Calcined Petroleum Coke, 3rd International Conference on Refining Processes.

List of Acronyms and Abbreviations

1THQ	1,2,3,4-tetrahydroquinoline
5THQ	5,6,7,8-tetrahydroquinoline
AEL	international zeolite code of AlPO4-11 material
AFOSR	Air Force Office of Scientific Research
ADN	Adsorptive Denitrogenation
ADS	Adsorptive Desulfurization
AlPO	aluminophosphate
ATTM	Ammonium Tetrathiomolybdate
API	American Petroleum Institute
BCH	bicyclohexane
BP	biphenyl
BT	benzothiophene
CFR	Cooperative Fuels Research
CHB	cyclohexylbenzene
DBT	dibenzothiophene
DDC	Detroit Diesel Corporation
DDS	direct desulfurization
DGC	dry-gel conversion
DHN	decahydronaphthalene
DHQ	decahydroquinoline
DMBP	dimethyl biphenyl
DMDBT	dimethyldibenzothiophene
DMDCH	dimethyl dicyclohexyl
DMN	dimethyl naphthalene
DPA	dipropylamine
EN	ethyl naphthalene
EPA	Environmental Protection Agency
FBP	final boiling point
FCC	fluid catalytic cracking
FID	flame ionizaton detector
FTIR	Fourier Transform Infrared
GCMS	gas chromatography-mass spectrometry
HDMDBT	hydrodimethyl dibenzothiophene
HDS	hydrodesulfurization
HDT	hydrotreated
HM	H-mordenite
HPLC	high performance liquid chromatography
HTS	hydrothermal synthesis
HY	H Y-type zeolite
HYD	hydrogenation pathway
HZSM	H-synthetic zeolite material
IBP	initial boiling point
IC	internal combustion
IQT	ignition quality test

JP-900	jet fuel prototype stable to 900 F
LCO	light cycle oil
LDMS	laser desorption mass spectrometry
LHSV	liquid hourly space velocity
LTHDA	low temperature hydrotreating and dearomatization
MAPO	metal substituted aluminophosphate
MCHT	methyl cyclohexyl toluene
MCM	mesopourous catalytic material
MDBT	methyldibenzothiophene
MN	methyl naphthalene
NTP	normal temperature and pressure
PARC	Pennsylvania Applied Research Corporation
PB	propyl benzene
PCH	propyl cyclohexane
PCHE	propyl cyclohexene
PFPD	pulsed flame photometric detector
PP	petroleum pitch
PSU	Penn State University
RCO	refined chemical oil
SARS	selective adsorption for removing sulfur
SAC	steam-assisted conversion
SAPO	silicon substituted aluminophosphate
SDA	structure-directing agent
SEM	scanning electron microscopy
SI	spark ignited
SpGr	specific gravity
SwRI	Southwest Research Institute
TEM	transmission electron microscopy
TEOS	tetraethyl orthosilicate
THDBT	tetrahydrodibenzothiophene
THDMDBT	tetrahydrodimethyldibenzothiophene
TLP	total liquid product
TMBT	trimethylbenzothiophene
TOS	time on stream
TPD	temperature programmed desorption
TPO	temperature programmed oxidation
TPR	temperature programmed reduction
VPT	vapor-phase transport
WHSV	weight hourly space velocity
XPS	x-ray photoelectron spectroscopy

Appendix 1-A

Data for distillation cuts and simulated distillation of cuts for RCO from Intertek PARC

Sample Name: **X1333 CUT1 OP-560F**
Acquired On: 20060628160136-0500
Recovered 100.00

BP Distribution

IBP	353.53
1%	402.51
2%	484.43
3%	499.12
4%	506.81
5%	508.06
6%	508.68
7%	508.47
8%	508.25
9%	509.12
10%	508.99
11%	508.86
12%	508.74
13%	509.65
14%	509.55
15%	509.45
16%	509.36
17%	509.26
18%	510.17
19%	510.05
20%	509.94
21%	509.82
22%	510.71
23%	510.42
24%	510.89
25%	514.15
26%	517.73
27%	518.15
28%	518.82
29%	518.62
30%	518.41
31%	519.27
32%	519.13
33%	518.98
34%	519.86
35%	519.73
36%	519.60
37%	519.47
38%	520.33
39%	520.12
40%	519.91
41%	522.90
42%	530.39
43%	536.83
44%	537.08
45%	537.79
46%	537.55
47%	538.39
48%	538.26
49%	538.12
50%	537.99
51%	538.90
52%	538.82
53%	538.74
54%	538.65
55%	538.57
56%	538.48
57%	539.42
58%	539.36
59%	539.30
60%	539.24
61%	539.17
62%	539.11
63%	539.05
64%	538.99
65%	539.93
66%	539.87
67%	539.82
68%	539.76
69%	539.70
70%	539.64
71%	539.58
72%	539.53
73%	540.47
74%	540.36
75%	540.25
76%	540.15
77%	540.04
78%	540.80
79%	541.86
80%	542.66
81%	543.92
82%	544.41
83%	544.99
84%	544.52
85%	545.86
86%	546.10
87%	547.10
88%	549.40
89%	549.70
90%	550.88
91%	552.72
92%	553.01
93%	554.38
94%	555.58
95%	563.04
96%	569.63
97%	574.75
98%	583.28
99%	592.48
FBP	607.91

Cut Points Listing

D86 Correlations

D1160 Correlations

Sample Name:	X1332 CUT1C 433-560F	X1332 CUT2 560-570F	X1332 CUT3 570-580F	X1332 CUT3 570-580F
Acquired On:	20060614095834-0500	20060614102642-0500	20060614110213-0500	20060614110213-0500
Recovered	100.00	100.00	100.00	100.00

BP Distribution

IBP	407.28	407.46	450.15	449.44
1%	407.61	487.32	497.22	497.26
2%	408.17	506.19	507.43	507.44
3%	408.88	507.96	508.61	508.61
4%	408.70	508.47	508.21	508.21
5%	408.53	509.16	508.98	508.98
6%	409.36	508.94	508.73	508.74
7%	409.23	508.72	509.54	509.54
8%	409.10	509.57	509.34	509.34
9%	408.97	509.41	510.12	510.13
10%	409.81	509.25	509.83	509.83
11%	409.65	510.10	510.24	510.26
12%	409.49	509.92	514.64	514.75
13%	410.19	509.74	518.16	518.18
14%	410.43	510.40	518.67	518.68
15%	424.45	512.14	519.34	519.35
16%	441.20	515.96	519.11	519.11
17%	447.41	518.05	518.87	518.88
18%	447.97	518.62	519.67	519.68
19%	448.62	519.32	519.45	519.46
20%	449.24	519.11	520.16	520.18
21%	449.63	518.90	520.66	520.71
22%	453.31	519.75	529.15	528.55
23%	453.56	519.59	537.45	536.53
24%	454.59	519.42	537.79	537.81
25%	472.27	520.25	538.43	538.45
26%	474.75	520.06	538.23	538.24
27%	475.12	520.84	538.02	538.03
28%	476.42	521.20	538.87	538.88
29%	482.17	529.13	538.74	538.74
30%	485.03	536.80	538.60	538.61
31%	485.82	537.83	538.47	538.48
32%	489.72	538.44	539.38	539.38
33%	490.71	538.22	539.28	539.29
34%	491.73	538.00	539.18	539.19
35%	496.26	538.85	539.09	539.09
36%	500.14	538.71	538.99	539.00
37%	507.98	538.56	539.90	539.91
38%	508.40	539.44	539.82	539.83
39%	509.10	539.34	539.73	539.74
40%	508.88	539.24	539.64	539.65
41%	509.69	539.15	539.56	539.56
42%	509.57	539.05	540.47	539.48
43%	509.44	539.96	540.33	540.34
44%	509.31	539.88	540.18	540.19
45%	510.20	539.80	540.03	540.04
46%	510.12	539.72	540.59	540.65
47%	510.03	539.64	542.94	542.09
48%	509.94	539.56	543.84	543.92
49%	509.85	539.48	544.13	544.20
50%	509.76	540.39	545.47	544.54
51%	510.69	540.30	546.43	545.55
52%	510.62	540.20	547.18	547.38
53%	510.54	540.11	549.09	549.22
54%	510.47	540.01	550.11	550.23
55%	510.39	540.81	552.73	552.89
56%	510.31	540.53	553.80	553.89
57%	510.24	542.21	553.97	554.09
58%	511.16	543.06	559.72	558.24
59%	511.06	544.33	565.84	563.90
60%	510.96	544.75	569.98	570.20
61%	510.86	545.08	572.17	571.51
62%	510.76	546.11	575.38	574.80
63%	511.55	547.91	581.43	580.90
64%	511.24	550.00	582.65	582.79
65%	515.06	550.14	583.64	583.79
66%	518.08	552.85	587.17	586.16
67%	518.54	553.86	589.48	589.56
68%	519.23	554.11	590.01	590.06
69%	518.99	557.35	589.72	589.76
70%	519.81	564.08	590.49	590.51
71%	519.64	570.18	590.31	590.33
72%	519.48	572.18	591.10	591.12
73%	520.33	576.00	590.98	591.00
74%	520.19	581.89	590.85	590.87
75%	520.05	583.24	590.73	590.75
76%	519.90	584.95	591.57	591.59
77%	520.69	589.58	591.48	591.49
78%	520.47	590.04	591.38	591.40
79%	521.81	589.73	591.29	591.31
80%	528.96	590.48	591.19	591.21
81%	537.22	590.29	592.06	592.08
82%	537.50	591.08	591.96	591.98
83%	538.19	590.94	591.87	591.89
84%	538.92	590.80	591.77	591.79
85%	538.72	590.67	591.68	591.70
86%	538.51	591.50	592.52	592.55
87%	539.31	591.38	592.35	592.39
88%	539.10	591.25	592.19	592.22
89%	539.84	592.09	592.87	592.95
90%	540.47	591.91	593.44	593.51
91%	542.68	591.72	593.07	593.15
92%	544.87	592.38	593.72	593.78
93%	547.40	592.82	594.32	594.41
94%	551.35	593.25	594.63	594.87
95%	556.72	593.72	598.34	598.67
96%	574.64	595.44	606.07	603.78
97%	588.92	600.96	619.80	616.52
98%	590.59	617.77	625.56	624.65
99%	591.86	634.59	657.52	649.06
FBP	596.47	657.89	677.71	667.21

Cut Points Listing

D86 Correlations

D1160 Correlations

150 Gallon Still Distillation

Distillation # X-1333 **Gross:** 640030 **Tare:** **Net Volume, Ml:** 608820 **Gal:** 160.8 **Date:** 6/14/2006
Project # 114014 (gms) (gms) **Net Weight,Gm:** 640030 **Reflux Ratio:** 20:10
Charge: PR-1660 **Takeoff Rate:** 3-5 GAL/HR **Max. Still Temp-°F:** 640
Charged by: AP **Obs.Temp:** **Grav:** 3.1 **Gravity:** 3.1 **SpGr:** 1.051 **Cuts:** 560f

Time			Distillation Yields														Temperatures °F								Coolant		Reflux		Heater						
		D	Weight (gms)							Volume			Gravity				Vapor		Still		Column						Timers(secs)		Amperage			Pot	Press	
SET	CUT	P	Cut		Cut Summary	Total				Ml	%	%	Observed		Calc.		@760	Ovhd	Btms	Top	Btms	Mid	Abv Rflx	Goose	IN	OUT	OFF	ON	#1	#2	#3	%	mm	Oper
		(in.H20)	Gross	Tare	Net	Total	%	Cum	%Cum			Cum	Temp	API	API	SpGr	mmHg	#13	#4	#7	#9	#11	#14	#16	19	18			btm	mid	top		Hg	
	1A		168240		168240	168240	26.3	168240	26.3	#DIV/0!	#####	#DIV/0!						429	471	451	436	432	428	427	45	50	20	10	22	20	22	50	ATMS	GS
	1B		183164		183164	183164	28.6	351404	54.9	#DIV/0!	#####	#DIV/0!						481	578	558	514	503	475	472	181	224	10	5	24	22	24	56	ATMS	HR
	1C		115214		115214	115214	18.0	466618	72.9	#DIV/0!	#####	#DIV/0!						560	637	621	595	577	556	554	224	225	10	5	26	24	26	58	ATMS	GS
	BTMS		159486		159486	159486	24.9	626104	97.8	#DIV/0!	#####	#DIV/0!																					

150 Gallon Still Distillation

Distillation # X-1332 **Gross:** 640937 **Tare:** **Net Volume, Ml:** 608324 **Gal:** 160.7 **Date:**
Project # 114014 (gms) (gms) **Net Weight,Gm:** 640937 **Reflux Ratio:** 20;10
Charge: PR-1660 **Takeoff Rate:** 3,5 **Max. Still Temp-°F:** 640
Charged by: GS **Obs.Temp:** **Grav:** 2.8 **Gravity:** 2.8 **SpGr:** 1.054 **Cuts:** 560 570 580

Time			Distillation Yields														Temperatures °F								Coolant		Reflux		Heater						
		D	Weight (gms)							Volume			Gravity				Vapor		Still		Column						Timers(secs)		Amperage			Pot	Press	
SET	CUT	P	Cut		Cut Summary	Total				Ml	%	%	Observed		Calc.		@760	Ovhd	Btms	Top	Btms	Mid	Abv Rflx	Goose	IN	OUT	OFF	ON	#1	#2	#3	%	mm	Oper
		(in.H20)	Gross	Tare	Net	Total	%	Cum	%Cum			Cum	Temp	API	API	SpGr	mmHg	#13	#4	#7	#9	#11	#14	#16	19	18			btm	mid	top		Hg	
	1		180306		180306	180306	28.1	180306	28.1	#DIV/0!	#####	#DIV/0!					428	428	474	452	430	428	427	420	49	52	20	10	24	22	24	54	ATMOS	EH
	1		181077		181077	181077	28.3	361383	56.4	#DIV/0!	#####	#DIV/0!					433	433	550	522	476	457	435	433	45	49	20	10	24	22	24	54	ATMOS	HR
	1		82555		82555	82555	12.9	443938	69.3	#DIV/0!	#####	#DIV/0!					560	420	559	542	510	421	415	409	47	56	20	5	30	28	30	60	100	HR
	2		8177		8177	8177	1.3	452115	70.5	#DIV/0!	#####	#DIV/0!					570	429	566	549	534	432	428	421	49	55	20	5	30	28	30	60	100	HR
	3		10140		10140	10140	1.6	462255	72.1	#DIV/0!	#####	#DIV/0!					580	438	570	552	538	438	434	427	47	55	20	5	30	28	30	60	100	HR
	BTMS		142793		142793	142793	22.3	605048	94.4	#DIV/0!	#####	#DIV/0!																					

150 Gallon Still Distillation

Distillation # X-1318 **Gross:** 648467 **Tare:** **Net Volume, Ml:** 614554 **Gal:** 162.4 **Date:** 4/25/2006
Project # 114014 (gms) (gms) **Net Weight,Gm:** 648467 **Reflux Ratio:** 20:10
Charge: PR-1660 **Takeoff Rate:** 3-5 gal/hr **Max. Still Temp-°F:** 640
Charged by: AP **Obs.Temp:** **Grav:** 2.6 **Gravity:** 2.6 **SpGr:** 1.055 **Cuts:** 560,570,580F

Time			Distillation Yields														Temperatures °F								Coolant		Reflux		Heater						
		D	Weight (gms)							Volume			Gravity				Vapor		Still		Column						Timers(secs)		Amperage			Pot	Press	
SET	CUT	P	Cut		Cut Summary	Total				Ml	%	%	Observed		Calc.		@760	Ovhd	Btms	Top	Btms	Mid	Abv Rflx	Goose	IN	OUT	OFF	ON	#1	#2	#3	%	mm	Oper
		(in.H20)	Gross	Tare	Net	Total	%	Cum	%Cum			Cum	Temp	API	API	SpGr	mmHg	#13	#4	#7	#9	#11	#14	#16	19	18			btm	mid	top		Hg	
	1 A		183118		183118	183118	28.2	183118	28.2	#DIV/0!	#####	#DIV/0!					418	418	472	453	425	422	420	418	52	55	20	10	24	22	24	52	760	GS
	1 B		208429		208429	208429	32.1	391547	60.4	#DIV/0!	#####	#DIV/0!					465	356	436	409	412	393	367	367	66	89	20	10	28	26	28	58	150	hr
	1 C		70308		70308	70308	10.8	461855	71.2	#DIV/0!	#####	#DIV/0!					560	430	506	486	479	461	432	430	48	58	10	10	30	28	31	60	120	hr
	2		3780		3780	3780	0.6	465635	71.8	#DIV/0!	#####	#DIV/0!					570	439	510	492	486	475	445	443	48	59	10	10	30	28	31	60	120	hr
	3		5130		5130	5130	0.8	470765	72.6	#DIV/0!	#####	#DIV/0!					580	449	513	497	491	481	459	455	48	60	10	10	30	28	31	60	120	GS
	BTMS		150368		150368	150368	23.2	621133	95.8	#DIV/0!	#####	#DIV/0!																					
								621133																										
	LOSS		27334		27334	27334	4.2	648467	100.0	#DIV/0!	#####	#DIV/0!																					

Appendix 1-B

Data for simulated distillation of cuts for LCO from Intertek PARC (material supplied by United Refining).

Sample Name: **PF-1639 LT CYCLE OIL**
Acquired On: 20060601161544-0500
Recovered 100.00

BP Distribution

IBP	233.03
1%	282.08
2%	333.54
3%	360.73
4%	389.05
5%	404.75
6%	413.18
7%	433.87
8%	445.31
9%	446.06
10%	447.29
11%	450.59
12%	452.04
13%	468.63
14%	478.77
15%	480.86
16%	482.77
17%	484.02
18%	485.07
19%	487.59
20%	487.89
21%	488.37
22%	489.82
23%	490.73
24%	493.94
25%	497.60
26%	503.14
27%	509.69
28%	513.00
29%	515.25
30%	516.20
31%	517.38
32%	519.91
33%	521.54
34%	522.41
35%	524.07
36%	526.93
37%	528.76
38%	531.28
39%	532.63
40%	535.77
41%	538.17
42%	540.28
43%	541.57
44%	543.10
45%	545.85
46%	548.25
47%	550.89
48%	553.28
49%	556.82
50%	561.27
51%	565.80
52%	567.97
53%	570.13
54%	571.43
55%	573.54
56%	575.71
57%	577.45
58%	580.53
59%	582.79
60%	586.60
61%	588.46
62%	590.77
63%	596.34
64%	599.24
65%	601.04
66%	604.07
67%	607.34
68%	609.51
69%	613.04
70%	616.46
71%	617.85
72%	618.97
73%	619.90
74%	623.17
75%	624.76
76%	626.06
77%	630.50
78%	634.65
79%	637.52
80%	640.01
81%	643.80
82%	646.46
83%	647.75
84%	649.39
85%	652.12
86%	652.93
87%	654.44
88%	657.05
89%	661.08
90%	664.88
91%	669.75
92%	672.49
93%	677.28
94%	680.03
95%	683.91
96%	690.74
97%	697.42
98%	708.18
99%	724.63
FBP	739.26

Cut Points Listing

D86 Correlations

D1160 Correlations

Sample Name: **PR-1850 LT CYCLE OIL**
Acquired On: 20060530120206-0500
Recovered 100.00

BP Distribution

IBP	284.21
1%	325.67
2%	371.73
3%	399.16
4%	414.19
5%	436.18
6%	445.32
7%	447.58
8%	448.14
9%	448.80
10%	448.47
11%	449.07
12%	450.11
13%	452.56
14%	453.91
15%	454.38
16%	454.53
17%	463.44
18%	470.06
19%	475.20
20%	479.16
21%	481.52
22%	481.84
23%	483.16
24%	483.81
25%	485.01
26%	485.57
27%	486.22
28%	485.89
29%	486.55
30%	487.08
31%	488.63
32%	489.67
33%	490.25
34%	489.93
35%	490.67
36%	490.42
37%	491.18
38%	490.92
39%	491.61
40%	492.23
41%	492.45
42%	495.66
43%	496.87
44%	497.11
45%	500.50
46%	501.18
47%	506.09
48%	508.83
49%	511.63
50%	513.46
51%	515.47
52%	516.55
53%	516.93
54%	518.26
55%	519.24
56%	520.75
57%	522.15
58%	523.17
59%	524.41
60%	524.67
61%	524.94
62%	526.49
63%	529.25
64%	530.40
65%	530.59
66%	532.74
67%	534.27
68%	535.38
69%	537.04
70%	539.24
71%	541.46
72%	542.37
73%	543.20
74%	544.20
75%	545.16
76%	546.77
77%	549.44
78%	550.95
79%	552.16
80%	553.50
81%	555.98
82%	558.61
83%	562.17
84%	565.05
85%	568.51
86%	570.58
87%	572.00
88%	574.23
89%	575.64
90%	576.75
91%	579.45
92%	582.40
93%	585.66
94%	589.30
95%	594.13
96%	599.79
97%	606.20
98%	615.51
99%	628.91
FBP	645.01

Cut Points Listing

D86 Correlations

D1160 Correlations

Appendix 4-A

Research Boiler Efficiency Calculations

Research Boiler Efficiency Calculations

Date of Operation	**8/2/06**
Test Fuel Burned	**X610**
Test Program	**Refinery Int.**

Operating Conditions

System Temperatures (°F)	
Primary Air	**340**
Condensate Return	**60**
Low Pressure Steam	**267**
Flue Gas Boiler Exit - West	**477**
Flue Gas Economizer Inlet	**483**
Flue Gas Boiler Exit - East	**486**
High Pressure Steam	**336**
Stack	**269**
Bag Filter Entrance	**362**
Quarl Top	**1246**
Secondary Air	**692**
Condensor Water Exit	**113**
Quarl Bottom	**1079**
Boiler Feed Water	**203**
Calorimeter	**276**
Liquid Fuel	**111**
Ambient (^{o}C)	**24** (75 F)

System Pressures	
High Pressure Steam (psig)	**96.6**
Low Pressure Steam (psig)	**5.4**
Liquid Fuel (psig)	**37.2**
Atomizing Media (psig)	**56.7**
Secondary Air (psig)	**63.4**
Primary Air (inch w.c.)	**3.5**

System Flow Rates	
Natural Gas (lb/hr)	**0.0**
Primary Air (lb/hr)	**1176**
High Pressure Steam (lb/hr)	**1152**
Liquid Fuel (lb/hr)	**83.7**
Atomizing Media (lb/hr)	**70.4**
Secondary Air (lb/hr)	**163**
Solid Fuel (lb/min)	**0.0**
Cooling Air (lb/hr)	**25.0**

Flue Gas Analysis (dry basis)	
Oxygen (%)	**4.1**
Carbon Monoxide (ppm)	**165**
Carbon Dioxide (%)	**13.6**
Sulfur Dioxide (ppm)	**13**
Nitrogen Oxides (ppm)	**186**
Hydrocarbons (ppm)	**0**

Additional System Data	
Steam Quality (%)	**99.0**
Primary Air Humidity (%RH)	**42.7**
Feeder Weight (lbs)	**0**
Combustion Efficiency (%)	**98.0**
Firing Rate (Btu/hr)	**1,497,393**

Primary Air Percent Humidity Calculation	
Water vapor press. @ ambient temp (atm)	**0.0287**
Partial press of water @ air temp (atm)	**0.0123**
Primary Air Percent Humidity (%H)	**42.0**

Liquid Fuel Analyses

	Weight %
Carbon	**89.10**
Hydrogen	**7.65**
Nitrogen	**0.12**
Sulfur	**0.06**
Oxygen	**3.05**
Moisture	**0.00**
Ash	**0.02**
Total =	**100.00**

HHV (determined at constant volume)	**17,890**	Btu/lb
HHV (determined at constant pressure)	**17,910**	Btu/lb

Steam Data

Enthalpy of Sat. Liq. (Btu/lb)	**307.1**	(saturated liquid @ absolute drum pressure)
Enthalpy of Sat. Vapor (Btu/lb)	**1,189.0**	(saturated vapor @ absolute drum pressure)
Enthalpy of Sat. Vapor (Btu/lb)	**1,180.6**	(saturated vapor @ absolute atomization pressure)
Entahlpy of Feed Water (Btu/lb)	**171.07**	(saturated liquid @ feedwater temperature)
Enthalpy of water vap. At Boiler Exit Temp (Btu/lb)	**1,278.85**	(Superheated steam @ 1psia & exit temperature)
Enhtalpy of water at reference temp. (Btu/lb)	**48.04**	(Sat. liquid @ fuel temperature - 80F)

Boiler Efficiency Calculations (Based on ASME PTC 4.1)

Input - Output Method

Efficiency = (Output/Input) * 100

Output = (steam flow rate)(steam quality/100)(enthalpy of steam @ drum pressure - enthalpy of feedwater) + (steam flow rate)((100 - steam quality)/100)(enthalpy of water @ drum pressure - enthalpy of feed water)

= **1,162,762** Btu/hr

Input = (fuel flow rate)(high-heat value of fuel) + heat credits

Heat Credits = heat supplied in dry primary air + heat supplied in preheated fuel + heat supplied in atomizing steam + heat supplied from moisture in primary air)

= Bae + Bfe + Bze + Bmae

Bae = (flow rate of primary air)(wt% dry air)(specific heat of air)(primary air temp - reference air temp)

= **73,486** Btu/hr (assumes primary air temperature of ~350F for Cp)

Bfe = (flow rate of fuel)(specific heat of fuel)(fuel inlet temp - reference air temp)

= **1,073** Btu/hr

Bze = (flow rate of atomizing steam)(enthalpy of atomizing steam - enthalpy of sat. vapor @ reference temp)

= **79,733** Btu/hr

Bmae = (flow rate of primary air)(wt% water vapor in dry air)(specific heat of water vapor)(primary air temp - reference air temp)

= **1,106** Btu/hr (assumes primary air temperature of ~350F for Cp)

Input = **1,652,791** Btu/hr

Boiler Efficiency = **70.4 %**

Heat Loss Method

Efficiency = (Losses/Input) * 100

Input = determined from Input-Output method
= **1,652,791** Btu/hr

Losses = heat loss due to dry gas + heat loss due to unburnt carbon + heat loss due to moisture in the fuel + heat loss due to moisture produced from burning hydrogen in the fuel + heat loss due to moisture in the combustion air + heat loss due to formation of carbon monoxide + heat loss due to heat in atomizing steam + heat loss due to surface radiation and convection
= Lg + Luc + Lmf + Lmfh + Lma + Lco + Lz + Lb

Dry Gas

Pounds of dry gas per pound of "as fired" fuel (Lg)

Wg' = ((c%)(C.Efficiency)(44.01 (CO2) + 32.00 (O2) + 28.02 (N2) + (28.01 (CO)/12.01 (CO2+CO)) + 12.01(S)/32.07

Wg' = **16.25** lb dry gas/lb of as fired fuel

Lg' = (Wg')(Cpg')(boiler exit temp - reference air temperature)(fuel flow rate)
= **131,153** Btu/hr

Unburnt Carbon

Luc = (% Carbon in the "as fired Fuel")(1-Comb.Efficiency)(fuel flow rate)(14500)
= **21,627** Btu/hr

Moisture in Fuel

Lmf = (lb moisture per lb of fuel)(entahlpy of water vapor at boiler exit temp - entahlpy of water at reference temperature)(fuel flow rate)
= **0** Btu/hr

Moisture from Burning Hydrogen

Lmfh = (8.936)(% hydrogen in "as fired" fuel)(enthalpy of water vapor @ boiler exit temp - enthalpy of water @ reference temperature)(fuel flow rate)
= **70,424** Btu/hr

Heat Loss Method - Continued

Moisture in Combustion Air (Primary air only)

Primary Air Flow Rate =	1176	lbs/hr	
lbs Air per lb of Fuel =	14.05	lbs air/lb fuel	
Primary Air % Humidity =	42.0		
Moisture in Primary Air =	0.008	lb water vapor/lb of dry air	(Figure 24-2, p. 748 McCabe and Smith, Unit Operations of Chemical Engineering - 3rd Edition)

Lma = (lbs air per lb of fuel)(lb of water vapor per lb of air)(enthalpy of water vapor @ boiler exit temp - enthalpy of water vapor @ reference temperature)(fuel flow rate)

= **11,579** Btu/hr

Formation of Carbon Monoxide

Lco = (CO/(CO2+CO))(10160)(Combustion Efficiency)(% carbon in 'as fired fuel)(fuel flow rate)

= **902** Btu/hr

Atomizing Steam

Lz = (lbs of atomizing steam per hour)(enthalpy of water vapor @ boiler exit temp - enthalpy of water vapor @ reference temp)

= **86,649** Btu/hr

Radiation

Maximum Continuous Boiler Output =	2,000,000	Btu/hr
Actual Output =	1,497,393	Btu/hr

Lb = **8.5 %** (Figure 8, p. 67, ASME PTC 4.1)

Total Heat Losses = **462,822** Btu/hr

Boiler Efficiency = **72.0 %**

Calculation of Pollutant Emission Factors

EPA CFR Title 40 Emissions Factor

Pollutant/MMBtu = $(1.194 \times 10^{-7}$ x (vol. concentration of pollutant - ppm)) x ((3.64(%H) + 1.53(%C) + 0.57(%S) + 0.14(%N) -0.46(%O_2))/GCV) x 10^6 x (20.9/(20.9 - %O_2))

(EPA, Code of Federal Register, Title 40, Part 75, Chapter 1, Section 3, pp. 321 -323.)

Pollutant	Emissions Factor (lbs./MM Btu)
CO	0.223
CO_2	183.0
SO_2	0.017
NO_x	0.251
Hydrocarbons (C_1-C_3)	0.000

Mass Balance Around the Boiler

Total Mass Input = lbs. of fuel (dry basis) + lbs. of primary air (dry basis) + lbs. of secondary air + lbs. of cooling air

= 1381 lbs/hr

Conversion of Gas Composition from Volume% to Wt%

	Mole %	lbs in each mole of gas	Weight %	Emission Factors (lbs/MM Btu)	
Oxygen	4.069921262	1.3024	4.29		
Carbon Monoxide	0.016489139	0.0046	0.02	0.140	<-- **CO**
Carbon Dioxide	13.6	5.9692	19.67	181.4	<-- **CO_2**
Sulfur Dioxide	0.00127356	0.0008	0.00	0.025	**<-- SO2**
Nitrogen Oxides	0.01859097	0.0056	0.02	0.260	**<-- NOx**
Nitrogen	82.3	23.0608	76.00		**<-- Hydrocarbons**
Total =	100.0	30.3433	100.00		

Research Boiler Efficiency Calculations

Date of Operation	**8/7/06**
Test Fuel Burned	**#6 Fuel Oil**
Test Program	**Refinery Int.**

Operating Conditions

System Temperatures (°F)

Primary Air	**340**
Condensate Return	**60**
Low Pressure Steam	**267**
Flue Gas Boiler Exit - West	**477**
Flue Gas Economizer Inlet	**483**
Flue Gas Boiler Exit - East	**486**
High Pressure Steam	**336**
Stack	**269**
Bag Filter Entrance	**362**
Quarl Top	**1246**
Secondary Air	**692**
Condensor Water Exit	**113**
Quarl Bottom	**1079**
Boiler Feed Water	**203**
Calorimeter	**276**
Liquid Fuel	**111**
Ambient (^{o}C)	**24** (75 F)

System Pressures

High Pressure Steam (psig)	**96.8**
Low Pressure Steam (psig)	**5.7**
Liquid Fuel (psig)	**40.9**
Atomizing Media (psig)	**59.6**
Secondary Air (psig)	**62.3**
Primary Air (inch w.c.)	**4.1**

System Flow Rates

Natural Gas (lb/hr)	**0.0**
Primary Air (lb/hr)	**1128**
High Pressure Steam (lb/hr)	**1153**
Liquid Fuel (lb/hr)	**81.4**
Atomizing Media (lb/hr)	**71.6**
Secondary Air (lb/hr)	**161**
Solid Fuel (lb/min)	**0.0**
Cooling Air (lb/hr)	**25.0**

Flue Gas Analysis (dry basis)

Oxygen (%)	**4.0**
Carbon Monoxide (ppm)	**43**
Carbon Dioxide (%)	**13.0**
Sulfur Dioxide (ppm)	**879**
Nitrogen Oxides (ppm)	**337**
Hydrocarbons (ppm)	**0**

Additional System Data

Steam Quality (%)	**99.0**
Primary Air Humidity (%RH)	**58.9**
Feeder Weight (lbs)	**0**
Combustion Efficiency (%)	**98.0**
Firing Rate (Btu/hr)	**1,500,772**

Primary Air Percent Humidity Calculation

Water vapor press. @ ambient temp (atm)	**0.0287**
Partial press of water @ air temp (atm)	**0.0169**
Primary Air Percent Humidity (%H)	**58.2**

Liquid Fuel Analyses

	Weight %
Carbon	**86.40**
Hydrogen	**11.30**
Nitrogen	**0.30**
Sulfur	**1.80**
Oxygen	**0.00**
Moisture	**0.00**
Ash	**0.20**
Total =	**100.00**

HHV (determined at constant volume)	**18,437**	Btu/lb
HHV (determined at constant pressure)	**18,467**	Btu/lb

Steam Data

Enthalpy of Sat. Liq. (Btu/lb)	**307.3**	(saturated liquid @ absolute drum pressure)
Enthalpy of Sat. Vapor (Btu/lb)	**1,189.1**	(saturated vapor @ absolute drum pressure)
Enthalpy of Sat. Vapor (Btu/lb)	**1,181.4**	(saturated vapor @ absolute atomization pressure)
Entahlpy of Feed Water (Btu/lb)	**171.07**	(saturated liquid @ feedwater temperature)
Enthalpy of water vap. At Boiler Exit Temp (Btu/lb)	**1,278.85**	(Superheated steam @ 1psia & exit temperature)
Enhtalpy of water at reference temp. (Btu/lb)	**48.04**	(Sat. liquid @ fuel temperature - 80F)

Boiler Efficiency Calculations (Based on ASME PTC 4.1)

Input - Output Method

Efficiency = (Output/Input) * 100

Output = (steam flow rate)(steam quality/100)(enthalpy of steam @ drum pressure - enthalpy of feedwater) + (steam flow rate)((100 - steam quality)/100)(enthalpy of water @ drum pressure - enthalpy of feed water)

= **1,163,818** Btu/hr

Input = (fuel flow rate)(high-heat value of fuel) + heat credits

Heat Credits = heat supplied in dry primary air + heat supplied in preheated fuel + heat supplied in atomizing steam + heat supplied from moisture in primary air)

= Bae + Bfe + Bze + Bmae

Bae = (flow rate of primary air)(wt% dry air)(specific heat of air)(primary air temp - reference air temp)

= **70,277** Btu/hr (assumes primary air temperature of ~350F for Cp)

Bfe = (flow rate of fuel)(specific heat of fuel)(fuel inlet temp - reference air temp)

= **1,044** Btu/hr

Bze = (flow rate of atomizing steam)(enthalpy of atomizing steam - enthalpy of sat. vapor @ reference temp)

= **81,146** Btu/hr

Bmae = (flow rate of primary air)(wt% water vapor in dry air)(specific heat of water vapor)(primary air temp - reference air temp)

= **1,454** Btu/hr (assumes primary air temperature of ~350F for Cp)

Input = **1,654,693** Btu/hr

Boiler Efficiency = **70.3 %**

Heat Loss Method

Efficiency = (Losses/Input) * 100

Input = determined from Input-Output method
= **1,654,693** Btu/hr

Losses = heat loss due to dry gas + heat loss due to unburnt carbon + heat loss due to moisture in the fuel + heat loss due to moisture produced from burning hydrogen in the fuel + heat loss due to moisture in the combustion air + heat loss due to formation of carbon monoxide + heat loss due to heat in atomizing steam + heat loss due to surface radiation and convection
= Lg + Luc + Lmf + Lmfh + Lma + Lco + Lz + Lb

Dry Gas

Pounds of dry gas per pound of "as fired" fuel (Lg)

Wg' = ((c%)(C.Efficiency)(44.01 (CO2) + 32.00 (O2) + 28.02 (N2) + (28.01 (CO)/12.01 (CO2+CO)) + 12.01(S)/32.07

Wg' = **16.40** lb dry gas/lb of as fired fuel

Lg' = (Wg')(Cpg')(boiler exit temp - reference air temperature)(fuel flow rate)
= **128,734** Btu/hr

Unburnt Carbon

Luc = (% Carbon in the "as fired Fuel")(1-Comb.Efficiency)(fuel flow rate)(14500)
= **20,396** Btu/hr

Moisture in Fuel

Lmf = (lb moisture per lb of fuel)(entahlpy of water vapor at boiler exit temp - entahlpy of water at reference temperature)(fuel flow rate)
= **0** Btu/hr

Moisture from Burning Hydrogen

Lmfh = (8.936)(% hydrogen in "as fired" fuel)(enthalpy of water vapor @ boiler exit temp - enthalpy of water @ reference temperature)(fuel flow rate)
= **101,167** Btu/hr

Heat Loss Method - Continued

Moisture in Combustion Air (Primary air only)

Primary Air Flow Rate =	1128	lbs/hr	
lbs Air per lb of Fuel =	13.86	lbs air/lb fuel	
Primary Air % Humidity =	58.2		
Moisture in Primary Air =	0.011	lb water vapor/lb of dry air	(Figure 24-2, p. 748 McCabe and Smith, Unit Operations of Chemical Engineering - 3rd Edition)

Lma = (lbs air per lb of fuel)(lb of water vapor per lb of air)(enthalpy of water vapor @ boiler exit temp - enthalpy of water vapor @ reference temperature)(fuel flow rate)

= **15,272** Btu/hr

Formation of Carbon Monoxide

Lco = (CO/(CO2+CO))(10160)(Combustion Efficiency)(% carbon in 'as fired fuel)(fuel flow rate)

= **230** Btu/hr

Atomizing Steam

Lz = (lbs of atomizing steam per hour)(enthalpy of water vapor @ boiler exit temp - enthalpy of water vapor @ reference temp)

= **88,126** Btu/hr

Radiation

Maximum Continuous Boiler Output = 2,000,000 Btu/hr

Actual Output = 1,500,772 Btu/hr

Lb = **8.5 %** (Figure 8, p. 67, ASME PTC 4.1)

Total Heat Losses = **494,574** Btu/hr

Boiler Efficiency = **70.1 %**

Calculation of Pollutant Emission Factors

EPA CFR Title 40 Emissions Factor

Pollutant/MMBtu = $(1.194 \times 10^{-7}$ x (vol. concentration of pollutant - ppm)) x ((3.64(%H) + 1.53(%C) + 0.57(%S) + 0.14(%N) -0.46(%O_2))/GCV) x 10^6 x (20.9/(20.9 - %O_2))

(EPA, Code of Federal Register, Title 40, Part 75, Chapter 1, Section 3, pp. 321 -323.)

Pollutant	Emissions Factor (lbs./MM Btu)
CO	0.060
CO_2	181.2
SO_2	1.225
NO_x	0.470
Hydrocarbons (C_1-C_3)	0.000

Mass Balance Around the Boiler

Total Mass Input = lbs. of fuel (dry basis) + lbs. of primary air (dry basis) + lbs. of secondary air + lbs. of cooling air

= 1300 lbs/hr

Conversion of Gas Composition from Volume% to Wt%

	Mole %	lbs in each mole of gas	Weight %	Emission Factors (lbs/MM Btu)	
Oxygen	3.951798069	1.2646	4.18		
Carbon Monoxide	0.004279794	0.0012	0.00	0.034	<-- **CO**
Carbon Dioxide	13.0	5.7247	18.91	163.8	<-- **CO_2**
Sulfur Dioxide	0.087923022	0.0563	0.19	1.611	**<-- SO2**
Nitrogen Oxides	0.033727238	0.0101	0.03	0.444	**<-- NOx**
Nitrogen	82.9	23.2244	76.70		**<-- Hydrocarbons**
Total =	100.0	30.2813	100.00		

Research Boiler Efficiency Calculations

Date of Operation	**8/7/06**
Test Fuel Burned	**#6 Fuel Oil**
Test Program	**Refinery Int.**

Operating Conditions

System Temperatures (°F)	
Primary Air	**344**
Condensate Return	**60**
Low Pressure Steam	**266**
Flue Gas Boiler Exit - West	**486**
Flue Gas Economizer Inlet	**487**
Flue Gas Boiler Exit - East	**487**
High Pressure Steam	**335**
Stack	**273**
Bag Filter Entrance	**368**
Quarl Top	**1254**
Secondary Air	**691**
Condensor Water Exit	**115**
Quarl Bottom	**1151**
Boiler Feed Water	**203**
Calorimeter	**276**
Liquid Fuel	**159**
Ambient (^{o}C)	**24** (75 F)

System Pressures	
High Pressure Steam (psig)	**96.6**
Low Pressure Steam (psig)	**5.9**
Liquid Fuel (psig)	**41.3**
Atomizing Media (psig)	**60.1**
Secondary Air (psig)	**64.0**
Primary Air (inch w.c.)	**4.0**

System Flow Rates	
Natural Gas (lb/hr)	**0.0**
Primary Air (lb/hr)	**1118**
High Pressure Steam (lb/hr)	**1164**
Liquid Fuel (lb/hr)	**81.0**
Atomizing Media (lb/hr)	**71.5**
Secondary Air (lb/hr)	**165**
Solid Fuel (lb/min)	**0.0**
Cooling Air (lb/hr)	**25.0**

Flue Gas Analysis (dry basis)	
Oxygen (%)	**4.0**
Carbon Monoxide (ppm)	**48**
Carbon Dioxide (%)	**13.0**
Sulfur Dioxide (ppm)	**881**
Nitrogen Oxides (ppm)	**344**
Hydrocarbons (ppm)	**0**

Additional System Data	
Steam Quality (%)	**99.0**
Primary Air Humidity (%RH)	**44.9**
Feeder Weight (lbs)	**0**
Combustion Efficiency (%)	**98.0**
Firing Rate (Btu/hr)	**1,493,397**

Primary Air Percent Humidity Calculation	
Water vapor press. @ ambient temp (atm)	**0.0287**
Partial press of water @ air temp (atm)	**0.0129**
Primary Air Percent Humidity (%H)	**44.2**

Liquid Fuel Analyses

	Weight %
Carbon	**86.40**
Hydrogen	**11.30**
Nitrogen	**0.30**
Sulfur	**1.80**
Oxygen	**0.00**
Moisture	**0.00**
Ash	**0.20**
Total =	**100.00**

HHV (determined at constant volume)	**18,437**	Btu/lb
HHV (determined at constant pressure)	**18,467**	Btu/lb

Steam Data

Enthalpy of Sat. Liq. (Btu/lb)	**307.2**	(saturated liquid @ absolute drum pressure)
Enthalpy of Sat. Vapor (Btu/lb)	**1,189.0**	(saturated vapor @ absolute drum pressure)
Enthalpy of Sat. Vapor (Btu/lb)	**1,181.5**	(saturated vapor @ absolute atomization pressure)
Entahlpy of Feed Water (Btu/lb)	**171.42**	(saturated liquid @ feedwater temperature)
Enthalpy of water vap. At Boiler Exit Temp (Btu/lb)	**1,281.12**	(Superheated steam @ 1psia & exit temperature)
Enhtalpy of water at reference temp. (Btu/lb)	**48.04**	(Sat. liquid @ fuel temperature - 80F)

Boiler Efficiency Calculations (Based on ASME PTC 4.1)

Input - Output Method

Efficiency = (Output/Input) * 100

Output = (steam flow rate)(steam quality/100)(enthalpy of steam @ drum pressure - enthalpy of feedwater) + (steam flow rate)((100 - steam quality)/100)(enthalpy of water @ drum pressure - enthalpy of feed water)

= **1,174,450** Btu/hr

Input = (fuel flow rate)(high-heat value of fuel) + heat credits

Heat Credits = heat supplied in dry primary air + heat supplied in preheated fuel + heat supplied in atomizing steam + heat supplied from moisture in primary air)

= Bae + Bfe + Bze + Bmae

Bae = (flow rate of primary air)(wt% dry air)(specific heat of air)(primary air temp - reference air temp)

= **66,164** Btu/hr (assumes primary air temperature of ~350F for Cp)

Bfe = (flow rate of fuel)(specific heat of fuel)(fuel inlet temp - reference air temp)

= **2,599** Btu/hr

Bze = (flow rate of atomizing steam)(enthalpy of atomizing steam - enthalpy of sat. vapor @ reference temp)

= **81,043** Btu/hr

Bmae = (flow rate of primary air)(wt% water vapor in dry air)(specific heat of water vapor)(primary air temp - reference air temp)

= **9,956** Btu/hr (assumes primary air temperature of ~350F for Cp)

Input = **1,653,159** Btu/hr

Boiler Efficiency = **71.0 %**

Heat Loss Method

Efficiency = (Losses/Input) * 100

Input = determined from Input-Output method
= **1,653,159** Btu/hr

Losses = heat loss due to dry gas + heat loss due to unburnt carbon + heat loss due to moisture in the fuel + heat loss due to moisture produced from burning hydrogen in the fuel + heat loss due to moisture in the combustion air + heat loss due to formation of carbon monoxide + heat loss due to heat in atomizing steam + heat loss due to surface radiation and convection
= Lg + Luc + Lmf + Lmfh + Lma + Lco + Lz + Lb

Dry Gas

Pounds of dry gas per pound of "as fired" fuel (Lg)

Wg' = ((c%)(C.Efficiency)(44.01 (CO2) + 32.00 (O2) + 28.02 (N2) + (28.01 (CO)/12.01 (CO2+CO)) + 12.01(S)/32.07

Wg' = **16.40** lb dry gas/lb of as fired fuel

Lg' = (Wg')(Cpg')(boiler exit temp - reference air temperature)(fuel flow rate)
= **129,593** Btu/hr

Unburnt Carbon

Luc = (% Carbon in the "as fired Fuel")(1-Comb.Efficiency)(fuel flow rate)(14500)
= **20,295** Btu/hr

Moisture in Fuel

Lmf = (lb moisture per lb of fuel)(entahlpy of water vapor at boiler exit temp - entahlpy of water at reference temperature)(fuel flow rate)
= **0** Btu/hr

Moisture from Burning Hydrogen

Lmfh = (8.936)(% hydrogen in "as fired" fuel)(enthalpy of water vapor @ boiler exit temp - enthalpy of water @ reference temperature)(fuel flow rate)
= **100,856** Btu/hr

Heat Loss Method - Continued

Moisture in Combustion Air (Primary air only)

Primary Air Flow Rate =	1118	lbs/hr	
lbs Air per lb of Fuel =	13.80	lbs air/lb fuel	
Primary Air % Humidity =	44.2		
Moisture in Primary Air =	0.08	lb water vapor/lb of dry air	(Figure 24-2, p. 748 McCabe and Smith, Unit Operations of Chemical Engineering - 3rd Edition)

Lma = (lbs air per lb of fuel)(lb of water vapor per lb of air)(enthalpy of water vapor @ boiler exit temp - enthalpy of water vapor @ reference temperature)(fuel flow rate)

= **110,287** Btu/hr

Formation of Carbon Monoxide

Lco = (CO/(CO2+CO))(10160)(Combustion Efficiency)(% carbon in 'as fired fuel)(fuel flow rate)

= **258** Btu/hr

Atomizing Steam

Lz = (lbs of atomizing steam per hour)(enthalpy of water vapor @ boiler exit temp - enthalpy of water vapor @ reference temp)

= **88,166** Btu/hr

Radiation

Maximum Continuous Boiler Output = 2,000,000 Btu/hr

Actual Output = 1,493,397 Btu/hr

Lb = **8.5 %** (Figure 8, p. 67, ASME PTC 4.1)

Total Heat Losses = **589,973** Btu/hr

Boiler Efficiency = **64.3 %**

Calculation of Pollutant Emission Factors

EPA CFR Title 40 Emissions Factor

Pollutant/MMBtu = $(1.194 \times 10^{-7}$ x (vol. concentration of pollutant - ppm)) x ((3.64(%H) + 1.53(%C) + 0.57(%S) + 0.14(%N) -0.46(%O_2))/GCV) x 10^6 x (20.9/(20.9 - %O_2))

(EPA, Code of Federal Register, Title 40, Part 75, Chapter 1, Section 3, pp. 321 -323.)

Pollutant	Emissions Factor (lbs./MM Btu)
CO	0.067
CO_2	181.6
SO_2	1.230
NO_x	0.480
Hydrocarbons (C_1-C_3)	0.000

Mass Balance Around the Boiler

Total Mass Input = lbs. of fuel (dry basis) + lbs. of primary air (dry basis) + lbs. of secondary air + lbs. of cooling air

= 1217 lbs/hr

Conversion of Gas Composition from Volume% to Wt%

	Mole %	lbs in each mole of gas	Weight %	Emission Factors (lbs/MM Btu)	
Oxygen	3.987976444	1.2762	4.21		
Carbon Monoxide	0.004811612	0.0013	0.00	0.036	<-- **CO**
Carbon Dioxide	13.0	5.7264	18.91	154.1	<-- **CO_2**
Sulfur Dioxide	0.088142452	0.0565	0.19	1.519	**<-- SO2**
Nitrogen Oxides	0.03441867	0.0103	0.03	0.426	**<-- NOx**
Nitrogen	82.9	23.2127	76.65		**<-- Hydrocarbons**
Total =	100.0	30.2834	100.00		

Research Boiler Efficiency Calculations

Date of Operation	**8/14/06**
Test Fuel Burned	**X1333**
Test Program	**Refinery Int.**

Operating Conditions

System Temperatures (°F)	
Primary Air	**347**
Condensate Return	**52**
Low Pressure Steam	**259**
Flue Gas Boiler Exit - West	**419**
Flue Gas Economizer Inlet	**418**
Flue Gas Boiler Exit - East	**422**
High Pressure Steam	**333**
Stack	**230**
Bag Filter Entrance	**304**
Quarl Top	**1169**
Secondary Air	**551**
Condensor Water Exit	**88**
Quarl Bottom	**1054**
Boiler Feed Water	**212**
Calorimeter	**273**
Liquid Fuel	**198**
Ambient (^{o}C)	**24** (75 F)

System Pressures	
High Pressure Steam (psig)	**92.9**
Low Pressure Steam (psig)	**2.5**
Liquid Fuel (psig)	**36.1**
Atomizing Media (psig)	**58.0**
Secondary Air (psig)	**63.9**
Primary Air (inch w.c.)	**7.7**

System Flow Rates	
Natural Gas (lb/hr)	**0**
Primary Air (lb/hr)	**742**
High Pressure Steam (lb/hr)	**794**
Liquid Fuel (lb/hr)	**67.2**
Atomizing Media (lb/hr)	**79.8**
Secondary Air (lb/hr)	**165**
Solid Fuel (lb/min)	**0.0**
Cooling Air (lb/hr)	**25.0**

Flue Gas Analysis (dry basis)	
Oxygen (%)	**5.1**
Carbon Monoxide (ppm)	**74**
Carbon Dioxide (%)	**13.5**
Sulfur Dioxide (ppm)	**299**
Nitrogen Oxides (ppm)	**505**
Hydrocarbons (ppm)	**0**

Additional System Data	
Steam Quality (%)	**98.9**
Primary Air Humidity (%RH)	**36.6**
Feeder Weight (lbs)	**0**
Combustion Efficiency (%)	**98.0**
Firing Rate (Btu/hr)	**1,130,506**

Primary Air Percent Humidity Calculation	
Water vapor press. @ ambient temp (atm)	**0.0287**
Partial press of water @ air temp (atm)	**0.0105**
Primary Air Percent Humidity (%H)	**35.9**

Liquid Fuel Analyses

	Weight %
Carbon	**90.30**
Hydrogen	**5.10**
Nitrogen	**0.35**
Sulfur	**0.54**
Oxygen	**3.68**
Moisture	**0.00**
Ash	**0.03**
Total =	**100.00**

HHV (determined at constant volume)	**16,823**	Btu/lb
HHV (determined at constant pressure)	**16,836**	Btu/lb

Steam Data

Enthalpy of Sat. Liq. (Btu/lb)	**304.4**	(saturated liquid @ absolute drum pressure)
Enthalpy of Sat. Vapor (Btu/lb)	**1,188.4**	(saturated vapor @ absolute drum pressure)
Enthalpy of Sat. Vapor (Btu/lb)	**1,181.0**	(saturated vapor @ absolute atomization pressure)
Entahlpy of Feed Water (Btu/lb)	**180.47**	(saturated liquid @ feedwater temperature)
Enthalpy of water vap. At Boiler Exit Temp (Btu/lb)	**1,249.79**	(Superheated steam @ 1psia & exit temperature)
Enhtalpy of water at reference temp. (Btu/lb)	**48.04**	(Sat. liquid @ fuel temperature - 80F)

Boiler Efficiency Calculations (Based on ASME PTC 4.1)

Input - Output Method

Efficiency = (Output/Input) * 100

Output = (steam flow rate)(steam quality/100)(enthalpy of steam @ drum pressure - enthalpy of feedwater) + (steam flow rate)((100 - steam quality)/100)(enthalpy of water @ drum pressure - enthalpy of feed water)

= **792,393** Btu/hr

Input = (fuel flow rate)(high-heat value of fuel) + heat credits

Heat Credits = heat supplied in dry primary air + heat supplied in preheated fuel + heat supplied in atomizing steam + heat supplied from moisture in primary air)

= Bae + Bfe + Bze + Bmae

Bae = (flow rate of primary air)(wt% dry air)(specific heat of air)(primary air temp - reference air temp)

= **44,772** Btu/hr (assumes primary air temperature of ~350F for Cp)

Bfe = (flow rate of fuel)(specific heat of fuel)(fuel inlet temp - reference air temp)

= **3,237** Btu/hr

Bze = (flow rate of atomizing steam)(enthalpy of atomizing steam - enthalpy of sat. vapor @ reference temp)

= **90,408** Btu/hr

Bmae = (flow rate of primary air)(wt% water vapor in dry air)(specific heat of water vapor)(primary air temp - reference air temp)

= **5,895** Btu/hr (assumes primary air temperature of ~350F for Cp)

Input = **1,274,818** Btu/hr

Boiler Efficiency = **62.2 %**

Heat Loss Method

Efficiency = (Losses/Input) * 100

Input = determined from Input-Output method
= **1,274,818** Btu/hr

Losses = heat loss due to dry gas + heat loss due to unburnt carbon + heat loss due to moisture in the fuel + heat loss due to moisture produced from burning hydrogen in the fuel + heat loss due to moisture in the combustion air + heat loss due to formation of carbon monoxide + heat loss due to heat in atomizing steam + heat loss due to surface radiation and convection
= Lg + Luc + Lmf + Lmfh + Lma + Lco + Lz + Lb

Dry Gas

Pounds of dry gas per pound of "as fired" fuel (Lg)

Wg' = ((c%)(C.Efficiency)(44.01 (CO2) + 32.00 (O2) + 28.02 (N2) + (28.01 (CO)/12.01 (CO2+CO)) + 12.01(S)/32.07

Wg' = **16.58** lb dry gas/lb of as fired fuel

Lg' = (Wg')(Cpg')(boiler exit temp - reference air temperature)(fuel flow rate)
= **91,053** Btu/hr

Unburnt Carbon

Luc = (% Carbon in the "as fired Fuel")(1-Comb.Efficiency)(fuel flow rate)(14500)
= **17,598** Btu/hr

Moisture in Fuel

Lmf = (lb moisture per lb of fuel)(entahlpy of water vapor at boiler exit temp - entahlpy of water at reference temperature)(fuel flow rate)
= **0** Btu/hr

Moisture from Burning Hydrogen

Lmfh = (8.936)(% hydrogen in "as fired" fuel)(enthalpy of water vapor @ boiler exit temp - enthalpy of water @ reference temperature)(fuel flow rate)
= **36,804** Btu/hr

Heat Loss Method - Continued

Moisture in Combustion Air (Primary air only)

Primary Air Flow Rate =	742	lbs/hr	
lbs Air per lb of Fuel =	11.04	lbs air/lb fuel	
Primary Air % Humidity =	35.9		
Moisture in Primary Air =	0.07	lb water vapor/lb of dry air	(Figure 24-2, p. 748 McCabe and Smith, Unit Operations of Chemical Engineering - 3rd Edition)

Lma = (lbs air per lb of fuel)(lb of water vapor per lb of air)(enthalpy of water vapor @ boiler exit temp - enthalpy of water vapor @ reference temperature)(fuel flow rate)

= **62,419** Btu/hr

Formation of Carbon Monoxide

Lco = (CO/(CO2+CO))(10160)(Combustion Efficiency)(% carbon in 'as fired fuel)(fuel flow rate)

= **331** Btu/hr

Atomizing Steam

Lz = (lbs of atomizing steam per hour)(enthalpy of water vapor @ boiler exit temp - enthalpy of water vapor @ reference temp)

= **95,900** Btu/hr

Radiation

Maximum Continuous Boiler Output = 2,000,000 Btu/hr

Actual Output = 1,130,506 Btu/hr

Lb = **8.5 %** (Figure 8, p. 67, ASME PTC 4.1)

Total Heat Losses = **412,464** Btu/hr

Boiler Efficiency = **67.6 %**

Calculation of Pollutant Emission Factors

EPA CFR Title 40 Emissions Factor

Pollutant/MMBtu = $(1.194 \times 10^{-7}$ x (vol. concentration of pollutant - ppm)) x ((3.64(%H) + 1.53(%C) + 0.57(%S) + 0.14(%N) -0.46(%O_2))/GCV) x 10^6 x (20.9/(20.9 - %O_2))

(EPA, Code of Federal Register, Title 40, Part 75, Chapter 1, Section 3, pp. 321 -323.)

Pollutant	Emissions Factor (lbs./MM Btu)
CO	0.108
CO_2	196.9
SO_2	0.436
NO_x	0.737
Hydrocarbons (C_1-C_3)	0.000

Mass Balance Around the Boiler

Total Mass Input = lbs. of fuel (dry basis) + lbs. of primary air (dry basis) + lbs. of secondary air + lbs. of cooling air

= 916 lbs/hr

Conversion of Gas Composition from Volume% to Wt%

	Mole %	lbs in each mole of gas	Weight %	Emission Factors (lbs/MM Btu)	
Oxygen	5.1	1.6320	5.37		
Carbon Monoxide	0.0074	0.0021	0.01	0.055	<-- **CO**
Carbon Dioxide	13.5	5.9414	19.55	158.5	<-- **CO_2**
Sulfur Dioxide	0.0299	0.0192	0.06	0.511	**<-- SO2**
Nitrogen Oxides	0.0505	0.0152	0.05	0.620	**<-- NOx**
Nitrogen	81.3	22.7755	74.96		**<-- Hydrocarbons**
Total =	100.0	30.3853	100.00		